Discovery of therapies for lymphomas and leukaemia: Synthesis and antiproliferative action of novel ethanoanthracenes

A thesis submitted to the University of Dublin for the degree of Doctor of Philosophy (PhD)

By

James P. Mc Keown, BSc. (Pharm), MPharm MPSI,

Statistics (P. Grad. Cert.), AMRSC

Volume 2

Under the supervision of

Dr. Niamh M. O'Boyle, BSc. (Pharm), PhD, MPSI

Prof.Mary J. Meegan, B.Sc. PhD (N.U.I), M.R.S.C., C.Chem.

School of Pharmacy and Pharmaceutical Sciences

Trinity College Dublin

January 2021

Chapter 3: Biological Evaluation

3.0 Introduction

The antiproliferative activity of the synthesised compound libraries was evaluated in the malignant CLL (chronic lymphocytic leukaemia) cell lines PGA-1 and HG-3. Antiproliferative activity was quantified using alamar Blue reagent, measuring cell viability post drug treatment.

These specific CLL cell lines were chosen for the development of the most potent maprotiline based analogues (*E*)-11,12-substituted-9-(2-nitrovinyl)-9,10-dihydro-9,10-ethanoanthracenes as they provided a more widely represented example (in terms of incidence) of a related B-cell malignancy than BL (Burkitt's lymphoma) in which the original biochemical studies were conducted[239]. The *in vitro* investigation of the effect of the representative examples in the CLL cell lines (HG-3 and PGA-1) was undertaken which will include the following biochemical experiments:

- Preliminary cell viability testing using alamar Blue reagent at two concentrations (10 µM and 1 µM) to identify compounds with promising biological activity. The results of these initial studies are presented in the form of bar charts (Mean value ± SEM).
- IC_{50} determination of the most potent compounds *via* the alamar Blue cell viability assay
- FACS (Fluorescence activated cell sorting) analysis of cell death using Annexin V / Propidium Iodide (PI) staining technique
- Lactate dehydrogenase (LDH) assay to assess cytotoxicity of most potent analogues
- Reactive Oxygen Species (ROS) assays using *N*-acetyl cysteine (NAC) (5 mM) and Trolox (10 mM) of most potent compounds to assess degree of ROS dependent activity
- Preliminary *ex vivo* toxicology study in Peripheral Blood Mononuclear Cells (PBMCs) to assess selective toxicity relative to CLL cancer cell lines
- Use of pan-caspase inhibitor Z-VAD-FMK to assess whether mechanism of cell death caused by synthesised compounds is caspase dependent
- Assessment of a representative set of synthesised compounds in the US National Cancer Institute (NCI) 60 cell-line panel

On the basis of biochemical results, a structure activity relationship (SAR) was established. The molecular properties of the compounds were calculated and assessed with the following cheminformatics and molecular modelling software:

- Swiss Institute of Bioinformatics (SIB)
- Molecular Operating Environment (MOE)
- National Cancer Institute (NCI) Compare analysis of 5-dose and 1-dose 60 cell-line biological results to standard and experimental agents in NCI database

The most potent compounds were identified and their drug-like properties determined for further progression to preclinical evaluation.

3.1 Materials and Methods

All reagents including FBS (foetal bovine serum) and RPMI-1640 (Roswell Park Memorial Institute) cell culture growth medium were purchased from BD Biosciences, Invitrogen or Sigma-Aldrich. Consumables such as 96 well plates, 6 well plates, sterile pipettes, centrifuge vials etc. were purchased from Cruinn Diagnostics. Fluorescence of 96 well plate for alamar Blue assay was read using a Gemini Spectramax plate reader. All data points were analysed using Graphpad PRISM (version 5) software (Graphpad software Inc., San Diego, CA). FACS analysis was carried out on the CyAn ADP (Beckman Coulter) flow cytometer and processed using FlowJo software (Version 10). The HG-3 and PGA-1 cell lines in addition to the periperheral blood mononuclear cells (PBMCs) were kindly supplied by Prof. Tony Mc Elligott (School of Medicine/St. James Hospital, Trinity College Dublin).

3.1.1 Cell Lines

HG-3: The HG-3 cell line is a cell line established from an *in vitro* EBV (Epstein Barr Virus) infection from an IGHV1–2 unmutated B1 lymphocyte origin CLL patient clone (70 year old caucasian male, clinical staging- Rai stage 2) and is representative of poor prognosis[378]. These cells grow in suspension cultures, mimicking the circulatory system and are distinctly round in shape. In addition, they have a tendency to clump and become slightly adherent as they approach confluency, represented in Figure 150. The molecular

karotype of the HG-3 cell line includes $CD5^+$ / $CD19^+$ /$CD20^+$ /$CD27^+$ /$CD43^+$ surface expression and production of IgM antibodies against filamin-B and ox-LDL on apoptotic cells[379].

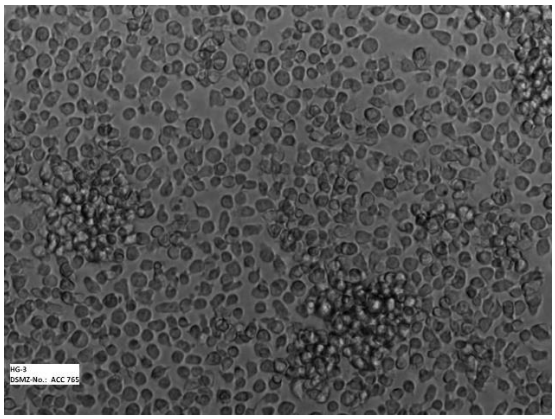

Figure 149: Image of HG-3 cells in suspension culture[378]

PGA-1: The PGA-1 cell line is a cell line established from leukemic B cells of a Caucasian man with CLL in 1988 with a mutated IGHV1-2 (representative of good prognosis)[380]. These cells grow in suspension culture mimicking being in circulatory system and are irregular in appearance, having the tendency to aggregate and become partially adherent as illustrated in Figure 151 below. The molecular karotype of the PGA-1 cell line include trisomy of chromosome 12 and 13q chromosomal deletion identified *via* fluorescence *in situ* hydridization (FISH)[381]. In addition, CD 5 surface expression is downregulated compared to other CLL cell lines such as HG-3, with Leibiniz DSMZ-German collection of microorganisms and cellcultures GmbH classifying the cell line as being CD 5^-.

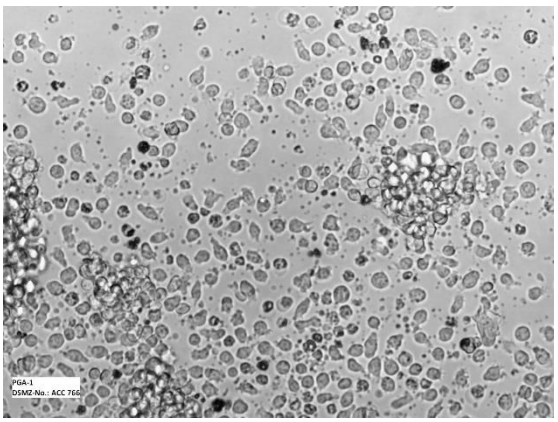

Figure 150: Image of PGA-1 cells in suspension culture[380]

3.1.2 Storage and Growth of Cultured Cells

When not in culture, stocks of cells were stored as a frozen solution in 10% DMSO/ 20% FBS/ 70% RPMI-1640 media. These stocks were initially stored overnight at -80 ˚C and were subsequently transferred into a vapour phase liquid nitrogen tank at -178 ˚C for long-term storage. When required for culture, these stocks were removed from cryogenic storage and quickly thawed in a 37 ˚C water bath. Once thawed, the stock was transferred into approximately 10 mL of pre-warmed fresh media in a centrifuge tube before centrifuging at 1200 rpm for 5 min. The supernatant layer were removed and the cells resuspended in 5 mL of the appropriate growth media (preheated to 37 ˚C) and transferred into a 25 cm^3 cell culture flask. The cells were then incubated at 37 ˚C under an atmosphere of 5 % CO_2/ 95 % air until confluent. At 70-80% confluence, the cells were transferred into a 250 cm^3 cell culture flask.

At high confluency levels cells need to be split in order to facilitate further healthy cell growth, prevent excessive cellular death, to prevent infection and limit possible cellular mutation through accelerated genetic drift. In order to lower confluency levels, an arbitrary aliquot of the cells were transferred into a new cell culture flask containing 20 mL of the required media (prewarmed to 37 ˚C), with each of these sub culture splitting events yielding a passage or generation of cells. This provides a means of monitoring cells against over-splitting and excessive continuous cell culture, helping to maintain integrity of conclusions derived from experimental results.

3.1.3 Seeding of cells

In order to prepare for the alamar Blue and FACS based assays, cells must first be counted to determine the number of cells / mL of culture media. By doing this, the necessary dilution factors can be calculated to produce stocks with appropriate cell density for the desired cell assay, dependent on cell line growth characteristics. A haemocytometer, a thick glass slide with a gridded central chamber of known area, is used for counting cells (Figure 152). After placing the coverslip over the gridded area, 10 µL of cells suspended in media is transferred using a micropipette to the loading area at the base of the grid. The 10 µL is then dispensed at the loading area, under the coverslip and covers the gridded area.

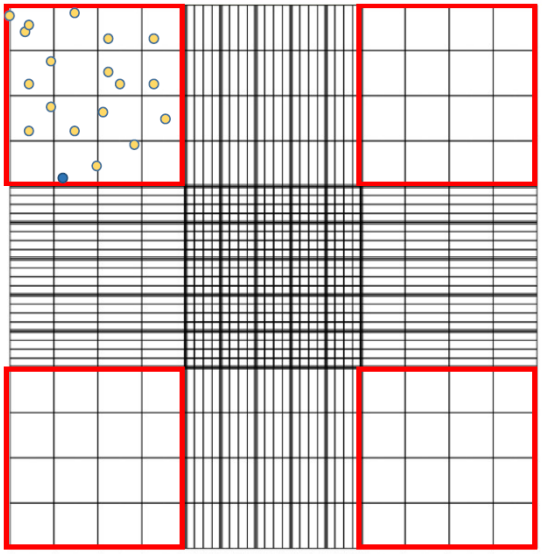

Figure 151: Diagram of haemocytometer and associated gridlines used in cell density determination

The number of cells on the grid were then counted using the four core areas of the grid. Not all cells fall directly within the confines of the grid and to account for this, cells that fell on the outer border of each grid box are counted on the left and right but not on the bottom or top (which is maintained for all following counts for consistency). This process was repeated for each of the four gridded areas of the haemocytometer. The number of cells / mL was then calculated using the following formula:

(No.of cells / 2) x 5 x 10,000 = No.of cells / mL

The antiproliferative effect of the compounds was evaluated using the alamar Blue cell viability assay. The active ingredient of the alamar Blue reagent is resazurin. Resazurin is a blue, low fluorescence compound and acts as a redox indicator and upon entering a viable cell, is reduced to resorufin – a highly fluorescent, red compound (Figure 153). Resazurin is actively reduced through the acceptance of electrons from electron carriers (NADH, NADPH, FADH) or cytochromes. This colorimetric change takes place over a 4-5 hour period for both cell lines and is subsequently measured using a fluorescence plate reader at Em λ 590 nm. These fluorescence readings are directly proportional to the quantity of viable cells remaining in each of the plate wells. From this quantitative relationship, a percentile of viable cells remaining can be calculated, taking media absorbance and vehicle effects into account.

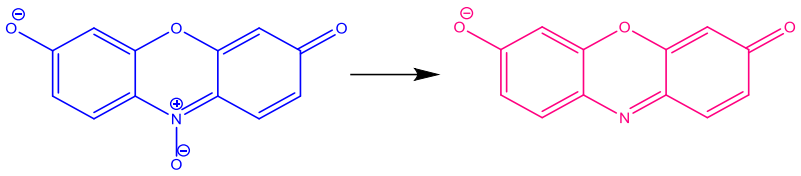

Figure 152: Alamar Blue mechanism of action-reduction of resazurin (blue) to resorufin (pink)

A 96 well plate was seeded at 200,000 cells / mL (200 µL per well) and treated with the desired drug concentration for a predetermined time frame. After treatment and incubation, each well was treated with 20 µL of alamar Blue (37˚C) and the plate was incubated in the dark at 37˚C for 4-6 hours. Fluorescence of the 96 well plate**s** was then read at Em λ 590 nm (Ex λ 544 nm). The control (untreated) wells were used to represent cells at 100% viability and by comparing these to the treated wells minus the background fluorescence of the media, the percentage of viable cells remaining was calculated. Compound **(24)** was used as an internal standard and resulted in ca. 90% cytotoxicity in each of the cell lines at a treatment concentration of 10 µM . Maprotiline was also used as an additional internal control due to its reproducible effects across both cell lines which resulted in 78% viable cells at 10 µM concentration in HG-3 cells and no effect at 1 µM. A vehicle control of 1% (v/v) DMSO was also used with no effect being seen at 10 µM and 1 µM concentrations in PGA-1 cells. Purine-nucleoside analogue fludarabine was used as a clinically relevant positive control for IC_{50} determination as it is one of the most widely used treatments in CLL across both single agent and combination therapies such as FCR (fludarabine, chlorambucil and rituximab)[123, 158].

3.2 Initial alamar Blue Screen Results

The panels of compounds evaluated in this project are arranged in the following groups (Figure 154):

- **Series 1:** (*E*)-9-(2-Nitrovinyl)-anthracenes
- **Series 2:** (*E*)-9-(2-Nitrovinyl)-9,10,11,15-tetrahydro -9,10-[3,4]epipyrroloanthracene-12,14-diones
- **Series 3:** Anthracene chalcones
- **Series 4:** Ethanoanthracene maleic anhydride chalcone adducts

- **Series 5-9:** Ethanoanthracene maleimide chalcone adducts

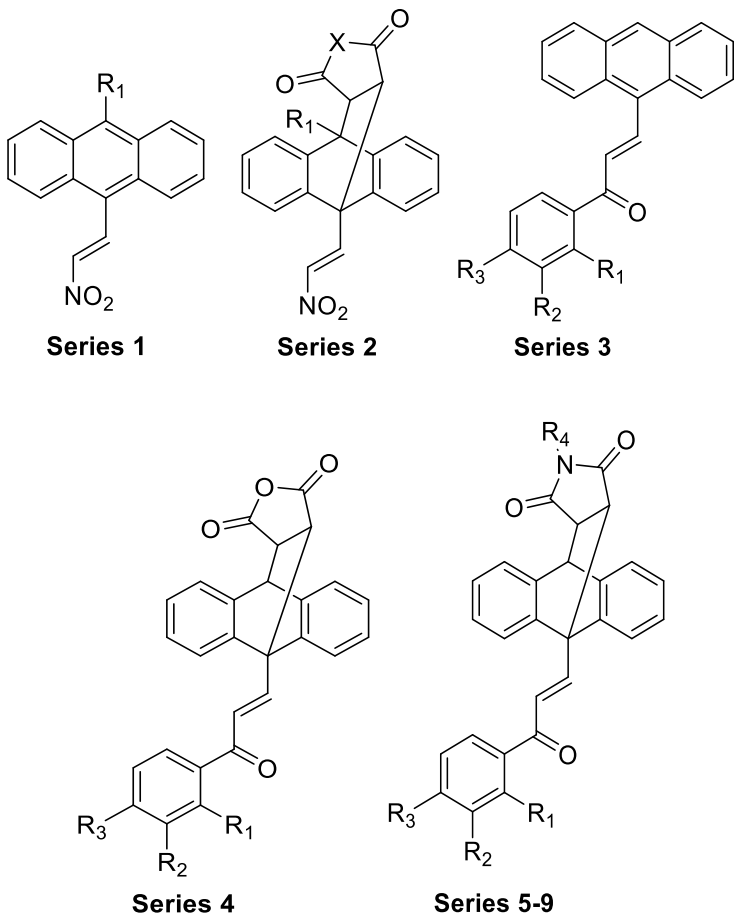

Figure 153: Example general structures of compound libraries evaluated in CLL cell lines with fludarabine and maprotiline structures

The HG-3 and PGA-1 cell lines were treated with a 10 µM and 1 µM concentration of each compound.

3.2.1 Series 1: *In vitro* antiproliferative activity of (*E*)-9-(2-nitrovinyl) anthracenes

The biochemical activity of the (*E*)-9-(2-nitrovinyl)anthracene derivatives compounds (**5, 7, 8, 21, 9**) (Figure 156) previously synthesised in the Meegan research group[382] in the HG-3 cell line are shown in Figure 155. At the 10 µM treatment concentration, all of the compounds tested were very effective, with **(21)** (compound with the isopropyl substituent at C10) being the most potent of the set (2.2% viable cells) and the others ranging from 4.2-6.1%. The sole exception was **(9)**, where the activity was approximately

fifteen-fold less (76%), where the double bond of the nitrovinyl moiety had been reduced to its corresponding alkane. At the lower 1 µM concentration, **(21)** (10-isopropyl derivative) also results in the best activity score (53%). The remaining compounds ranged between 75-92% cell viability (Figure 155).

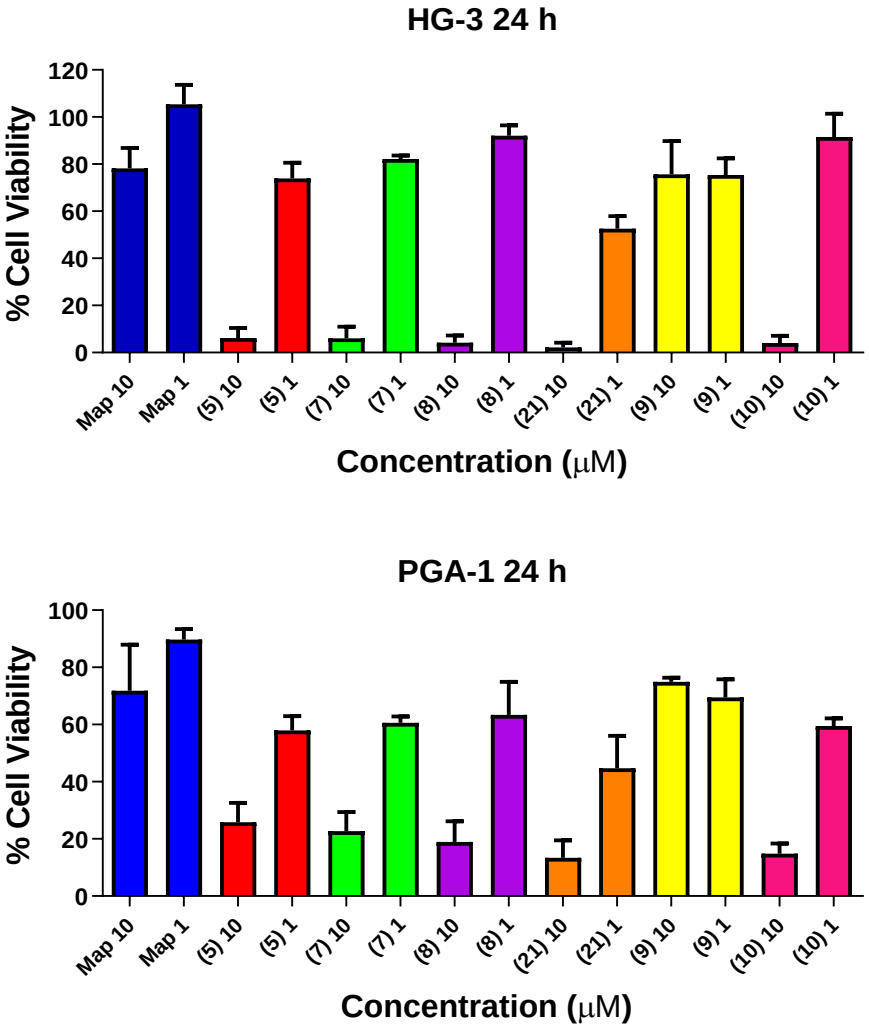

Figure 154: Biochemical activity of (*E*)-9-(2-nitrovinyl)anthracene derivatives (5, 7, 8, 9, 10, 21) in HG-3 and PGA-1 CLL cell lines (Map=maprotiline)

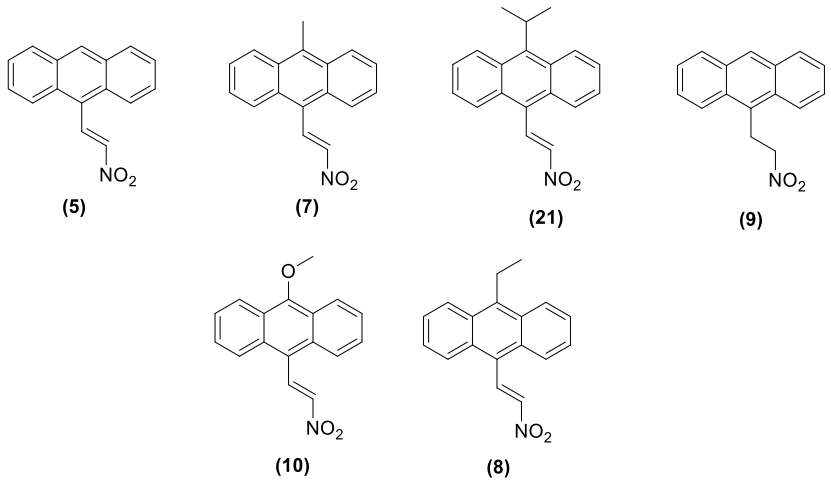

Figure 155: (*E*)- 9-(2-Nitrovinyl)anthracene derivatives (5,7, 8, 9, 10, 21)

The cell viability results of the (*E*)-9-(2-nitrovinyl)anthracene derivatives **(5, 7, 8, 21, 9, 10)** (Figure 156) in the PGA-1 cell line are shown in Figure 155. At the 10 µM treatment concentration, all of the compounds tested were very effective, with **(21)** (10-isopropyl) leading to the best observed value (13% viable cells) and the other compounds ranging from 15-26%. Furthermore, similar to the HG-3 cell results, the reduced **(9)** had the least activity of the group (75%). These results indicate the importance of the intact double bond for antiproliferative activity. At 1 µM treatment concentration, **(21)** was also the most active (45%) with the rest of the compounds falling within the range of 58-70% including **(9)** (nitroalkane at C9) which had a minor increase in activity (70% viable cells).

The antiproliferative activity of the (*E*)-9-(2-nitrovinyl)anthracene derivatives **(11, 12, 13, 14, 15, 16)** (Figure 158) in the HG-3 cell line are shown in Figure 157. At the 10 µM treatment concentration, the most effective compounds were (in order of potency): **(13)** (19% viable cells, 10-phenyl derivative), **(15)** (20%, phenanthrene derivative), **(16)** (49%, 3-nitrobutenyl derivative) and **(12)** (60%, 2-nitrobutenyl derivative). The remaining two compounds **(11)** (2-nitropropenyl derivative) and **(14)** (10-chloro-3-propenyl derivative) only had very minor activity (83 and 69% respectively). The extension of the alkyl chain on the 2-nitrovinyl unit confers a modest activity increase at 10 µM (23% reduction in cell viability) from **(11)** to **(12)**. At the lower 1 µM treatment concentration, the responses were more uniform across the compound set, with the activity of the compounds being represented in the range of 58-72% viable cells. The most effective within this range in order of potency was **(15)** (58%), **(13)** (59%), **(14)** (60%), **(16)** (62%), **(11)** (67%) and

the least potent was **(12)** (72%) (Figure 157). From these results, the 10-chloro substitution on **(14)** confers a small advantage in biological activity compared to the unsubstituted analogue **(11)**. The most potent molecule, **(13)** had the sole modification of a 10-phenyl substitution to the anthracene core and the second most effective was **(15)**, where the anthracene core was replaced by a phenanthrene structure.

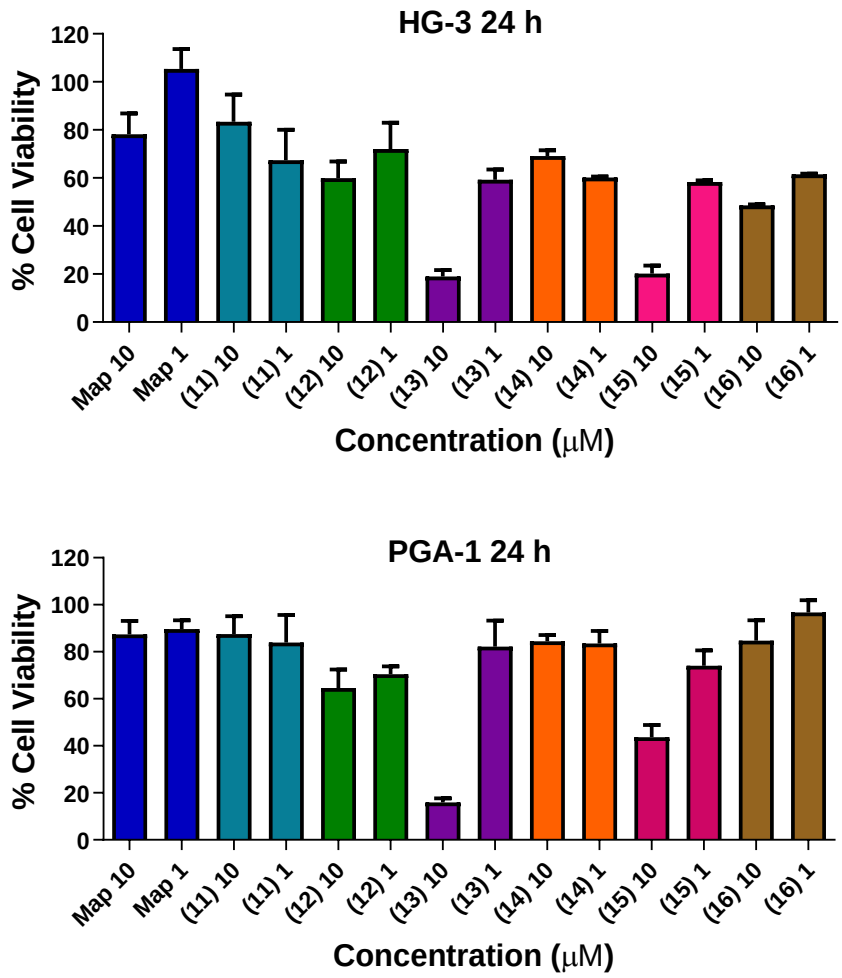

Figure 156: **Biochemical activity of (*E*)-9-(2-nitrovinyl)anthracene derivatives (11-16) in HG-3 and PGA-1 CLL cell lines (Map=maprotiline)**

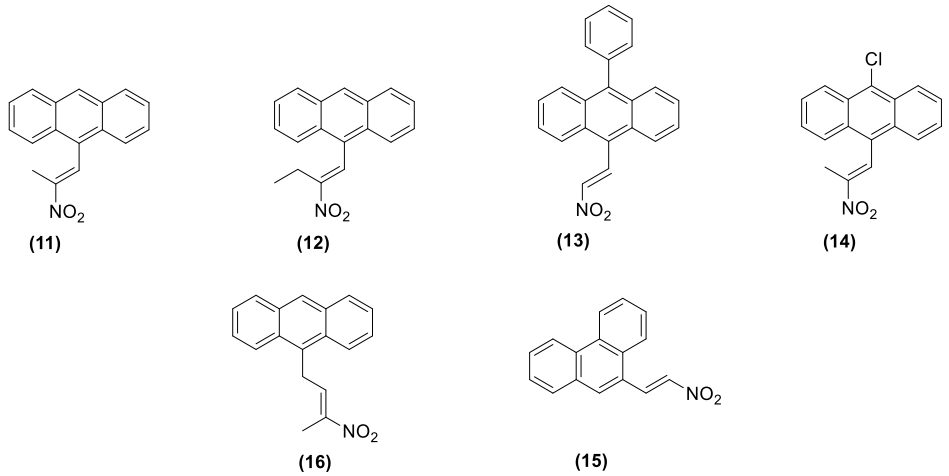

Figure 157: (*E*)- 9-(2-nitrovinyl)anthracene derivatives (11-16)

The cell viability of the (*E*)-9-(2-nitrovinyl)anthracene derivatives **(11-16)** (Figure 158) in the PGA-1 cell line are shown in Figure 157. At the 10 µM treatment concentration, the most potent compounds were found to be **(13)** (16% viable cells), **(15)** (44%,) and **(12)** (65%). The remaining compounds (**11**, **14**, **16**) were consistent in activity, ranging from 85-88% viable cells. At the lower 1 µM concentration, **(12)** and **(15)** were observed to have the best activity, leading to percentage viability values of 71% and 74% respectively. The other compounds of the set (**11**, **13**, **14**, **16**) had little to no appreciable activity (82-97%). Overall, the most active compound across both cell lines was **(13)** (compound with the phenyl substituent at C-10), yielding greater activity in PGA-1 (16% viable cells) as opposed to HG-3 (19%) at 10 µM. Furthermore, at 10 µM, the other compounds were marginally more effective in HG-3 cells than PGA-1, the largest difference being produced by **(16)** (3-nitrobutenyl derivative), where the 2-nitrovinyl chain was extended by a single bond, where a 14-21% variance was noted, depending on the compound concentration used.

The biochemical activity of (*E*)-9-(2-nitrovinyl)anthracene derivatives **(6** and **17-20)** (Figure 160) in the HG-3 cell line is shown in Figure 159. At the 10 µM treatment concentration, all of the compounds tested were considered to be inactive apart from **(20)** (83% viable cells, 10-bromo derivative) (Figure 159). At 1 µM, a similar result was achieved with only the dicyano **(18)** having very weak activity (89%). The addition of 10-chloro to **(19)** to yield compound **(18)** brought about a minor increase in antiproliferative activity at 1 µM only.

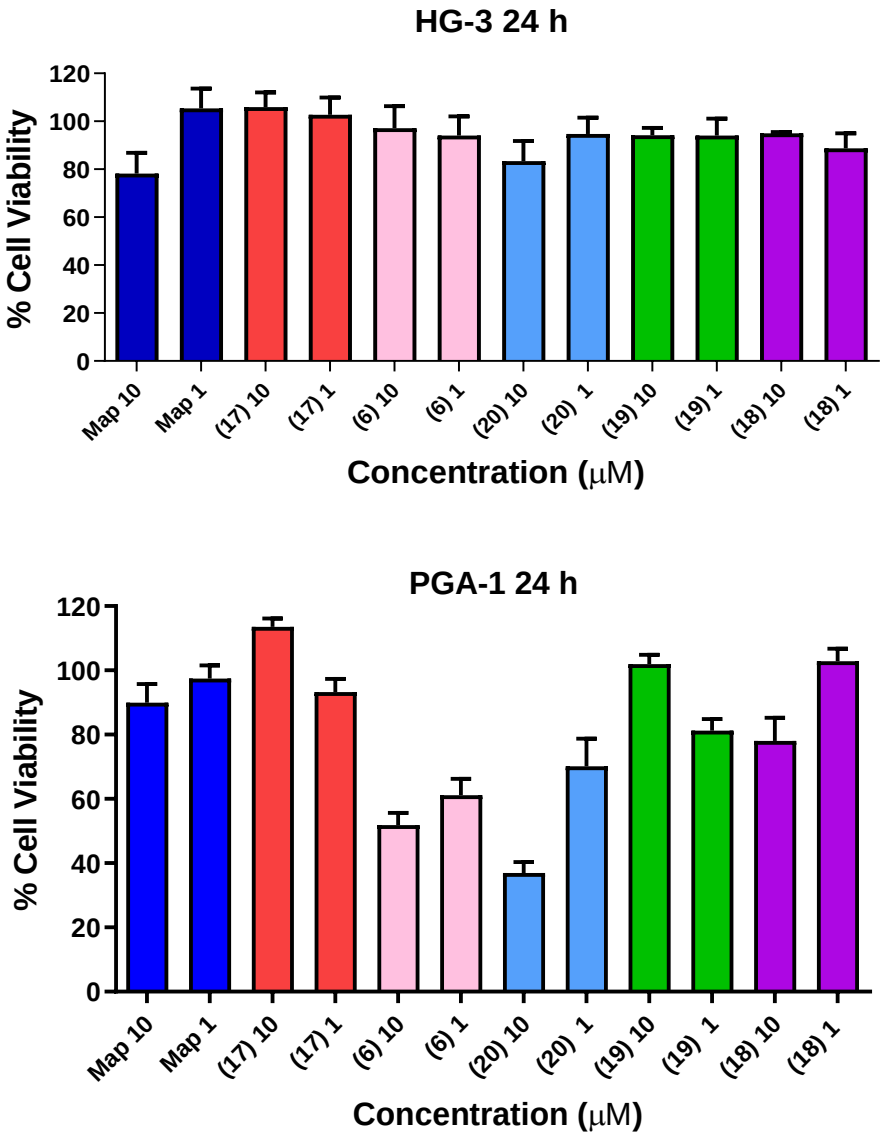

Figure 158*:* Biochemical activity of (*E*)-9-(2-nitrovinyl)anthracene derivatives (6 and 17-20) in HG-3 and PGA-1 CLL cell lines (Map=maprotiline)

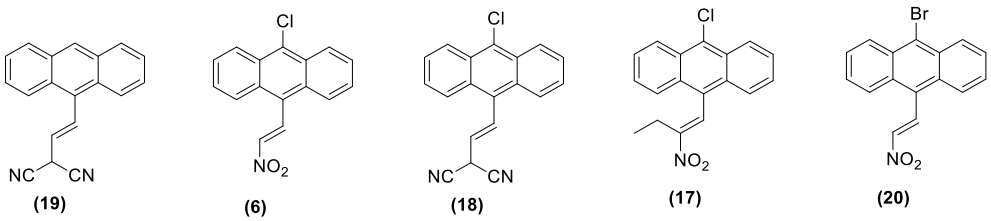

Figure 159: (*E*)- 9-(2-nitrovinyl)anthracene and (*E*)-2-(2-(anthracen-9-yl)vinyl)malononitrile derivatives (6 and 17-20)

The biochemical activity of (*E*)-9-(2-nitrovinyl)anthracene derivatives **(6** and **17-20)** (Figure 160) in the PGA-1 cell line are shown in Figure 159. At the 10 µM treatment concentration, the most effective compounds were **(20)** (38% viable cells), **(6)** (55%) and **(18)** (81%), while **(17)** and **(19)** were considered inactive. At 1 µM, a comparable trend emerged with **(6)** exhibiting the greatest biological activity (63% viable cells), followed by **(20)** (73%) and **(19)** (82%) while the other compounds displayed no effect (Figure 159). Overall, the molecules listed appeared to be more effective in PGA-1 over the HG-3 cell line. This was clear in the cases of **(6)** and **(20)**. For **(6)**, a 31-42% difference in response existed across cell lines and concentrations tested. Moreover, a large change existed for **(20)** with a 45% difference over the cell lines at the 10 µM concentration. Overall, the most potent compounds from series 1 **(5, 8, 10** and **20)** were chosen for IC_{50} determination and evaluation (section 3.2.7).

3.2.2 Series 2 : *In vitro* antiproliferative activity of (*E*)-9-(2-nitrovinyl)-9,10,11,15-tetrahydro-9,10-[3,4]epipyrroloanthracene-12,14-diones

The antiproliferative activity of the (*E*)-9-(2-nitrovinyl)-9,10-dihydro-9,10-[3,4]epipyrolloanthracene-12,14-dione and (*E*)-10-(2-nitrovinyl)-9,10-dihydro-9,10-ethanoanthracene-11-carbonitrile derivatives **(24-28)** (Figure 162) in the HG-3 and PGA-1 cell lines are shown in Figure 161. These were among the most potent compounds initially tested in previous work within the group by A. Byrne (2015)[382] in the related B-cell malignancy Burkitt's lymphoma cell lines MUTU-1 (chemosensitive) and DG-75 (chemoresistant). In HG-3 cells, at the 10 µM treatment concentration, the most potent compounds were observed to be **(28)** (12% cell viability, *p*-benzophenone derivative), followed closely by **(25)** (13%, *p*-chlorophenyl) (Figure 161). Compound **(26)** displayed a low cell viability (17%, cyano derivative), with **(24)** (*N*-phenyl) and **(27)** (maleimide) showing activities of 31% and 45% respectively. However, at the lower 1 µM concentration, **(24)** exerted the greatest effect (38% viable cells), which was only marginally more than was discovered at a ten-fold compound concentration increase (31% at 10 µM treatment). The observed activity of the remaining compounds were as follows in the order of most to least potent: **(28)** (44% cell viability), **(25)** (54%), **(27)** (64%) and **(26)** (82%).

The cell viability results of compounds **(24-28)** (Figure 162) in the PGA-1 cell line are shown in Figure 161. At the 10 µM treatment concentration, the most effective compounds were (**25)** (3% viable cells), **(28)** (6%) and **(26)** (4%) The remaining compounds **(24)** and **(27)** displayed activites of 13% and 19% respectively. At the lower 1 µM concentration, **(26)** was the most potent (19% viable cells), while the remaining compounds (**24**, **27**, **25**, **28**) exerted good activity in the range of 27-35 % cell viability, the least effective being **(24)** (35%). Overall, (*E*)-9-(2-nitrovinyl)-9,10-dihydro-9,10-[3,4]epipyroloanthracene-12,14-dione derivatives exhibited better overall activity in PGA-1 than in HG-3 cells across both concentrations, with the *p*-chloro and benzophenone based maleimides **(25)** and **(28)** as well as the acrylonitrile adduct **(26)**, acting as the most promising antiproliferative agents.

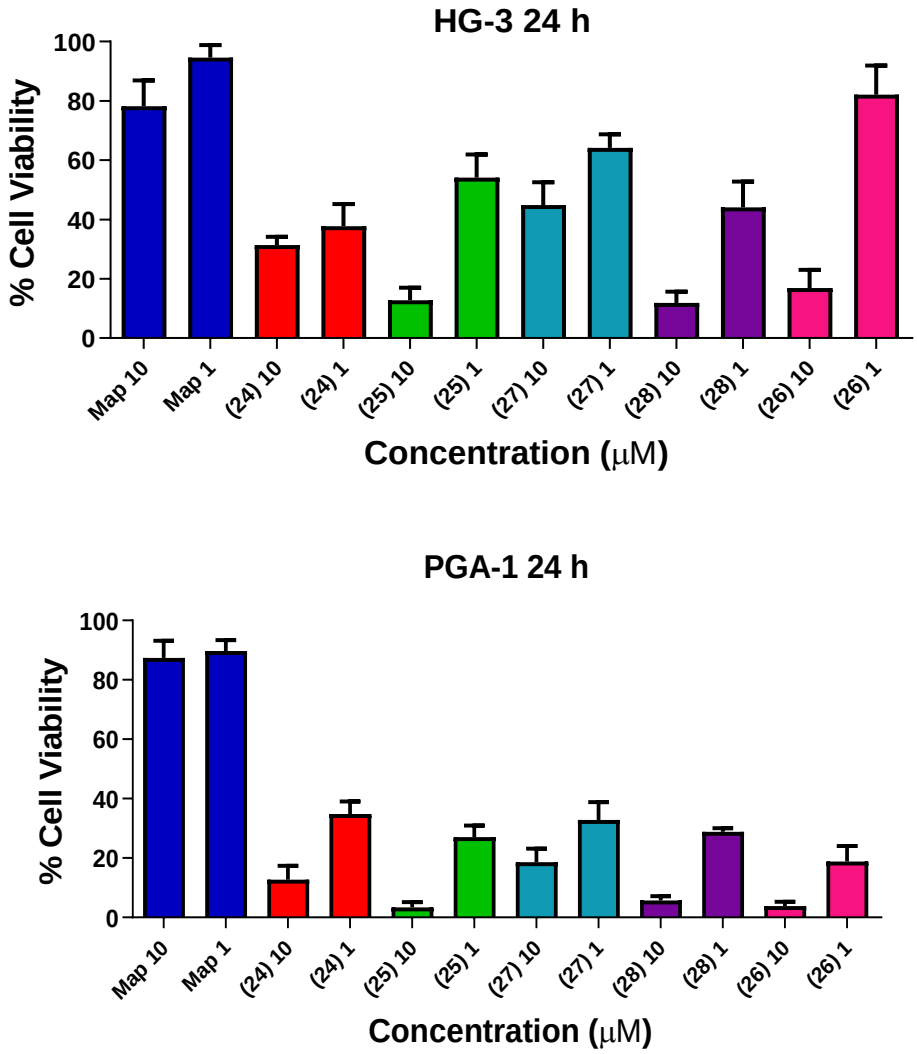

Figure 160*:* Biochemical activity of (*E*)-9-(2-nitrovinyl)-9,10,11,15-tetrahydro-9,10-[3,4]epipyrroloanthracene-12,14-dione derivatives (24-28) in HG-3 and PGA-1 CLL cell lines (Map=maprotiline)

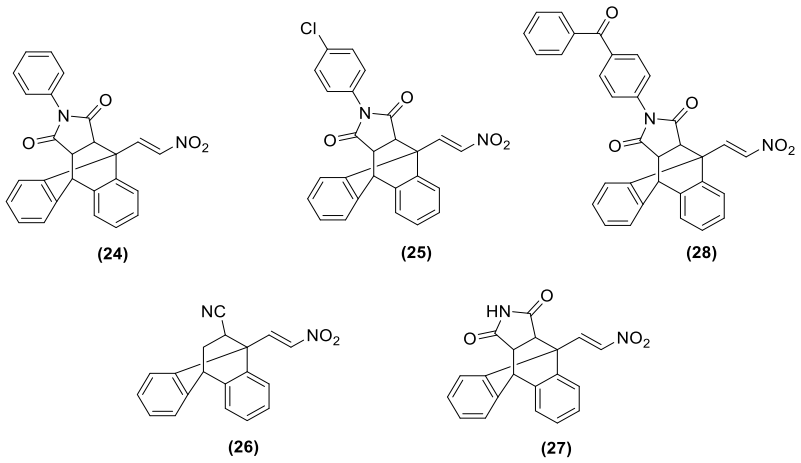

Figure 161: (*E*)-9-(2-Nitrovinyl)-9,10,11,15-tetrahydro-9,10-[3,4]epipyrroloanthracene-12,14-diones (24-38)

3.2.3 Series 3: *In vitro* antiproliferative activity of (*E*)-3-(anthracen-9-yl)-1-phenylprop-2-en-1-ones

The biochemical activity of (*E*)-3-(anthracen-9-yl)-1-phenylprop-2-en-1-ones compounds **(34-50)** (Figure 164) in the HG-3 cell line are shown in Figure 163, with maprotiline and compound **(5)** acting as internal standards across both cell lines.

From the initial HG-3 cell line screen, five main active compounds were observed at the 10 µM treatment concentration; these were compounds **(38), (47), (44), (37)** and **(46)**. The 3,4-dimethoxy aryl ring of **(38)** confers the best activity of the set (37% cell viability), followed closely by the 2-pyridyl derivative **(47)** (43%). The 3,4,5-trimethoxy aryl ring of **(44)** is observed to cause a marginally lower decrease in cell viability (49%), with the 2,4-dichloro aryl **(37)** and 4-pyridyl **(46)** analogues ranking the lowest of the five compounds with cell viability scores of 53% and 54% respectively. However, at 1 µM, **(37)** has the most activity (50% cell viability), followed closely by **(47)** (53%). **(38)**, **(44)** and **(46)** and have similar biological activity, yielding cell viability results of 60%, 61% and 61% respectively. Furthermore, an interesting effect on activity with different halogen atoms at the *para* position of the acetophenone - derived aromatic ring was noted. At the higher treatment concentration of 10 µM, the fluoro chalcone **(41)** was the most potent (61% cell viability), then followed by the chloro chalcone **(45)** (76%), the unsubstituted chalcone **(39)** (81%) the iodo chalcone **(40)** (96%) and the bromo chalcone **(34)** (104%). This suggests that factors such as electronegativity and atomic radius of the *para* substituent have the ability to affect activity in the HG-3 CLL cell lines. However,

the activity trend observed at the lower 1 µM concentration presents differently with **(39)** being the most effective (84%), followed by **(45)** (86%), **(41)** (87%), **(40)** (101%), **(34)** (104%) being the least effective. Taking this into account, it is possible that similar factors are at play (as the bromo substitution is consistently the least potent across both concentrations) but there is a potential concentration dependent effect (Figures 163 and 165).

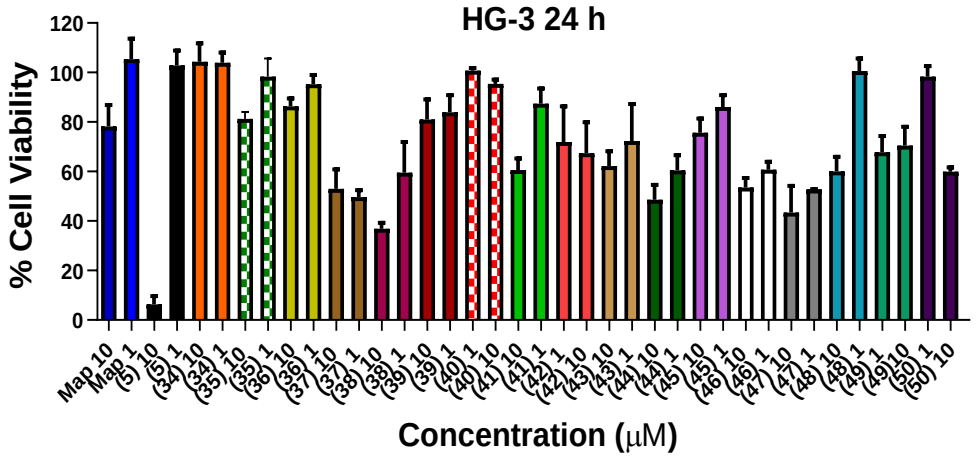

Figure 162: Biochemical activity of (*E*)-3-(anthracen-9-yl)-1-phenylprop-2-en-1-one derivatives (34-50) in HG-3 cell line (Map=maprotiline)

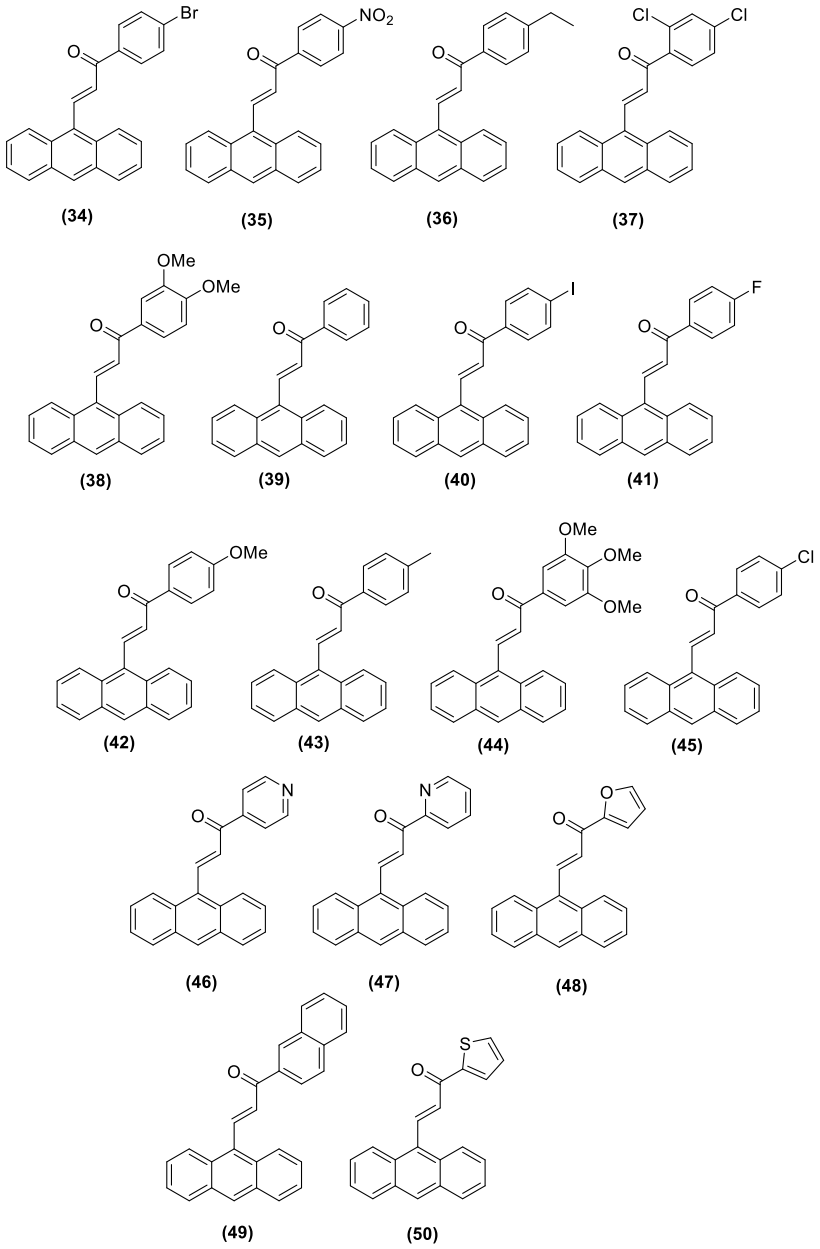

Figure 163: (*E*)-3-(anthracen-9-yl)-1-phenylprop-2-en-1-ones (34-50)

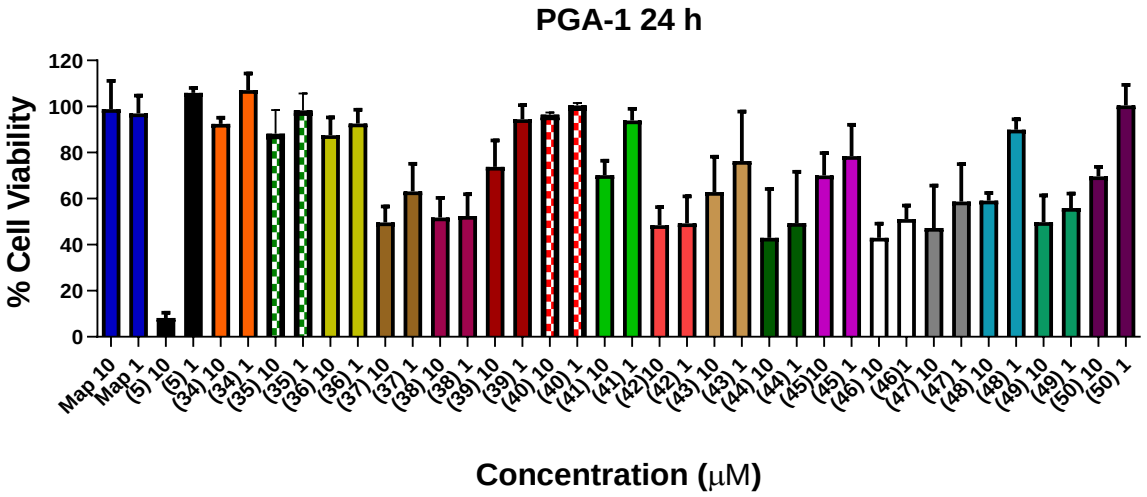

Figure 164: Biochemical activity of (*E*)-3-(anthracen-9-yl)-1-phenylprop-2-en-1-one derivatives (34-50) in PGA-1 CLL cell line (Map=maprotiline)

The biochemical activity of (*E*)-3-(anthracen-9-yl)-1-phenylprop-2-en-1-one compounds (Figure 164) in the PGA-1 cell line are shown in Figure 165. The most potent compounds at the 10 µM treatment concentration (in order of most to least active) were: **(46)** (43% cell viability,4-pyridyl derivative), **(44)** (43%, 3,4,5-trimethoxy), **(47)** (47%, 2-pyridyl), **(42)** (49%, 4-methoxy), **(37)** (50%, 2,4-dichloro), **(38)** (52% 3,4-dimethoxy) and **(49)** (50%, 2-naphthyl). At the lower 1 µM treatment concentration, the compounds that displayed the best activity were (in order of most to least active): **(42)** (49% cell viability, 4-methoxy derivative), **(44)** (50%, 3,4,5-trimethoxy), **(46)** (51%, 4-pyridyl), **(38)** (53%, 3,4-dimethoxy) and **(49)** (56%, 2-naphthyl).

A similar notable variability in biological response dependent on halogen substitution was observed at 10 µM with the 4-fluoro chalcone **(41)** and **(45)** (4-chloro) being more potent (70% cell viability), followed by the unsubstituted chalcone **(39)** (74%), the bromo chalcone **(34)** (92%) and the iodo chalcone **(40)** (96%) in PGA-1 cells (Figure 165). For the 4-halogen compounds, the lower concentration of 1 µM, the activity order changed, with **(45)** being the most effective (79%), followed by **(41)** (94%), **(39)** (95%) and **(40)** (101%) and **(34)** (107%). Again, similar factors to those previously discussed for the HG-3 cell line results seem to be present.

Overall from the compound series, **(38)** (3,4-dimethoxy aryl derivative), **(47)** (2-pyridyl) and **(44)** (3,4,5-trimethoxy) were more potent across 10 µM concentration in the HG-3 cell line. This varied at the 1 µM with compounds **(37)** (2,4-dichloro derivative), **(47)** (2-pyridyl) and **(38)** being the most effective in HG-3 cell lines. In the PGA-1 cell line at

the 10 µM concentration, **(46)** (4-pyridyl), **(44)** and **(47)** were found to display the best activity. At the 1 µM treatment concentration, the most promising activity was shown by **(42)** (4-methoxy derivative), **(44)**, **(46)** and **(38)**. The activity of **(36)** (4-ethyl), **(34)** (4-bromo derivative) and **(5)** remained constant over both concentrations and cell lines while maprotiline had greater biological activity at the 10 µM treatment concentration in HG-3 cells (78% viable cells) than in PGA-1 cells (99%). Despite being the most potent compounds of series 3, compounds **(37**, **38**, **47, 42, 44)** (Figure 166) were not selected for progression to IC_{50} determination. This decision was supported by preliminary in-house IC_{50} studies completed on **(41)** with a value > 100 µM noted.

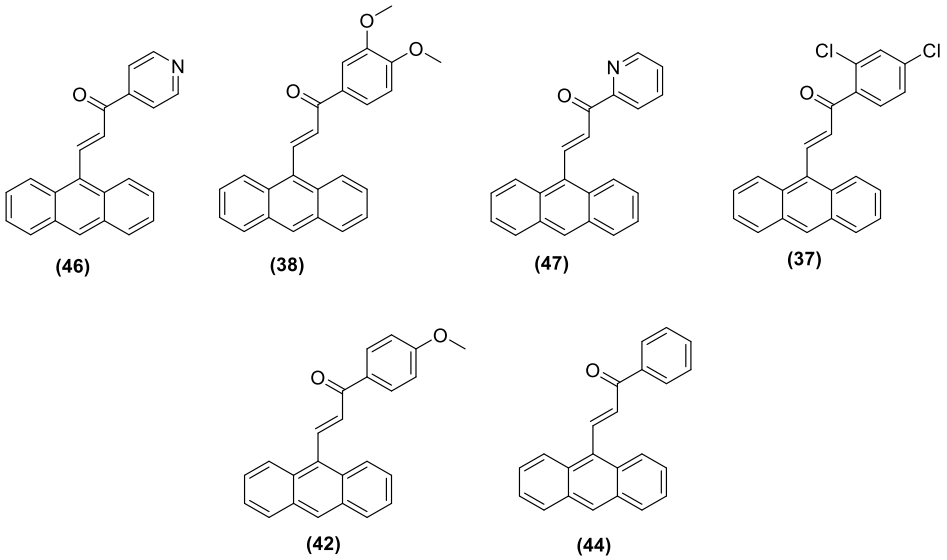

Figure 165: Most potent (*E*)-3-(anthracen-9-yl)-1-phenylprop-2-en-1-ones identified from biochemical screening

3.2.4 Series 4: *In vitro* antiproliferative activity of of 9-(*E*)-3-oxo-3-phenylprop-1-en-1-yl)-9,10-dihydro-9,10-[3,4]furanoanthracene-12,14-diones

The cell viability of fifteen 9-(*E*)-3-oxo-3-phenylprop-1-en-1-yl)-9,10-dihydro-9,10-[3,4]furanoanthracene-12,14-dione compounds **(71-85)** (Figure 168) in the HG-3 cell line are shown in Figure 167. The majority of this compound set was inactive across both 10 µM and 1 µM treatment concentrations with the exception of **(84)** [which displayed fair activity at 10 µM (77% viable cells, 2-naphthyl derivative) and 1 µM (86%)] and **(74)** (88% at 1 µM concentration, 3,4-dimethoxy derivative) (Figure 167).

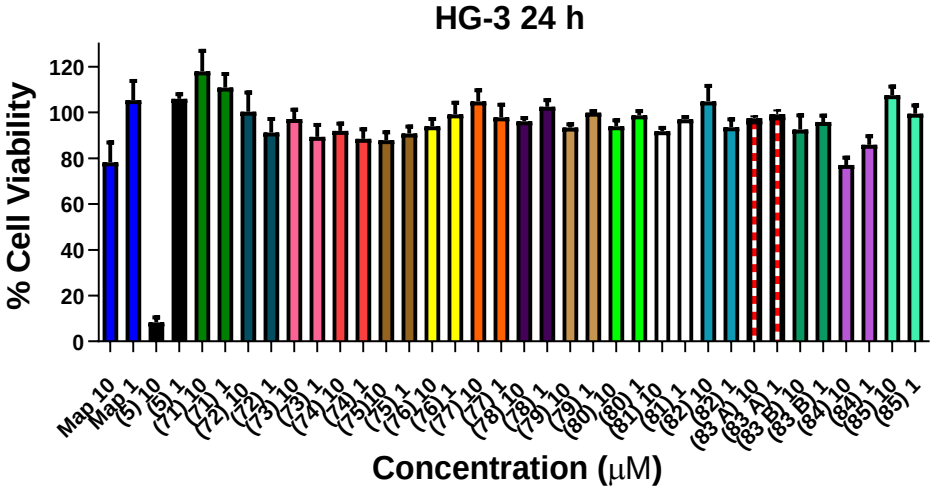

Figure 166: Biochemical activity of 9-(*E*)-3-oxo-3-phenylprop-1-en-1-yl)-9,10-dihydro-9,10-[3,4]furanoanthracene-12,14-diones (71-85) in the HG-3 CLL cell line

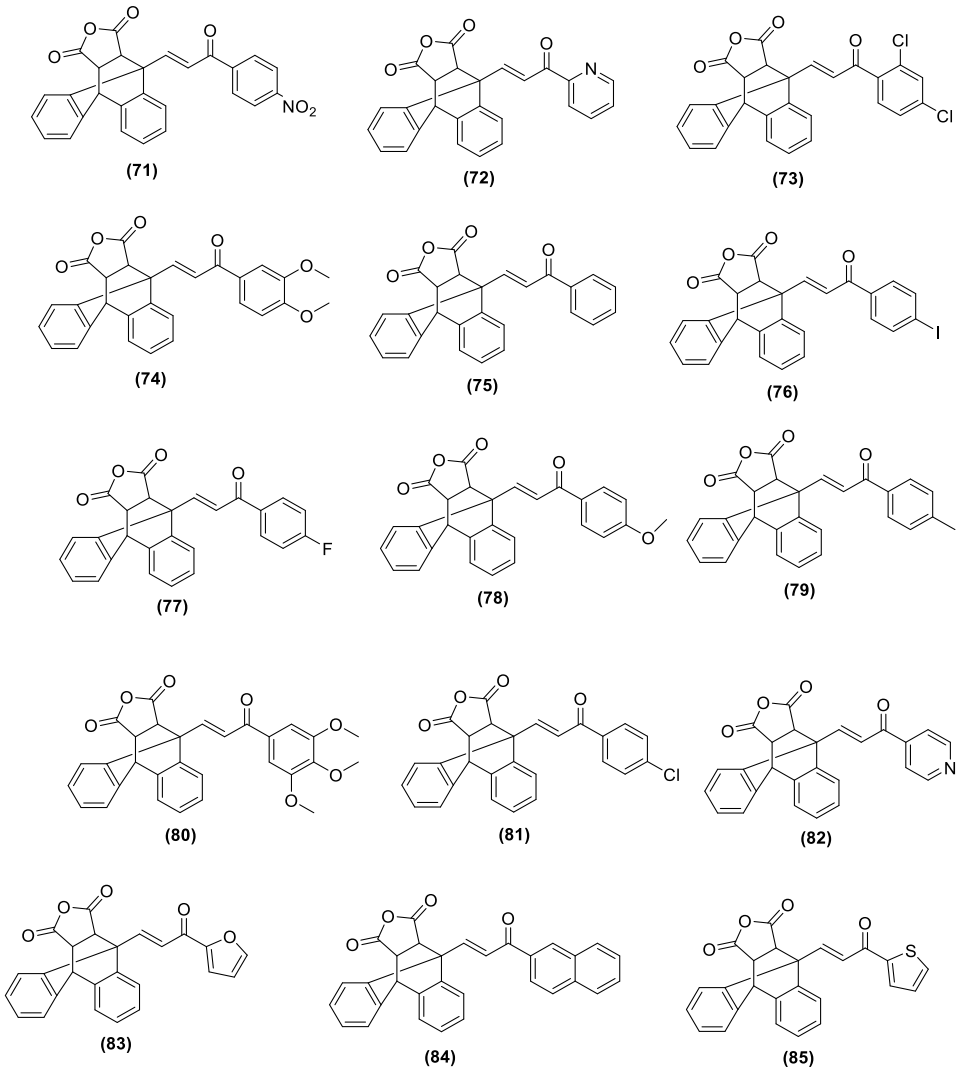

Figure 167: 9-(*E*)-3-oxo-3-phenylprop-1-en-1-yl)-9,10-dihydro-9,10-[3,4]furanoanthracene-12,14-diones (71-85)

The biochemical activity of the 9-(*E*)-3-oxo-3-phenylprop-1-en-1-yl)-9,10-dihydro-9,10-[3,4]furanoanthracene-12,14-diones **(71-85) (**Figure 168) series 4 in the PGA-1 cell line are shown in Figure 169. The most potent compounds of the series were **(84)** (79% cell viability at 10µM concentration, 2-naphthyl), **(71)** (observed to have fair activity of 79% and 83% at treatment concentrations of 10 µM and 1 µM respectively, 4-nitro derivative), and **(74)** (90% cell viability at 1 µM, 3,4-dimethoxy derivative). The remaining analogues were relatively inactive across both 10 µM and 1 µM treatment concentrations.

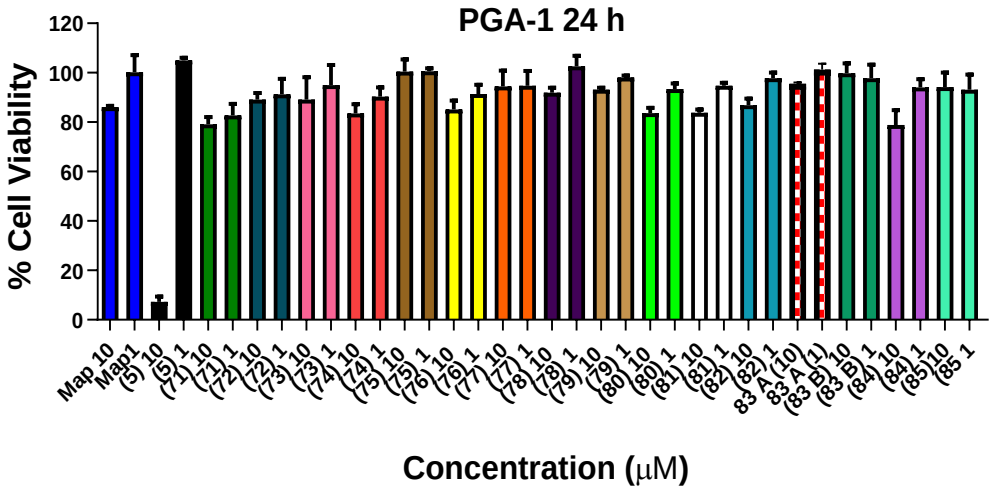

Figure 168: Biochemical activity of 9-(*E*)-3-oxo-3-phenylprop-1-en-1-yl)-9,10-dihydro-9,10-[3,4]furanoanthracene-12,14-diones (71-85) in the PGA-1 CLL cell line

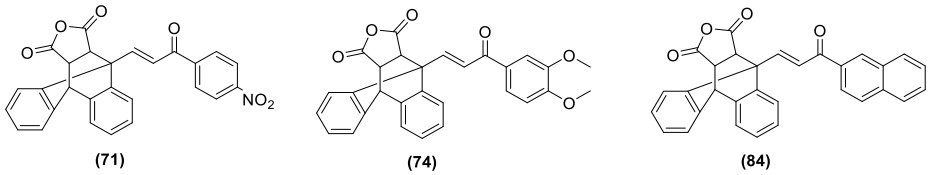

Figure 169: Most potent 9-(*E*)-3-oxo-3-phenylprop-1-en-1-yl)-9,10-dihydro-9,10-[3,4]furanoanthracene-12,14-dione compounds identified from biochemical screening

Figure 170 above illustrates the most potent compounds identified from the series 4 structural class **(71, 74, 84)** from initial biochemical testing in both cell lines. The weak activity displayed by these compounds did not merit further investigation. These structures suggest a wide tolerability for diverse functional group substitutions on the α,β-unsaturated ketone tail ranging from ring activating groups (4-nitro aryl, **71**), ring deactivating groups (3,4-dimethoxy aryl, **74**) and polyaromatic systems (2-naphthyl, **84**).

While varation at this position causes little impact on biological activity, choice of the resident structure at the ethanoanthracene bridge proves crucial (as will now be discussed in Series 5-9).

3.2.5 Series 5: *In vitro* antiproliferative activity of 9-(*E*)-3-oxo-3-phenylprop-1-en-1-yl)-9,10-dihydro-9,10-[3,4] epipyrroloanthracene -12,14-diones

The biochemical activity of 9-(*E*)-3-oxo-3-phenylprop-1-en-1-yl)-9,10-dihydro-9,10-[3,4] epipyrroloanthracene-12,14-diones **(86-102)** (Figure 172) in the HG-3 cell line are shown in Figure 171. All tested compounds in the set showed promising activity with the least effective at 10 µM treatment concentration being **(87)** (50% viable cells). The most potent of the panel screened at the higher 10 µM concentration were, in order of most to least effective; **(101)** (2-naphthyl derivative, 0% viable cells), **(92)** (4-iodo derivative, 0% viable cells), **(86)** (4-bromo derivative, 0.5%), **(97)** (4-chloro derivative, 0.7%), **(91)** (unsubstituted aryl, 2%) and **(99)** (2-pyridyl dervative, 2%). The remaining compounds were also very effective, with activity ranges from approximately 5-25% viable cells remaining. At the lower treatment concentration of 1 µM, the order of the most potent compounds changes with **(101)** (2-naphthyl derivative, 46% viable cells) being the most effective then **(90)** (3,4-dimethoxy, 60%), **(96)** (3,4,5-trimethoxy derivative, 62% cell viability), followed by **(97)** (66%), **(91)** (68%) and **(99)** (72%).

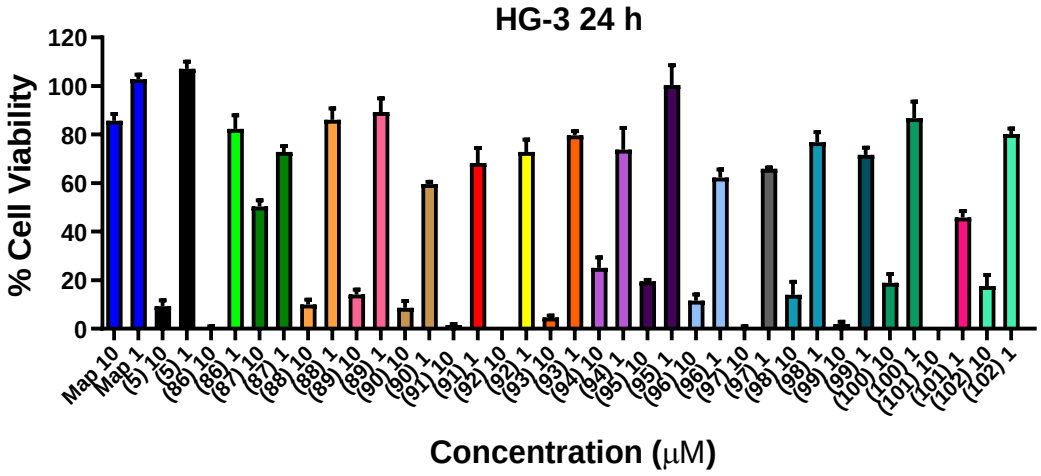

Figure 170: Biochemical activity of 9-(*E*)-3-oxo-3-phenylprop-1-en-1-yl)-9,10-dihydro-9,10-[3,4] epipyrroloanthracene -12,14-diones derivatives (86-102) in the HG-3 CLL cell line

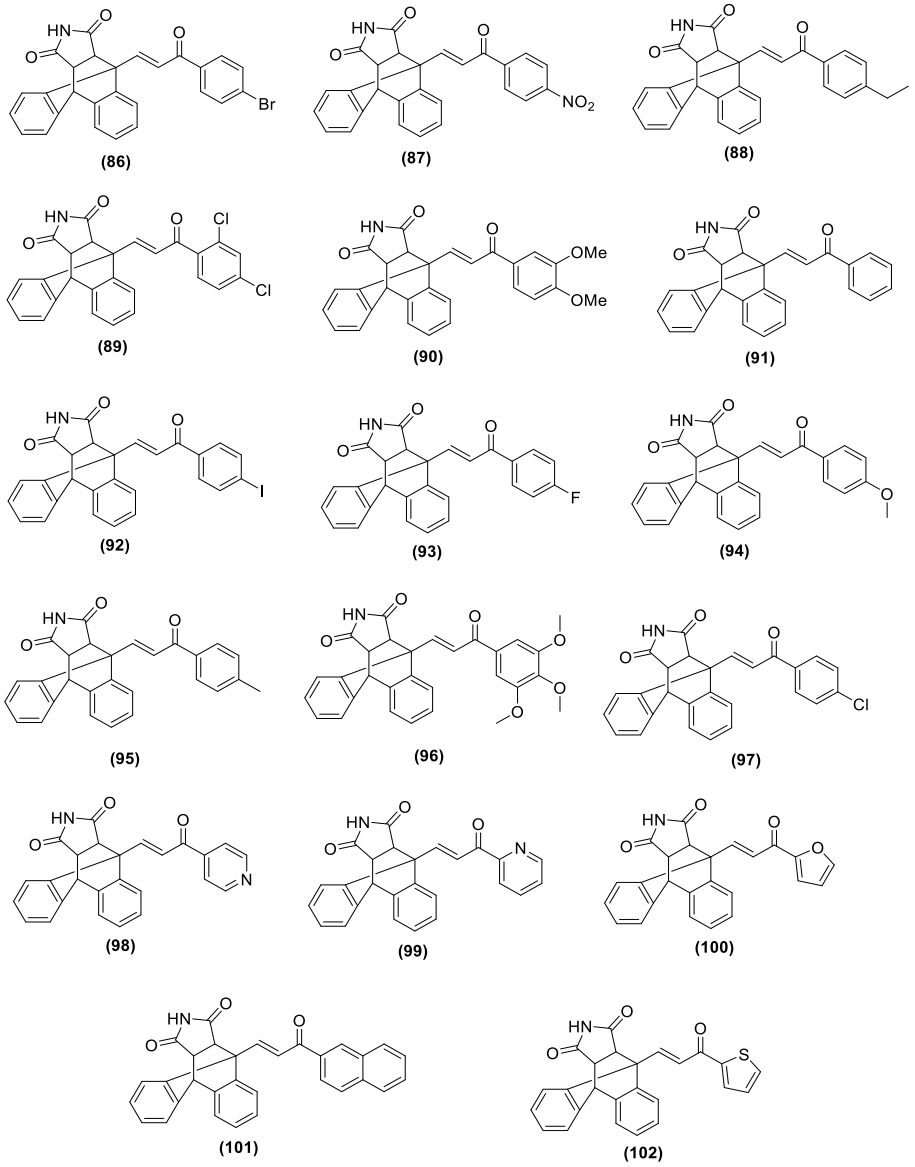

Figure 171: 9-(*E*)-3-Oxo-3-phenylprop-1-en-1-yl)-9,10-dihydro-9,10-[3,4] epipyrroloanthracene -12,14-diones (86-102)

Considering the previous results of (*E*)-3-(anthracen-9-yl)-1-phenylprop-2-en-1-ones (Series 3) with respect to the trend of increased biological activity relative to the halogen substitution pattern (generally greater activity with smaller halogen atoms), it was noteworthy that a contrary effect on activity was seen in 9-(*E*)-3-oxo-3-phenylprop-1-en-1-yl)-9,10-dihydro-9,10-[3,4] epipyrroloanthracene-12,14-diones derivatives (Series 4) at 10 µM concentration. With increasing size of the halogen and increasing electronegativity on the *para* position of the acetophenone-derived aromatic ring, compound potency increases in a sequential manner (I>Br>Cl>F) at the 10 µM concentration.

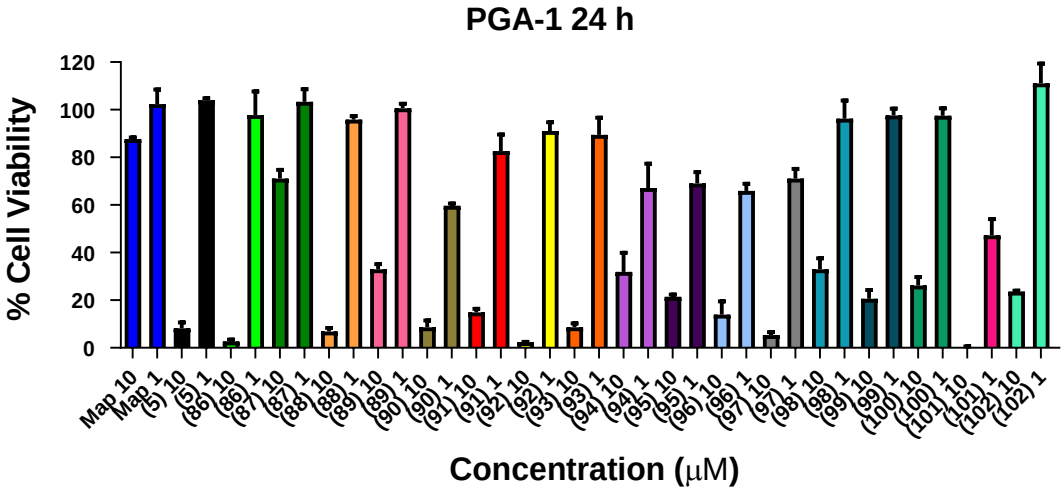

Figure 172: Biochemical activity of 9-(*E*)-3-oxo-3-phenylprop-1-en-1-yl)-9,10-dihydro-9,10-[3,4] epipyrroloanthracene -12,14-diones (86-102) in the PGA-1 CLL cell line

The biochemical activity of 9-(*E*)-3-oxo-3-phenylprop-1-en-1-yl)-9,10-dihydro-9,10-[3,4] epipyrroloanthracene-12,14-diones **(86-102)** (Figure 172) in the PGA-1 cell line are shown in Figure 173.

The most potent of the panel screened at the 10 μM treatment were, in order of most to least effective; **(101)** (0% viable cells), **(92)** (2%), **(86)** (3%), **(97)** (5%), **(88)** (4-ethyl derivative, 7%) and **(93)** (4-fluoro derivative, 9%). The remaining compounds were also moderately effective, with activity ranges from approximately 14-71% viable cells remaining. A similar trend of activity with *para*-halogen substitution of the acetophenone aromatic ring was observed in the PGA-1 cell line with activity being correlated to halogen increasing atom size and decreasing electronegativity (I>Br>Cl>F). At the lower treatment concentration of 1 μM, the order of the most potent compounds changes with **(101)** (47% cell viability, 2-naphthyl derivative) having the greatest antiproliferative effect, with the next most active being **(90)** (58%, 3,4-dimethoxy derivative), followed by **(96)** (66%, 3,4,5-trimethoxy derivative), **(94)** (4-methoxy derivative, 67%) and **(95)** (4-methyl derivative, 69%).

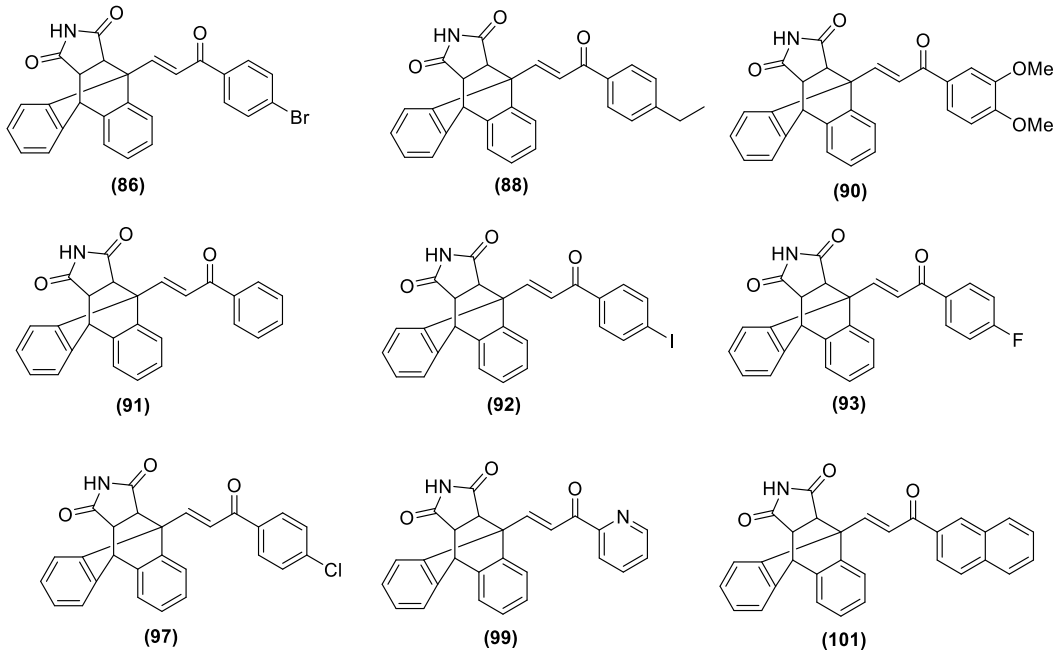

Figure 173: Most potent 9-(*E*)-3-oxo-3-phenylprop-1-en-1-yl)-9,10-dihydro-9,10-[3,4] epipyrroloanthracene-12,14-diones compounds identified from biochemical screening

Compared to maleic anhydride (Series 4), the maleimide head group elicits greater biological activity across all compounds at both concentrations, in both cell lines tested. In this series and across both cell lines, more favourable activity was observed for compounds (**86, 88, 90, 91, 92, 93**, **97, 99, 101**) (Figure 174). These diverse sets of functional groups (alkyl, aryl halogens), heterocycles and aromatics eliciting a similar degree of antiproliferative activity suggests a moderate tolerence of variation on the acetophenone-derived tail of the synthesised molecules in relation to their anticancer effect.

The compounds in this series exhibit a general trend of greater effectiveness in the aggressive HG-3 CLL cell type than in PGA-1 cells (Table 32). Two interesting instances were **(99)** (2-pyridyl derivative) and **(91)** (unsubstituted benzoyl derivative). These compounds were notably less effective at the 10 μM in PGA-1 cells (19% higher for **(99)** and 13% higher for **(91)** compared to HG-3 cell results). This could possibly be due to the reduced steric bulk of the acetophenone-derived tail, which may be more of a requirement for activity in the mutated IGHV PGA-1 cell line.

Compound no.	PGA-1 10µM (% viability)	PGA-1 1 µM (% viability)	HG-3 10 µM (% viability)	HG-3 1 µM (% viability)
(86)	3	98	1	82
(88)	7	96	10	86
(101)	0	47	0	-
(99)	21	98	2	72
(90)	9	60	9	60
(93)	9	90	5	80
(92)	2	91	0	73
(97)	5	71	1	66
(91)	15	83	2	68

Table 32: Percentage cell viability results of most potent 9-(*E*)-3-oxo-3-phenylprop-1-en-1-yl)-9,10-dihydro-9,10-[3,4] epipyrroloanthracene-12,14-dione compounds identified from biochemical screening

3.2.6 Series 6: *In vitro* antiproliferative activity of (*E*)-9-(3-oxo-3-phenylprop-1-en-1-yl)-13-phenyl-9,10-dihydro-9,10-[3,4]epipyrroloanthracene-12,14-diones

The cell viability results of (*E*)-9-(3-oxo-3-phenylprop-1-en-1-yl)-13-phenyl-9,10-dihydro-9,10-[3,4]epipyrroloanthracene-12,14-diones **(103-119)** (Figure 176) in the HG-3 cell line are shown in Figure 175. All compounds were found to be relatively effective at the higher 10 µM concentration with the lowest activity being **(107)** (3,4-dimethoxy derivative, 65%). The most potent of the panel screened were, in order of most to least effective were; **(117)** (3% viable cells remaining, furan derivative), **(116)** (4% viable cells remaining, 2-pyridyl), **(104)** (10%, 4-nitro derivative), **(103)** (14%, 4-bromo), **(114)** (24%, 4-chloro) and **(119)** (24%, 2-thiophene). The remaining compounds were also moderately effective, with activity ranges covering from approximately 29-65% viable cells remaining. At the lower treatment concentration of 1 µM, the order of potency changes with **(116)** having the greatest activity (48% viable cells remaining), then **(105)** (53%, 4-ethyl derivative) **(103)** (63%), **(117)** (63%), **(104)** (64%), **(114)** (65%) and **(109)** (68%).

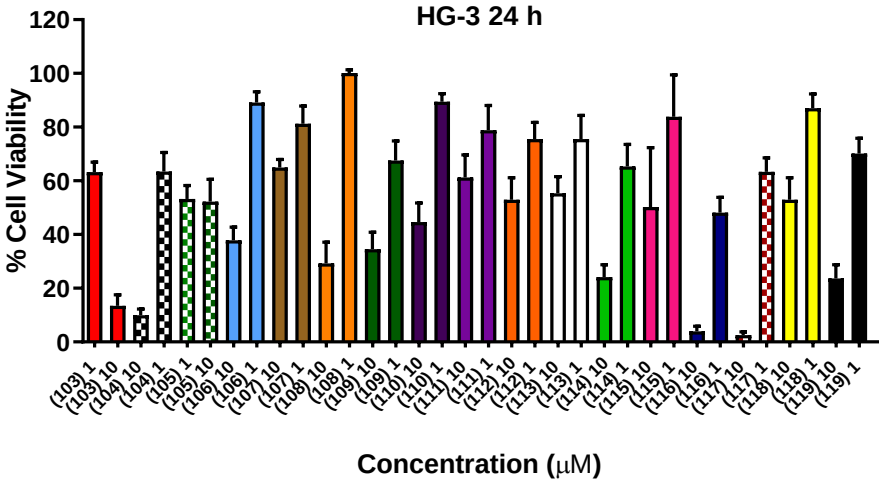

Figure 174: (*E*)-9-(3-Oxo-3-phenylprop-1-en-1-yl)-13-phenyl-9,10-dihydro-9,10-[3,4]epipyrroloanthracene-12,14-diones (103-119) in the HG-3 CLL cell line

The biochemical activity of (*E*)-9-(3-oxo-3-phenylprop-1-en-1-yl)-13-phenyl-9,10-dihydro-9,10-[3,4]epipyrroloanthracene-12,14-diones **(103-119)** (Figure 176) in the PGA-1 cell line are shown in Figure 177. All compounds were found to be relatively effective at the higher 10 µM concentration with the lowest activity being **(115)** (4-pyridine derivative, 81%). The most potent of the panel screened were, in order of most to least effective were; **(117)** (furan derivative, 9% viable cells remaining, **(114)** (4-chloro derivative, 17%), **(104)** (4-nitro derivative, 22%), **(103)** (4-bromo derivative, 25%) and **(108)** (unsubstituted aryl, 26%). The remaining compounds were also moderately effective, with activity ranges covering from approximately 35-81% viable cells remaining. At the lower treatment concentration of 1 µM, the order of potency changes with **(111)** having the greatest activity (4-methoxy derivative, 66% viable cells remaining), **(114)** (70%), **(117)** (71%), **(109)** (72%), **(112)** (72%), **(104)** (73%), and **(113)** (3,4,5-trimethoxy derivative, 84%). The most potent compounds of the series are illustrated in Figure 178.

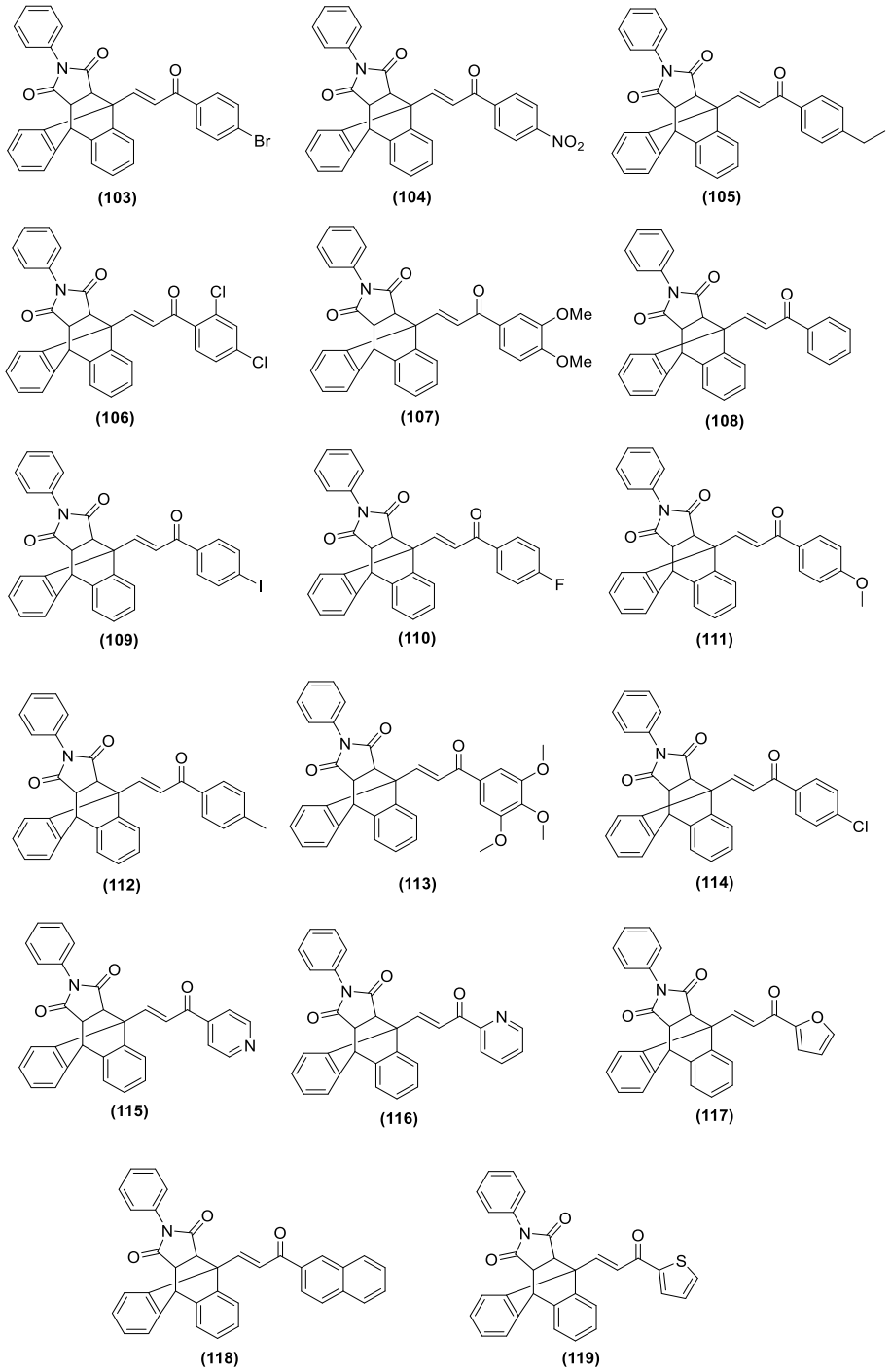

Figure 175: (*E*)-9-(3-Oxo-3-phenylprop-1-en-1-yl)-13-phenyl-9,10-dihydro-9,10-[3,4]epipyrroloanthracene-12,14-diones (103-119)

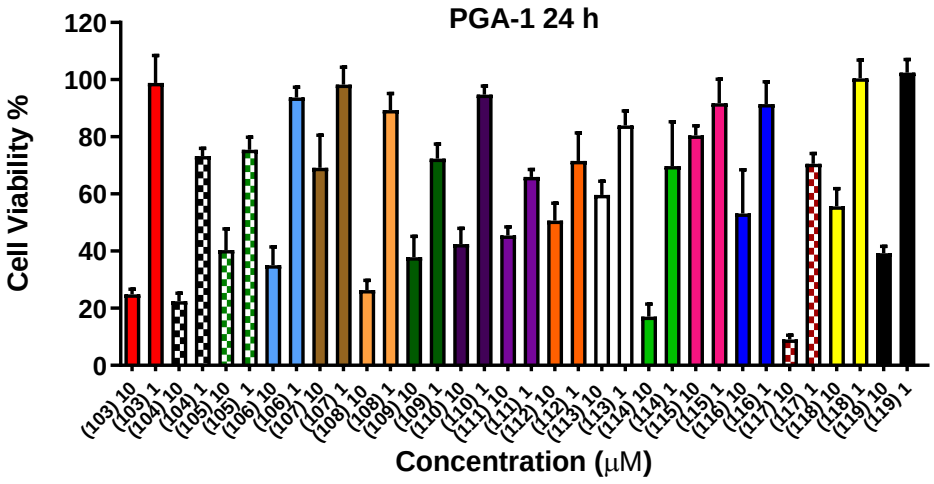

Figure 176: Biochemical activity of (*E*)-9-(3-oxo-3-phenylprop-1-en-1-yl)-13-phenyl-9,10-dihydro-9,10-[3,4]epipyrroloanthracene-12,14-diones (103-119) in the PGA-1 CLL cell line

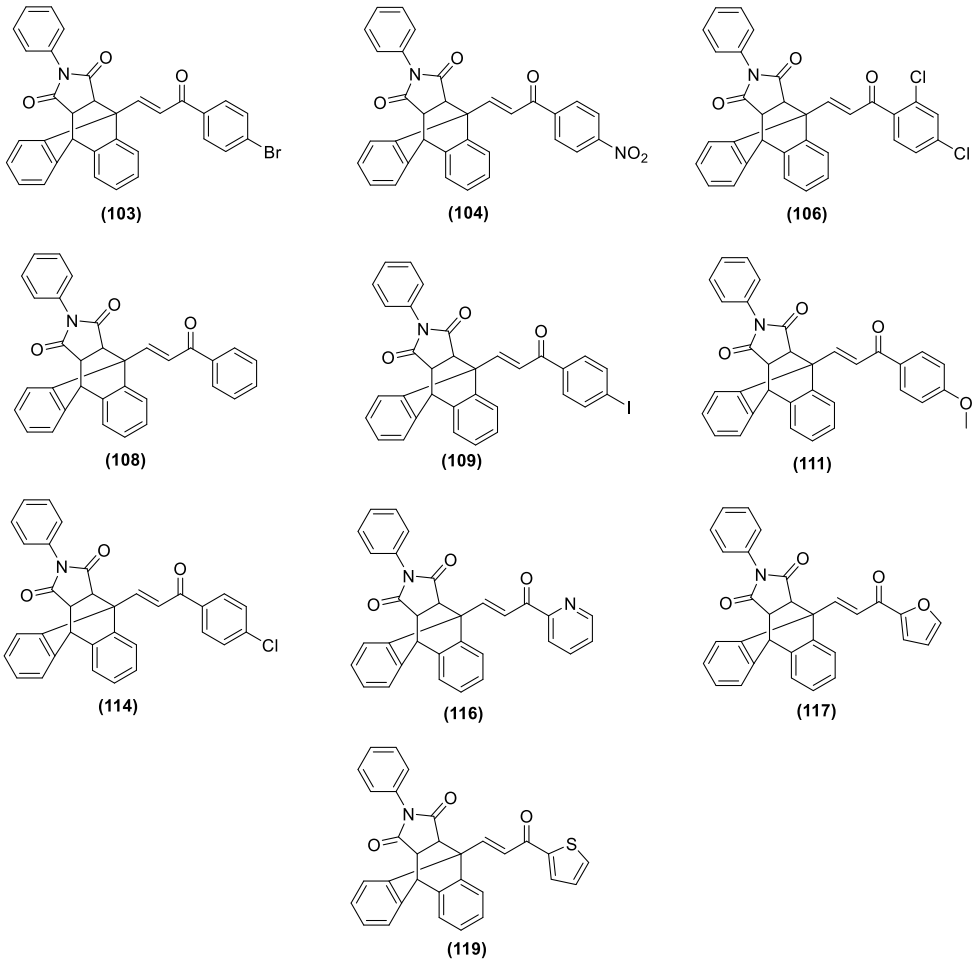

Figure 177: Most potent (*E*)-9-(3-oxo-3-phenylprop-1-en-1-yl)-13-phenyl-9,10-dihydro-9,10-[3,4]epipyrroloanthracene-12,14-dione compounds identified from biochemical screening

3.2.7 Series 7: *In vitro* antiproliferative activity of (*E*)-13-(4-chlorophenyl)-9-(3-oxo-3-phenylprop-1-en-1-yl)-9,10-dihydro-9,10-[3,4]epipyrroloanthracene-12,14-diones

The antiproliferative activity of seventeen (*E*)-13-(4-chlorophenyl)-9-(3-oxo-3-phenylprop-1-en-1-yl)-9,10-dihydro-9,10-[3,4]epipyrroloanthracene-12,14-diones **(120-136)** (Figure 180) in the HG-3 cell line are shown in Figure 179. At the higher treatement concentration of 10 µM, the most potent of the series screened (werein order of most to least effective) were: (**133)** (2% viable cells, 2-pyridyl), (**134)** (5%, 2-acetyl furan derivative), (**132)** (8%, 4-pyridyl), **(127)** (35%, 4-fluoro), **(121)** (35%, 4-nitro) and **(136)** (47%, 2-thiophene). The remaining compounds were also moderately effective, with activity ranges covering from approximately 48-79% viable cells remaining. At a lower treatment concentration of 1 µM, the order of potency changes with **(133)** having the greatest activity (30% cell viability), followed by **(132)** (52%), **(123)** (54%, 2,4-dichloro derivative), **(120)** (63%), **(129)** (76%) and **(124)** (84%).

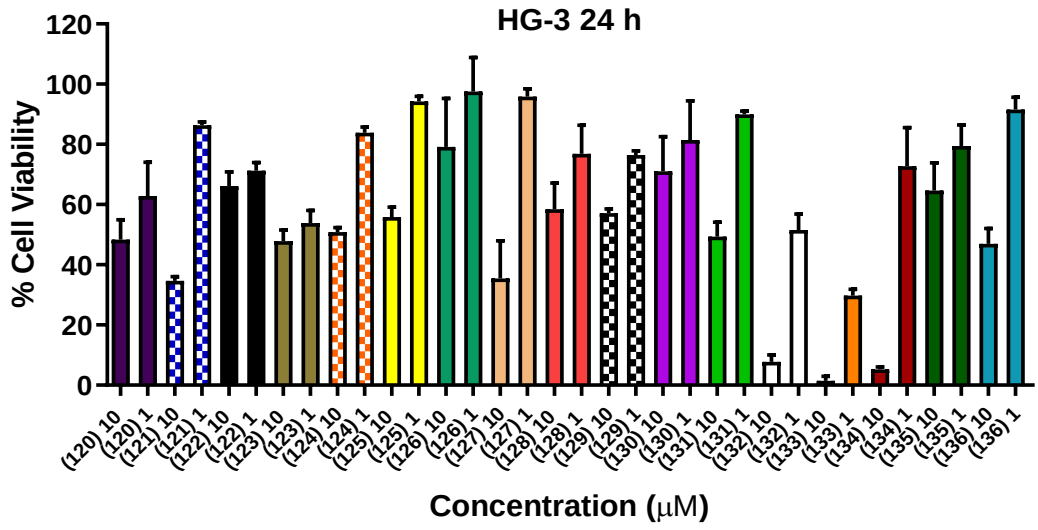

Figure 178: Biochemical activity of (*E*)-13-(4-chlorophenyl)-9-(3-oxo-3-phenylprop-1-en-1-yl)-9,10-dihydro-9,10-[3,4]epipyrroloanthracene-12,14-dione compounds derivatives (120-136) in HG-3 CLL cell line

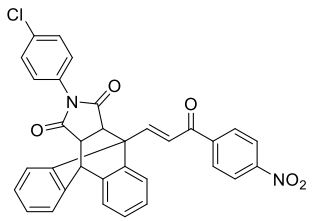

(121)

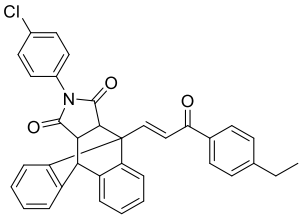

(122)

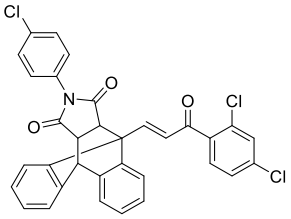

(123)

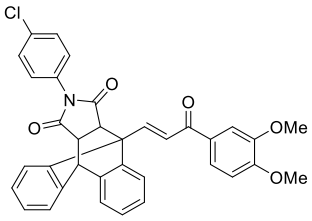

(124)

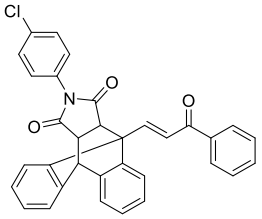

(125)

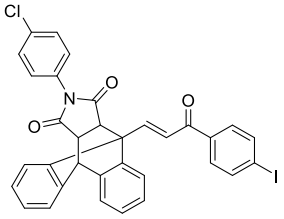

(126)

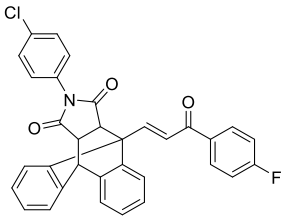

(127)

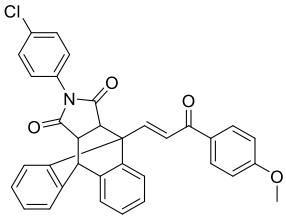

(128)

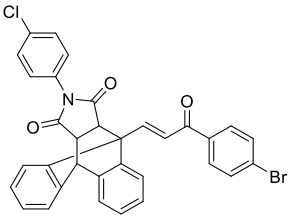

(120)

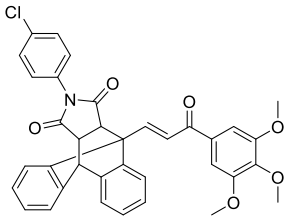

(130)

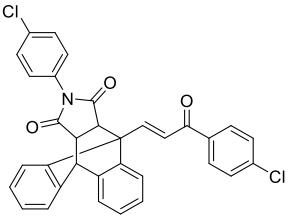

(131)

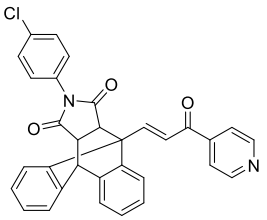

(132)

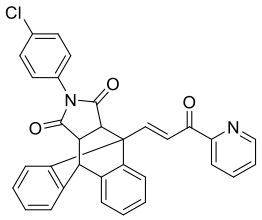

(133)

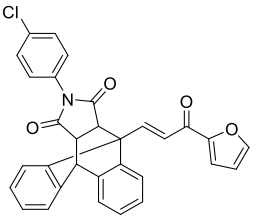

(134)

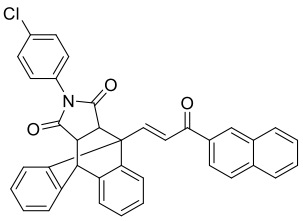

(135)

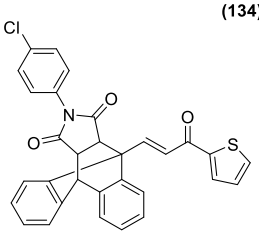

(136)

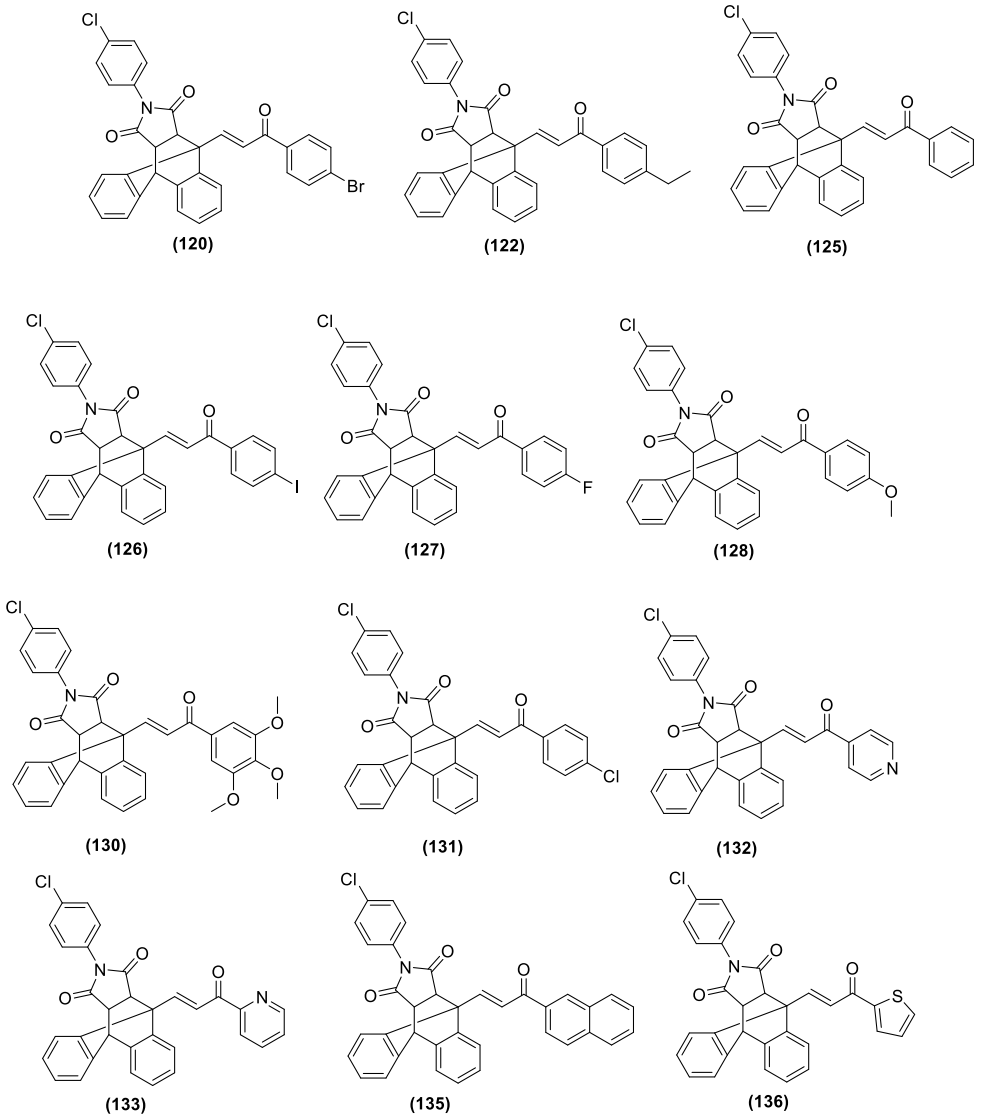

Figure 179: 9-(*E)*-3-oxo-3-phenylprop-1-en-1-yl)-9,10-dihydro-9,10-[3,4] epipyrroloanthracene -12,14-diones (120-136)

The biochemical activity of 9-(*E*)-3-oxo-3-phenylprop-1-en-1-yl)-9,10-dihydro-9,10-[3,4] epipyrroloanthracene -12,14-diones **(120-136)** (Figure 180) in the PGA-1 cell line are shown in Figure 181. At the higher 10 µM concentration the most potent of the panel screened (in the order of most to least effective were): (**133)** (7% viable cells), (**134)** (14%), **(131)** (24%, 4-chloro), **(132)** (28%), **(120)** (33%), **(126)** (33%) and **(121)** (34%). The remaining compounds were also moderately effective, with activity ranges covering from approx. 39-90% viable cells remaining. At a lower treatment concentration of 1 µM, the order of potency changes with **(133)** having the greatest activity (25% cell viability), followed by **(126)** (49%), (**132)** (50%), **(134)** (60%) and **(123)** (62%). The most potent of the series are illustrated in Figure 182.

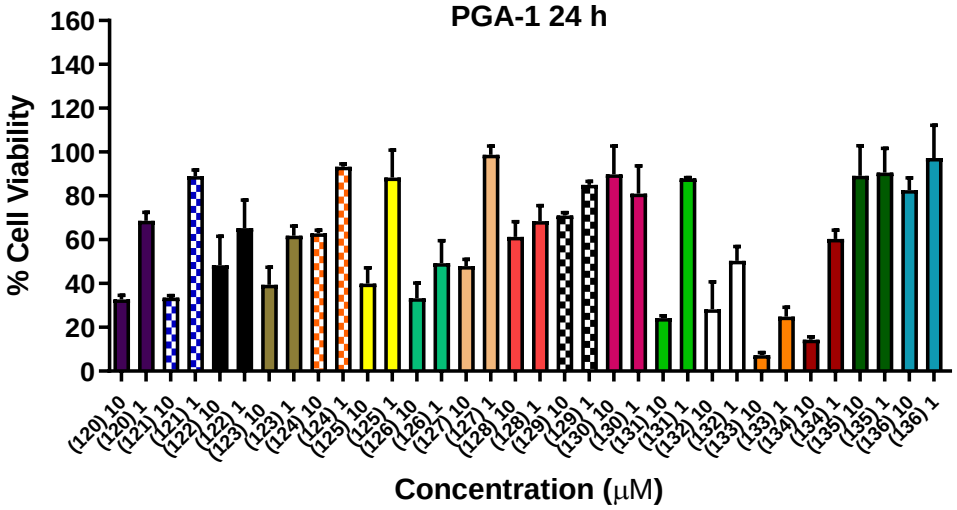

Figure 180: Biochemical activity of (*E*)-13-(4-chlorophenyl)-9-(3-oxo-3-phenylprop-1-en-1-yl)-9,10-dihydro-9,10-[3,4]epipyrroloanthracene-12,14-dione compounds) derivatives (120-136) in PGA-1 CLL cell line

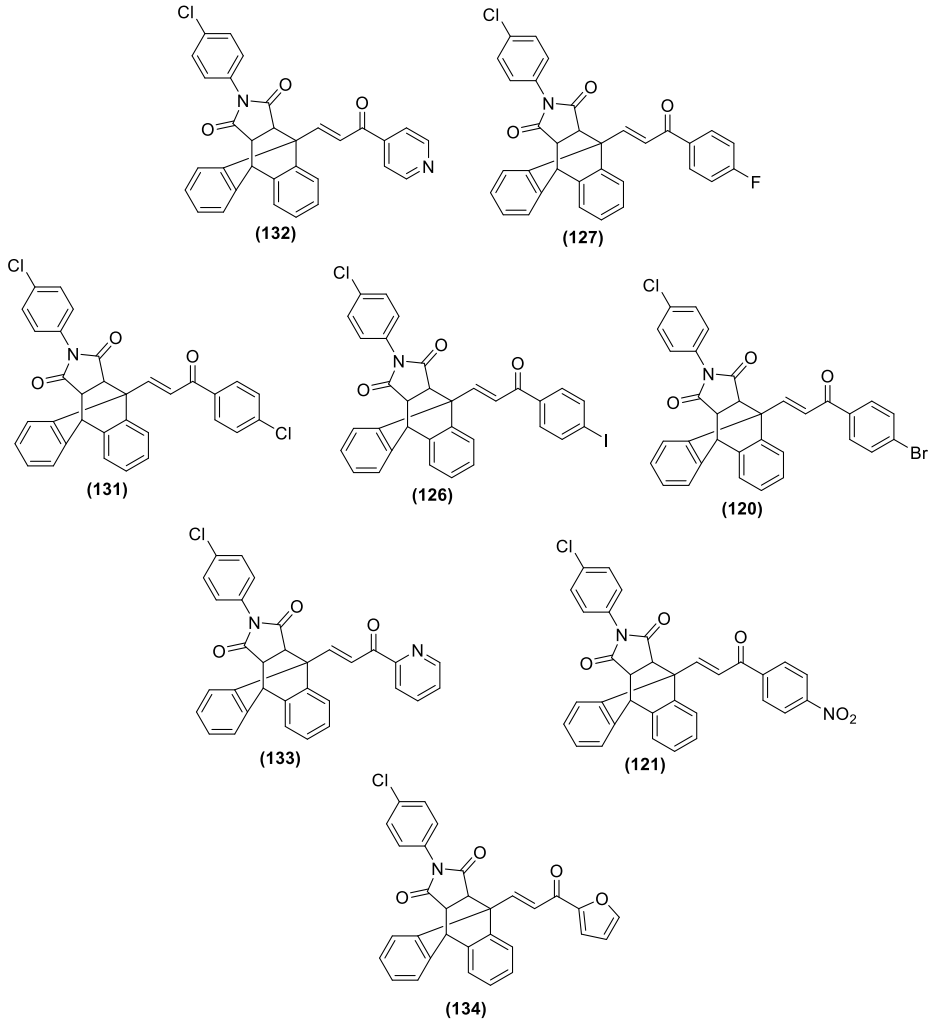

Figure 181: Most potent 9-(*E*)-3-oxo-3-phenylprop-1-en-1-yl)-9,10-dihydro-9,10-[3,4] epipyrroloanthracene -12,14-diones identified in biochemical screening

3.2.8 Series 8: *In vitro* antiproliferative activity of (*E*)-13-(4-benzoylphenyl)-9-(3-oxo-3-phenylprop-1-en-1-yl)-9,10-dihydro-9,10-[3,4]epipyrroloanthracene-12,14-diones

The biochemical activity of (*E*)-13-(4-benzoylphenyl)-9-(3-oxo-3-phenylprop-1-en-1-yl)-9,10-dihydro-9,10-[3,4]epipyrroloanthracene-12,14-diones **(137-153)** (Figure 184) in the HG-3 cell line are shown in Figure 183. At the higher treatment concentration of 10 µM, the most potent of the panel screened in order of most to least effective were; **(150)** (4% viable cells, 2-pyridyl derivative), **(151)** (15%, 2-furan) **(149)** (27%, 4-pyridyl), **(153)** (56%, 2-thiophene), **(137)** (57%, 4-bromo) and **(143)** (60%, 4-iodo). The remaining compounds had fair to negligible activity ranging from approx. 63-97 % viable cells remaining. At a lower treatment concentration of 1 µM, the order of potency changes

with **(137)** having the greatest activity (32% cell viability), followed by **(153)** (61%), **(149)** (62%), **(150)** (62%) and **(151)** (65%). The remaining compounds had a had fair to negligible activity ranging from approx. 66-107% viable cells remaining.

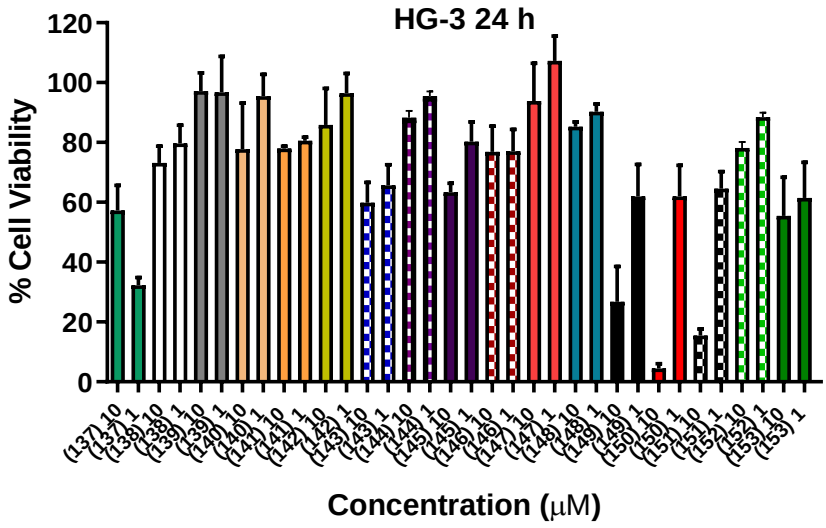

Figure 182: Biochemical activity of (*E*)-13-(4-benzoylphenyl)-9-(3-oxo-3-phenylprop-1-en-1-yl)-9,10-dihydro-9,10-[3,4]epipyrroloanthracene-12,14-diones derivatives (137-153) in the HG-3 CLL cell line

The biochemical activity of **(137-153)** (Figure 184) in the PGA-1 cell line are shown in Figure 185. At the higher treatment concentration of 10 μM, the most potent of the panel screened in order of most to least effective were: **(151)** (9% viable cells remaining, 2-furan derivative) **(149)** (17%, 4-pyridyl), **(150)** (18%, 2-pyridyl), **(153)** (51%, 2-thiophene) and **(140)** (52%, 2,4-dichloro). The remaining compounds had fair to negligible activity ranging from approx. 68-104 % viable cells remaining. At a lower treatment concentration of 1 μM, the order of potency changes with **(137)** having the greatest activity (29% cell viability, 4-bromo), followed by **(149)** (44%), **(140)** (61%), **(151)** (64%) and **(147)** (68%, 3,4,5-trimethoxy derivative). The remaining compounds had fair to negligible activity ranging from approx. 75-114% viable cells remaining. The most potent compounds of the series are illustrated in Figure 186.

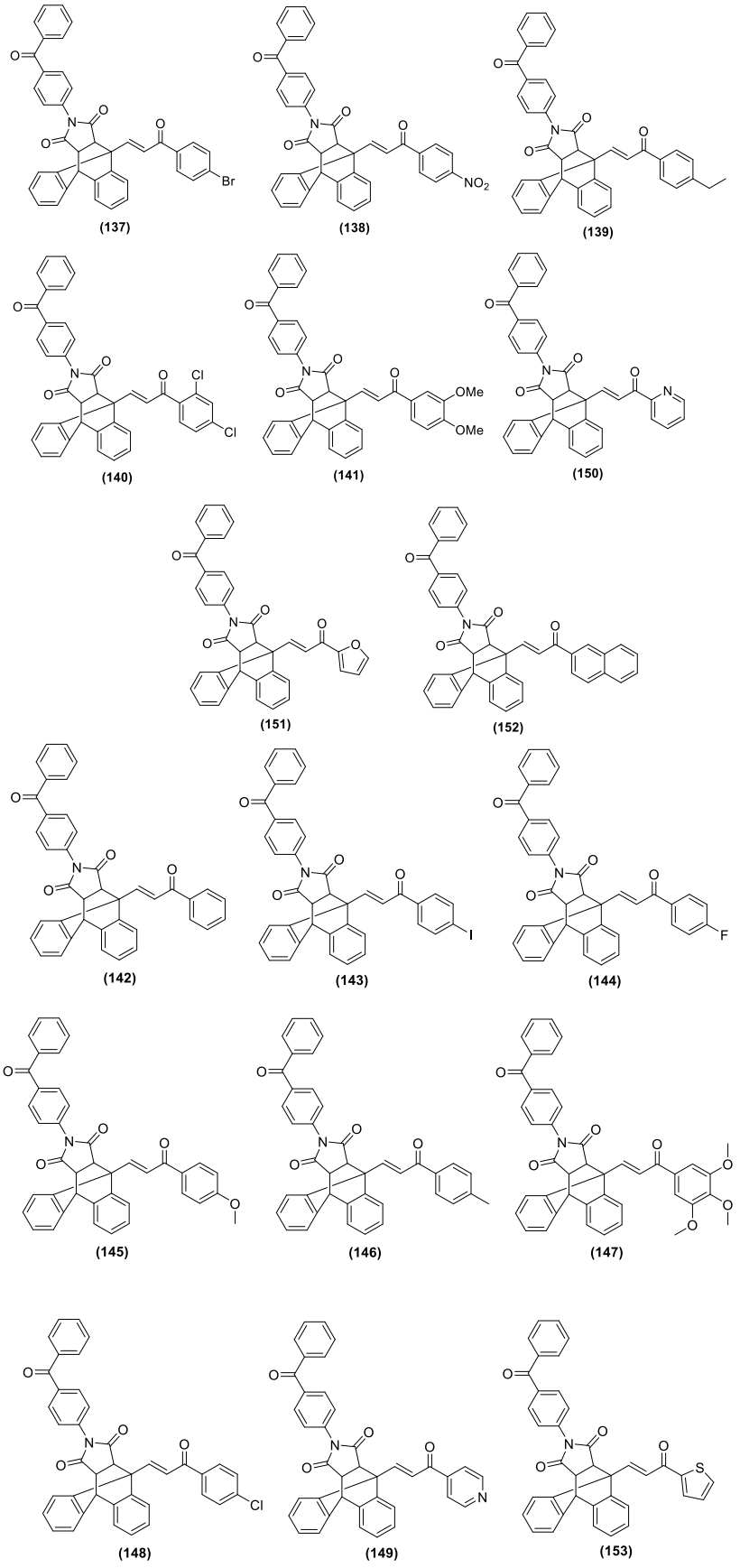

Figure 183: (*E*)-13-(4-benzoylphenyl)-9-(3-oxo-3-phenylprop-1-en-1-yl)-9,10-dihydro-9,10-[3,4]epipyrroloanthracene-12,14-dione compounds (137-153) (series 8)

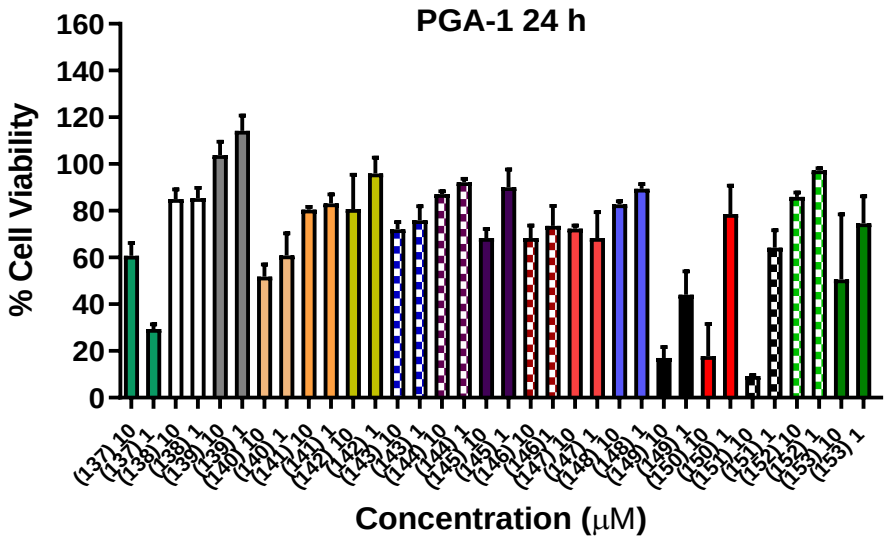

Figure 184: Biochemical activity of (*E*)-13-(4-benzoylphenyl)-9-(3-oxo-3-phenylprop-1-en-1-yl)-9,10-dihydro-9,10-[3,4]epipyrroloanthracene-12,14-diones derivatives (137-153) in the PGA-1 CLL cell line

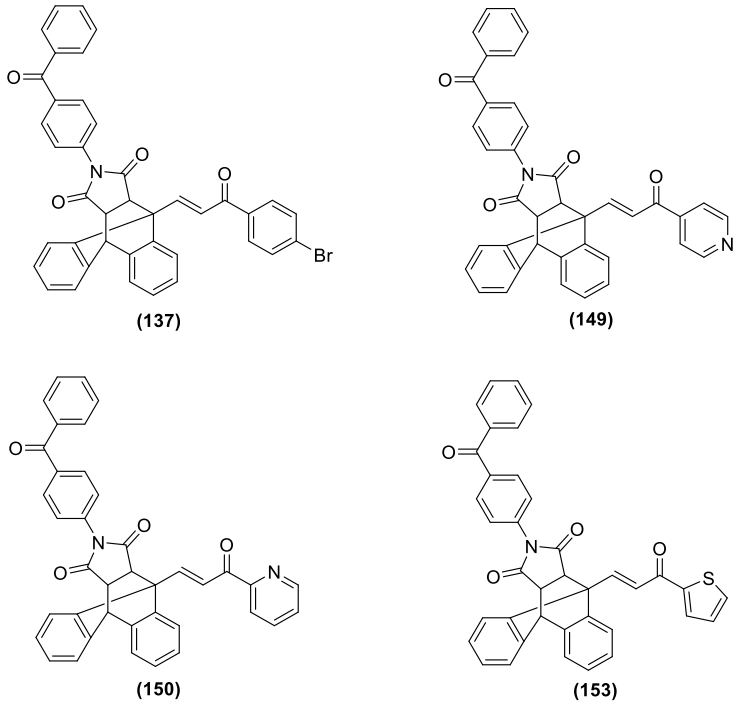

(137) (149) (150) (153)

Figure 185: Most potent (*E*)-13-(4-benzoylphenyl)-9-(3-oxo-3-phenylprop-1-en-1-yl)-9,10-dihydro-9,10-[3,4]epipyrroloanthracene-12,14-dione compounds identified from biochemical screening

Overall in this series and across both cell lines, more favourable activity was observed when heterocycles (pyridine [**149, 150**], thiophene [**153**]) (Figures 183 and 185) replaced the unsubstituted benzoyl aromatic ring (**142**) on the molecular scaffold (Table 33). The 4-pyridine derivative **(149)** led to a notable decrease in cell viability of 64% (to 17% viable cells) at the 1 μM treatment concentration in comparison to the unsubstituted **(142)**

in the PGA-1 cell line (Table 33). In HG-3 cells, a 59% improvement in reducing cell viability was observed at 10 µM for **(149)** and a 64% decrease at the 1 µM concentration comapred to **(142)**. With **(150)** (2-pyridyl derivative), a significant reduction in cell viability was noted in PGA-1 cells showing decreases of 63% and 20% at 10 µM and 1 µM respectively. Similarly, in HG-3 cells, **(150)** showed substantial decreases in cell viability compared to **(142)** (82% greater decrease in cell viability at 10 µM and 34 % greater decrease at 1 µM). In addition, the presence of a bromine atom at position 4 of the benzoyl aromatic ring (**137**) resulted in a significant increase in biological activity when compared to **(142)** leading to a 20 % reduction in cell viability at 10 µM and a 70% reduction at 1 µM in PGA-1 cells. Moreover in HG-3 cells, this resulted in a decrease of 29% in cell viability at 10 µM treatment concentration and a 64% decrease at 1 µM (Table 33).

Compound no.	PGA-1 10 µM (% viability)	PGA-1 1 µM (% viability)	HG-3 10 µM (% viability)	HG-3 1 µM (% viability)
(149)	17	44	27	62
(153)	51	75	56	61
(137)	61	29	57	32
(150)	18	79	4	62
(142)	81	96	86	96

Table 33: Percentage viability results of most potent (*E*)-13-(4-benzoylphenyl)-9-(3-oxo-3-phenylprop-1-en-1-yl)-9,10-dihydro-9,10-[3,4]epipyrroloanthracene-12,14-diones compared to (142) (unsubstituted benzoyl ring)

3.2.9 *In vitro* antiproliferative activity (IC_{50}) of the most potent nitrostyrene, nitrostyrene-based ethanoanthracene and chalcone-based ethanoanthracene derivatives

The IC_{50} values of the most promising anti-proliferative nitrostyrene, nitrostyrene-based ethanoanthracene and chalcone-based ethanoanthracene compounds identified from preliminary biological screening at 10 µM and 1 µM concentrations were obtained for both HG-3 and PGA-1 cell lines. Fludarabine was used as a clinically relevant positive

control. Compounds **(5)**, **(7)**, **(8)**, **(10)** and **(21)** were selected from the (*E*)-9-(2-nitrovinyl)anthracene derivatives (of which **(21)**, **(8)**, **(10)** , **(7)** were synthesised by Byrne et al. in previous work[239]).

3.2.10 *In vitro* IC_{50} determination of the most potent (*E*)-9-(2-nitrovinyl)anthracene derivatives (Series 1)

Compounds **(5**), **(7**), **(8)**, **(10)** and **(21)** were selected and were tested across a concentration range of 10 µM, 7.5 µM, 5 µM, 2.5µM, 1.5 µM, 1 µM and 0.5 µM and assessed at the 24 h timepoint (Figure 187 and Table 34). The compounds exerted a more potent effect than the fludarabine control ([5-40 fold greater in HG-3 cells, 4-25 fold greater in PGA-1 cells]) across both HG-3 and PGA-1 cell lines with IC_{50} ranges of 0.7-3.85 µM and 1.29-9.1 µM respectively. In HG-3 cells, the most potent compounds identified were 10-methoxy derivative **(10)** (IC_{50} 0.17 µM) and the 10-isopropyl derivative **(21) (**IC_{50} 0.7 µM); while in PGA-1 cells the most potent compounds were **(10)** (IC_{50} 1.29 µM) and 10-ethyl derivative **(8)** (IC_{50} 1.3 µM). Overall, the two most potent compounds across both cell lines were **(10)** (average IC_{50} 0.73 µM) and **(05)** (average IC_{50} 2.77 µM). These results suggest that alkyl and alkoxy substituents present at the 10-position on the anthracene core can lead to greater anti-proliferative activity in CLL compared to the unsubstituted **(5)**. However, this effect was observed to be subject to disease subtype, steric bulk and substituent size. The steric bulk of 10-isopropyl group of **(21)** caused a 13-fold greater response in HG-3 as opposed to PGA-1 cells (0.7 µM vs 9.1 µM) and 3.5-fold activity increase compared to **(5)**. This is in contrast to the less bulkier 10-ethyl substituent of **(8)** causing an increase in the HG-3 IC_{50} value of 3 µM while reducing the PGA-1 IC_{50} value by 2 µM [relative to **(5)**].Interestingly, the smaller 10-methyl substitutient of **(7)** had a negative impact on both cell lines, leading to an approximate increase of 1.4 µM in the respective IC_{50} values.Furthermore, the 10-methoxy of **(10)** led to a 7.8-fold better IC_{50} value in HG-3 than in PGA-1 cells and a similar activity to **(8)** (10-ethyl) in PGA-1 cells.

These results suggest the potential for similar, yet distinct compound attributes for potent anti-proliferative activity in the main two CLL disease cell subtypes.

Compound Number	HG-3 (μM)	PGA-1 (μM)	Average (μM)
	IC_{50}	IC_{50}	IC_{50}
(5)	**2.43**	**3.1**	**2.77**
(7)	**3.85**	**4.4**	**4.13**
(8)	**5.4**	**1.3**	**4.85**
(10)	**0.17**	**1.29**	**0.73**
(21)	**0.7**	**9.1**	**4.9**
Fludarabine	**28.1**	**32**	**30.1**

Table 34: IC_{50} values of the most potent (*E*)-9-(2-nitrovinyl)anthracene derivatives in both HG-3 and PGA-1 CLL cell lines

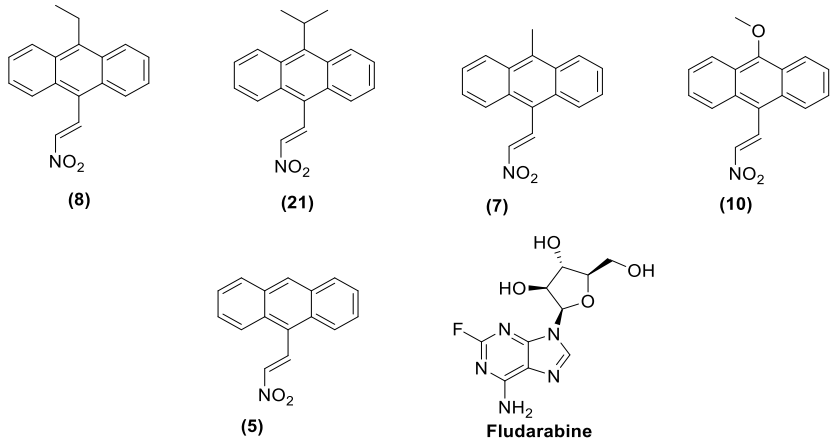

Figure 186: Most potent (*E*)-9-(2-nitrovinyl)anthracene derivatives in both HG-3 and PGA-1 CLL cell lines

3.2.11 *In vitro* IC_{50} determination of (*E*)-9-(2-nitrovinyl)-9, 10, 11, 15-tetrahydro-9, 10-[3, 4] epipyroloanthracene-12, 14-dione derivatives (Series 2)

Compounds **(24-28**) were selected and tested across a concentration range of 5 μM, 1 μM, 0.4μM, 0.2 μM, 0.1 μM and 0.01 μM and assessed at the 24 h timepoint (Figure 188 and Table 35) in collaboration with Adam Bergin. The compounds exerted a more potent effect than the fludarabine control (18-59 fold greater in HG-3 cells, 29-53 fold greater in PGA-1 cells) across both HG-3 and PGA-1 cell lines with IC_{50} ranges of 0.48-1.6 μM and 0.61-1.1 μM respectively. In HG-3 cells, the most potent compounds identified were **(24)** (IC_{50} 0.48 μM, *N*-phenyl derivative) and **(28)** (IC_{50} 0.71 μM, *p*-benzophenone); while in PGA-1 cells the most potent compounds were **(24)** (0.61 IC_{50} μM) and **(25**) (IC_{50} 0.66

µM, *p*-chlorophenyl). Overall, the two most potent compounds across both cell lines were **(24)** (average IC_{50} 0.55 µM) and **(25)** (average IC_{50} 0.77 µM). In both cell lines, **(26)** (cyano derivative) had the lowest relative IC_{50} values (Table 35) with the remaining compounds having sub-micromolar activity. This suggests that the general maleimide structure plays an important role in the biological activity observed. In addition, the presence of an unsubstituted aromatic ring on the maleimide-derived funcitonal group **(24)** leads to better activity over the unsubstituted maleimide (**27**), *p*-chloromaleimide (**25**) and the *p*-benzophenone maleimide (**28**) adduct.

Compound Number	HG-3 (µM) IC_{50}	PGA-1 (µM) IC_{50}	Average (µM) IC_{50}
(24)	**0.48**	**0.61**	**0.55**
(25)	**0.85**	**0.66**	**0.76**
(26)	**1.6**	**1.1**	**1.4**
(27)	**0.78**	**0.76**	**0.77**
(28)	**0.71**	**0.88**	**0.8**
Fludarabine	**28.1**	**32**	**30.1**

Table 35: IC_{50} values of the most potent (*E*)-9-(2-nitrovinyl)-9, 10, 11, 15-tetrahydro-9, 10-[3, 4] epipyrolloanthracene-12, 14-dione derivatives (24-28) in both HG-3 and PGA-1 CLL cell lines

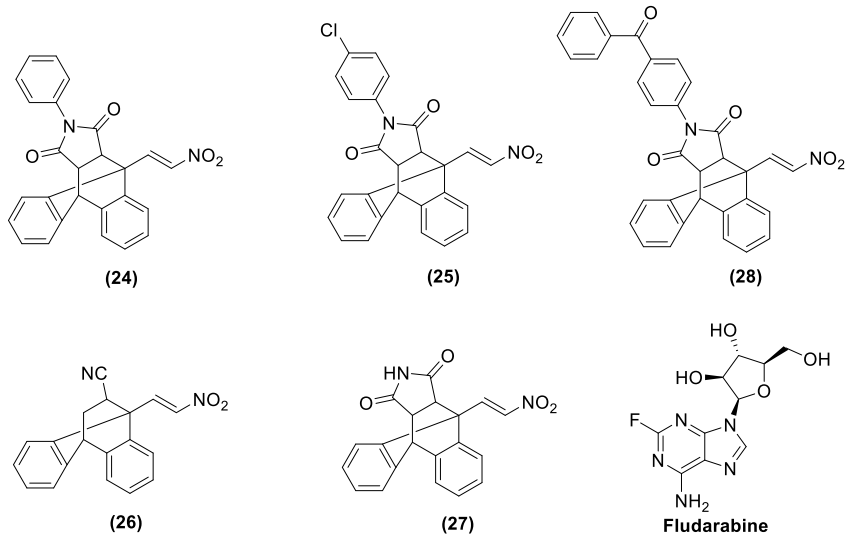

Figure 187: Structures of the most potent (*E*)-9-(2-nitrovinyl)-9, 10, 11, 15-tetrahydro-9, 10-[3, 4] furanoanthracene-12, 14-dione derivatives in both HG-3 and PGA-1 CLL cell lines

3.2.12 *In vitro* IC_{50} determination of 9-(*E*)-3-oxo-3-phenylprop-1-en-1-yl)-9,10-dihydro-9,10-[3,4]epipyrroloanthracene-12,14-dione derivatives (Series 5-9)

Compounds **(86**, **88**, **101**, **99**, **93**, **92**,**133 ,150 , 91**, **97**, **94**, **96, 108** and **114)** were selected and tested across a concentration range of 50 μM, 20 μM, 10 μM, 5 μM, 1 μM, 0.1 μM and 0.01 μM and assessed at the 24 h timepoint (Table 36). An example of the cell viability dose response curves used to determine the IC_{50} values for these compounds in HG-3 and PGA-1 cells is illustrated in Figure 189. The compounds exerted a more potent effect than the fludarabine control (3-22 fold greater in HG-3 cells, 3-37 fold greater in PGA-1 cells) across both HG-3 and PGA-1 cell lines with IC_{50} ranges of 1.31-10.28 μM and 0.31-12.6 μM respectively.

In HG-3 cells, the most potent compounds identified were **(133)** (IC_{50} 1.31 μM, 2-pyridyl, *p*-chlorophenyl derivative) and (**101)** (IC_{50} 1.41 μM, 2-naphthyl, maleimide derivative) while in PGA-1 cells the most potent compounds were **(114)** (0.31 IC_{50} μM, 4-chloro, maleimide derivative) and **(150)** (IC_{50} 0.39 μM, 2-pyridyl, *p*-benzophenone maleimide derivative). Overall, the two most potent compounds across both cell lines were **(133)** (average IC_{50} 1.09 μM) and **(150)** (average IC_{50} 1.12 μM). The most potent analogs are are shown in Figure 190.

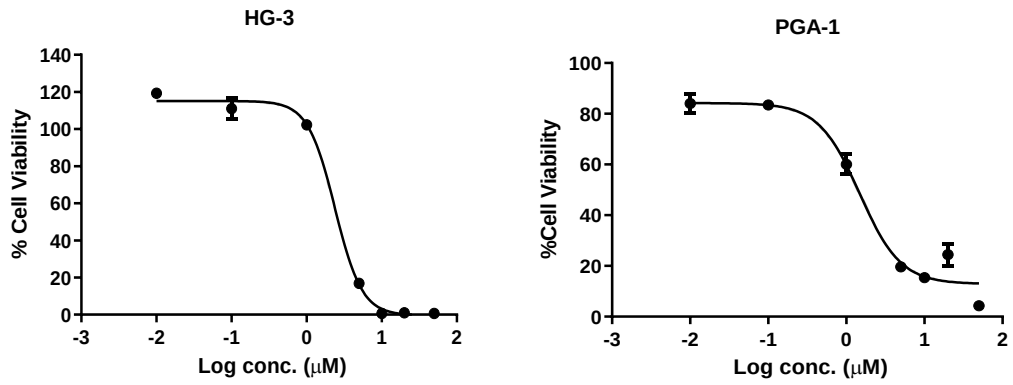

Figure 188: Representative IC_{50} curve of compound (99) used to determine the μM concentration at which the CLL cells experience 50% reduction in cell viability

Compound Number	HG-3 (µM) IC_{50}	PGA-1 (µM) IC_{50}	Average (µM) IC_{50}
(86)	2.69	1.97	2.33
(88)	4.61	2.72	3.67
(101)	1.41	1.30	1.36
(99)	2.39	1.48	1.94
(93)	4.65	2.88	3.77
(92)	4.47	2.77	3.62
(133)	1.31	0.87	1.09
(150)	1.85	0.39	1.12
(91)	3.55	11.3	7.43
(97)	2.23	3.21	2.72
(94)	10.28	12.6	11.4
(96)	4.9	5.38	5.19
(108)	7.35	7.13	7.24
(114)	3.45	0.31	1.88
Fludarabine	28.1	32	30.1

Table 36: IC_{50} values of the most potent 9-(*E*)-3-oxo-3-phenylprop-1-en-1-yl)-9,10-dihydro-9,10-[3,4]epipyrroloanthracene-12,14-dione derivatives in both HG-3 and PGA-1 CLL cell lines

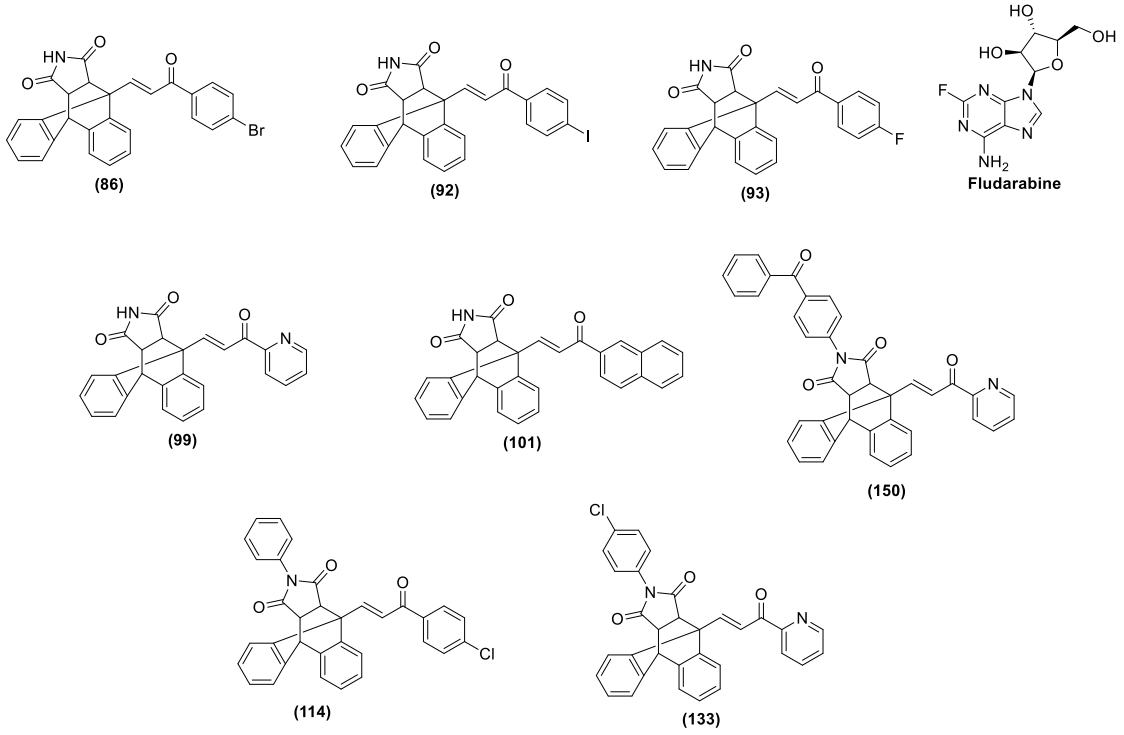

Figure 189: Most potent compounds 9-(*E*)-3-oxo-3-phenylprop-1-en-1-yl)-9,10-dihydro-9,10-[3,4]epipyrroloanthracene-12,14-diones

3.2.13 *In vitro* antiproliferative activity of 13,13'-(ethane-1,5-diyl)bis(9-((E)-2-nitrovinyl)-9,10-dihydro-9,10-[3,4]epipyrroloanthracene-12,14-dione) (156)

Identified previously as a potent anti-proliferative in Burkitt's lymphoma by Byrne et al.[239], the novel dimer compound **(156)** was selected and tested across a concentration range of 50 μM, 20 μM, 10 μM, 5 μM, 1 μM, 0.1 μM and 0.01 μM and assessed at the 24 h timepoint. The compound **(156)** exerted a more potent effect than the fludarabine control (165-fold greater in HG-3 cells, 91-fold greater in PGA-1 cells) across both HG-3 and PGA-1 cell lines with IC_{50} values of 0.17 μM and 0.35μM respectively. Overall, across both cell lines, **(156)** displayed an average IC_{50} value of 0.53 μM (Table 37, Figure 191).

Compound Number	IC_{50} HG-3 (μM)	IC_{50} PGA-1 (μM)	IC_{50} Average (μM)
(156)	**0.17**	**0.35**	**0.26**
Fludarabine	**28.1**	**32**	**30.1**

Table 37: IC $_{50}$ value of 13,13'-(Ethane-1,5-diyl)bis(9-((*E*)-2-nitrovinyl)-9,10-dihydro-9,10-[3,4]epipyrroloanthracene-12,14-dione) (156)

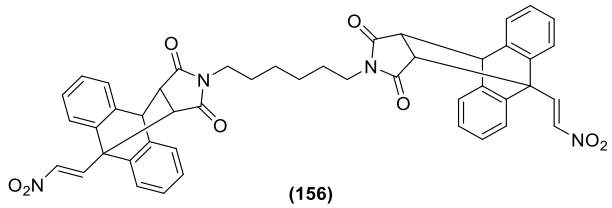

(156)

Figure 190: 13,13'-(Ethane-1,5-diyl)bis(9-((*E*)-2-nitrovinyl)-9,10-dihydro-9,10-[3,4]epipyrroloanthracene-12,14-dione) (156) chemical structure

3.3 National Cancer Institute (NCI) 60 Cell line panel

Founded in the 1950s, the NCI-60 high throughput screening initiative was one of the first of its kind involving the testing of agents with preliminary or believed anticancer activity in a diverse immortalized cancer cell line panel. Still utilized today as a valuable, publicly available drug discovery resource, this panel is subdivided into nine subcategories based on cancer tissue types which include leukaemia, ovarian, central

nervous system, breast, lung, prostate, skin, renal and colon. A number of our most promising compounds identified through preliminary cell viability testing were selected for NCI drug screening in the 60 cell line panel and were initially assessed in a one-dose assay at a fixed treatment concentration of 10 μM. On the basis of these reports, the compounds deemed worthy of further investigation were progressed to a five-dose assay across the concentration range of 0.01, 0.1, 1, 10 and 100 μM[383].

The end points assessed as part of the screening protocol were:

1. **GI_{50}**-concentration at which the drug would cause 50 % growth inhibition in the cell line of interest
2. **TGI**-concentration of drug at which the growth of the cell line of interest is completely inhibited (i.e. 0 % cell growth)
3. **LC_{50}**-concentration of drug which causes 50% lethality in the cell line of interest (i.e. 50% cell death)[384]

Five-dose assay results

As the main focus of this thesis is the antiproliferative and anti-cancer effects of ethanoanthracenes in CLL, attention will be given primarily to leukaemia cell line results within the wider 60 cell line panel.

The leukaemia cell lines used for the assessment were as follows:

- **CCRF-CEM-** acute lymphoblastic leukaemia
- **HL-60 (TB)-** acute promyelocytic leukaemia
- **K-562-** chronic myeloid leukaemia
- **MOLT-4-** acute lymphoblastic leukaemia
- **RPMI-8226-** plasmacytoma/myeloma
- **SR-** large cell immunoblastic lymphoma

The compounds accepted and screened as part of the NCI Developmental Therapeutics testing program were **(88, 89, 91, 93, 97, 98, 99, 100, 108, 114, 133, 150)** (Figure 192). The resultant GI_{50} values are represented in Table 38 and Table 39. The compound biological activity will now be briefly discussed by leukaemia cell line by their respective GI_{50} values.

In the CCRF-CEM cell line, compound bioactivity was represented by GI_{50} values in the range of 0.321-2.66 µM with the most potent agents being (**133)** (0.32 µM), **(99)** (1.44 µM), **(114)** (0.57 µM) and **(89)** (1.24 µM). With the HL-60 (TB) cell line, the antiproliferative activity varied from GI_{50} values of 0.02-1.90 µM with the compounds displaying the most activity being **(93)** (0.02 µM), **(88)** (0.07 µM), **(133)** (0.29 µM), and **(100)** (0.32 µM). In K-562 cells, the observed GI_{50} values fell between 0.29-2.57 µM. The most active analogues noted were **(133)** (0.29 µM), **(99)** (1.37 µM), **(108)** (1.39 µM) and **(93)** (1.42 µM). With MOLT-4 cells, the GI_{50} values ranged from 0.32-2.57 µM and the most potent compounds were **(133)** (0.32 µM), **(93)** (0.46 µM), **(114)** (0.76 µM) and **(108)** (1.23 µM). In RPMI-8226 cells, the GI_{50} values ranged from 0.25-2.49 µM and the most active adducts were **(133)** (0.25 µM), **(89)** (1.10 µM), **(114)** (1.16 µM) and **(99)** (1.22 µM). With the SR cell line, the GI_{50} values noted ranged from 0.28-2.15 µM. The compounds displaying the most potent biological activity were **(133)** (0.28 µM), **(93)** (0.29 µM), **(99)** (0.78 µM) and **(114)** (1.07 µM).

Cell Line		**Drug no.**					
		(89) µM GI_{50}	**(100) µM GI_{50}**	**(88) µM GI_{50}**	**(99) µM GI_{50}**	**(98) µM GI_{50}**	**(93) µM GI_{50}**
CCRF-CEM		1.24	1.89	2.66	1.44	2.39	2.45
HL-60 (TB)		1.58	0.32	0.07	1.02	1.76	0.02
K-562		2.19	2.57	2.42	1.37	1.88	1.42
MOLT-4		2.16	1.77	2.23	2.11	2.57	0.46
RPMI-8226		1.10	1.68	1.87	1.22	2.11	1.62
SR		1.25	1.59	1.37	0.78	1.76	0.29
Average		1.59	1.64	1.77	1.32	2.08	1.00

Table 38: NCI five dose leukaemia cell panel GI_{50} values for compounds (88,89,93,98-100)

Cell Line		Drug no.					
		(91) µM GI_{50}	(108) µM GI_{50}	(97) µM GI_{50}	(114) µM GI_{50}	(133) µM GI_{50}	(150) µM GI_{50}
CCRF-CEM		2.16	1.45	1.66	0.57	0.32	2.59
HL-60 (TB)		1.50	1.02	1.47	0.8	0.29	1.90
K-562		1.94	1.39	1.99	1.55	0.29	1.77
MOLT-4		2.17	1.23	1.70	0.76	0.32	2.29
RPMI-8226		1.52	1.55	1.66	1.16	0.25	2.49
SR		1.57	2.03	2.15	1.07	0.28	1.37
Average		1.81	1.45	1.77	0.98	0.29	2.07

Table 39: NCI five dose leukaemia cell panel GI_{50} values for compounds (91, 97 108, 114, 133, 150)

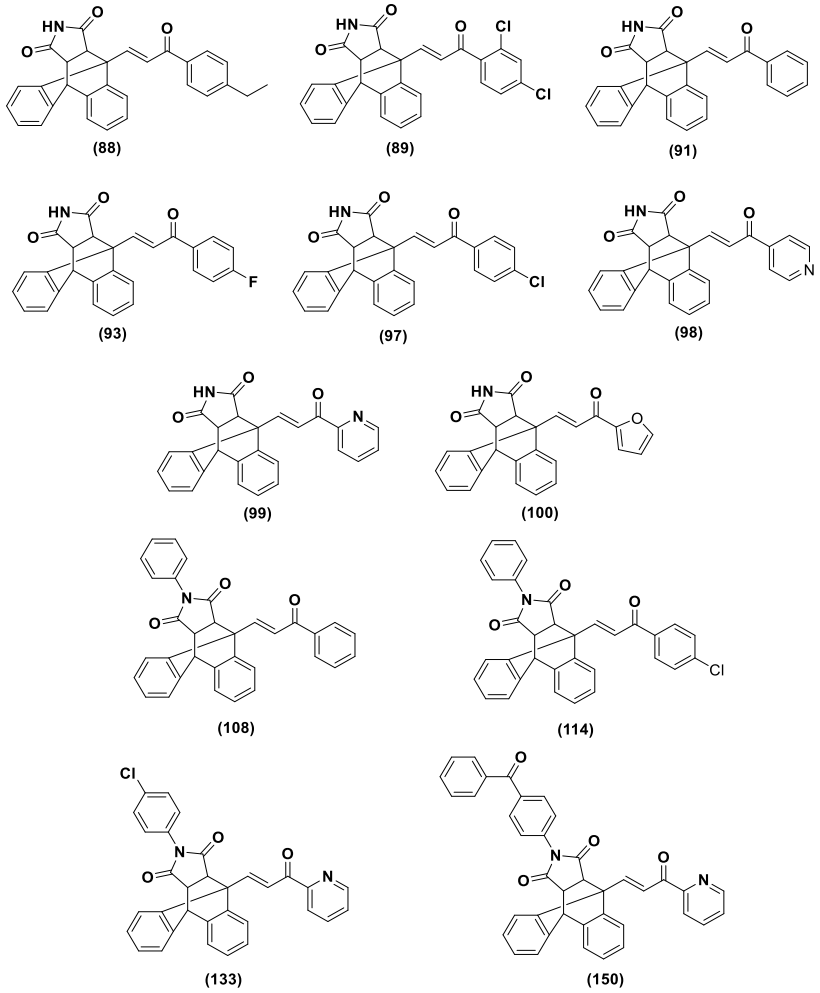

Figure 191: Compounds assessed with NCI 60 cell line panel

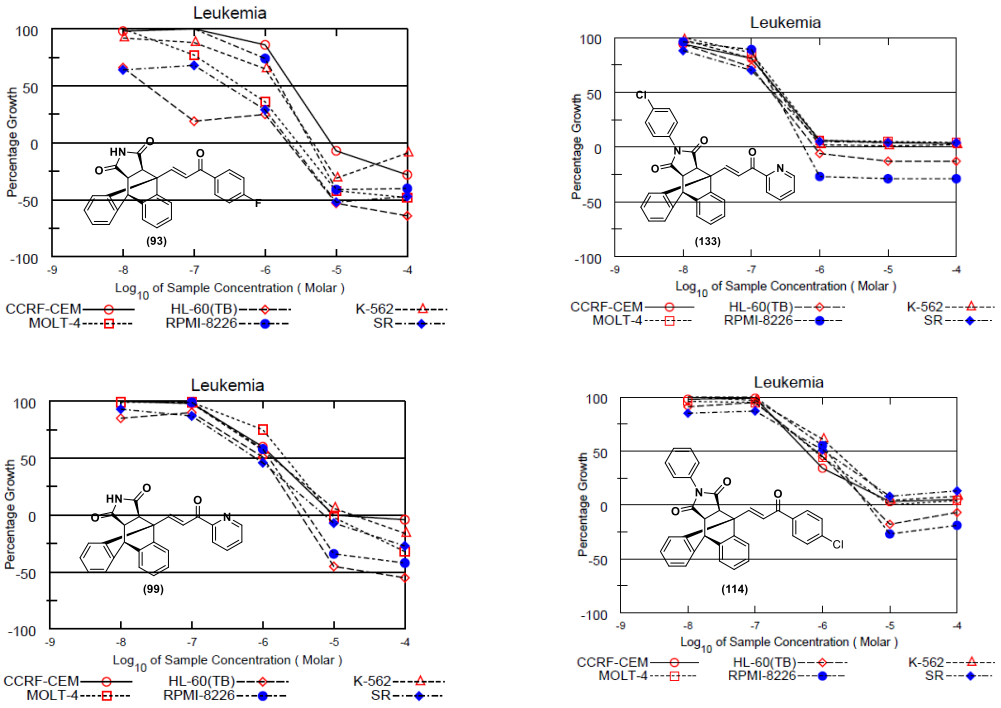

Figure 192: Dose-response curves generated in NCI leukaemia cell lines for compounds (93) (top left), (133) (top right), (99) (bottom left) and (114) (bottom right)-the most potent compounds identified through NCI 60 cell screening

The average biological activity represented by GI_{50} values across the leukaemia cell panel was also calculated and fell within the range of 0.29-2.08 µM. **(133)** (0.29 µM), **(114)** (0.98 µM), **(93)** (1.00 µM) and **(99)** (1.32 µM) were the most promising overall anti-leukaemic agents screened and warrant further study as lead compounds for the development of more selective and potent anti-cancer agents (Table 40). The leukaemia dose respose-curves used to determine the GI_{50} values of **(133, 114, 93, 99)** and their associated chemical structures are illustrated in Figure 193. These results match those determined in this work in HG-3 and PGA-1 CLL cell lines as shown in Table 40 with the exception of **(91)** which has a marked decrease in potency in CLL (average 7.43 µM IC_{50}), predominately in PGA-1 (good prognosis) cell lines (11.30 µM IC_{50}) as opposed to HG-3 cell line (3.55 µM IC_{50}). This further supports the potential of these particular molecular scaffolds to act as lead compounds for the generation of novel antileukaemic agents.

In addition to the above, promising anticancer activity was observed across the NCI 60 cell line panel with particularly interesting activity in melanoma and breast cancer cell

lines with notable GI_{50} value ranges of: **(133)** (melanoma 0.20-1.07 µM, breast 0.30-0.63 µM), **(93)** (melanoma 1.66-2.46 µM, breast 1.66-3.02 µM), **(99)** (melanoma 1.12-2.14 µM, breast 0.56-3.24 µM) and **(97)** (melanoma 1.58-2.46 µM, breast 0.89-1.86 µM). These values suggest potential exploration of these compounds in breast and skin cancers in the future.

Compound	Average NCI Leukaemia panel GI_{50} (µM)	Average CLL data IC_{50} (µM) (determined in-house)
(89)	1.59	2.33
(100)	1.64	3.67
(88)	1.77	1.94
(99)	1.32	3.77
(98)	2.08	3.62
(93)	1.0	3.77
(133)	0.293	1.09
(150)	2.07	1.12
(91)	1.81	7.43
(108)	1.45	7.24
(97)	1.77	2.72
(114)	0.98	1.88

Table 40: Comparison of IC_{50} and GI_{50} values determined in CLL cell lines and NCI leukaemia panel

3.3.1 COMPARE-NCI algorithm: Prediction of Biochemical Mechanism of Action

This is a computer algorithm developed from the work of Paull et al[385],which allows for the the recognition and comparison of compound activity profiles across the NCI 60 cell line panel. It was noted that compounds that displayed similar activity profiles often brought about cell growth inhibition through related mechanisms of action with robust correlations in mean profiles across multiple screening assays. The method used consists of the calculation of a linear Pearson correlation coefficient between all of the data obtained over the NCI 60 cell line panel for the seed (pattern of interest) and the NCI database (implemented through a web-interface using the C programming language). As COMPARE variables can include database used (e.g. standard agents, synthetic agents), seed used (molecular target, compound of interest) and parameters set (minimum

variance needed for significance, minimum number of cell lines to be included in calculations), the methodology used in this work is outlined briefly below.

Representative compounds **(93, 99**, **114, 133)** were used as COMPARE seeds, where their mean recognition patterns used were from their respective NCI five-dose screening assays. The database selected for comparison was the NCI Standard Agents data set and all other parameters were kept as their default settings. The top five ranked compounds for each seed based on Pearson correlation coefficient were chosen and researched to identify their possible mechanisms of action (Tables 41-44).

Rank	Compound	Correlation
1	Anguidine	0.422
2	Bleomycin	0.37
3	3-HP	0.364
4	O6-Methylguanine	0.36
5	4-Ipomeanol	0.344

Table 41: Top five ranking compounds with (133) according to NCI-COMPARE Pearson correlation coefficient analysis of GI_{50} profiles

Rank	Compound	Correlation
1	Dichloroallyl lawsone	0.505
2	Anguidine	0.496
3	Triazinate	0.496
4	Tamoxifen	0.488
5	Diglycoaldehyde	0.486

Table 42: Top five ranking compounds with (99) according to NCI-COMPARE Pearson correlation coefficient analysis GI_{50} profiles

Rank	Compound	Correlation
1	2-Deoxycoformycin	0.918
2	Caracemide	0.663
3	Fluorodopan	0.631
4	Hydroxyurea	0.587
5	Melphalan	0.538

Table 43: Top five ranking compounds with (93) according to NCI-COMPARE Pearson correlation coefficient analysis GI $_{50}$ profiles

Rank	Compound	Correlation
1	Fluorodopan	0.631
2	Pyrimidine-5-glycoaldehyde	0.531
3	Hydroxyurea	0.512
4	Glyoxylic acid	0.505
5	(Carboxyphthalato)platinum	0.496

Table 44: Top five ranking compounds with (114) according to NCI-COMPARE Pearson correlation coefficient analysis of GI_{50} profiles

The top five ranked compounds for each seed compound based on Pearson correlation coefficient will now have their mechanism of action briefly outlined.

Anguidine exerts growth inhibitory effect on rapidly proliferating cells such as lymphocyctes through protein synthesis inhibition (*via* ribosome binding) and cytotoxic activity through cell-cycle interference and apoptosis induction (mitochondrion dependent or independent)[386, 387]. **Bleomycin** induces cancer cell death through complexation of iron, subsequently reducing molecular oxygen to ROS including hydroxide and superoxide radical, causing ssDNA and dsDNA breaks, leading to cell-cycle arrest predominantly in the G2 phase[388, 389]. **3-HP (Pyridine-2-carboxaldehyde, 3-hydroxy-thiosemicarbazone)** exerts its anti-neoplastic effect through the inhibition of the enzyme ribonucleoside diphosphate reductase, effecting both DNA and RNA synthesis[390]. **O6-Methylguanine** is derivative of guanine is formed through the

alkylation of guanine on the position 6 oxygen through the action of alkylating agents such as temozolomide.The resultant biological effect is the initiation of DNA base mismatch repair and cell death through apoptosis[391, 392]. **4-Ipomeanol** is a naturally occuring phytoalexin prodrug, which when it undergoes metabolism by CYP4B1. It forms a highly reactive DNA alkylating agent capabile of causing DNA-protein cross link sand DNA strand breaks, ultimately resulting in apoptotic cell death[393]. **Dichloroallyl lawsone** is a potent pyrimidine biosynthesis inhibitor through action on dihydroorotate dehydrogenase, a key enzyme in the *de novo* pyrimidine biosynthetic pathway[385]. **Triazinate** is a triazine based antifolate drug which (similar to methotrexate) interferes with malignant cell growth through the inhibition of dihydrofolate reductase (DHFR) and subsequent nucleotide biosynthesis[394]. **Tamoxifen** is a nonsteroidal selective estrogen receptor modulator which inhibits the DNA synthesis and cellular response to estrogen through binding to the estogen receptor, preventing the activation of the estrogen response element expressed on cellular DNA[395]. **Diglycoaldehyde** is an inosine oxidation derivative causes potent inhibition of RNA (through termination of growing RNA strands/ RNA strand template interference) and DNA (due to ribonuclease reductase inhibition) synthesis[396, 397]. **2-Deoxycoformycin (Pentostatin)** is an antimetabolite, purine nucleotide analogue used in the treatment of haemaological malignancies.It exerts its anticancer action through the inhibtion of the enzyme adenine deaminase, which plays a central role in purine metabolism.It becomes incorporated into DNA and RNA, leading to S-phase specific cell-cycle arrest[398, 399]. **Caracemide** is derived from acetohydroxamic acid and it mediates its antineoplastic effect through the inhibition of the enzyme ribonuclease reductase, leading to subsequent decrease in tumour growth through decreasing DNA synthesis[400]. **Fluorodopan** is an antineoplastic agent. It is a monofunctional alkylating agent which acts by alkylating DNA base guanine on the position 7 nitrogen resulting in cytotoxicity, thereby damaging DNA and interfering with DNA replication and cell division[401]. **Hydroxyurea** is an antimetabolite with a hydroxycarbamate structure that can selectively inhibit the enzyme ribonucleoside diphosphate reductase, resulting in cell-cycle arrest in the G_1/S Phase and through DNA interference[402]. **Melphalan** is a nitrogen mustard derivative of phenylalanine. It mediates its cytotoxic effect by alkylation of the nitrogen atom at position 7 of guanine.This leads to DNA strand crosslinkage taking place, and subsequent inhibition of DNA and RNA synthesis. **Pyrimidine-5-glycoaldehyde** is a compound that mediates its proapoptotic effect on cancer cells through the inhibition of the enzyme ribonuclease reductase[403].

Glyoxylic acid is an experimental small molecule is thought to act through targeting of the metabolic ATP cascade through enzymes such as malate synthase G, isocitratelyase and 4-hydroxy-4-methyl-2-oxoglutaratealdolase[404]. **(Carboxyphthalato)platinum** is a second generation derivative of platinum anticancer agents exerts its cytotoxic effect through the classic mechanism of action of platinum chemotherapeutics such as cisplatin. These involve cancer cell uptake, formation of the active aquated species, subsequent crosslinkage of DNA through covalent bond formation, followed by apoptosis[405, 406].

Based on the correlated chemotherapeutic agents which have fair to strong positive Pearson correlation coefficients (0.34-0.92), experiments to assess these compounds effects on DNA and/or RNA synthesis (focused on key enzymes such as ribonuclease reductase) and cell-cycle analysis to confirm specific phase of cellular arrest would be of particular interest. Furthermore, investigation of potential DNA binding (covalent bond formation), evidence of DNA crosslinkage and DNA strand breaks would be warranted given the vast majority of positively correlated chemotherapeutic agents mediating cytotoxicity through affecting DNA synthethic pathway and resultant DNA functionality (whether through direct or indirect downstream effects) .

3.4 Lactate dehydrogenase (LDH) cytotoxicity assay

The lactate dehydrogenase (LDH) assay (Thermo Scientific™ Pierce™ LDH Cytotoxicity Assay Kit) is a straightforward colorimetric assay used to assess membrane integrity of cells as a function of cytoplasmic LDH released. LDH is a cytosolic mammalian enzyme present in cells, retained intracellularly by the plasma membrane. The loss of cell membrane integrity (due to cytotoxic insult) is detectable through LDH release into the cell growth medium. The assay is initiated by the reduction of cellular co-factor NAD^+ to NADH catalysed by LDH enzyme. Newly formed NADH catalyses the acidic reduction of the tetrazolium salt iodonitrotetrazolium (INT) to the highly coloured formazan (red) (mediated by the diaphorase enzyme). The degree of LDH released is proportional to formazan concentration and this can be measured spectroscopically[407, 408] (Figure 194). The LDH assay lysis solution was used to quantify formazan concentration at 100% cell lysis.

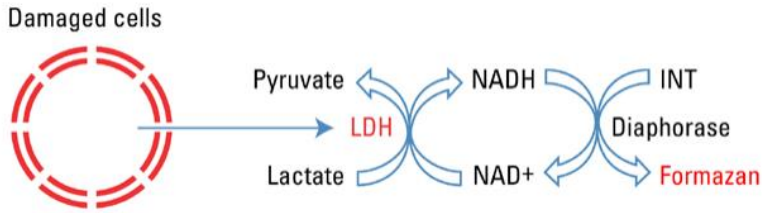

Figure 193: Process for formazan formation during LDH assay[409]

A 96 well plate was seeded with $2x10^5$ cells/well and treated with 10 µM and 1 µM of the desired drugs and relevant spontaneous (sterile water-only) and maximum LDH activity controls for a predetermined time frame of 24 h. After treatment and incubation, 50 µL of each sample medium was then placed in a new 96 well plate and 50 µL LDH reaction mixture was added to each sample. The plate was protected from light and incubated at RT for 30 min. The reaction was terminated by addition of 50 µL of LDH stop solution to each well. The absorbance of each sample was obtained at 490 nm and 690 nm respectively. Individual sample values were obtained by subtracting the measurement at 690 nm from the corresponding primary measurement at 490 nm. The lysis solution wells were used to represent cells at 100% lysis and by comparing this to the treated wells minus the background LDH reading of the media; the percentage of LDH released and hence cytotoxicity, was calculated as per the formula displayed in Figure 195. A vehicle control of 1% (v/v) DMSO was also included. The assay was conducted in triplicate on two independent days.

$$\% \text{ Cytotoxicity} = \frac{\text{Compound-treated LDH activity} - \text{Spontaneous LDH activity}}{\text{Maximum LDH activity} - \text{Spontaneous LDH activity}} \times 100$$

Figure 194: Method of calculating percentage cytotoxicity *via* LDH release

3.4.1 *In vitro* LDH cytotoxicity investigation of select lead compounds (24, 86, 133, 156

The results for LDH cytotoxicity assay for compounds **(24, 86, 133, 156)** (Figure 197) (which were representative of the most potent compounds identified in preliminary biochemical screening) in HG-3 cell lines are shown in Figure 196. At the 10 µM treatment concentration, compound activity ranged from mild to moderate cytotoxicity

(19-47%). **(156)** displayed the lowest LDH release at 19%, then **(86)** with 25%, **(24)** with 33% and **(133)** with the highest value of 47%. At the lower treatment concentration of 1 µM, cytotoxicity remains mild to moderate with an observed range of 12-37%. Similar to the higher 10 µM treatment concentration, **(156)** displays the lowest % LDH release at 12%, then **(24)** with 19%, followed by **(86)** with 22% and **(133**) with the largest value at 37%.

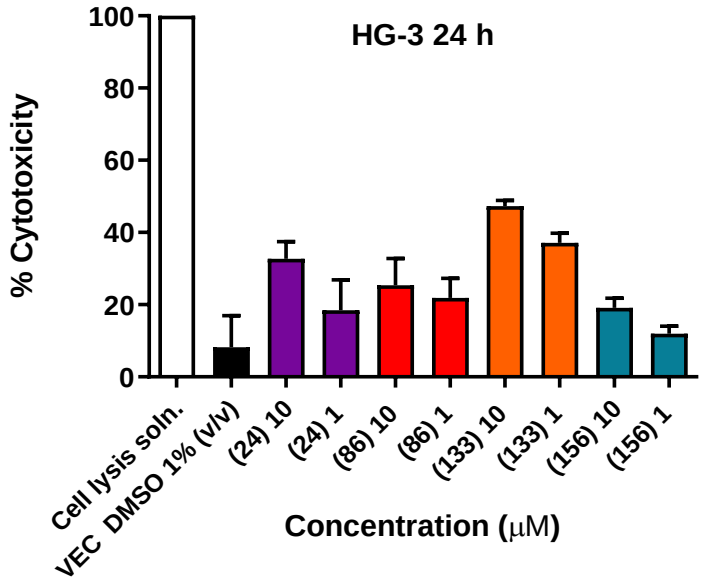

Figure 195: LDH assay results for compounds (24, 86, 133, 156) in the HG-3 cell line (Cell lysis soln.=100 % cell lysis and LDH release, n=2)

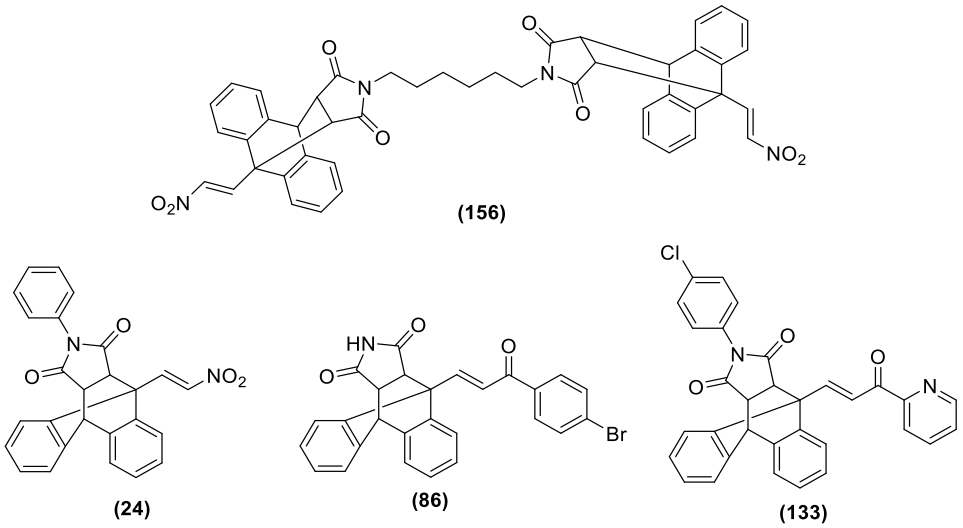

Figure 196: Compounds investigated for cytotoxicity in HG-3 and PGA-1 cell lines using LDH assay (24, 86, 133, 156)

The results for LDH cytotoxicity assay results for compounds **(24, 86, 133, 156)** (Figure 197) in PGA-1 cell lines are shown in Figure 198. At the 10 µM treatment concentration, compound activity ranged from low to mild cytotoxicity (9-23%). **(24)** displayed the lowest LDH release at 9%, then **(133**) with 15%, **(156)** with 19% and **(86)** with the highest value of 23%. At the lower treatment concentration of 1 µM, cytotoxicity remains low to mild with a range of 4-18% observed. In contrast to the higher 10 µM treatment concentration, **(86)** displays the lowest % LDH release at 4%, then **(133)** with 5%, followed by **(24)** with 9% and **(156)** with the largest value at 18%.

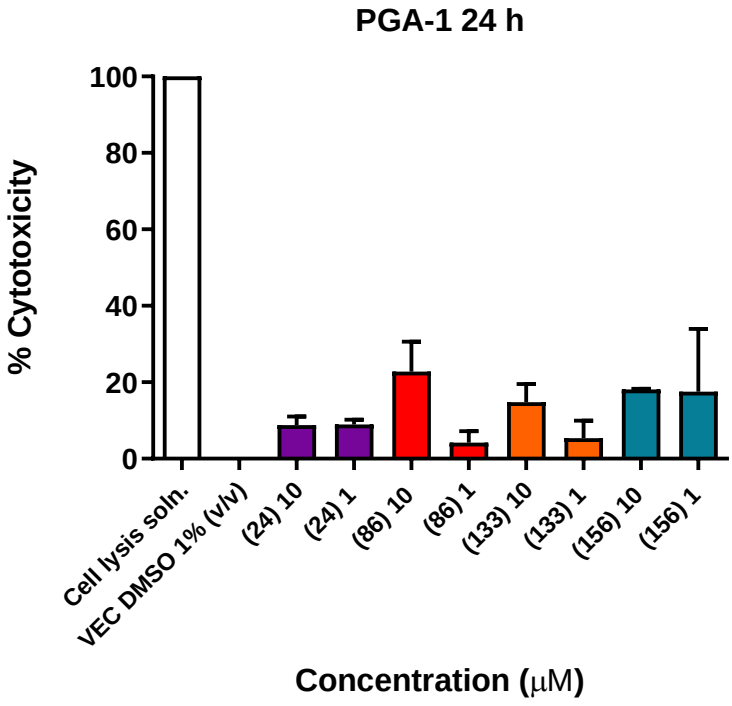

Figure 197 : LDH assay results for compounds (24, 86, 133, 156) in the PGA-1 cell line (Cell lysis solution=100 % cell lysis and LDH release, n=2)

In summary, the compounds **(24, 86, 133, 156)** were found to be of low to moderate toxicity across both HG-3 and PGA-1 CLL cell lines. Furthermore, this supports further investigation of these lead compounds and related adducts due to reduced potential for membrane rupture and necrosis (which can cause detrimental clinical syndromes such as tumour lysis syndrome[410] if advanced to preclincial animal testing). Interestingly, the assessed compounds were observed to cause a greater degree of LDH release from HG-3 cells compared to PGA-1, suggesting greater cytotoxicity against more aggressive variants of CLL.

3.5 Investigations into potential pro-apoptotic effects of select lead compounds- FITC Annexin V / PI FACS analysis

FITC (fluorescein isothiocyanate) Annexin V / PI (propidium iodide) FACS (fluorescence activated cell sorting) analysis was used to characterise the mode of cellular death induced by the compounds tested. In healthy cells, phosphatidylserine (PS) is restricted to the cytoplasmic surface of the plasma cell membrane. In apoptotic cells, PS translocates from this inner cell membrane to outer surface, where PS exposure acts as a signal mediator of cell phagocytosis[411-413]. Annexin V is a human cellular protein with proposed placental anticoagulant activity and is known to exhibit phospholipase A2 and protein kinase C inhibitory actions[414]. Moreover, Annexin V has a high binding affinity for PS. Once labelled with a specific fluorophore of known emission wavelength or colour, Annexin V can be used to identify apoptotic cells by binding to PS in a calcium-dependent manner on the outer surface of the plasma cell membrane. PI (propidium iodide) is a nucleic binding dye that stains dead cells with red fluorescence and PI cannot permeabilise an intact cellular membrane or stain healthy cells. Four populations are produced during the assay Annexin V and PI negative (Q4, healthy cells), Annexin V positive and PI negative (Q3, early apoptosis), Annexin V and PI positive (Q2, late apoptosis) and Annexin V negative and PI positive (Q1, necrosis). These populations can be easily identified and quantified using a BD Accuri™ C6 Plus Flow Cytometer (BD Biosciences) flow cytometer[415, 416]. An example of the quadrant diagram generated by compound **(21)** at 10 µM in HG-3 cells is illustrated in Figure 199 below.

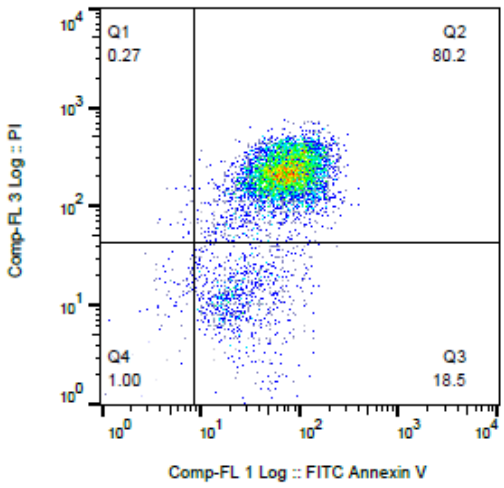

Figure 198: Flow cytometry output of Annexin V / PI FACS analysis of compound (21) at 10 µM treatment concentration in HG-3 cells

For the purpose of the analyses carried out in the present work, apoptosis was assessed as % total apoptosis. This was achieved through the addition of early and late apoptosis in quadrant 3 (Q3) and quadrant 2 (Q2) respectively. Untreated cells and vehicle treated cells acted as experiment controls with the exact treatment concentrations used varying depending on the compound class tested (either 10 µM and 1 µM, or 10 µM, 5 µM, 1 µM). The experiment was carried out as individual replicates on three independent days.

3.5.1 Investigation of mode of cell death induced by most potent (*E*)-9-(2-nitrovinyl)anthracenes (Series 1)

The following results from Annexin V/ PI studies of the lead (*E*)-9-(2-nitrovinyl)anthracene compounds **(10, 7**, **21**, **8**) (Figure 202) are shown in Figures 200 and 201. The treatment concentrations assessed were 10 µM and 1 µM. In HG-3 cells, all compounds tested produced a marked proapoptotic effect (Figure 200). **(8)** (10-ethyl) caused the greatest apoptotic response at 10 µM at 74%, followed by **(7)** (10-methyl) and **(21)** (10-isopropyl) producing 70% and 69% total apoptosis respectively. **(10)** (10-methoxy) produced the lowest pro-apoptotic response at the 10 µM with 54% total apoptosis. The observed results in the CLL cell lines HG-3 and PGA-1 suggest that these compounds act by a pro-apoptotic mechanism of action, with higher amounts of apoptosis being observed at the higher treatment concentrations (10 µM).

In initial studies in PGA-1 cells, all compounds tested produced a marked proapoptotic effect with **(7)** (10-methyl derivative) and **(8)** (10-isopropyl derivative) producing 80% and 82 % total apoptosis respectively, followed by **(21)** (74%). **(10)** produced the lowest pro-apoptotic response at 10 µM with 52% total apoptosis (Figure 201).

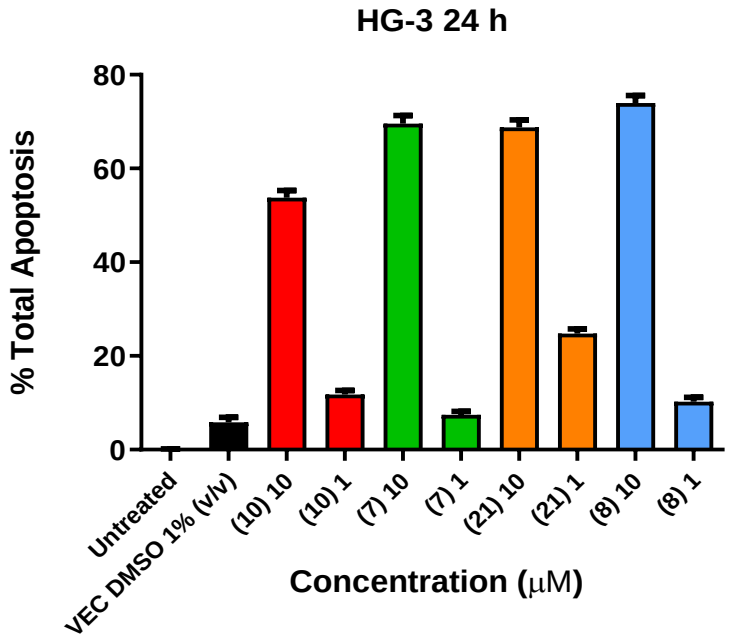

Figure 199: Proapoptotic activity of (*E*)-9-(2-nitrovinyl)anthracenes in HG-3 cell line (n=3)

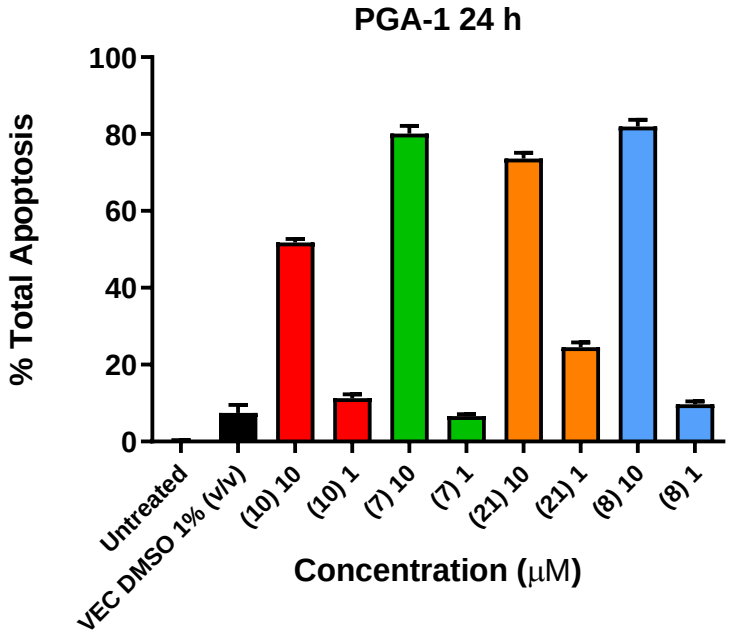

Figure 200: Total apoptosis induced by (*E*)-9-(2-nitrovinyl)anthracenes in PGA-1 cell line (n=3)

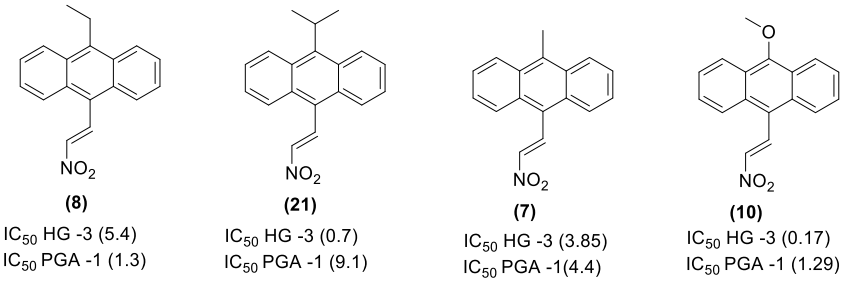

Figure 201: (*E*)-9-(2-nitrovinyl)anthracenes (8, 21, 7, 10) and associated IC_{50} values (µM) in HG-3 and PGA-1 cell lines

Across both cell lines, alkyl substitution at position 10 of the anthracene core was observed to lead to more favourable pro-apoptotic action in CLL cell lines at the 10 µM. The noticeable decrease in apoptosis with the introduction of an oxygen atom in the form of a methoxy group at position 10 in **(10)**, compared to the alkyl side-chain of **(8)** suggests the potential role of hydrophobic groups in favourable biological activity (30% activity decrease in PGA-1, 20% activity decrease in HG-3). This was in contrast to the 1 µM treatment concentration where **(21)** was the most potent compound by a 14% margin in total apoptosis induced (25% apoptosis), followed by **(10)** (11% apoptosis). Furthermore, with decreasing steric bulk of the hydrophobic alkyl group, there was a decreasing pro-apoptotic trend (**21** [isopropyl] > **8** [ethyl] > **7** [methyl]) at the lower compound concentration.

3.5.2 Investigation of mode of cell death induced by select potent ethanoanthracene nitrovinyl and chalcone derivatives (Series 2-9)

The following results are Annexin V/ PI studies of representative potent lead ethanoanthracene compounds **(24**, **86**, **133**, **156, 5)** (Figure 204). The treatment concentrations assessed were 10 µM, 5 µM and 1 µM.

In HG-3 cells, all compounds produced significant apoptosis that was observed to be largely concentration-dependent (Figure 203). At the 10 µM concentration, the most active compounds were **(86)** (95% total apoptosis, 4-bromo, maleimide) and **(24)** (95%, N-phenylmaelimide, nitrostyrene). The next most potent were **(133)** (93% apoptosis, 2-pyridyl, p-chlorophenylmaleimide) and **(5)** (93%, anthracene nitrostyrene), **(156)** (82%, nitrostyrene dimer). The dimer compound **(156)** was the least effective with 82% apoptosis induced. With the 5 µM treatment concentration, **(24)** was the most potent pro-apoptotic compound (94% total apoptosis) and followed closely in activity by **(133)** (93%

total apoptosis). **(156)** was the next most effective compound showing 82% apoptosis and chalcone ethanoanthracene **(86)** had a similar activity of 80% apoptosis. The least potent pro-apoptotic agent at the 5 µM concentration was **(5)** (unsubstituted nitrostyrene) with 69% apoptosis. At the lowest treatment concentration of 1 µM, the most potent pro-apoptotic agents noted were the nitrostyrene derivatives **(24)** and **(156)** (both compounds causing 82% total apoptosis). Compound **(133)** was the next most biologically active, causing 37 % apoptosis. Chalcone ethanoanthracene **(86)** and nitrostyrene derivative **(5)** were the least potent compounds at the 1 µM treatment concentration with 33% and 21% apoptosis respectively being observed.

A similar trend is observed in HG-3 cells with chalcone based ethanoanthracenes **(86)** (4-bromo, maleimide) and **(133)** (2-pyridyl, *p*-chloromaleimide) and the nitrostyrene **(5)** causing apoptosis in a concentration dependent manner as was shown in PGA-1 cells. Interestingly, **(24)** (*N*-phenylmaleimide, nitrostyrene) appears to have the opposite activity trend in HG-3 cells than in PGA-1 cells, increasing apoptosis with decreasing compound concentration. A possible explanation for this unusual observation could be potential solubility issues at higher concentrations. Furthermore, for the nitrostyrene dimer **(156)**, apoptotic activity remained constant across all three concentrations, due to its low IC_{50} value of 0.17 µM in HG-3 cells (Figure 203).

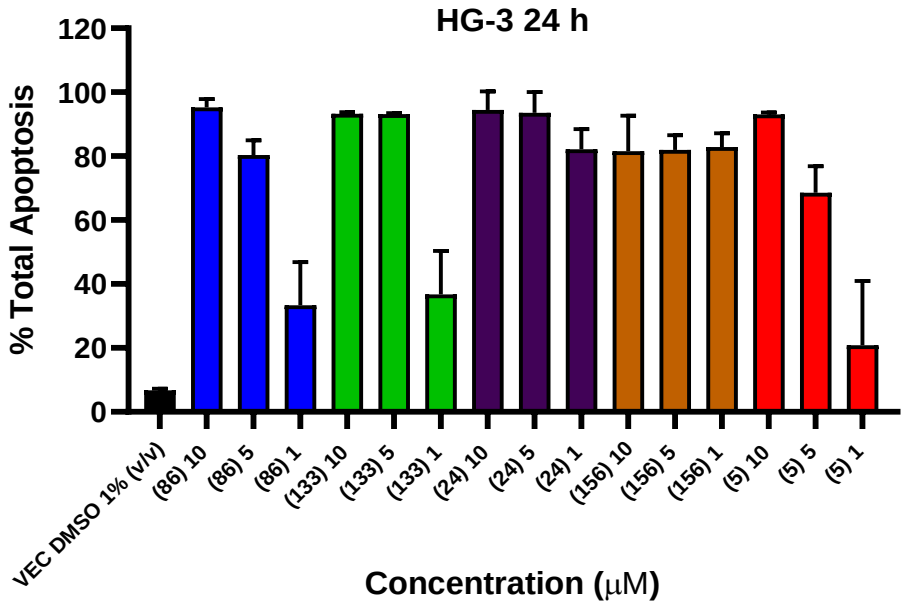

Figure 202: % Total apoptosis of compounds (24, 86, 133, 156, 5) at the treatment concentrations 10 µM, 5 µM and 1 µM in HG-3 CLL cells (n=3)

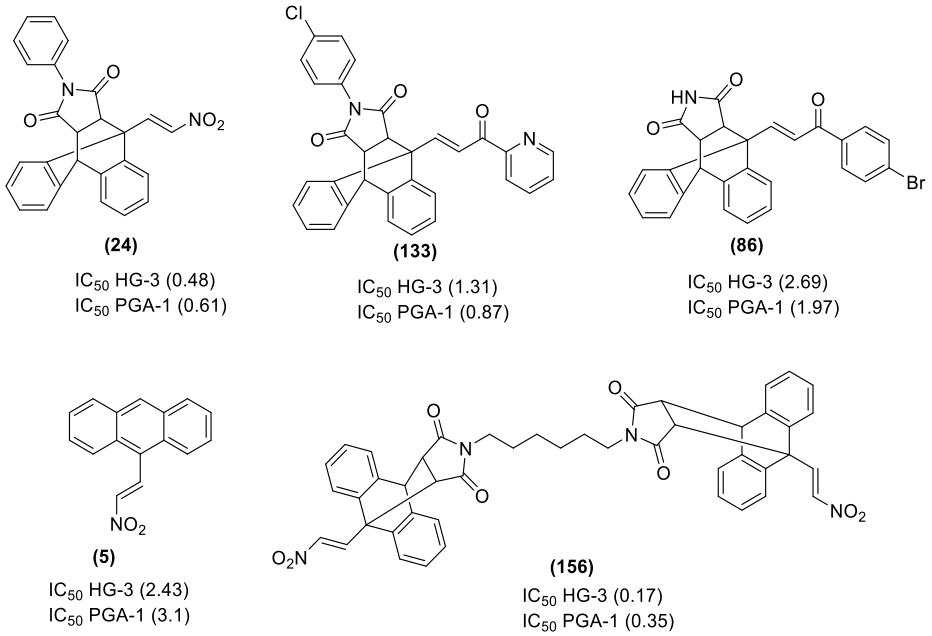

Figure 203: Representative potent compounds (24, 86, 133, 156, 5) assessed for pro-apoptotic activity in CLL cell lines and associated IC_{50} values (µM) in HG-3 and PGA-1 cell lines

In PGA-1 cells, all compounds produced significant apoptosis that was observed to be concentration-dependent (Figure 205). At the 10 µM treatment concentration, **(24)** (*N*-phenyl nitrostyrene) induces the highest amount of apoptosis (97% total apoptosis) along with **(5)** (94%, anthracene nitrostyrene) and **(86)** (89%, 4-bromo, maleimide). Compound **(156)** was the next most potent inducer of apoptosis (88% apoptosis, nitrostyrene dimer), with **(133)** displaying the lowest effect at the 10 µM concentration (87%). With the 5 µM treatment concentration, **(24)** displayed the most pro-apoptotic cell death (97%), followed by **(156)** (87%) and **133** (86%). Compound **(86)** (4-bromo, maleimide derivative) was the next most potent inducer of apoptosis at 71% and **(5)** was the least effective at the 5 µM treatment concentration with 67% apoptosis observed. At the lowest concentration tested of 1 µM, the nitrovinyl compounds **(24)** and **(156)** produced the highest amount of apoptosis (83% and 76% respectively), then **(133)** (60%) and **(86)** (42%). Compound **(24)** was the lowest performing at the 1 µM treatment concentration with 40% apoptosis induced. With chalcone based ethanoanthracene **(133)** and nitrovinyl ethanoanthracene **(24)**, the amount of cellular apoptosis is maintained with decreasing treatment concentration from 10 µM to 5 µM. However, at 1 µM, a notable drop off in activity is observed. This is in contrast to the steady decrease of pro-apoptotic activity induced by **(86)** proportional to drug concentration.

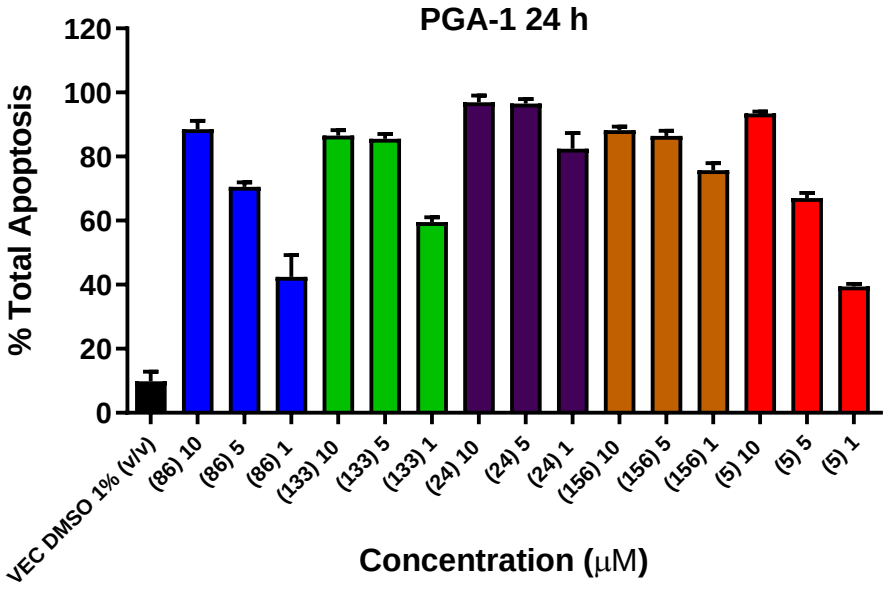

Figure 204: % Total apoptosis of compounds (24, 86, 133, 156, 5) at the treatment concentrations 10 µM, 5 µM and 1 µM in PGA-1 CLL cells (n=3)

In summary, across both cell lines compounds **(24, 86, 133, 156, 5)** (Figure 204), induce significant apoptosis in a largely concentration dependent manner and would warrant further investigation e.g. cell cycle analysis. Hence, these results support a pro-apoptotic mechanism of action with the trend of greater degree of apoptosis being experienced at higher treatment concentrations (10 µM) in CLL cell lines HG-3 and PGA-1 (Figures 203 and 205).

3.6 *Ex vivo* assessment of selected compounds (24, 86, 133) in donor peripheral blood mononuclear cells (PBMCs)

Representative examples of the most potent compounds of (*E*)-9-(2-nitrovinyl)-9, 10, 11, 15-tetrahydro-9,10-[3,4]epipyroloanthracene-12,14-diones and 9-(*E*)-3-oxo-3-phenylprop-1-en-1-yl)-9,10-dihydro-9,10-[3,4]epipyrroloanthracene-12,14-diones (**24**, **86**, **133**) were assessed in collaboration with Prof. Tony Mc Elligott (Trinity Translational Medicines Institute-Molecular Haematology) in St. James's Hospital Dublin. This testing involved working with whole blood samples from healthy donors and was conducted with the approval of the Tallaght University Hospital / St. James's Hospital Joint Research Ethics Committee. The PBMCs from five donors were isolated, prepared and treated as per the protocol described below.

Peripheral Blood Mononuclear Cells (PBMCs) were isolated from CLL patients by density gradient centrifugation using Lymphoprep® (Axis-Shield, UK). The blood samples were diluted by adding an equal volume of RPMI (1:1 ratio) and layered on top of Lymphoprep maintaining a relative ratio of 2:1 (diluted whole blood : Lymphoprep). The tubes were capped and centrifuged at 800x*g* with no brake for 30 minutes at room temperature. After centrifugation, the cells were removed from the sample/medium interface using a Pasteur pipette. The isolated PBMCs were then rinsed three times using wash buffer (diluted 1:1 with RPMI without FBS) being centrifuged at 400x*g* for 10 minutes at RT per wash. The cells were then resuspended in RPMI media containing 10% FBS, 1% penicillin/streptomycin (P/S). The cells were then counted using a haemocytometer and seeded into 96 well plates at a density of 100,000 cells/well (200 µl) and were left to incubate at 37°C for 1 h prior to compound treatment. The Annexin V/ PI assay was used as a preliminary method of assessing selective toxicity of the above compounds when compared with previous FACS testing in CLL lines.

Percentage total apoptosis observed in the treatment of isolated donor PBMCs with compound **(133)** (normalised against vehicle 0.5% v/v DMSO) is illustrated in Figure 206. Compound **(133)** was observed to be only moderately toxic to healthy donor PBMCs when treated at the highest concentration of 5.00 µM (%). This was in contrast to the relatively low toxicity (12-16%) experienced at the concentrations representative of the compounds IC_{50} values in both HG-3 and PGA-1 CLL cell lines which were 1.31 µM and 0.87 µM respectively. The dose response behaviour was noted to follow general concentration dependent trend, with reduced apoptotic cell death as treatment concentration decreased.

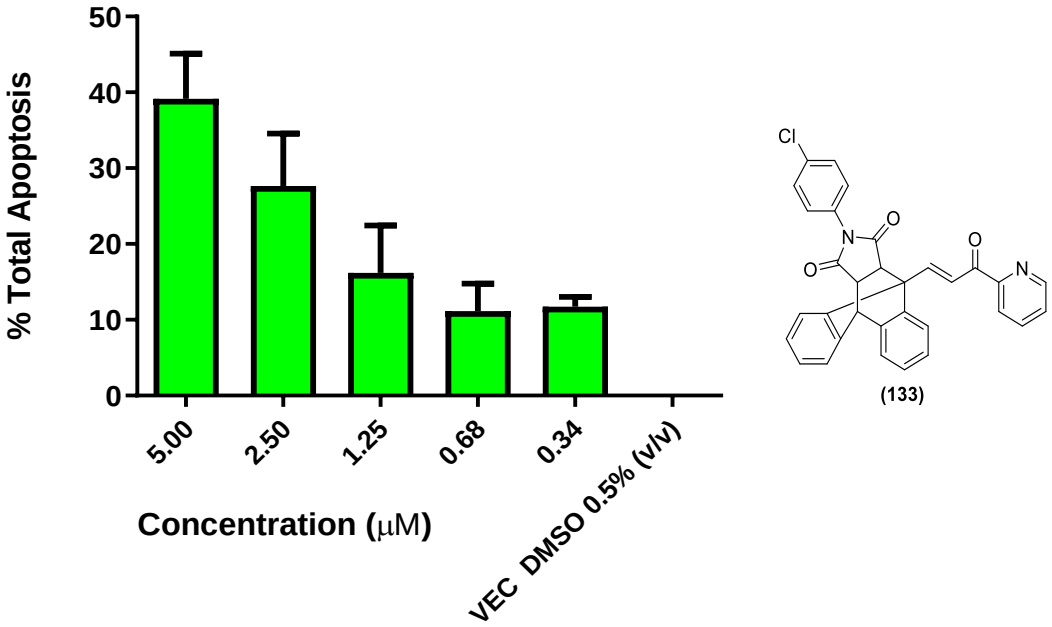

Figure 205: Percentage total apoptosis observed on treatment of isolated donor PBMCs with compound (133) (normalised against vehicle 0.5% (v/v) DMSO) and (133) chemical structure

Percentage total apoptosis observed in the treatment of isolated donor PBMCs with compound **(24)** (normalised against vehicle 0.5% (v/v) DMSO) is llustrated in Figure 207. **(24)** exhibited similar behaviour in PBMC testing, having moderate toxicity towards the healthy donor lymphocytes at the highest concentration tested of 1.25 µM. When compared to the IC_{50} values in both HG-3 and PGA-1 CLL cell lines of 0.48 µM and 0.61 µM respectively, relatively low-moderate amounts of apoptotic death in healthy cells was noted (10-35% at 0.34 and 0.68 µM). Like **(133)**, **(24)** followed a general dose response behaviour that was concentration dependent, with reduced apoptotic cell death as treatment concentration decreased.

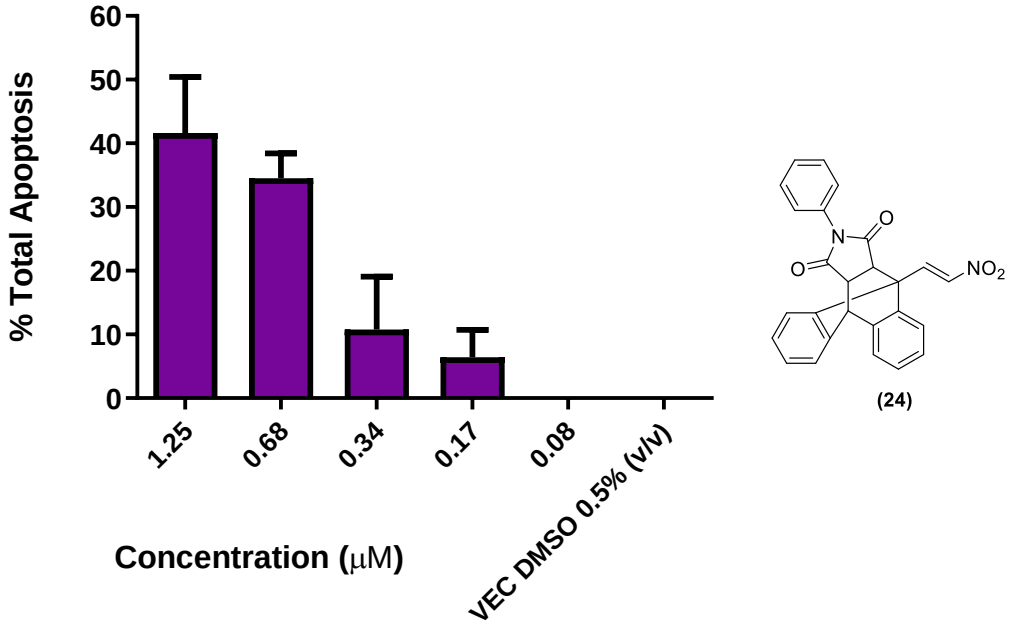

Figure 206: Percentage total apoptosis observed on treatment of isolated donor PBMCs with compound (24) (normalised against vehicle 0.5% (v/v) DMSO)

Percentage total apoptosis observed in the treatment of isolated donor PBMCs with compound **(86)** (normalised against vehicle 0.5% (v/v) DMSO) is illustrated in Figure 208. **(86)** was noted to exhibit the lowest toxicity of the three compounds evaluated to healthy donor PBMCs at its highest treatment concentration of 5 µM with an observed total apoptosis of 28%. When these results were compared to the IC_{50} values in both HG-3 and PGA-1 CLL cell lines of 2.69 µM and 1.97 µM respectively, very low amounts of lymphocyte cell death were detected (5-14 % at 1.25-2.5 µM). Like **(133)** and **(24)**, **(86)** followed a general dose response behaviour that was concentration dependent, with reduced apoptotic cell death as treatment concentration decreased. An exception to this trend was noted at the lower concentration of 0.34 µM.

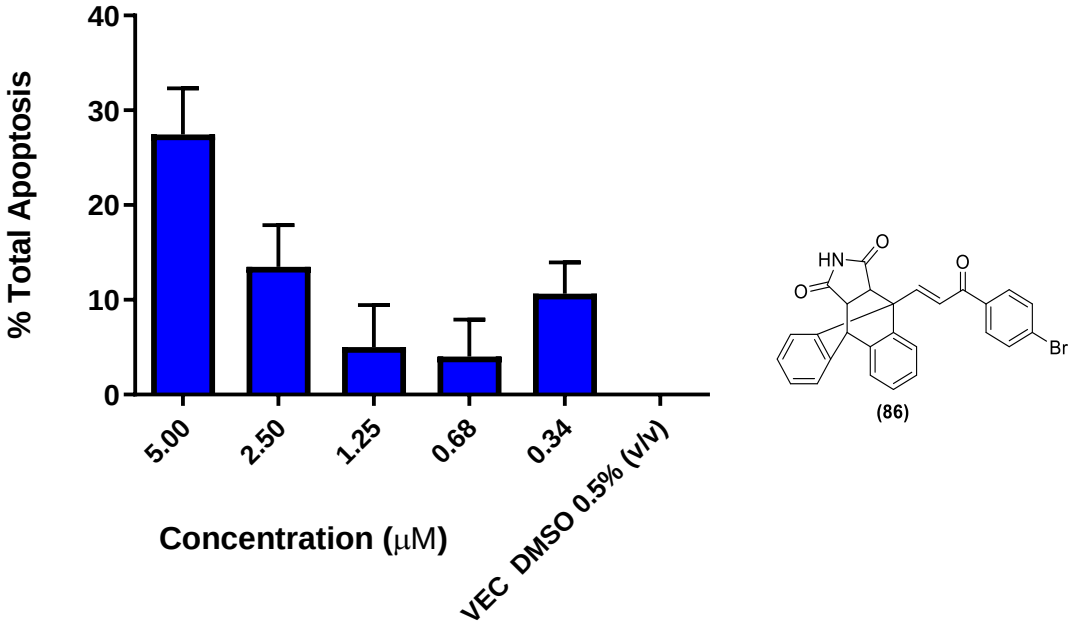

Figure 207: Percentage total apoptosis observed on treatment of isolated donor PBMCs with compound (86) normalised against vehicle 0.5% (v/v) DMSO)

3.7 ROS (Reactive Oxygen Species) cell viability assays to investigate dependence of compound biological activity on ROS flux

Reactive Oxygen Species are a broad class of reactive intermediates that are formed through sequential loss of one electron from molecular oxygen producing water molecules as a by-product of cellular aerobic respiration. These transient metabolic by-products include hydrogen peroxide, superoxide, singlet oxygen and the hydroxyl radical among others [417]. In addition to these, similar reactive nitrogen intermediates (RNI) are generated which can affect ROS levels such as peroxynitrile and nitric oxide radicals.

Sources of such reactive species can be broadly classified into two main groups:

- Endogenous sources
- Exogenous sources

Endogenous sources include peroxisomes, mitochondria as well as a range of other cytosol based enzymatic systems like the Cytochrome P450 family and NADPH oxidases involved in normal intracellular metabolism. Whereas, in contrast, exogenous sources are those generated as a result of external influences on cellular homeostasis including xenobiotics, ionizing radiation, UV light and environmental pollutants[418]. In low

concentrations, ROS act as intracellular signalling molecules and secondary messengers, playing a central role in the maintenance of cellular homeostasis, immune system modulation and cell development including the cell cycle, cellular differentiation and cell death e.g. apoptosis [419].

This highly regulated redox balance is controlled through catabolic antioxidant defence mechanisms the principal of which are:

- Catalase- This tetrameric heme protein is a metalloprotein oxidoreductase, converts hydrogen peroxide into less harmful oxygen and water. It is mostly confined to peroxisomes and exist in both membrane associated and soluble forms[420, 421].
- Superoxide Dismutase (SOD)- This detoxification enzyme is involved in the catalysis of superoxide anion conversion to hydrogen peroxide and molecular oxygen. The reaction (dismutation) consists of simultaneous oxidation and reduction. Depending on the SOD isotype and location, the enzyme can be associated with either copper and zinc (cytoplasm and extracellular SOD 1, SOD 3 respectively) or manganese (mitochondria SOD 2)[422-424].
- Glutathione (GSH)- This tripeptide cellular thiol is one of the central antioxidant and radical scavenging species in the cellular environment. Glutathione [also known as (γ-L-glutamyl-L-cysteinylglycine)] is synthesised from a two-step ATP dependent process, combining glycine, cysteine and glutamic acid. It is predominantly present in its reduced form intracellularly (approximately 98%), with the rest existing in a dimeric oxidised GSSG form, with GSH/GSSG ratios ranging from 30:1 to 100:1 depending the cellular environment[425, 426].
- Thioredoxins (Trx)- Apart from glutathione based redox systems, thioredoxins represent the other major thiol-dependent antioxidant modulators in the cellular environment. In mammalian cells, two main type exist; Txr1 (located in the cytosol) and Txr2 (located in the mitochondria)[427]. This reductase family of enzymes are responsible for maintaining the balance of disulphides/dithiols in proteins through the provision of electrons to thiol-dependent peroxidases, which then rapidly eliminate reactive nitrogen and oxygen species[428, 429].
- Peroxiredoxins- These subclass of reductive enzymes are a family of peroxidases which catabolise hydrogen peroxide and other organic peroxides in a thiol-dependent manner. Furthermore, the redox state of the cysteine residues at their

catalytic site is closely regulated by the thioredoxin / thioredoxin reductase system. In mammals, there exist six different isotypes (Prx I–VI)[430, 431] :

- Prx1, Prx2 are localised in the cytoplasm and nucleus
- Prx3 in the mitochondria
- Prx4 in the endoploasmic reticulum
- Prx5 associated with cytosol, peroxisomes and mitochondria
- Prx6 in the cytosol

- Methionine Sulfoxide reductases (Msr)- These antioxidant enzymes, through the acceptance of electrons provided by the thioredoxin system, are responsible for the stereospecific reduction of methionine sulfoxides to corresponding methionines. As a result, they can restore the functions of affected protein residues and transform free methionines to their original state that have been altered by oxidative stress. The enzymes exist as three distinct subclasses:

- MsrA- responsible for the reduction of methionine-*S*-sulfoxide and located in the mitochondria
- MsrB- responsible for the reduction of methionine-*R*-sulfoxide and can be divided into MsrB1,MsrB2 and MsrB3 respectively
- fMsr- reduces free methionine-*R*-sulfoxide

In addition, catabolism of ROS is accomplished through ROS non-enzymatic based small molecules such as ascorbate (Vitamin C) or α-tocopherol (Vitamin E) acting as a renewable buffer to neutralise these highly reactive intermediates and limit any potential damage as a result[432-434].

3.7.1 ROS and Cancer

While ROS contributes to normal metabolic functioning (regulation, growth and function of healthy cells, inflammation and prevention of tumourigenesis), they are likewise pivotal in the cancer cell development, adaptation and progression[435, 436]. It is believed that through the exploitation of conventional cellular machinery, cancer cells generate consistently higher amounts of ROS through hypermetabolism relative to their non-transformed counterparts through the combination of metabolic, genetic and tumour microenvironment modifications. In terms of pro-tumorigenic metabolic changes, the

vast majority involve bioenergetic pathways found in the synthesis of essential cellular components such as nucleotides and fatty acids. One of the most famous cases of metabolic programming involved in many cancers is that of aerobic glycolysis or the "Warburg Effect" (Figure 209). First observed by Nobel laureate Otto Heinrich Warburg and colleagues in 1924, cell glycolysis and lactate production continues in the tumour cells independent of oxygen levels present in the microenvironment[437]. While first observed more than 95 years ago and thousands of papers researching its purpose are published, no one prevalent theory of this phenomenon's function has been established[438].

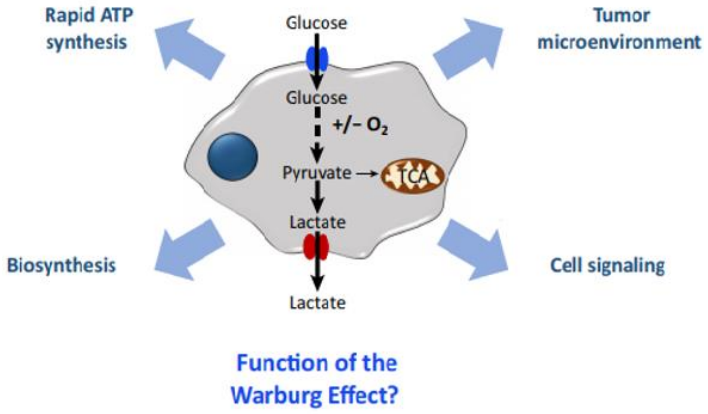

Figure 208: The Warburg effect and associated hypotheses[439]

Four of the main working theories considered in the current scientific literature are:

1. **Rapid ATP (Adenosine Triphosphate) synthesis:** Preference for the inefficient glycolytic pathway of aerobic glycolysis is supported through theoretical studies into evolutionary game theory such as Slavov et al. which estimate a lower yielding, yet increase rate of ATP output[440]. From this, a potential selective advantage could be conferred on such malignant cells. This is further supported by studies by Shestov et al. and Epstein et al. which show a far greater rate of ATP production per unit time using in cancer cells using aerobic glycolysis as well as this form of rapidly accessible energy being harnessed preferentially in periods of heavy metabolic activity, while oxidative phosphorylation (OXPHOS) rate remains constant[441, 442].

2. **Biosynthesis:** Driven by selective activation of oncogenes such as HER2 (Human Epidermal Growth Factor 2) in breast cancer, this theory proposes that the Warburg effect is a selective adaptation which acts indirectly as a fast-tracked carbon source for related biosynthetic pathways (nucleotides, fatty acids and proteins) governing the production of the molecular building blocks necessary for unhindered cellular proliferation[443-445]. This has been documented in tissue cultured cells *via* PET (Positron Emission Tomography).

3. **Tumour microenvironment**: In the presence of multiple cellular types, the Warburg effect is thought to confer a selective advantage to the growth of malignant cells through the establishment of an acidotic state. This would be through elevated glucose metabolism and subsequent lactate and proton secretion, lowering the pH of the local cellular microenvironment[446], with the cancer cell itself maintaining a slightly alkaline intracellular pH.

   Observable impacts were increased cancer cell mobility and migration through extracellular matrix remodelling mediated by tumour associated macrophages and fibroblasts, induced changes cell polarisation and altering of tumour-stroma cell interactions[447]. Additionally, it has been noted that tumour infiltrating lymphocytes (TILs) directly compete for glucose utilization with tumour cells, thus having a significant impact on anti-malignant immune system response, further promoting cancer cell expansion[442]. Thus, this preferential environmental engineering promotes immune cell evasion and provides an ideal support structure to facilitate malignant cell growth/expansion[448].

4. **Cell signalling-** The final proposed function of the Warburg effect is the provision of a means of cell signalling to tumour cells. The first of the two main mechanisms documented in the literature would be control of the generation and flux of ROS[449, 450].

As previously mentioned, a delicate balance exists between the ROS levels that promotes tumorigenesis / drives proliferation and those that can be catastrophic to a cellular viability[451, 452]. As a result of the excessive metabolic demands of tumour cells, the potential for ROS generation vastly increases as the majority of ROS is generated

by the activity of mammalian mitochondria through the activity of the electron transport chain[453, 454].

One of the most important factors that determines a cell's redox capacity is maintenance the cofactor ratio of NADH/NAD^+. Normally, cells can regenerate NAD^+ through the action of the malate-aspartate shuttle however when capacity of this system is exceeded, this balance become skewed towards NADH and excessive ROS generation. In cancer cells, this is combatted through the conversion of pyruvate to lactate via lactate dehydrogenase, regenerating NAD^+ and has recently been implicated in control of oncogene-induced senescence (OIS) [439, 455, 456]. Furthermore, other metabolic pathways that have been upregulated in conjunction with the Warburg effect include serine catabolism (which provides an additional source of NADPH) and increased glutamine uptake / utilization (contributing to glutathione synthesis and increased cysteine based antioxidant reserves) [425, 457, 458].

The second of the cell signalling pathways that have been explored with regard to the Warburg effect and cancer development is that of chromatin structure. Chromatin status plays a central role in the regulation of key cellular functions such as gene transcription and DNA repair. Links have been found between the acetylation status of histones in mammalian cells and glycolytic flux[459, 460] causing neutralisation of the DNA–histone charge attraction and making DNA more available for transcription[461]. This occurs in response to changes in cellular acetyl CoA availability provided through glycolysis, fatty acid metabolism and acetate produced in the nucleus[462]. Furthermore, studies have shown how this mechanism of acetylation affects the regulation of growth genes and supports cellular proliferation[318, 463]. Similarly, deacetylation can also be dependent on the energetic state of the cell, with the primary example being sirtuins (class 3 histone deacetlyases), which depend on NAD^+ as a co-factor. Overall, this provides evidence of the ability of the Warburg effect to influence pro-tumorigenic cell signalling[464, 465].

3.7.2 ROS-based experimental and therapeutic agents

Due to the pivotal role ROS is observed to play in such malignant cell transformation and progression, a wide variety of chemotherapeutic agents which rely on ROS modulation

(either directly or indirectly) have been researched. Piperlongumine (piplartine, 5,6-dihydro-1-[(2*E*)-1-oxo-3-(3,4,5-trimethoxyphenyl)-2-propenyl]-2(1*H*)-pyridinone) is one such example (Figure 210). This alkaloid is present in the *Piper* plant species and is the major biologically active component of *Piper longum* (Long Pepper) with longstanding use in Ayruvedic medical treatment for a wide variety of conditions from tumours to asthma[466]. In light of the broad activities of piperlongumine (anti-atherosclerotic, antibacterial, antifungal among others), its promising anticancer activity was investigated extensively and was patented as a result [467]. Piperlongumine has been documented to selectively increase the oxidative stress in cancer cells (increasing ROS levels) along with depletion of intracellular GSH. An additional proposed mechanism through which such compounds are thought to mediate their activity is though protein glutathionylation via electrophilic functional group reactivity with cellular protein cysteine residues such as GSTp1 and CRB1[468-470]. Furthermore, quinone based anticancer agents are a major class of therapeutic agents which mediate their cytotoxic effects through a ROS-based mechanism among others. Examples include doxorubicin (topoisomerase inhibitor and DNA intercalator), mitomycin C (DNA alkylator) and bleomycin (DNA intercalator and DNA gyrase inhibitor) have been used clinically as single treatments / combinations for breast, small cell lung, haematological cancers as well as pancreatic and gastric carcinomas[25, 471].

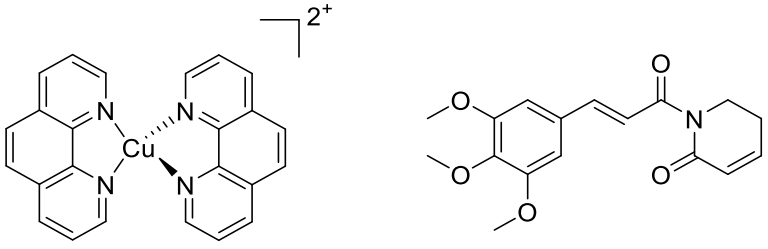

Figure 209: Bioorganic copper complex example-(Cu-phen) (left) and piperlongumine (right) that exert anticancer effects through ROS-dependent mechanisms

One specific scaffold that is of particular interest for its wide versatility and promising ROS directed biological potential are bioorganic copper complexes. Among the most notable of this class of chemotherapeutic compounds was synthesised by Sigman et al. and was the first synthetic chemical nuclease to be designed [Cu(1,10-phenanthroline)2]2^+ (Cu-phen)[472-474] (Figure 210). Such compounds are known to partly intercalate between bases of DNA and bind to its minor groove. Moreover, mechanistic

work into the cell death induced by such copper 1,10-phenanthroline complexes conducted by Kellett et al. have identified mitochondrial dysfunction, ROS induction and formation of genomic DNA double-strand breaks as contributors to their potent antitumour activity[475]. In addition to this, interest exists in their development due to possible attenuation of off-target toxicity concerns that are present in current platinum based complexes such as cisplatin including nephro and neurotoxicity[476, 477].

3.7.3 ROS-*N*-acetyl cysteine (NAC) assay

The ROS cell viability assay included pre-treatment of the CLL cells with *N*-acetyl cysteine or Trolox (6-hydroxy-2,5,7,8-tetramethylchroman-2-carboxylic Acid). *N*-acetyl cysteine (NAC) (Sigma) was dissolved in sterile water and subsequently diluted to obtain a 5 mM stock solution concentration. Trolox (Sigma) was dissolved in ethanol to yield a stock solution concentration of 10 mM. Fresh solutions were prepared for each experiment. CLL cells were seeded at a density of 2 x 10^5 cells / mL. The cells were pre-treated with NAC or Trolox (2 µL) for 1 hr, protecting from light before then treating with compound. The remainder of the assay was carried out as described for the alamar Blue cell viability assay previously. **(86**, **133**, **156, 24)** were chosen as representative potent compounds from the chalcone and nitrostyrene based ethanoanthrcene libraries respectively and were assessed at treatment concentrations of 10 µM and 1 µM in the absence and presence of NAC 5 mM solution. NAC and Trolox were chosen to assess the potential for the synthesised compounds to mediate their antiproliferative effect through ROS flux. They also represent antioxidant structures that would be encountered *in vivo* by therapeutic agents e.g. glutathione and vitamin E[433, 478, 479].

In HG-3 cells at the 10 µM treatment concentration, NAC addition impacts on the ability of all compounds to reduce cell viability to varying degrees (Figure 211). With **(86)**, a dramatic increase of 78 % in cell viability was noted upon pretreatment with NAC. Similarly, for **(24)** a large increase of 103% is observed on treatment with NAC. These are both in contrast to **(133)** and **(156)** whereby smaller relative increases in cell viability take place (17% and 14% respectively). At the lower 1 µM treatment concentration, the trends observed at 10 µM remain with **(86)** showing a 34% cell viability increase on NAC treatment. Comparably, **(24)** exhibits a marked increase of 73% ,while **(133)** displays a

small increase of 5% cell viability. This is in contrast to the effect of NAC addition on **(156)** treated cell viability, where negligible a difference of 1% was noted.

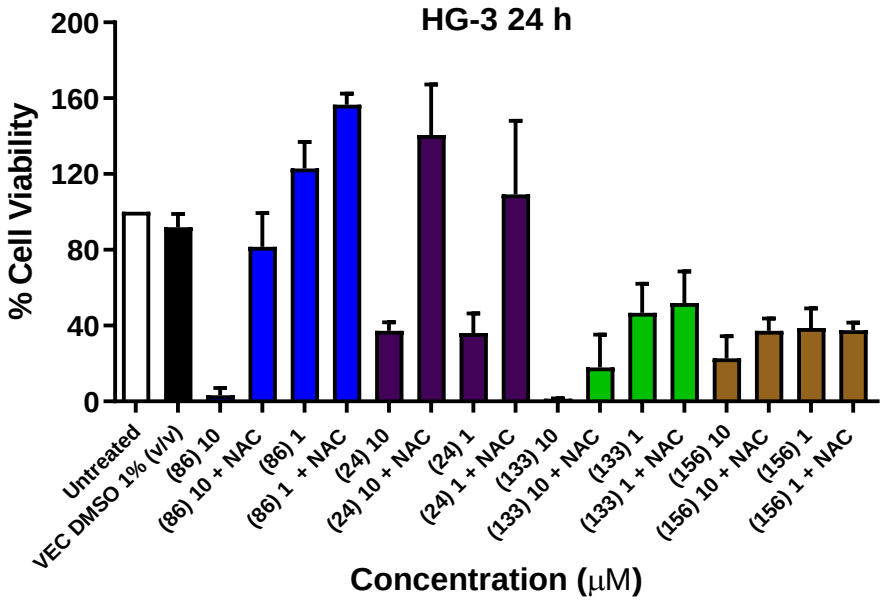

Figure 210: NAC ROS assay % viability results for compounds (86, 133, 156, 24) in HG-3 cell line (n=3)

In PGA-1 cells at the 10 µM treatment concentration, NAC addition impacts on the ability of all compounds to reduce cell viability to varying degrees (Figure 212), but comparitively less than in HG-3 cells (Figure 211). With **(86)**, a moderate increase of 48 % in cell viability was noted upon pretreatment with NAC. Similarly, for **(24)** a large increase of 130% is observed on treatment with NAC. These are both in contrast to **(133)** and **(156)** whereby smaller relative increases in cell viability take place (3% and 5% respectively). At the lower 1 µM treatment concentration, the trends observed at 10 µM remain with **(86)** showing a 37 % cell viability increase on NAC treatment. Comparably, **(24)** exhibits a marked increase of 92% , while **(133)** displays a small increase of 10% cell viability. The effect of NAC addition on **(156)** cell viability exhibited a small difference of 5%.

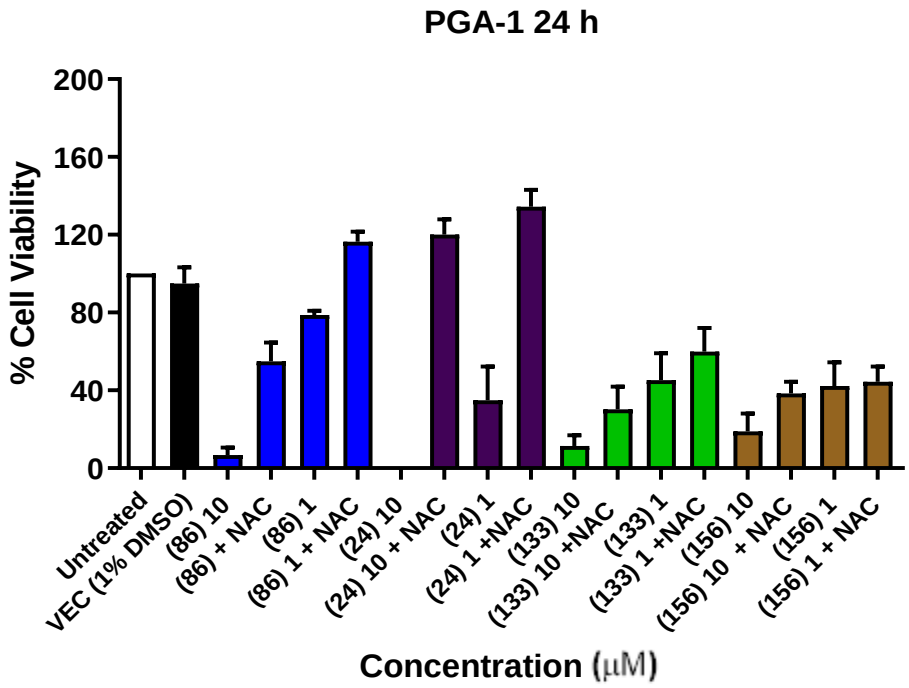

Figure 211: NAC ROS assay % viability results for compounds (86, 133, 156, 24) in PGA-1 cell line

These results strongly suggest a potential ROS-dependent mechanism for compounds **(86)** and **(24)**, while **(133)** and **(156)** appear to have less of a response to NAC pretreatment, hence may be less dependent on ROS than the other compounds assessed for their ability to decrease the % viable cells remaining.

3.7.4 ROS -Trolox (6-hydroxy-2,5,7,8-tetramethylchroman-2-carboxylic acid) assay

In addition to NAC, the ability of Trolox (6-hydroxy-2,5,7,8-tetramethylchroman-2-carboxylic acid) (a cell permeable water soluble analogue of vitamin E) at a 10 mM solution concentration was also assessed in compouds (**86, 133, 156, 24)** at both 10 µM and 1 µM treatment concentrations.

In HG-3 cells at the 10 µM treatment concentration, Trolox addition impacts on the ability of all compounds to affect cell viability to varying degrees (Figure 213). With **(86)**, a small decrease of 5 % in cell viability was noted. This was in contrast to **(24)** which showed a small increase of 8% on treatment with Trolox. Similarly, **(133)** and **(156)**

followed this trend where by small to negligible changes in cell viability were noted (no change and 8% respectively). At the lower 1 µM treatment concentration, the trends observed at 10 µM remain with **(86)** showing a 21% cell viability decrease on Trolox treatment. Comparably, **(24)** exhibits a small decrease of 7% ,while **(133)** displays a small increase of 5% cell viability. Moreover, a marked effect of Trolox addition on **(156)**-treated cell viability was observed, leading to a cell viability decrease of 18% at 10 µM and 15% at 1 µM.

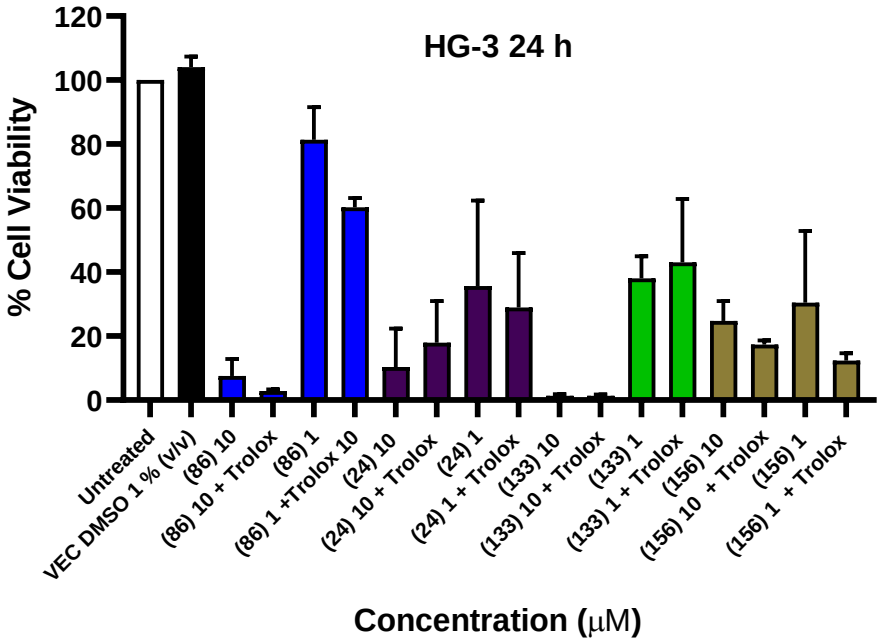

Figure 212: Trolox ROS assay % viability results for compounds (86, 133, 156, 24) in HG-3 cell lines

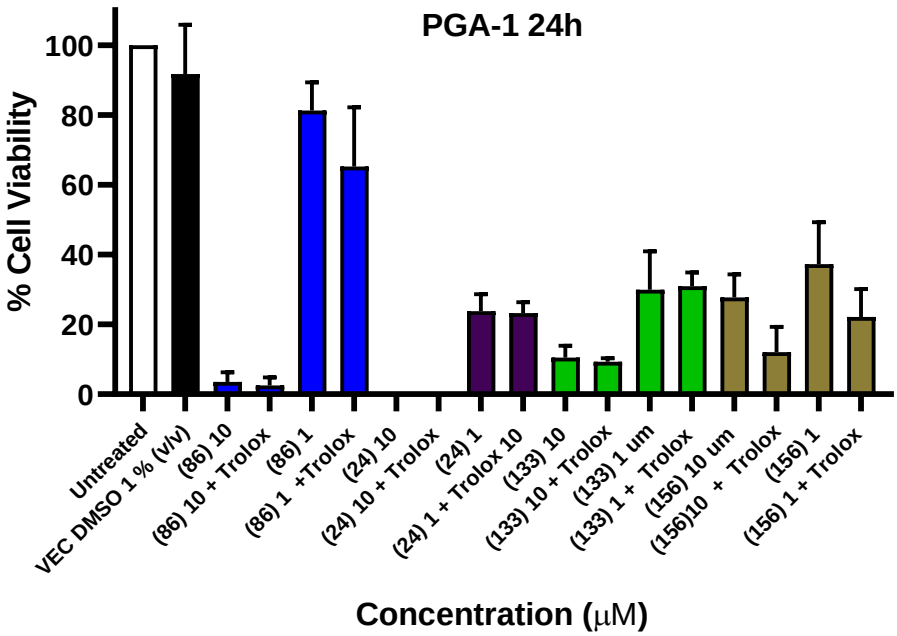

Figure 213: Trolox ROS assay % viability results for compounds (86, 133, 156, 24) in PGA-1 cell line

In PGA-1 cells at the 10 µM treatment concentration, Trolox addition impacts on the ability of all compounds to reduce cell viability to varying degrees (Figure 214). With **(86)**, a small decrease of 1% in cell viability was noted. Similarly, **(24)** a small increase of 1% was observed on treatment with Trolox. These are both in contrast to **(133)** and **(156)** whereby small relative decreases in cell viability take place (2% and 16% respectively). At the 1ower 1 µM treatment concentration, the trends observed at 10 µM remain with **(86)** showing a 26 % cell viability decrease on Trolox treatment. Comparably, **(24)** exhibits a negligible decrease of 1% ,while **(133)** also displays a small increase of only 1% cell viability. Moreover, a marked effect of Trolox addition on **(156)** treated cell viability was observed, leading to a marginal cell viability decrease of 8% at 10 µM and 18% at 1 µM.

These results suggest that the impact of Trolox treatment on cell viability is mutlifactorial and observed to be compound structure, treatment concentration and and cell line dependent. Across both cell lines, compounds **(86)** and **(156)** display increased effectiveness on cotreatment with Trolox, being greater at 1 µM treatment concentration than 10 µM. Interestingly, compound **(133)** has a minimal effect at both treatment concentrations and in both cell lines. This is in contrast to compound **(24)** which has decreased activity at 10 µM on addition of Trolox and an enhanced activity against HG-

3 cells at 1 µM cotreatment. No appreciable effect was observed for the same in PGA-1 cells at both concentrations.

3.8 Caspase inhibition assay

Caspases (cysteine-aspartic proteases) are a family of aspartic acid residue specific regulatory cysteine proteases that play an essential role in key cellular homeostatic processes such as inflammation and programmed cell death through induction of apoptosis[480, 481]. The majority of human caspases can be broadly divided wih respect to these two main cellular processes; with caspases -2, -3, -7, -8, -9 and -10 involved in apoptotic cascade and caspases-1, -4, -5, -11 and -12 being involved in the inflammatory process[482]. Focussing on the apoptotic caspases, these can be subdivided into initiator caspases (caspases-2, -8, -9, -10, whose function is the cleavage and activation of inactive executioner procaspases) and executioner caspases (caspases-3, -6, -7, which when activated, are responsible for propagation of an accelerated caspase activation loop which leads to apoptotic cell death). Apoptosis is mediated by such caspases through two main pathways, extrinsic and intrinsic.

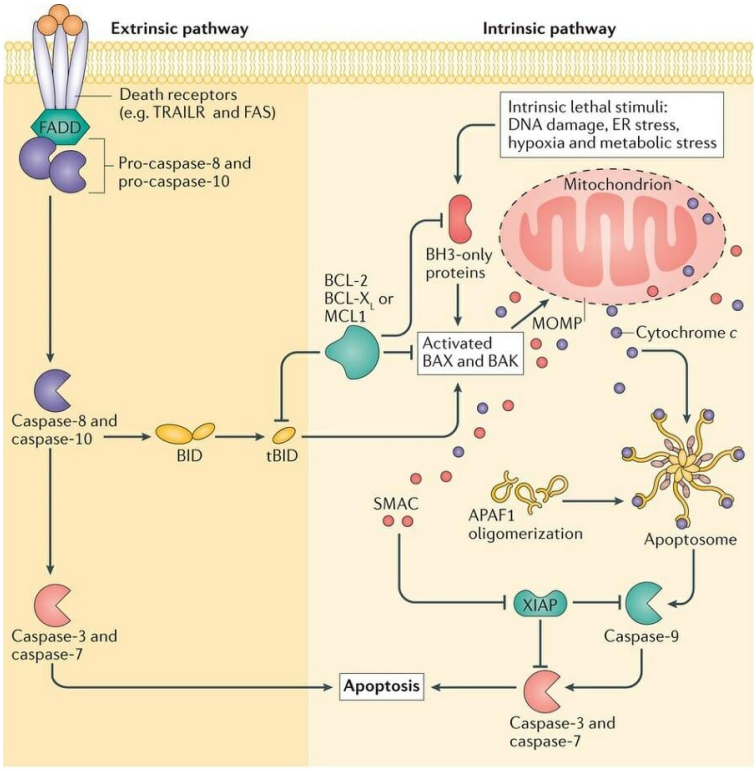

Figure 214: The extrinsic and intrinsic pathways of apoptosis[26]

The extrinsic pathway is where the apoptotic process is triggered through the binding of an extraceullar ligand e.g. TNF-α to a death receptor of tumor necrosis receptor superfamily e.g. tumour necrosis factor receptor 1 (TNFR1), located on the surface on the cancer cell. This is in contrast to the intrinsic pathway, where by the process is mediated through the mitochondria and Bcl-family of proteins in response to cellular and metabolic stress e.g. in response to cytotoxic drug, excessive ROS production or DNA damage (Figure 215)[483, 484].

To assess whether the biological activity of both major ethanoanthracene classes (nitrostyrene and chalcone-based) is caspase dependent, compounds **(86)** and **(24)** (representing Series 5 and Series 2 respectively) (Figure 217) were selected for evaluation at two treatment concentrations, 10 µM and 1 µM across both CLL cell lines. CLL cells were seeded at a density of 2x 10^5 cells / mL and were subsequently pre-treated with 20 µM of pan-caspase inhibitor Z-VAD-FMK (G-Biosciences, Geno Technology Inc. , USA) per well 4 h prior to compound treatment. The capase assay protocol was adapted from Bright et al. [485] and the remainder of the assay was carried out as described for the alamar Blue cell viability assay previously and was completed in triplicate on two-independent days. The output was also statistically analysed using a one-way ANOVA with Bonferroni multiple comparison test. Statistical significance was defined as any comparison with a generated p-value of <0.05.

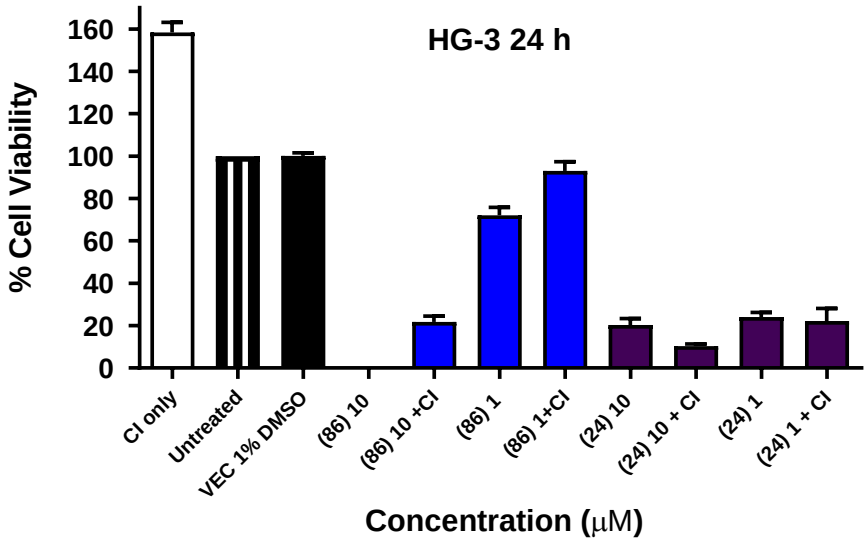

Figure 215: Caspase-inhibitor results of compounds (86) and (24) in HG-3 CLL cell line (CI=caspase inhibitor) (n=2)

In HG-3 cell lines, the pretreatment with of 20 µM of pan-caspase inhibitor **Z-VAD-FMK**[486, 487] (Figure 217) leads to an increase in viable cell remaining of 24% for compound **(86)** at a 10 µM (Figure 216). Similarly, at a 1 µM, an increase in viable cells remaining of 21 % was observed. In contrast to this, with compound **(24)**, a decrease of 10% in cell viability was noted at 10 µM and a decrease of 2% at 1 µM. While the increases in cell viability caused by compound **(86)** were statistically significant (p-values of 0.02 and 0.048), no significant difference was found between cell viability response (with or without CI) at both 10 µM and 1 µM concentrations for compound **(24).**

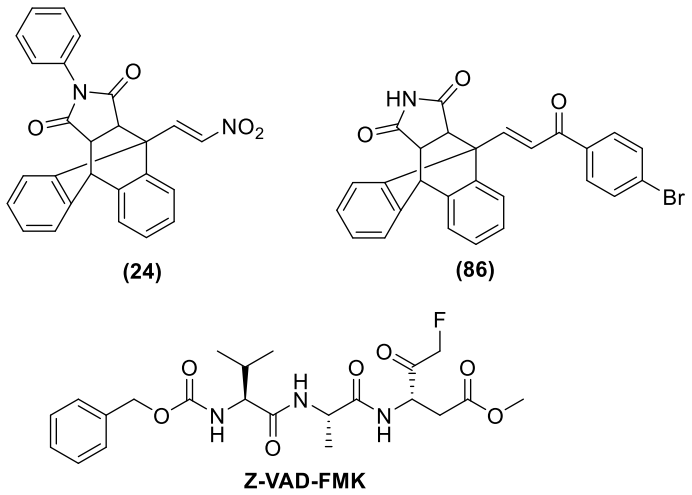

Figure 216: Chemical structures of compounds (24) and (86) used in the caspase assay, structure of pan-caspase inhibitor Z-VAD-FMK[486]

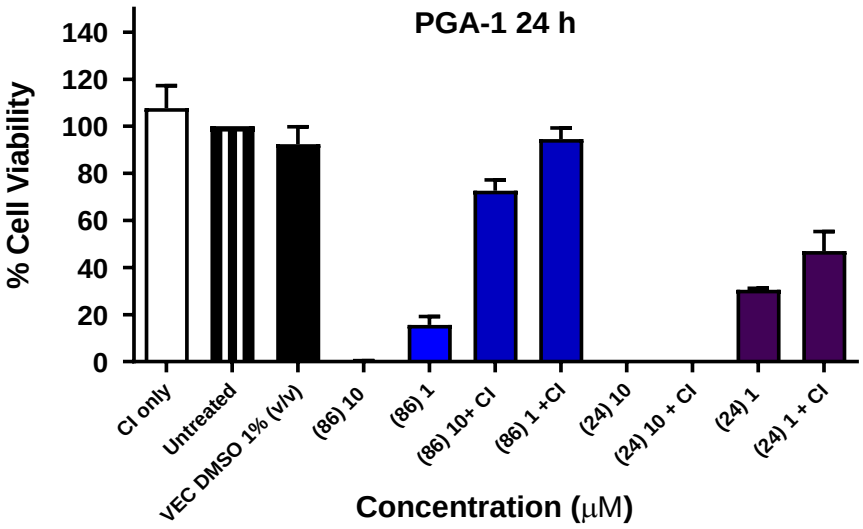

Figure 217: Caspase-inhibitor results of compounds (86) and (24) in PGA-1 CLL cell line (CI=caspase inhibitor) (n=2)

In PGA-1 cell lines, the pretreatment with 20 µM of pan-caspase inhibitor **Z-VAD-FMK** leads to an increase in viable cells remaining of 16 % for compound **(86)** at a 10 µM (Figure 218). Similarly, at a 1 µM, an increase in viable cells remaining of 22% was observed. In contrast to this, with compound **(24)**, a decrease of 0.7 % in cell viability was noted at 10 µM and an increase of 17% at 1 µM. However, none of the differences observed were deemed of statistical significance (p-value < 0.05 in comparison to the compound-only controls) . This is in contrast to the correlation between **(24)** concentration, antiproliferative activity and apoptotic cell death induced.

The assay results illustrated in Figure 216 and Figure 218 may suggest the involvement of caspases in the ability of compound **(86)** to reduce the cell viability in HG-3 CLL cells. However, beyond this observation, the evidence of caspases being involved in the compound activity (**86** in PGA-1 cells and **24** in both cell lines) is lacking. Due to the unclear role caspases play in ethanoanthracene compound activity in CLL cell lines informed by this assay, further investigation may be warranted to establish an unambigious conclusion. Recommendations for future caspase assay design include further increasing of CI concentration to elicit more easily defined differences (if any) in cell viabiliy with treatment. In addition, the investigation of caspase inhibition on compound pro-apoptotic activity would be warrented given the previously outlined potent induction of apoptosis in HG-3 and PGA-1 cell lines.

3.9 Exploration of a potential molecular target-p53

In the absence of a specific molecular drug target and the observation that the most potent ethanoanthracene compounds cause pro-apoptotic cell death, the current scientific literature was searched for existing chemical agents which could be similar in structure (Michael acceptor functionality, carbon bridges) and elicit a similar effect on cancer cell lines. Two such agents selected for investigation on this basis were MIRA and PRIMA-1 (Figure 220), which target mutated p53 in cancer cell lines, causing it to refold and completely or partly restore its anti-tumorigenic functions[488].

Both of these compounds have been shown to exert this biological effect through covalent bond formation with exposed thiol groups in the mutant p53 core domain *via* reactive

Michael acceptor double bond functionalities.In addition to this main mechanism of action, MIRA has also been observed to prevent the unfolding of wild-type and mutated p53 proteins, leading to greater p53 functionality[489]. Furthermore, such covalently binding compounds are of particular interest in the realm of breast cancer drug discovery due to their impressive selectivity between malignant and healthy cells e.g. APR-246 (methylated analogue of PRIMA-1) and PK11007 (2-sulfonylpyrimidine based agent)[490, 491] (Figure 219).

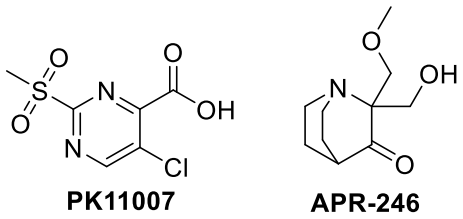

Figure 218: Structures of the covalent p53 bonding agents PK11007 (left) and APR-246 (right)

As previously mentioned (chapter 2), α,β-unsaturated ketone functional groups in chalcones may work through similar molecular mechanism of covalent bond formation. This, along with the demonstrated activity in breast cancer cell lines MCF-7 and MDA-MB 231 (in-house unpublished results) as well as the breast cancer cell lines of the NCI 60 panel, **(24)** was explored as a potential p53 binding agent. MIRA and PRIMA-1 (two covalent p53 cysteine residue binders) underwent flexible alignment analysis with one of our identified lead compounds **(24)** shown in Figure 220 below. The spatial distribution of key functional groups and atoms (carbonyl groups, hydroxyl groups and nitrogen atoms) necessary for binding to mutated p53 exposed cysteine residues show good complementarity of fit between the maleimide derived region of **(24)** and the PRIMA-1 and MIRA molecules. Hence, this may indicate similar binding and mechanism of action. This investigation of p53 is further supported through in-house NMR binding experiment of chalcone ethanoanthracene compound **(99)** with cysteamine, providing evidence of covalent thiol group binding[492].

To verify whether the biological effect of the synthesised compounds was p53 specific, one of the most promising lead compounds (**24**) was explored in a study with our collaborator Dr. Naoise Synnott in UCD. This involved initial antiproliferative assessment in a series of breast cancer cell lines (BT549, Hs579T, Hs579T (i8), SKBR3,

CAMA1 and MCF-7) of compound **(24),** utilizing the MTT (methylthiazolyldiphenyl-tetrazolium bromide) viability assay (Figure 221).

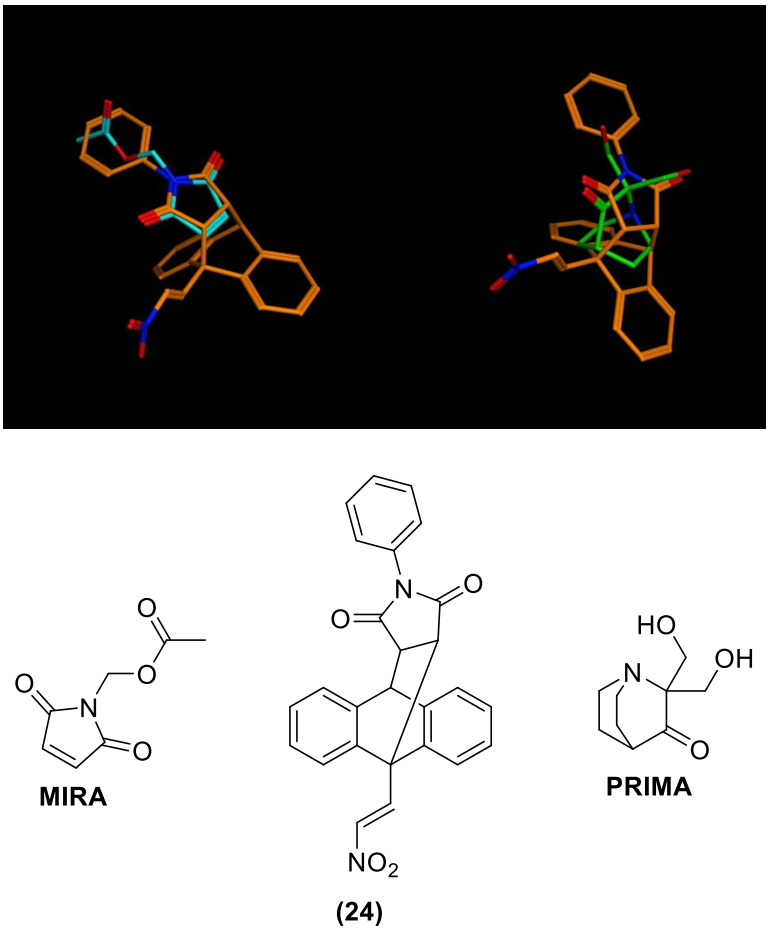

Figure 219: Flexible allignment of MIRA (cyan) and (24) (orange) (left), flexible allignment of PRIMA-1 (green) and (86) (orange) (right), chemical structures of MIRA, (24) and PRIMA-1 (bottom)

A brief description of the cell types and variants used in these studies are as follows:

- **BT549 :** Ductal carcinoma with mutated p53 (triple negative)[493]
- **Hs579T:** Breast carcinoma with mutated p53 (triple negative)
- **Hs579T (i8):** Invasive ductal carcinoma with mutated p53 (triple negative)
- **SKBR3:** Adenocarcinoma with mutated p53 [494]
- **CAMA-1:** Adenocarcinoma (luminal) with mutated p53 [495]
- **MCF-7:** Adenocarcinoma with wild-type p53[496]

Figure 220: MTT (methylthiazolyldiphenyl-tetrazolium bromide) colorimetric assay

The chemical basis for this widely used assay is the metabolic reduction of the tetrazolium salt (MTT) 3-(4, 5-dimethylthiazolyl-2)-2, 5-diphenyltetrazolium bromide (yellow) to the intracellular (*E*,*Z*)-5-(4,5-dimethylthiazol-2-yl)-1,3-diphenylformazan (formazan) (dark blue/purple).This reduction is facilitated by the action of NAD(P)H-dependent cellular oxidoreductase enzymes located in the mitochondria, cytoplasm and non-mitrochondrial memebranes (e.g.plasma membrane).The quantification of cell viabilty is then correlated with this metabolic activity as only live cells can facilitate this reaction[497, 498] (Figure 221).

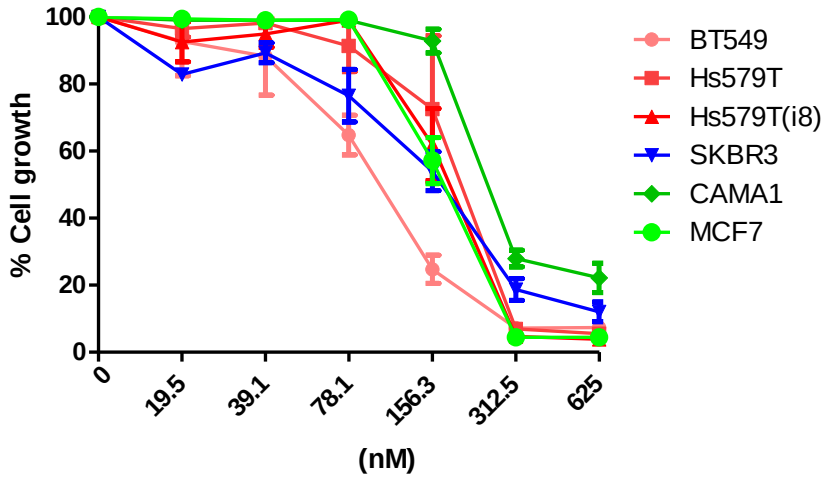

Figure 221: Dose response curves of (24) in breast cancer cell line panel

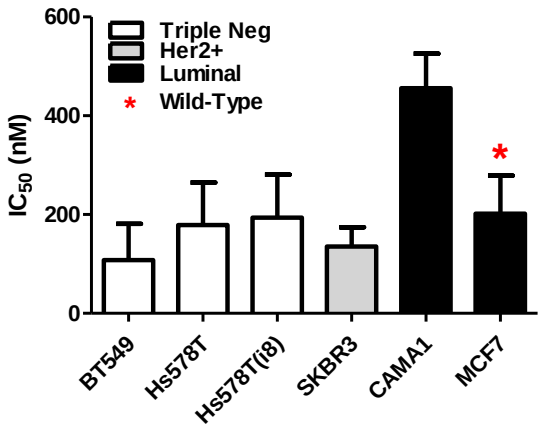

Figure 222: (24) cell viability results in breast cancer cell panel

Breast Cancer cell line	IC_{50} (24) (nM)	IC_{50} APR-246 (nM)
BT549	107.9	3.11
Hs579T	178.7	7.09
Hs579T (i8)	194	11.91
SKBR3	135.4	5.13
CAMA1	456	3.33
MCF7	201.8	31.06

Table 45: Comparison of IC_{50} values of compounds (24) and APR-246

The results of **(24)** treatment on the breast cancer cell line panel are shown in in Figure 222, Figure 223 and Table 45. The cell lines were treated with a concentration range of **(24)** dissolved in DMSO. Promising antiproliferative activity across the breast cancer cell lines was observed for compound **(24)** with an IC_{50} value range between 107.9-456 nM. The most potent activity noted for compound **(24)** was in cell lines BT549 and SKBR3 (both with mutated p53) with IC_{50} values of 107.9 and 135.4 nM respectively. Interesting antiproliferative activity of **(24)** observed in the triple negative and HER 2 positive breast cancer cell lines Hs579T and Hs579T (i8) with IC_{50} values of 178.7 and 194 nM respecively. However, a drastic decline in potency in CAMA-1 luminal cells leading to the highest IC_{50} value observed for compound **(24)**.

Furthermore, the determined activity of **(24)** in the breast cancer cell panel was compared directly to APR-246 (Figure 224), a prodrug of the anti-cancer research compound PRIMA-1, which is converted *in vivo* to Michael acceptor methylene quinuclidinone (MQ). This reactive moiety then facilitates cell death through reactivation of mutated p53 through convalent cysteine residue modification, in addition to impacting on ROS balance through inhibition of thioredoxin reductase and glutathione (GSH) depletion[499]. APR-246 vastly outperformed **(24)** across the breast cancer cell line panel with IC_{50} values ranging between 3.11-31.06 nM (14-35 fold more potent in the breast cancer panel tested).

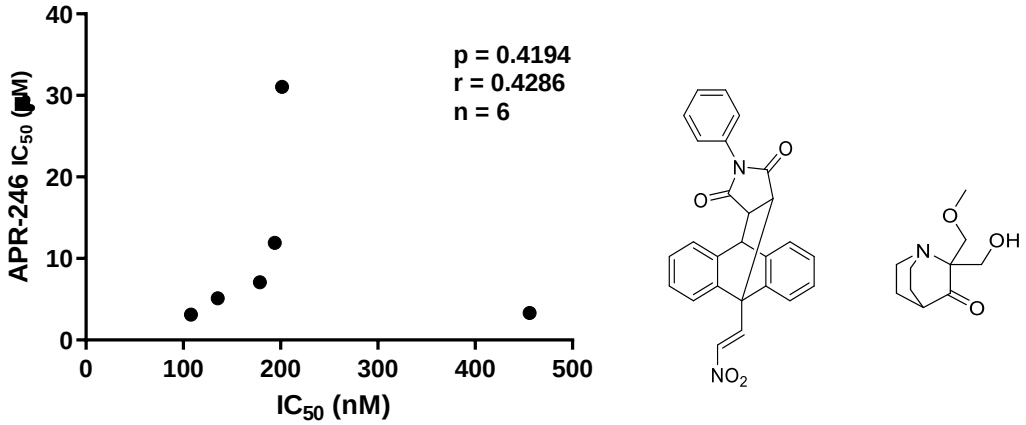

Figure 223: Correlation of APR-246 and (24) breast cancer panel activity, chemical structures of (24) and APR-246 (right)

The Pearson correlation coefficient (p=0. 4194) and the corelation coefficient (r= 0. 4286) indicate a weak positive correlation between the compound activities in the cell panel tested, proposing that there may be a small chance that they operate through a similar mechanism of action. However, in light of the clear linear trend in compound activities in the absence of the final two outlier data points along with the small sample size (n=6), further testing should be undertaken to firmly exclude this possibility. To assess whether treatment had any effect on p53 protein expression or related p53-family proteins (p63 and p73), both Western blots and ELISAs (enzyme-linked immunosorbent assay) were undertaken. It was noted that little evidence existed of a correlation between p53 protein expression and **(24)** activity as four of six samples remained on the baseline (Western blot) or slighly above it (ELISA) with increasing treatment concentration (Figure 225).

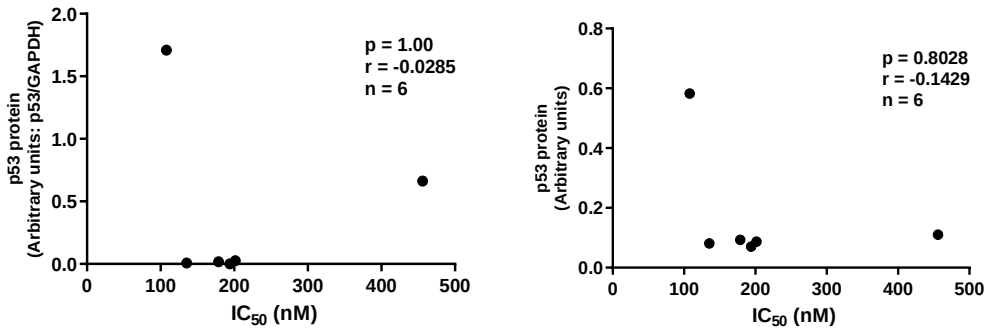

Figure 224: Western blot and ELISA of p53 protein expressed vs (24) activity

In contrast to p53, p63 (a p53 homologue) shows a weak to moderate correlation (p=0.5639, r=0.2732) with its protein expression appearing to increase with increasing **(24)** treatment concentration (five of the six samples showing elevation above 0.5 units). P73 (another p53 homologue) showed a similar, yet weaker correlation between its protein expression and treatment concentration (p=0.5639, r=0.2732) (Figure 226).

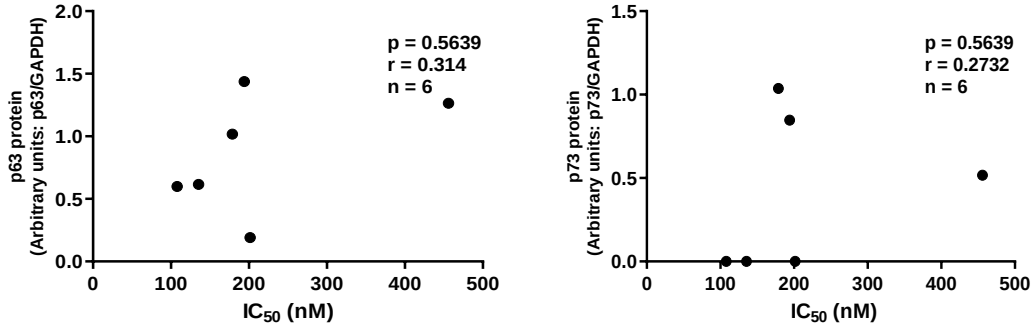

Figure 225: Correlation plots of (24) IC $_{50}$ values in cells lines assessed against degree of protein expression of p63 (left) and p73 (right)

In conclusion, from the studies of p53 and related homologue proteins, the apoptotic cell death induced by lead compound **(24)** in the breast cancer cell panel appears to be p53-independent while involving the upregulation of related transcriptional proteins p63 and p73 (to lesser extent). Due to highly conserved genetic domains (e.g. DNA binding domain >60% similarity to p53) across the p53 family, transactivators of these distinct yet similar regulator proteins exist which can allow for selective expression of pro-apoptotic genes in the absence of p53 influence such as MDM2 (murine double minute 2)[500], BAX (BCL2 associated X, apoptosis regulator)[501], PERP (p53 apoptosis effector

related to PMP22)[502] and NOXA[503] [latin for damage, also know as phorbol 12-myristate 13-acetate-induced protein 1 (PMAIP1)] [504-507].

3.10 Cheminformatics analysis of lead compounds-Swiss ADME

Swiss ADME is a free cheminformatics webtool package developed by the moleuclar modelling group at the Swiss Institute of Bioinformatics (SIB). It offers a series of robust reliable and easily interpretable predictive computational models from which key drug development parameters can be estimted and modelled *in silico*. These include pharmacokinetics, physicochemical parameters, druglikeness and medicinal chemistry suitability and accessibility. With a user friendly interface, it provides an important, accessible drug discovery platform in early stage preclinical development for both experienced computational chemists and those not familiar with computer aided-drug design[508]. An example of the output generated for compound **(86)** is illustrated in Figure 227.

From the following Swiss ADME calculation results shown for lead compounds, the following parameters will be discussed:

- Physicochemical Properties-Molar refractivity (MR), TPSA (total polar surface area) (Table 46)
- Lipophilicity-Consensus Log P value from five separate calculation methods
- Water solubility-Calculated across three different methods
- Pharmacokinetics-Estimations of degree of gastroinstestinal (GI) absorption, blood-brain barrier (BBB) permeability, p-glycoprotein (P-gp) substrate potential, specific cytochrome P450 (CYP450) isozyme inhibition propensity, skin permeation coefficient (Table 47)
- Druglikeness assessment methods (Lipinski, Ghose, Veber, Egan and Muegge) (Table 48)
- Medicinal chemistry structure alert assessments PAINS (pan assay interference compounds), BRENK filters

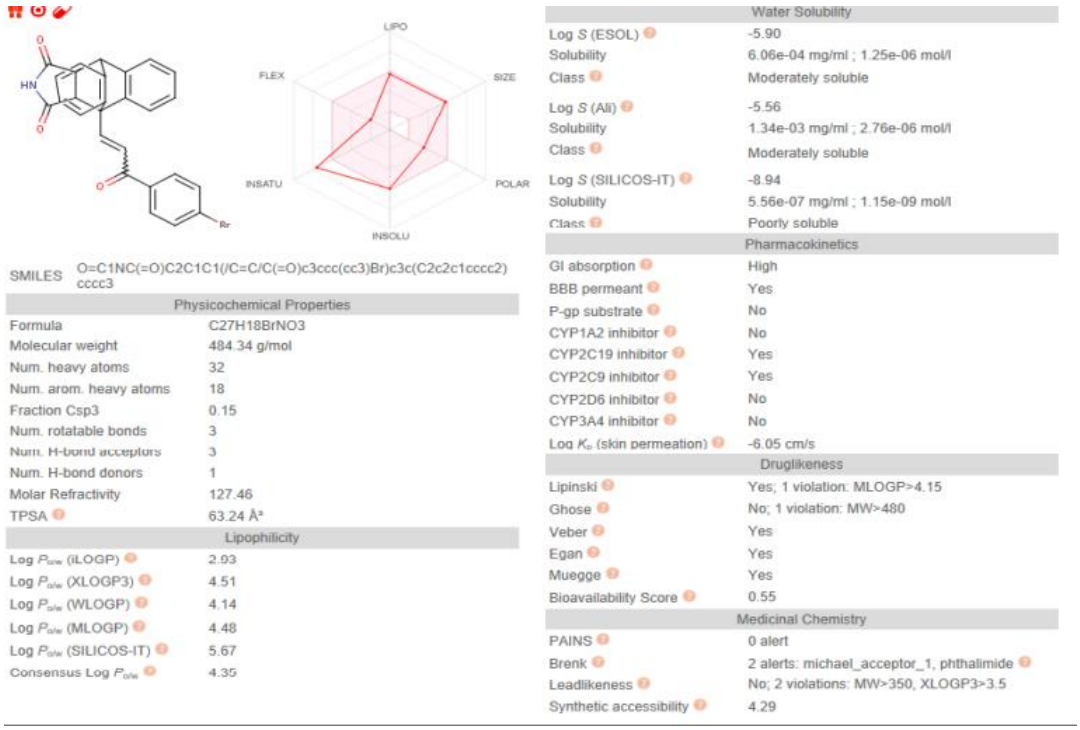

Figure 226: Example of (86) result readout generated using Swiss ADME web software[508]

Compound	Molar Refractivity (m^3/mol)	TPSA (Å²)	Log P (consensus)	Water Solubility (consensus) (mg/mL)	GI Absorption	BBB permeable	Skin permeation Coefficient (cm/s)	Average CLL IC_{50} (in-house) (µM)
(86)	127.46	63.24	4.35	-6.80	High	(+)	-6.05	2.33
(99)	117.56	76.13	3.03	-5.56	High	(+)	-6.59	1.94
(93)	119.72	63.24	4.05	-6.18	High	(+)	-6.10	3.77
(92)	132.48	63.24	4.38	-6.89	High	(+)	-6.37	3.62
(88)	129.53	63.24	4.36	-6.73	High	(+)	-5.66	3.67
(101)	137.27	63.24	4.62	-7.35	High	(+)	-5.48	1.36
(150)	172.57	84.41	5.51	-9.02	High	(-)	-5.50	1.12
(133)	147.71	67.34	4.98	-7.80	High	(-)	-5.58	1.09
(91)	119.76	63.24	3.73	-6.00	High	(+)	-6.06	7.43
(97)	124.77	63.24	4.27	-6.61	High	(+)	-5.82	2.72
(94)	126.25	72.47	3.72	-6.12	High	(+)	-6.27	11.4
(96)	139.24	90.93	3.66	-6.34	High	(-)	-6.27	5.19

Table 46: Physicochemical descriptors and average CLL IC_{50} values of compounds (86, 99, 93, 92, 88, 101, 150, 133, 91, 97, 94, 96)

Molar refractivity (MR) (also known as molecular refractivity) is considered as a measure of the overall polarisability of the drug molecule being studied. It is based on the physicochemical Lorenz-Lorentz formula (Equation 1), which relates the measured refractive index of a molecular system with its polarisability. As the refractive index measured is dependent on the wavelength used, MR represents the true molecular volume

of a molecule as wavelength tends to infinity. In the realm of drug design and measuring of drug-likeness, compounds that fall within the range of 40-130 tend to display favourable physicochemical behaviour[509-511].

$$MR = (n^2-1)/(n^2+2) \times (M/\rho)$$

Where M= molar mass of the material, n=refractive index, ρ=material density and MR=molecular volume

Equation 1: Lorenz-Lorentz equation used for the determination of the Molar refraction parameter[509-511]

The MR range of the lead compounds assessed in this work was 117.56-172.57 m^3/mol. While the vast majority of molecules were estimated to be within the ideal range that supports compound druggability, an interesting difference was noted with **(150)** and **(96)** in context of biological activity. Although, while compound **(150)** was found to have the highest MR value of 172.57, **(96)** (MR value 139.24) was 5-fold less potent. This observation may point towards greater steric tolerability at the ethanoanthracene bridge rather than on the acetophenone functional group aromatic ring.

Polar surface area (PSA) can be defined as the area of van der Waals force that is derived from the presence of oxygen and nitrogen atoms with the hydrogens attached to such atoms. The descriptor is related to the potential of a compound to undergo hydrogen bonding[512]. Excellent correlations between dynamic PSA (PSAd) and passive intestinal absorption (R-squared=0.99)[513] were noted by Palm et al. In a later study, Palm et al.[514] discovered that PSAd could be used to identify poorly absorbed compounds prior to synthesis through the limits of > 140 Å^2, only 10% of the drug fraction was absorbed and that < 60 Å^2, greater than 90% was absorbed, calculated across multiple conformers. Topological polar surface area (TPSA) is the most commonly used and simplest technique for evaluating PSA of a molecule. TPSA is defined as the sum of polarity contributions of the solvent-accessible surface areas of atoms with partial charges and is represented in Equation 2[511, 515].

$$TPSA = \Sigma\, n_i\, C_i$$

Where n_i = number of a particular substituent contributing to the total molecular polarity and C_i = the individual polarity contribution of each type of substituent

Equation 2: Method of TPSA calculation

In terms of TPSA, the values of the focussed library of lead compounds were observed to be between 63.24-90.93 Å^2. When compared to the ideal consensus TPSA value of <60-70 Å^2 [which correlates to near complete drug absorption (>90%)] and the widely

accepted upper limit of 140 $Å^2$, all assessed compounds fall within these cut-off thresholds. However, a TPSA value of <75 $Å^2$ could potentially cause toxicity when combined with a highly lipophilic Log P value[515].With the exceptions of **(99)** and **(150)**, compounds with a TPSA value of >70 $Å^2$ tended to be less potent (**94, 96**), suggesting that biological potency may correlate to drug TPSA.

Hydrophobicity for compounds can be expressed through the estimated or experimentally derived distribution of the drug between the organic 1-octanol layer and aqueous layer of a two-phase system. The relative concentration between the organic and aqueous layer can be expressed as the partition coefficient (P) (Equation 3)[516]. The logarithm (base 10) of the partition coefficient (log P) is then used as a classic measure of lipophilicity of a molecule in decimal form[517]. Calculated Log P values were found to be in the range of 3.03-5.51, the majority of which fell within the cut-off value of Log P=5. The compounds could be considered lipophilic due to their moderately positive values with favourable activity appearing to span this entire log P range. Of particular interest is **(133)**, which had the most promising biological activity and one of the highest estimated Log P values at 4.98. Hence, it is unlikely that a classic linear relationship exists between the Log P parameter and compound potency.

P= (concentration of drug in octanol layer/ concentration of drug in aqueous layer)

Equation 3: Partition coefficient of drug

P-glycoprotein is a Na^+/K^+ ATPase pump utilised in the human body for maintenance of normal homeostatic conditions in the cellular environment such as resting membrane potential and nerve transmission through differential ion concentration gradients[53]. In malignant conditions, this usually benign and essential part of molecular machinery is utilised and exploited through overexpression as an efflux pump for a wide variety of chemotherapeutics, increasing resistance through decreased exposure hence mediating cancer resistance to otherwise effective treatments. This biological "efflux pump" is also central to the protection of the central nervous system (CNS) from xenobiotics and flux from the wall of the GIT to the lumen[518, 519].

From nearly all screened compounds, with the exception of **(96)**, they are not predicted to be P-gp substrates (Table 47). This supports the possibility that the presence of the 3,4,5-trimethoxy moiety may affect compound action through P-gp efflux (which may

partly contribute to the relatively low biological activity when compared to other similar potent compounds synthesised).

Cytochrome P 450 (CYP 450) is a superfamily of isozymes central to Phase 1 metabolism of toxins and xenobiotics, facilitating subsequent elimination from the body through improving compound aqueous solubility *via* oxidation[520]. Among the most pharmacokinetically relevant of these enzymes are CYP3A4, CYP2D6, CYP2C9, CYP2C19 and CYP1A2 responsible for the metabolism of between 50-90% of clinically administered therapeutics[521]. Prone to induction (which may cause sub-therapeutic drug plasma concentrations and hence sub-optimal clinical outcomes) and inhibition (responsible for drug-drug interactions and/or toxic side effects due to rapid increases in plasma drug concetration) by drugs and their metabolites[522, 523], the propensity of a compound influence CYP isozyme function is an important consideration in the process of drug development. Overall, the lead compounds tested are estimated to inhibit at least one CYP subtype e.g. **(101)** and others up to as many as three CYP subtypes e.g. **(96)**. All compounds tested were predicted to act as CYP2C9 inhibitors.

Compound	P-gp substrate	CYP1A2 Inhibitor	CYP2C19 inhibitor	CYP2C9 inhibitor	CYP2D6 Inhibitor	CYP3A4 Inhibitor	Average CLL IC_{50} (in-house) (μM)
(86)	(-)	(-)	(+)	(+)	(-)	(-)	2.33
(99)	(-)	(+)	(+)	(+)	(-)	(-)	1.94
(93)	(-)	(-)	(+)	(+)	(-)	(-)	3.77
(92)	(-)	(-)	(+)	(+)	(-)	(-)	3.62
(88)	(-)	(-)	(+)	(+)	(-)	(-)	3.67
(101)	(-)	(-)	(-)	(+)	(-)	(-)	1.36
(150)	(-)	(-)	(-)	(+)	(-)	(-)	1.12
(133)	(-)	(-)	(+)	(+)	(-)	(-)	1.09
(91)	(-)	(-)	(+)	(+)	(-)	(-)	7.43
(97)	(-)	(-)	(+)	(+)	(-)	(-)	2.72
(94)	(-)	(-)	(+)	(+)	(-)	(+)	11.4
(96)	(+)	(-)	(+)	(+)	(-)	(+)	5.19

Table 47: Pharmacokinetic interaction estimations of lead compounds with P-gp and CYP 450 isozymes

3.10.1 Drug-likeness asssessment methods

With regard to drug-likeness, this can be defined as the qualitative assessment of the chance that an experimental molecule could be developed as an orally-administered therapeutic (tied closely to bioavailability-the amount of drug that will present for pharmacological action at the target or active site)[508]. The most well-known of such

screening criteria and high-throughput filters for synthetic compound libraries being Lipinski's rule of 5. Lipinski's rules are a series of chemical parameters in relation to predicted behaviour of a given molecule in a bio-physiological system. Using defined ranges and values for specific physiochemical parameters, the suitability of a drug candidate for oral drug development can be investigated. These conservative biological constraints where coined by chemist Christopher A. Lipinski and colleagues working in the Pfizer central research division over two decades ago[524].

In order for experimental drug candidates to have the pharmacokinetic characteristics to be orally viable, the following conditions have to be met:

- Molecular weight (MW) of the compound has to be < 500 Da (Daltons)
- Log P value (measure of lipophilicity) has to be < 5
- Number of hydrogen bond donors <5
- Number of hydrogen bond acceptors < 10

In support of the importance of these initial guidelines in drug development, over 90% of oral drugs that have fallen within these limits have progressed to Phase 2 clinical trials. Furthermore, the aqueous solubility and intestinal absorption tend to be within the ideal scope to facilitate oral bioavailability (where bioavailability is defined as the relative amount of an administered dose that reaches the systemic circulation)[525].

Aside from the popularised Lipinski adapted methods of druggability, there exist some others of note that are routinely used in medicinal chemistry and pharmaceutical industry as a means of compound screening for lead development. One such method was developed by Mueege et al.[526, 527] at Bayer AG, which involved a pharmacophore point filter. The key feature or underlying principle of this approach is the presence or absence of four key functional groups such as carboxylic acids and alcohols, which mediate target protein-compound interactions through hydrogen bonding. These groups can combine in numerous ways to form "pharmacophore points" e.g. amides. These pharmacophore points are then used to distinguish between drug and non-drug candidates, where a suitable compound will have between 2-7 of these features. However, when a compound goes outside these ranges it can be considered either under or over-functionalised.

Another method, was developed by Ghose et al.[528] at Amgen Inc., focussed on the superimposition of a diverse array of active molecules to compare and contrast common

structural features e.g. hydrogen bond donors and defined torsion angles. Furthermore, with the computational model utilizing multiples distance matrices to represent molecular diversity and conformational flexibility, potential biologically active conformations could be assesed for the inhibition of a specific molecular pathway or discovering potential active conformations of lead compounds through molecular docking in enzyme X-ray structures.

In addition, Veber et al.[529] at GlaxoSmithKline (GSK) developed a modified version of Lipinski's rule of 5 based on oral bioavailability studies of approximately 1100 drug candidates in rats. Their studies suggested that TPSA (values of 140 $Å^2$ or less) and the number of rotatable bonds (10 or less) in a molecule had a far higher probability of predicting favourable candidates for oral drug development than the assumption of a molecular weight (MW) greater than 500 Da. Veber also noted that in artificial membrane permeation studies that compound TPSA was a more accurate predictor of permeation rate than clogP (lipophilicity) and that increasingly higher numbers of rotatable bonds correlated with a decreased permeation rate. Hence, a more streamlined and holistic measure than its predecessor and more importantly included potential invaluable drug candiates otherwise excluded from further development due to high MW [529].

Furthermore, Egan et al. in Pharmacopeia Inc. developed a method of predicting human passive-intestinal absorption of a drug utilizing PSA and AlogP98 as molecular descriptors in a multivariate statistical pattern-recognition model. Hence, the model is only based on the three molecular properties of lipophilicity, size and hydrophilicity. This not only has the advantage of ease of interpretation but also active transport and efflux mechanisms were taken into account (which often bias such predictive absorption models). Moreover, it has the advantage of using a large dataset as opposed to to the smaller ones many other passive absorption models use. This provides a more comprehensive cover of the chemical space with regard to human passive intestinal absorption, potentially reducing false conclusions derived from limited diversity and number within datasets assessed[530]. Such methods have come to play an integral role in modern drug development using (HTS) High Throughput Screening, moving away from the time and resource consuming method of identifying suitable drug candidates to identification of suitable lead compounds. Hence, reducing the burden of lead optimisation, enhancing the efficiency and cost effectiveness of the drug pipeline production process leading to better starting points for lead generation projects[531, 532].

Since the "rule of 5" was developed on the basis of results computed from several thousand drug compounds, it is logical that some drug candidates fall outside these confines. The main classes of molecules which tend differ from said boundaries are macrolide antibiotics, vitamins, antifungals and cardiac glycosides. This is accomplished through the presence of distinct functional groups in the molecules, allowing them to act as substrates for active protein transporters[533]. For example, 90 USAN (United States Adopted Names) cardiac glycosides with MW >500 Da and very low Log P values. However, according to Lipinski et al., when these categories were excluded, little to no molecular violations where noted[524]. Additionally, other examples of clinically relevant compounds which have a high incidence of generating violations include HIV protease inhibitors, cyclic peptide-based immunosuppresants and tyrosine kinase inhibitors[534]. Despite its usefulness, there are pitfalls to reliance on such a system as outlined by both Lipinski and Hopkins et al., whereby all compounds that are validated against these parameters will not necessarily be drug-like and potentially successful compounds may be rejected in failing to meet one of the physiochemical requirements[525, 535].

Compound	Lipinski	Ghose	Veber	Egan	Muegge	PAINS	Brenk	Average CLL IC_{50} (in-house (μM)
(86)	(+)	(-)	(+)	(+)	(+)	0 alerts	2 alerts	2.33
(99)	(+)	(+)	(+)	(+)	(+)	0 alerts	2 alerts	1.94
(93)	(+)	(+)	(+)	(+)	(+)	0 alerts	2 alerts	3.77
(92)	(-) 2 violations	(-) 2 violations	(+)	(+)	(+)	0 alerts	3 alerts	3.62
(88)	(+) 1 violation	(+)	(+)	(+)	(+)	0 alerts	2 alerts	3.67
(101)	(+) 1 violation	(-) 1 violation	(+)	(+)	(-) 1 violation	0 alerts	2 alerts	1.36
(150)	(-) 2 violations	(-) 4 violations	(+)	(-) 1 violation	(-) 1 violation	0 alerts	2 alerts	1.12
(133)	(-) 2 violations	(-) 2 violations	(+)	(+)	(-) 1 violation	0 alerts	2 alerts	1.09
(91)	(+)	(+)	(+)	(+)	(+)	0 alerts	2 alerts	7.43
(97)	(+)	(+)	(+)	(+)	(+)	0 alerts	2 alerts	2.72
(94)	(+)	(+)	(+)	(+)	(+)	0 alerts	2 alerts	11.4
(96)	(+)	(-)	(+)	(+)	(+)	0 alerts	2 alerts	5.19

Table 48: Drug-likeness of representative compounds assessed *via* leadlikeness and reactivity/toxicity filters

Taking the output generated by the various physicochemical drug-likeness filters into account, the majority the compounds satisfy the criteria deemed necessary for effect oral

drug development (Table 48). However, notable exceptions to this were compounds **(101)** (2-naphthyl, maleimide), **(150)** (2-pyridyl, *p*-benzophenonemaleimide) and **(133)** (2-pyridyl, *p*-chloromaleimide) which were flagged by 60-80% of the filters . Despite this prediction, these compounds are observed to have among the most potent average IC_{50} values in CLL cell lines HG-3 and PGA-1 (average CLL IC_{50} values 1.09-1.36 µM).

3.10.2 Pan Assay Interference Compounds (PAINS) filter

PAINS are compounds which contain functional groups or moeities make them highly reactive, giving them the appearance of promising lead agents against a wide and diverse range of protein targets e.g. epoxides. The pitfall of such structures as outlined by Baell et al.[536] is not only research time but also project funding, while legitimate "hits" may go unnoticed. With an estimated 5-12% of academic screening libraries containing PAINS, lead compounds (**86**, **99**, **93**, **92**, **88**, **101**, **150**, **133**, **91, 97**, **94**, **96**) were screened according to PAINS filters to reduce the chance of such compounds being selected for progression and optimisation. Despite the presence of a Michael acceptor in the form of the α,β-unsaturated ketone on the lead molecules considered, no PAINS alerts were flagged for any of our compounds assessed.

As well as this structural filtering system, an additional structural alert was employed, created by Daina et al.[508] from the study of Brenk et al.[537] into leadlikeness of drug screening libraries for drug discovery and their assessment. This included approximately 105 compound fragments that were associated with some or all of the following criteria:

- known to induce toxicity directly or post-metabolic activation
- highly reactive functional groups and non-selective action
- have poor pharmacokinetic characterisitcs such as being metabolically labile

All compounds assessed (**86**, **99**, **93**, **92**, **88**, **101**, **150**, **133**, **91, 97**, **94**, **96**) had two structural alerts on the "Brenk filter" , one for the presence of a phthalimide in the form of the maleimide bridgehead structure and the other for the presence of a Michael acceptor in the form of the α,β-unsaturated ketone. While this doesn't discount the promise of these hits as developable leads for CLL treatment, care should be taken going forward in the assessment of potential mechanisms of action as well as further structural modification.

To assess whether any correlation existed between compounds biological activity and the physicochemical properties estimated (molar refractivity, TPSA, log P (consensus), water solubility (consensus), BBB penetration, skin permeation coefficient), using a multiple variable table and subsequent correlation matrix generation using GraphPad Prism Version 8. Potential correlations were assessed using the calculation of Pearson correlation coefficients (r) and illustration of the results in the form of a heat map, where (r)=1 indicates a perfect positive correlation , (r)= -1 a perfect negative correlation and a value of (r)=0, no correlation existing between the variables assessed.

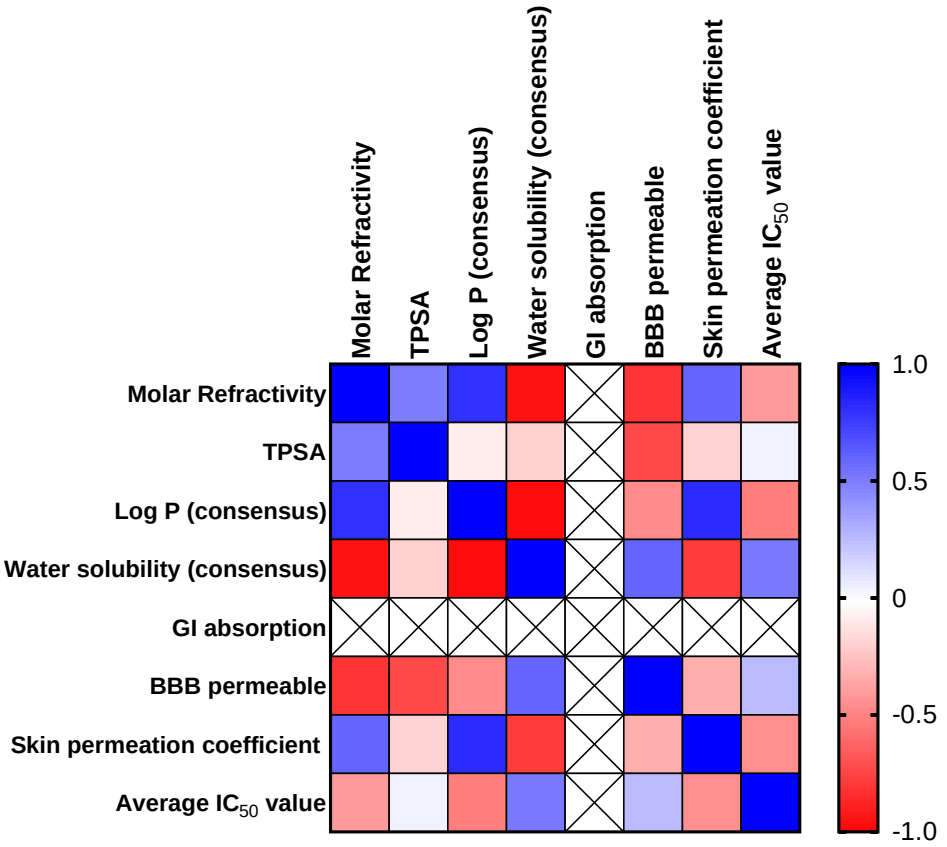

Figure 227: Heat map of Pearson correlation coefficients calculated for lead compounds (86, 99, 93, 92, 88, 101, 150, 133, 91, 97, 94, 96) assessed (blue-indicating positive correlation, red-indicating negative correlation, white-indicating no correlation)

On observation of both the heat map (Figure 228) and the corresponding statistical output in Table 49 four variables (molar refractivity, log P (consensus), water solubility (consensus), skin permeation coefficient) were noted to be approaching statistical significance (p-value <0.05). This would warrant monitoring of such parameters in future work, especially as the number of compounds assessed in this manner increases as the

sample size is quite small to definitively rule particular correlations as being central to compound potency. These four variables will be now briefly discussed.

Variable	Pearson correlation coefficient values (r)	p-values
Molar Refractivity	-0.394	0.205
TPSA	0.052	0.873
Log P (consensus)	-0.503	0.096
Water solubility (consensus)	0.524	0.080
GI absorption	----------	----------
BBB permeable	0.267	0.401
Skin permeation coefficient	-0.442	0.15

Table 49: Pearson correlation coefficients (r) and associated p-values comparing average IC_{50} values with assessed variables (where p-value <0.05 indicates statistical significance)

Molar refractivity appears to have weak to moderate negative correlation (-0.394) with compound biological activity which could mean that activity appears to increase with lower MR values and therefore decreased steric bulk of the molecule. However, while the p-value approaches the point termed to be "almost significant" ($p<0.1$), the current observations are considered not to be staisitically significant. With log P (consensus) there was a moderate negative correlation with biological activity (-0.503), therefore suggesting that with lower lipophilicity, molecules may tend towards greater activity.Water solubility (consensus) provided the only positive correlation coeffcient (0.524), proposing that with an increasing degree of water solubility of a molecule, the greater the biological activity. While both of these outputs are classfied as almost significant, currently none fufil the criteria of statistical signifiance. The final variable considered, the skin permeability coefficient, had a negative correlation (-0.442), signifying the potential for the activity to increase as the predicted degree of skin permeation would decrease. Similar to other parameters previously mentioned, skin

permeation approaches the threshold of being almost significant (p-value 0.15), therefore while the correlation is not currently of statistical significance, such parameters such be followed closely as the compound library assessed expands to more robustly identify any trends present.

To summarise, from initial biochemical screening in CLL cell lines HG-3 and PGA-1, potent lead compounds were identified spanning nitrostyrene, nitrostyrene-ethanoanthracene and chalcone-ethanoanthracene series scaffolds. The compounds chosen displayed highly effective antiproliferative activity in the CLL cell lines and were subsequently found to induce cell death by a pro-apoptotic mechanism that was concentration-dependent. Evidence for ROS involvement in their antiproliferative activity suggested a structure-dependent factor linked to the potential degree of ROS involvement. Caspase-dependence could not be definitively confirmed for representative compounds, however the correlation between cell viability, compounds concentration and apoptosis was noted. All compounds assessed were predicted to act as CYP2C9 inhibitors with only three of the twelve compounds not falling within druggability filter criteria. Overall, the identified lead compounds represent promising potential scaffolds for CLL drug development.

Chapter 4: Conclusions and Future Work

4.1 Conclusions

Chronic lymphocytic leukaemia is the most common leukaemia present in the Western world. Despite increased understanding of the CLL tumour microenvironment and the development of increasingly specific and effective targeted therapeutics such as imatinib and ventetoclax, disease maintenance remains the treatment goal. CLL remains incurable and disease relapse due to drug resistance is a major clinical hurdle faced in haematooncology.

Previous work in our laboratory identified a series of (*E*)-1,3-bis(aryl)-2-nitro-1-propenes with potent anticancer activity in BL cell lines. The nitrostyrenes and related nitrovinyl compounds are biologically active compound classes which have a pro-apoptotic mechanism and antiproliferative effects across a range of different cancers e.g. breast, ovarian and CNS cancers. As part of these studies, various antidepressants were screened, with maprotiline being chosen as a lead compound scaffold for related nitrostyrene drug development. As a result, the (*E*)-9-(2-nitrovinyl)anthracenes and (*E*)-9-(2-nitrovinyl)-9,10,11,15-tetrahydro-9,10-[3,4]furanoanthracene-12,14-diones were designed and synthesised, which demonstrated promising pro-apoptotic activity in BL. The most potent of these two classes were progressed to CLL, a related B-cell malignancy to investigate their potential to be developed into novel therapeutics.

This study reports the synthesis, characterisation and biochemical evaluation of a number of nitrostyrene, related nitrovinyl, chalcone and related chalcone compounds in two CLL cell lines: HG-3 and PGA-1. A diverse library of compounds related in structure to the previous lead scaffold and the tetracyclic antidepressant maprotiline were synthesised and initially evaluated for anti-proliferative effect in the two CLL cell lines. These compounds were divided into 9 series of compounds as follows:

- **Series 1:** (*E*)-9-(2-Nitrovinyl)anthracenes
- **Series 2:** (*E*)-9-(2-Nitrovinyl)anthracene-maleimide adducts
- **Series 3:** Anthracene chalcones and related compounds
- **Series 4:** Ethanoanthracene chalcone-maleic anhydride adducts
- **Series 5-9:** Ethanoanthracene chalcone-maleimide adducts and related compounds

The structure activity relationships for each series will now be discussed.

4.1.1 Series 1: (*E*)-9-(2-Nitrovinyl)anthracenes

A focused library of 17 anthracene nitrovinyl derivatives underwent preliminary biochemical screening at two concentrations (10 and 1 μM) in HG-3 and PGA-1 cell lines. A number of potent antiproliferative agents were identified. A summary of SAR findings for this series is illustrated in Figure 229.

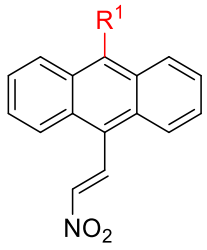

$R^1 = OCH_3 > H > CH_3 > C_2H_5 > -CH-(CH_3)_2$

Figure 228: Summary of SAR findings in Series 1 nitrostyrene compounds

The most potent of series 1 compounds **(5)**, **(8)**, **(10) (21)** and **(7)** were found to have IC_{50} values of 0.7-5.4 μM in HG-3 and 1.29-9.1 μM in PGA-1 cells , exihibiting high pro-apoptotic activity in HG-3 and PGA-1 CLL cell lines.The most promising of these compounds was **(10)** (Figure 230).

IC_{50} HG-3 :
(0.7-5.4 μM)

IC_{50} PGA-1:
(1.29-9.1 μM)

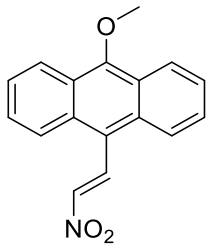

% Total Apoptosis
(both cell lines) :

(10 μM) (52-54%)

(1 μM) (11-12%)

(10)

Figure 229: Most potent compound of series 1 (10)

4.1.2 Series 2: (*E*)-9-(2-Nitrovinyl)anthracene-maleimide adducts

A small library of five potent (*E*)-9-(2-nitrovinyl)anthracene-maleimide adducts previously identified as antiproliferative agents in BL cell lines were assesed for antiproliferative activity in CLL cell lines HG-3 and PGA-1. All lead compounds (**24-**

28) were potent antiproliferative agents in CLL cells, predominantly in the sub-micromolar region. The most potent (**24**) was chosen as a proof of concept for Annexin V/PI studies, showing the presence of a concentration dependent pro-apoptotic effect in HG-3 and PGA-1 CLL cells. Futhermore, LDH studies noted low cytotoxicity of **24** in the identified CLL cells at the IC_{50} value range in both cell lines (**24** IC_{50} HG-3 048 µM , IC_{50} PGA-1 0.61 µM). In addition, ROS assays using both NAC and Trolox pretreatment and their ability to modulate the antiproliferative effect of **(24)** suggests the potential for a ROS dependent mechanism of action. Caspase inhibition assays conducted suggest a non-caspase dependent mechanism, however this results is to be confirmed in future studies. From all series tested, series 2 were found to be the most potent with IC_{50} values ranging from 0.48-1.6 µM HG-3 cells and 0.61-1.1 µM in PGA-1 cells. Based on the antiproliferative results of the most potent compounds, the SAR summary of the series is outlined in Figure 231. The most potent of the series 2 compounds identified was (**24)** (Figure 232).

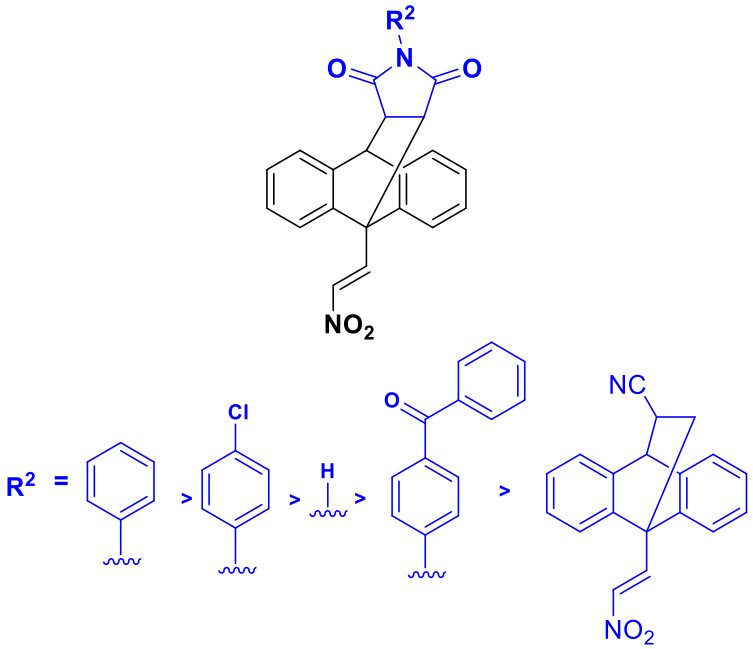

Figure 230: Summary of antiproliferative SAR for Series 2 compounds in CLL cell lines HG-3 and PGA-1

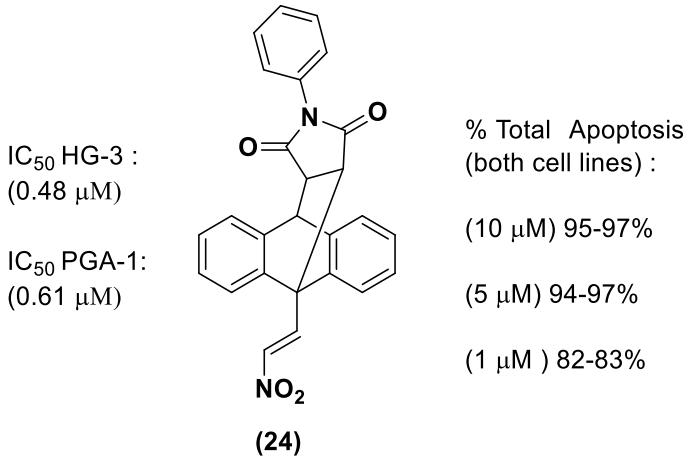

(24)

Figure 231: Most potent compound of series 2 (24)

4.1.3 Series 3: Anthracene chalcones and related compounds

A structurally diverse library of 16 anthracene chalcones was screened for antiproliferative actvity in HG-3 and PGA-1 cell lines. Based on the cell screening viability results, these compounds were accepted as useful intermediates for functionalisation of the final drug chemical structure and were not progressed further in these studies.

4.1.4 Series 4-9: Ethanoanthracene chalcone-maleic anhydride and maleimide adducts

A substantial library of 80 chalcone ethanoanthracene compounds was synthesised using Diels–Alder cycloaddition chemistry. They were divided into 5 subclasses according to the dienophile used, each consisting of 17 compounds. Variation at the ethanoanthracene bridge consisted of anhydride, imide (unsubstituted, *N*-phenyl, *p*-chlorophenyl and *p*-benzophenone) while variation at the C9 position of the anthracene core was dictated by the functionalities of the chalcones used.These consisted of pyridyl, aromatic, furan and thiophene heterocycles and diversely substituted benzyl rings. A summary of the SAR for the compounds is shown in Figure 233.

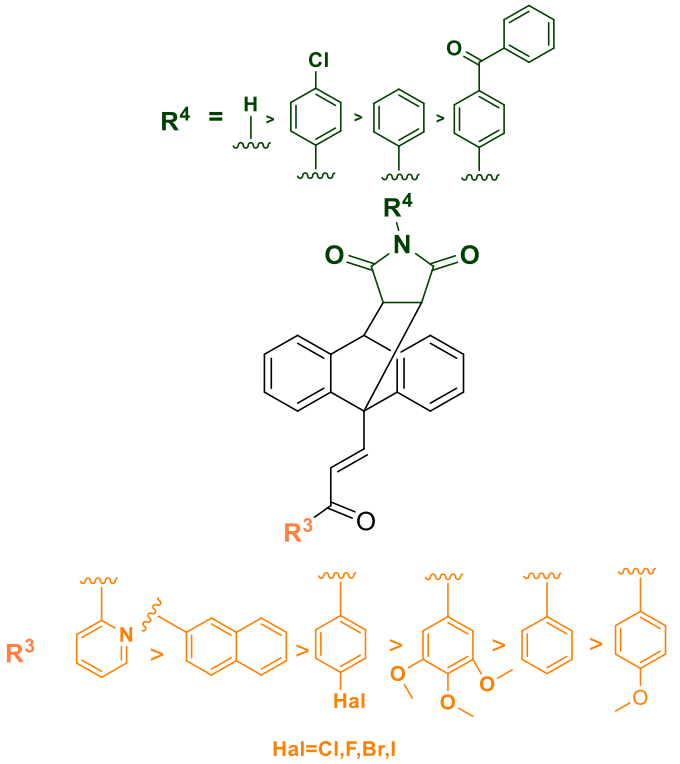

Figure 232: SAR summary of antiproliferative effect of series 4-9 ethanoanthracene chalcone-maleic anhydride and maleimide adducts in CLL cell lines

A moderate number of 14 ethanoanthracene chalcones (**86**, **88**, **101**, **99**, **93**, **92**, **133**, **150**, **91**, **97**, **94**, **95**, **108**, **114**) were classed as being potent enough to warrant further biochemical investigation, with observed CLL cell IC_{50} values of 1.31-10.28 µM in HG-3 and 0.31-12.6 µM PGA-1 cells. From these compounds two examples were investigated further e.g. **(86)** and **(133)**. LDH assays showed low to moderate cytotoxicity in PGA-1 and HG-3 respectively at the lower treatment concentration close to both compound IC_{50} values (**133** IC_{50} HG-3 1.31 µM , IC_{50} PGA-1 0.87 µM), (**86** IC_{50} HG-3 2.69 µM , IC_{50} PGA-1 1.97µM).These compounds also outperformed the standard clinical CLL drug fludarabine, which had IC_{50} values significantly larger than either compound **(133)** or **(86)** (fludarabine IC_{50} HG-3 28.1 µM, IC_{50} PGA-1 32 µM) .Strong evidence for ROS involvement in the effect compound **(86)** was seen with NAC co-treatment; however was weak with Trolox. This was in contrast to weak evidence of ROS involvement with both antioxidants and compound **(133)**. This result potentially points to structure dictating the degree (if any) of ROS involvement in compound bioactivity in this series.**(86)** had a caspase-dependent bioactivity in the HG-3 CLL cell line, however, this difference was not of statistical significance in the PGA-1 cell line. **(133)** and **(86)** both showed low

toxicity to PBMCs in *ex vivo* testing compared to their IC_{50} values across both cell lines, supporting possible selective compound toxicity (Figure 234).

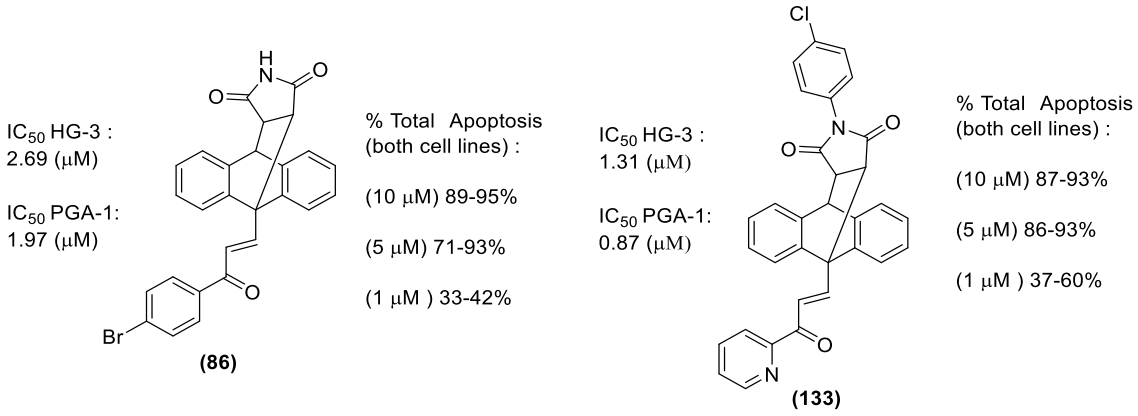

Figure 233: Two of the most potent compounds of series (4-9); compound (86) (left) and compound (133)

4.2 Future Work

Future work will include analysis of potential DNA binding and interference of lead compounds supported by NCI COMPARE analysis through correlation with known chemotherapeutic agents. This will be explored in an effort to discover potential molecular targets eliciting the observed pro-apoptotic effects in CLL cell lines.

Moreover, the use of polymerase chain reaction microarrays relevant to apoptotic cell death and the literature documented activites / cellular pathways of nitrostyrene and chalcone-based compounds (e.g. protein kinases, Nrf2) would help to inform future efforts for molecular targets, allowing efficient screening of large numbers of potential possibilities in a relatively short timeline. Another avenue worth assessing (informed by the NCI correlations to DNA interference agents) would be the exploration of compounds potential for DNA binding and/or DNA damage which could be pursued through use of techniques such as COMET assays and UV-Vis.

Futhermore, in terms of the role caspases may play in compound bioactivity, the caspase inhibitior concentration should be further optimised in PGA-1 and HG-3 cell lines and the assay repeated to draw a definitive conlusion. Also, the effect of caspase inhibition on compound-induced apoptosis is warranted to lend further evidence to whether a caspase-dependent or independent mechanism of cell death is present and if so, to elucidate the role of structural variations.

In addition to the above suggestions, another worthwhile avenue to expore would be the separation, physicochemical and biological characterisation of the racemate enantiomers of the most promising ethanoanthracene compounds.

Moreover, in terms of utilising the large amount of compound structural data generated to inform future compound modification, a working qualitative structure activity relationship (QSAR) model for these novel pro-apoptotic agents should be developed and in turn, a series pharmacophore developed using molecular modelling and computational chemistry approaches.

Structural modifications that would be of interest are:

- Reduction of α,β-unsaturated chalcone and subsequent Diels–Alder products to investigate impact of loss of Michael acceptor structure

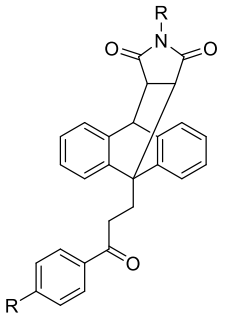

- Synthesis of further maleimide dimer-like compounds to investigate if potency similar to **(156)** can be optimised

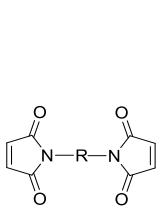

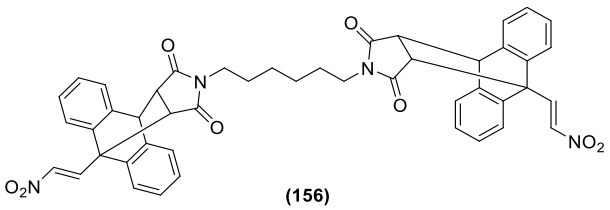

(156)

- Direct bioisosteric replacement of the nitro group of nitrostyrene with a pyridine ring and synthesis of Diels–Alder adducts

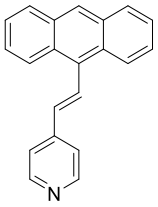

- Retention of the maleimide double bond on the ethanoanthracene bridge

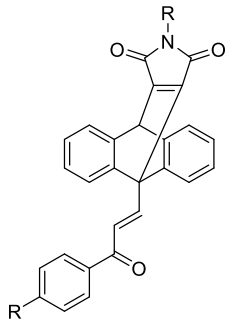

- Further biochemical evaluation of synthesised libraries by IC_{50} determination in CLL cell lines is also necessary to identify other potent structure scaffolds of interest

Efforts directed at curative and effective management therapies are of the utmost importance as CLL, like many other malignancies, remains incurable[538].Moreover, even though relatively successful treatments exist, emerging resistance, decreased efficacy and morbidity/quality of life impacts that result from conventional chemotherapeutic regimen side-effects[133, 150, 156]. Therefore, the discovery of novel CLL therapeutics represents a significant gap in patient treatment that warrants further exploration and investigation.

Chapter 5: Experimental

5.0 General Information- Experimental Note

Uncorrected melting points were measured on a Gallenkamp apparatus.Infra-red (IR) spectra were recorded on a Perkin Elmer FT-IR Paragon 1000 spectrometer. ^{1}H and ^{13}C nuclear magnetic resonance (NMR) spectra were recorded at 27 °C on a Bruker DPX 400 spectrometer (400.13 MHz, ^{1}H; 100.61 MHz, ^{13}C) in either $CDCl_3$ or DMSO-d_6 [Internal standard tetramethylsilane (TMS)]. For $CDCl_3$, ^{1}H-NMR spectra were assigned relative to the TMS peak at 0.00 ppm and ^{13}C-NMR spectra were assigned relative to the middle peak of the $CDCl_3$ triplet at 77.00 ppm. For ^{1}H-NMR assignments, chemical shifts are reported: shift value (number of protons, multiplicity, coupling constant(s) where applicable). Electrospray ionisation mass spectrometry (ESI-MS) and atmospheric – pressure chemical ionisation (APCI) mass spectrometry was performed in the positive ion mode on a liquid chromatography time-of-flight mass spectrometer (Micromass LCT, Waters Ltd., Manchester, UK). The samples were introduced to the ion source by an LC system (Waters Alliance 2795, Waters Corporation, USA) in acetonitrile:water (60:40 %v/v) at 200 μL / min. The capillary voltage of the mass spectrometer was at 3 kV. The sample cone (de-clustering) voltage was set at 40 V. For exact mass determination, the instrument was externally calibrated for the mass range m/z 100 to m/z 1000. A lock (reference) mass of leucine–enkephalin (m/z 556.2771) was used. Mass measurement accuracies of < ±5 ppm were obtained. Retnetion factor (R_f) values are quoted for thin layer chromatography on silica gel Merck F-254 plates, unless otherwise stated. Flash column chromatography was carried out on Merck Kieselgel 60 (particle size 0.040-0.063 mm), Aldrich aluminium oxide (activated, neutral, Brockmann I, 50 mesh) or Aldrich aluminium oxide (activated, acidic, Brockmann I, 50 mesh). Microwave experiments were carried out using the Discover CEM microwave synthesiser on standard power setting unless otherwise stated. On standard power setting, the maximum power supplied is 300 W.

Analysis of synthesised compounds by HPLC

Analytical high-performance liquid chromatography (HPLC) was performed using a Waters 2487 Dual Wavelength Absorbance detector, a Waters 1525 binary HPLC pump and a Waters 717plus Autosampler. The column used was a Thermo Scientific Hypersil

GOLD C18 reverse phase 5 μm 150 × 4.6 mm chromatography column. Samples were detected using wavelengths of 232 nm compounds **(24)** and **(99)**. All samples were analysed using and acetonitrile (75%): TFA (0.1%) in water (25%) over 15 min and a flow rate of 1 mL/min.

Phosphate buffer stability study method

Buffers were prepared according to methods from the 2019 version of the British Pharmacopoeia[539].

Phosphate buffer pH 4.0: 6.8 g of potassium dihydrogen orthophosphate was dissolved in 700 mL of water and the pH was adjusted to 4 with a 10% v/v solution of orthophosphoric acid.The solution was then diluted up to 1000 mL, ensuring constant pH while mixing using a pH meter.

Phosphate buffer pH 7.4: Potassium dihydrogen phosphate (0.2 M, 250 mL) was added to of sodium hydroxide (0.1 M, 393 mL) and mixed to form a buffer of pH 7.4.A constant pH while mixing was ensured using a pH meter.

Phosphate buffer pH 9.0: 1.74 g of potassium dihydrogen phosphate was dissolved in 80 mL of water and the pH was adjusted to pH 9 with a 1 M potassium hydroxide solution prepared from potassium hydroxide and then diluted to 100 mL with water. A constant pH while mixing was ensured using a pH meter.

Method

300 μL of stock solution (1mg/mL ACN) for compounds **(24)** and **(99)** were added to a vial containing 9.7 mL of buffer. Prior to HPLC analysis, this solution was pre-heated to 37˚C and uniformly mixed to induce a temperature similar to *in vivo* conditions. 1 mL of the solution was added to a HPLC glass vial and 10 μL was injected, followed by hourly injections for a 24 hour period.

5.1 General procedure for the synthesis of (*E*)-9-(2-nitrovinyl)anthracene derivatives *via* Henry Knovenagel Condensation

To a solution of 9-anthraldehyde 2.0 g (9.7 mmol) in the appropriate nitroalkane 15 mL was added 1.5 g of piperidinium acetate (10.3 mmol). Piperidinium acetate was prepared from 6.6 mL piperidine and 3 mL of acetic acid. The solution was heated at 90℃ for 1.5

h under nitrogen. After one hour the reaction was cooled to room temperature and poured onto 100 mL of ice cold H_2O. The resultant mixture was extracted into DCM, washed with brine and the organic layers were combined, dried over Na_2SO_4 and solvent removed *in vacuo.* The product was recrystallized from methanol and diethyl ether.

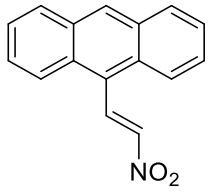

(*E*)-9-(2-Nitrovinyl) anthracene (5)

(*E*)-9-(2-Nitrovinyl)anthracene was prepared from 9-anthraldehyde (9.7 mmol, 2.0 g) and nitromethane (0.28 moles, 15 mL) according to general procedure (1). The product was recrystallized from methanol and diethyl ether, red crystals (99%)

Melting Point: 145-147 ˚C (lit.M.p.142 ˚C [191])

IR*Vmax* (ATR): 3050, 2948 (C-H), 1617, 1553 (C=C), 1498, 1330 (NO2), 1250 (C-N) cm^{-1}

^{1}H NMR (400 MHz, $CDCl_3$) δ ppm 7.40 - 7.66 (m, 5 H, ArH ,CH=C), 7.80 - 8.05 (m, 2 H, ArH), 8.05 - 8.25 (m, 2 H, ArH), 8.45 (br.s., 1 H), 8.90 (d, *J* = 13.43 Hz, 1 H, CH=C)

^{13}C NMR (101 MHz, $CDCl_3$) δ ppm 124.3, 125.7, 127.5, 129.2, 129.2, 129.8, 130.4, 131.1, 135.6, 142.6

HRMS (APCI) calculated for $C_{16}H_{12}NO_2$ [M^++H] 250.0868: found 250.0879. Mass accuracy (-4.39 ppm)

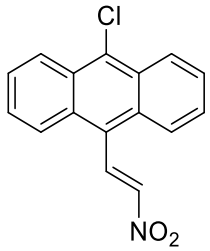

(*E*)-9-Chloro-10-(2-nitrovinyl) anthracene (6)

(*E*)-9-Chloro-10-(2-nitrovinyl)anthracene was prepared from 10-chloroanthracene-9-carbaldehyde (5 mmol, 1.2 g) and nitromethane (15 mL) according to general procedure

(1). The product was recrystallized from methanol and diethyl ether, orange crystals (71%)

Melting Point: 231-233˚C

IR*Vmax* (ATR): 3066, 2973 (C-H), 1623 (C=C), 1439 (C=C), 1538, 1326 (NO_2), 1110 (C-N) cm^{-1}

^{1}H NMR (400 MHz, $CDCl_3$) δ ppm 7.52 (d, *J* = 14.04 Hz, 1 H, CH=C), 7.60 - 7.77 (m, 4 H, ArH), 8.20 (d, *J* = 8.55 Hz, 2 H, ArH), 8.62 (d, *J* = 8.55 Hz, 2 H, ArH), 8.96 (d, *J* = 14.04 Hz, 1 H, CH=C)

^{13}C NMR (101 MHz, $CDCl_3$) δ ppm 124.8, 125.8, 127.1, 127.6, 128.5, 130.1, 135.4, 143.3

HRMS (APCI) calculated for $C_{16}H_{11}ClNO_2$ $[M^+ + H]$ 284.0478: found 284.0492. Mass accuracy (4.93 ppm)

5.2 General Procedure (2) for synthesis of (*E*)-9-(2-nitrovinyl)-9,10,11,15-tetrahydro-9,10-[3,4]epipyrroloanthracene-12,14-dione derivatives

To a solution of the appropriate nitrovinyl anthracene analog (1.0 mmol) in toluene (2 mL) was added a specific dienophile (1.3 mmol). The mixture was heated, with stirring at 90 ˚C for 48 h. The reaction was then cooled to RT and the resulting solid was isolated by filtration. The solid product was sequentially washed with toluene (2 mL) and diethyl ether (2 mL). The product was then recrystallized from toluene if necessary.

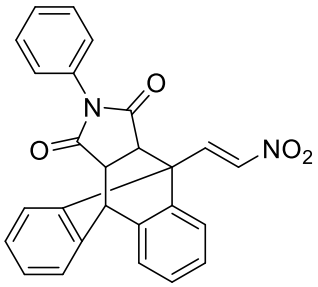

(*E*)-9-(2-Nitrovinyl)-13-phenyl-9,10-dihydro-9,10-[3,4]epipyrroloanthracene-12,14-dione (24)

(*E*)-9-(2-Nitrovinyl)-13-phenyl-9,10-dihydro-9,10-[3,4]epipyrroloanthracene-12,14-dione was prepared from (*E*)-9-(2-nitrovinyl) anthracene (1.0 mmol, 0.25 g) and *N*-

phenylmaleimide (1.3 mmol, 0.23 g) according to general procedure (2), colourless solid (30%)

Melting Point: 256-257 ˚C

IR*Vmax* (KBr): 3108.83, 3046.54, 3035.26, 2961.81 (Ar C-H), 1709.98 (C=O), 1529.34, 1349.99 (NO_2), 1596.99, 1498.62, 1457.12 (Ar C=C), 1201.34 (C-N) cm^{-1}

^{1}H NMR (400 MHz, DMSO-*d*$_6$) δ ppm 3.51 (m, *J*=8.24, 2.75 Hz, 1H), 3.91 (d, *J*=8.54 Hz, 1 H), 4.86 - 4.98 (m, 1H), 6.28 - 6.46 (m, 2 H), 7.14 - 7.34 (m, 10 H, ArH), 7.58 (d, *J*=6.71 Hz, 1 H, ArH), 8.08 (d, *J*=14.04 Hz, 1 H), 8.28 (d, *J*=14.04 Hz, 1 H)

^{13}C NMR (101 MHz, DMSO-*d*$_6$) δ ppm 44.78, 47.63, 47.92 , 123.07 , 123.51 , 124.48 , 125.29 , 126.47 , 126.97 , 127.16 , 127.31 , 128.57 , 128.85 , 131.53, 137.29, 138.47, 140.94, 141.28 , 145.22 , 174.72, 175.06 (C=O)

HRMS (APCI) calculated for $C_{26}H_{19}N_2O_4$ [M^++H] 423.1345: found 423.1364. Mass accuracy (4.49 ppm)

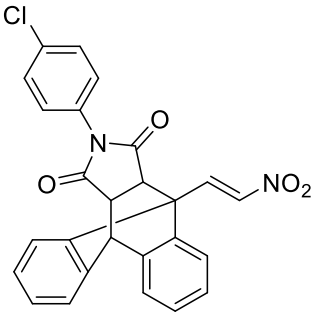

(*E*)-13-(4-Chlorophenyl)-9-(2-nitrovinyl)-9,10-dihydro-9,10-[3,4]epipyrroloanthracene-12,14-dione (25)

(*E*)-13-(4-Chlorophenyl)-9-(2-nitrovinyl)-9,10-dihydro-9,10-[3,4]epipyrroloanthracene-12,14-dione was prepared from (*E*)-9-(2-nitrovinyl)anthracene (1.0 mmol, 0.25 g) and 1-(4-chlorophenyl)-1*H*-pyrrole-2,5-dione (1.3 mmol, 0.27 g) according to general procedure (2), colourless solid (51 %)

Melting Point: 238-241˚C

IR*Vmax* (KBr): 3129.50, 3097.50, 3051.15, 3035.88, 2946.49 (Ar C-H), 1714.9 (C=O), 1659.56 (C=C), 1537.76, 1493.14, 1459.86 (Ar C=C), 1191.36 (C-N) cm^{-1}

^{1}H NMR (400 MHz, DMSO-*d*$_6$) δ ppm 3.55 (dd, *J*=8.54, 3.05 Hz, 1 H), 3.95 (d, *J*=7.93 Hz, 1 H), 4.97 (d, *J*=3.05 Hz, 1 H), 6.48 (d, *J*=8.54 Hz, 2 H), 7.21 - 7.47 (m, 10 H, ArH), 7.61 (d, *J*=6.71 Hz, 1 H), 8.12 (d, *J*=14.04 Hz, 1 H), 8.32 (d, *J*=14.04 Hz, 1 H)

^{13}C NMR (101 MHz, DMSO-*d*$_6$) δ ppm 44.78, 47.67, 49.65, 123.04, 123.54, 124.51, 125.26, 126.51, 126.99, 127.18, 127.34, 128.13, 129.00, 130.29, 133.13, 137.22, 138.42, 138.49, 140.85, 141.20, 145.24, 174.51, 174.87 (C=O)

HRMS (APCI) calculated for $C_{26}H_{18}ClN_2O_4$ [M^++H] 457.0955: found 457.0968. Mass accuracy (2.84ppm)

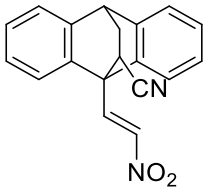

(*E*)-10-(2-Nitrovinyl)-9,10-dihydro-9,10-ethanoanthracene-11-carbonitrile (26)

(*E*)-10-(2-Nitrovinyl)-9,10-dihydro-9,10-ethanoanthracene-11-carbonitrile was prepared from (*E*)-9-(2-nitrovinyl)anthracene (1.0 mmol, 0.25 g) and acrylonitrile (3.0 mmol, 0.2 mL) according to general procedure (2), orange crystals (30%)

Melting Point: 223-225 °C

IR*Vmax* (ATR): 3113, 3072, 2952 (C-H), 1658 (C=C), 1485, 1457 (C=C), 1526, 1354 (NO_2), 1190 (CN) cm^{-1}

^{1}H NMR (400 MHz, DMSO-*d*6) δ ppm 1.93 (dt, *J* = 12.82, 3.36 Hz, 1 H), 2.27 (ddd, *J* = 12.67, 10.53, 2.44 Hz, 1 H), 3.66 (dd, *J* = 10.68, 3.97 Hz, 1 H), 4.60 (s, 1 H), 7.11 - 7.31 (m, 5 H, 5 x ArH), 7.34 - 7.49 (m, 3 H, 3 x ArH), 8.04 (d, *J* = 13.43 Hz, 1 H), 8.33 (d, *J* = 14.04 Hz, 1 H)

^{13}C NMR (101 MHz, DMSO-*d*6) δ ppm 31.2, 34.0, 41.7, 48.9, 121.0, 123.1, 123.2, 123.8, 124.2, 126.1, 126.3, 127.3, 127.4, 138.1, 138.7, 139.9, 142.1, 142.5, 144.0

HRMS (APCI) calculated for $C_{19}H_{14}N_2O_2$ [M^+] 302.1055: found 302.1055. Mass accuracy (0 ppm)

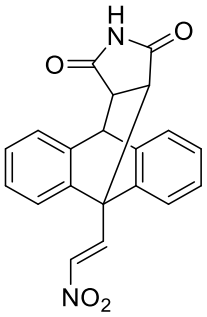

(*E*)-9-(2-Nitrovinyl)-9,10-dihydro-9,10-[3,4]epipyrroloanthracene-12,14-dione (27)

(*E*)-9-(2-Nitrovinyl)-9,10-dihydro-9,10-[3,4]epipyrroloanthracene-12,14-dione was prepared from (*E*)-9-(2-nitrovinyl)anthracene (1.0 mmol, 0.25 g) and maleimide (1.3 mmol, 0.13 g) according to general procedure (2), colourless solid (50 %)

Melting Point: 176-178 ^{o}C

IR*Vmax* (KBr): 3551.15 (N-H), 3133.67, 3091.21, 3058.51, 2963.34 (Ar C-H), 1722.27 (C=O), 1527.78, 1354.70 (NO_2), 1167.49 (C-N) cm^{-1}

^{1}H NMR (400 MHz, DMSO-*d*$_6$) δ ppm 3.28 (br.s., 1 H), 3.70 (d, *J*=8.54 Hz, 1 H), 4.79 (br.s., 1 H), 6.99 - 7.36 (m, 7 H, ArH), 7.51 (d, *J*=6.71 Hz, 1 H, ArH), 8.04 (d, *J*=14.04 Hz, 1 H), 8.24 (d, *J*=13.43 Hz, 1 H), 10.89 (br.s., 1 H)

^{13}C NMR (101 MHz, DMSO-*d*$_6$) δ ppm 44.34, 48.6 , 49.22, 122.89, 123.25, 124.26, 125.25, 126.31, 126.71, 126.99, 127.15, 137.51, 138.54, 138.72, 141.43, 141.66, 145.05, 176.88, 177.05 (C=O)

HRMS (APCI) calculated for $C_{20}H_{13}N_2O_4$ [M^+-H] 345.0881: found 345.0896. Mass accuracy (-4.34 ppm)

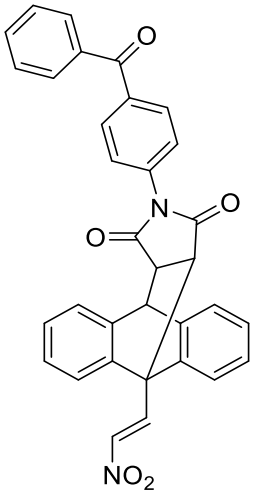

(*E*)-13-(4-Benzoylphenyl)-9-(2-nitrovinyl)-9,10-dihydro-9,10-[3,4]epipyrroloanthracene-12,14-dione (28)

(*E*)-13-(4-Benzoylphenyl)-9-(2-nitrovinyl)-9,10-dihydro-9,10-[3,4]epipyrroloanthracene-12,14-dione was prepared from (*E*)-9-(2-nitrovinyl) anthracene and maleimide according to general procedure (2), yellow solid (40%)

Melting Point: 232-234 ˚C

IR*Vmax* (ATR): 3071, 2966 (C-H), 1708 (C=O), 1660 (C=C), 1458, 1448 (C=C), 1529, 1353 (NO_2), 1195 (C-N) cm^{-1}

^{1}H NMR (400 MHz, DMSO-*d*6) δ ppm 3.60 (dd, *J* = 8.55, 3.05 Hz, 1 H), 3.99 (d, *J* = 8.55 Hz, 1 H,), 5.00 (d, *J* = 3.05 Hz, 1 H), 6.69 (d, *J* = 8.55 Hz, 2 H), 7.22 - 7.35 (m, 5 H, ArH), 7.35 - 7.46 (m, 2 H, ArH), 7.50 - 7.60 (m, 2 H, ArH), 7.60 - 7.74 (m, 6 H, ArH), 8.14 (d, *J* = 14.04 Hz, 1 H), 8.34 (d, *J* = 14.04 Hz, 1 H)

^{13}C NMR (101 MHz, DMSO-*d*6) δ ppm 44.8, 47.8, 48.1, 49.7, 123.1, 123.6, 124.5, 125.3, 126.4 , 126.5, 127.1, 127.2, 127.4, 128.2, 128.6, 129.6, 130.2, 132.9 , 134.9, 136.5, 136.9, 137.2 , 138.4, 138.5, 140.9, 141.2, 145.3, 174.5, 174.8, 194.8 (C=O)

HRMS (APCI) calculated for $C_{33}H_{23}N_2O_5$ [M^++H] 527.1607: found 527.1599. Mass accuracy (-1.52 ppm)

5.3 General Procedure (3) for the synthesis of (*E*)-3-(anthracen-9-yl)-1-phenylprop-2-en-1-ones

To a solution of NaOH (6 mmol, 0.24g) in 50% aqueous EtOH (20 mL) was added the appropriate acetophenone (5.02 mmol). After dissolution of the acetophenone derivative, 9-anthracenecarboxaldehyde (5.02 mmol, 1.035 g) was added, resulting in a coloured

solution. This was left to stir at RT for 24 h to give a coloured suspension. The suspension was filtered, washed with minimal cold EtOH and left to dry to afford the crude product. The product was then recrystallized from the minimal amount of hot EtOH or dry MeOH, cooling the hot solution to RT to allow the resulting solid to precipitate out of solution and washing it with cold EtOH or MeOH to afford pure product as a coloured solid.

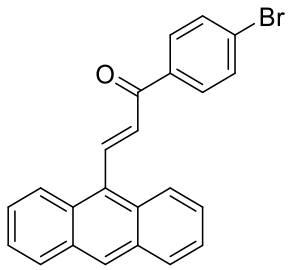

(*E*)-3-Anthracen-9-yl)-1-(4-bromophenyl) prop-2-en-1-one (34) [540]

(*E*)-3-(Anthracen-9-yl)-1-(4-bromophenyl)prop-2-en-1-one was synthesised from 4-bromoacetophenone (5.02 mmol, 1g) and 9-anthracenecarboxaldehyde (5.02 mmol, 1.035 g) according to the general procedure (3), yellow crystals (65%)

Melting Point: 164˚C (lit Mp.164˚C)[540]

^{1}H NMR (400 MHz,$CDCl_3$) δ ppm 7.46 - 7.54 (m, 5 H, 4xArH, 1x C=CH), 7.61 - 7.66 (m, 2 H, ArH), 7.89 - 7.95 (m, 2H, ArH), 7.99 - 8.04 (m, 2 H,ArH), 8.24 - 8.29 (m, 2 H, ArH), 8.46 (br.s, 1 H, ArH), 8.80 (d, *J*=15.76 Hz, 1 H, C=CH)

^{13}C NMR (101 MHz,$CDCl_3$) δ ppm 125.15, 125.43, 125.35, 126.5, 128.26, 128.62, 128.95, 129.61, 129.84, 130.18, 130.37, 131.27, 132.05, 136.58, 142.47, 188.50 (C=O)

IR*ν_{max}* (ATR): 3048.16 (Ar C–H), 1593.87, 1332.11 (Ar C=C), 1730.51 (*trans* C=C), 1657.97 (C=O), 1070.45 (Ar Br) cm^{-1}

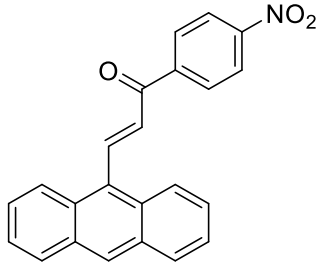

(*E*)-3-(Anthracen-9-yl)-1-(4-nitrophenyl) prop-2-en-1-one (35)

(*E*)-3-(Anthracen-9-yl)-1-(4-nitrophenyl)prop-2-en-1-one was synthesised from 4-nitroacetophenone (5.02 mmol, 829.1 mg) and 9-anthracenecarboxaldehyde (5.02 mmol, 1.035 g) according to the general procedure (3), Red Crystals (78%)

Melting point: 159-162°C (lit.Mp.154-155°C) [540, 541]

^{1}H NMR (400 MHz,$CDCl_3$) δ ppm 7.48 - 7.56 (m, 5 H, 4x ArH, 1x C=CH), 8.01 - 8.07 (m, 2 H, ArH), 8.18 - 8.24 (m, 2 H, ArH), 8.24 - 8.30 (m, 2 H, ArH), 8.33 - 8.38 (m, 2 H, ArH), 8.51 (br.s, 1 H, ArH), 8.87 (d, *J*=15.34 Hz, 1 H, C=CH)

^{13}C NMR (101 MHz,$CDCl_3$) δ ppm 123.93, 124.92, 125.5, 126.78, 129.05, 129.13, 129.58, 129.67, 130.01, 131.26, 142.57, 143.87, 188.08 (C=O)

IR*Vmax* (ATR): 3104.08, 3081.04, 3048.01, 2981.55 (Ar C-H), 1659.87 (C=O), 1624.09 (*trans* C=C), 1598.52, 1582.22, 1441.80, 1407.66 cm (Ar C=C), 1523.92, 1344.05 (Ar NO_2) cm^{-1}

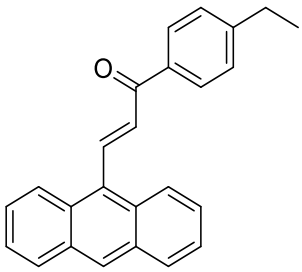

(*E*)-3-(Anthracen-9-yl)-1-(4-ethylphenyl) prop-2-en-1-one (36)

(*E*)-3-Anthracen-9-yl)-1-(4-ethylphenyl)prop-2-en-1-one was synthesised from 4-ethylacetophenone (5.02 mmol, 744 mg) and 9-anthracenecarboxaldehyde (5.02 mmol, 1.035 g) according to the general procedure (3), Yellow/Orange Crystals (61%)

Melting Point: 128-129˚C

^{1}H NMR (400 MHz,$CDCl_3$) δ ppm 1.27 (t, *J*=7.67 Hz, 3 H, CH_3) 2.73 (q, *J*=7.60 Hz, 2 H,CH_2) 7.33 (d, *J*=8.29 Hz, 2 H) 7.47 - 7.57 (m,5H,4x ArH ,1xC=CH),7.98 - 8.05 (m, 4 H, ArH) 8.27 - 8.34 (m, 2 H, ArH) 8.45 (br.s, 1 H, ArH) 8.77 (d, *J*=16.17 Hz, 1 H,C=CH)

^{13}C NMR (101 MHz, $CDCl_3$) δ ppm 15.20, 28.99, 125.35, 125.40, 126.34, 128.27, 128.87, 128.96, 129.61, 130.33, 131.13, 131.30, 135.56, 141.40, 150.16, 189.19 (C=O)

IR*Vmax* (ATR): 3318.10, 3048.93, 3081.76, 2970.29, 2883.67 (Ar C-H), 1658.74 (C=O), 1622.32 (*trans* C=C), 1591.76, 1518.23, 1441.48, 1409.24 (Ar C=C), 1463.79 (CH_2), 1376.63 (CH_3) cm^{-1}

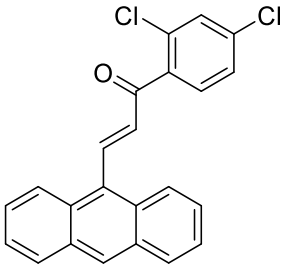

(*E*)-3-(Anthracen-9-yl)-1-(2, 4-dichlorophenyl) prop-2-en-1-one (37)

(*E*)-3-(Anthracen-9-yl)-1-(2,4-dichlorophenyl)prop-2-en-1-one was synthesised from 2',4'-dichloroacetophenone (5.02 mmol, 949 mg) and 9-anthracenecarboxaldehyde (5.02 mmol, 1.035 g) according to the general procedure (3), yellow solid (75%)

Melting Point: 142-143 ˚C

^{1}H NMR (400 MHz $CDCl_3$) δ ppm 7.14 (d, *J*=16.17 Hz, 1 H, C=CH), 7.41 (dd, *J*=8.29, 1.66 Hz, 1 H, ArH,) 7.46 - 7.56 (m, 5 H, ArH), 7.61 (d, *J*=8.29 Hz, 1 H, ArH), 7.99 - 8.04 (m, 2 H, ArH), 8.20 - 8.26 (m, 2 H,ArH), 8.48 (br.s, 1 H, ArH), 8.52 (d, *J*=16.59 Hz, 1 H, C=CH)

^{13}C NMR (101 MHz, $CDCl_3$) δ ppm 124.98, 125.46, 126.66, 128.95, 128.97, 129.05, 129.52, 130.29, 130.67, 131.24, 134.38, 137.33, 143.64, 191.96 (C=O)

IR*ν_{max}* (ATR): 3085.39, 3050.17 (Ar C-H), 1622.99 (*trans* C=C), 1663.97, 1588.07, 1556.09, 1465.62, 1013.77 (Ar-Cl) cm^{-1}

LRMS (ESI) calculated for C_{23} H12 $O^{2\bullet 2+}$ [M^{+}- (2HCl)] 304.0877 : found 304.2624 .

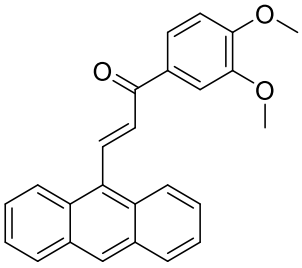

(*E*)-3-(Anthracen-9-yl)-1-(3, 4-dimethoxyphenyl) prop-2-en-1-one (38)

(*E*)-3-Anthracen-9-yl)-1-(3, 4-dimethoxyphenyl)prop-2-en-1-one was synthesised from 3', 4'-dimethoxyacetophenone (5.02 mmol, 904.6 mg) and 9-anthracenecarboxaldehyde (5.02 mmol, 1.035 g), according to the general procedure (3), yellow powder (85%)

Melting Point: 138-139 ˚C

^{1}H NMR (400 MHz, $CDCl_3$) δ ppm 3.97 (d, *J*=11.61 Hz, 6 H, 2xCH_3), 6.91 (d, *J*=8.71 Hz, 1 H), 7.40 - 7.53 (m, 4 H, ArH), 7.54-7.58 (d, *J*=15.76 Hz, 1 H,CH=C), 7.65 - 7.72 (m, 2 H, ArH), 8.01 - 8.05 (m, 2H, ArH), 8.29 - 8.32 (m, 2H, ArH), 8.47 (br.s, 1H, ArH), 8.77 (d, *J*=15.76 Hz, 1H, ArH)

^{13}C NMR (101 MHz, $CDCl_3$) δ ppm 53.07, 53.11, 110.07, 110.85, 123.34, 125.39, 126.31, 128.20, 128.87, 129.61, 130.80, 131.03, 131.31, 141.00, 187.81 (C=O)

IR*Vmax* (ATR): 3081.44, 3049.16, 2968.80 (Ar C-H), 1656.98 (C=O), 1622.51 (*trans* C=C), 1591.24, 1580.66, 1515.04, 1442.23, 1416.45 (Ar C=C), 1266.73, 1014.80 (C-O) cm^{-1}

HRMS (ESI) calculated for C_{25} H_{20} NaO_3 [M^++ Na] 391.130465: found 391.130730 . Mass accuracy (-0.7 ppm).

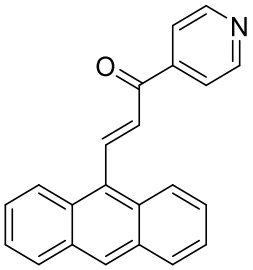

(*E*)-3-(Anthracen-9-yl)-1-(pyridin-4-yl) prop-2-en-1-one (46) [542]

(*E*)-3-(Anthracen-9-yl)-1-(pyridin-4-yl) prop-2-en-1-one was synthesised from 4-acetylpyridine (5.02 mmol, 0.55 mL) and 9-anthracenecarboxaldehyde (5.02 mmol, 1.035 g), according to the general procedure (3), orange crystals (49%)

Melting Point: 170-173 ˚C

^{1}H NMR (400 MHz, $CDCl_3$) δ ppm 7.44 - 7.48 (d, 1H, CH=C), 7.49 - 7.56 (m, 3H, ArH), 7.80 - 7.85 (m, 2H, ArH), 7.98 - 8.05 (m, 2H, ArH), 8.21 - 8.28 (m, 2H, Ar H), 8.46 (br.s, 1H), 8.80 - 8.87 (m, 3H, ArH, C=CH)

^{13}C NMR (101 MHz, $CDCl_3$) δ ppm 121.57, 124.92, 125.49, 126.75, 129.03 129.09, 129.64, 129.84, 131.23, 143.86, 143.90, 150.94, 188.94 (C=O)

IR*Vmax* (ATR): 3047.23, 2971.86 (Ar C-H), 1587 (C=O), 1621.69 (*trans* C=C), 1661. 62, 1597.45, 1518.42, 1441.76 (Ar C=C), 1266.30 (C-N) cm^{-1}

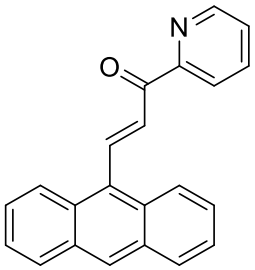

(*E*)-3-(Anthracen-9-yl)-1-(pyridin-2-yl) prop-2-en-1-one (47)

(*E*)-3-(Anthracen-9-yl)-1-(pyridin-2-yl)prop-2-en-1-one was synthesised from 2-acetylpyridine (5.02 mmol, 0.56 mL) and 9-anthracenecarboxaldehyde (5.02 mmol, 1.035 g), according to the general procedure (3), green solid (58%)

Melting point: 97-101 ˚C

^{1}H NMR (400 MHz, $CDCl_3$) δ ppm 7.44 - 7.53 (m, 5H, ArH, CH=C), 7.90 (td, *J*=7.78, 1.87 Hz, 1 H, ArH), 7.99 - 8.04 (m, 2H, ArH), 8.23 - 8.30 (m, 2H, ArH), 8.33 - 8.38 (m, 2H, ArH), 8.46 (br.s, 1H, ArH), 8.66 - 8.70 (m, 1H, ArH), 8.92 (d, *J*=16.17 Hz, 1H, C=CH)

^{13}C NMR (101 MHz, $CDCl_3$) δ ppm 123.1, 125.4, 125.5, 126.4, 127.0, 128.5, 128.9, 130.2, 137.1, 137.9, 141.8, 149.1, 172.4 (chalcone C=O)

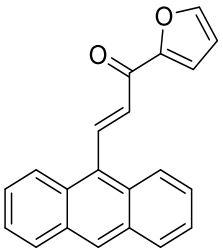

(*E*)-3-(Anthracen-9-yl)-1-(furan-2-yl) prop-2-en-1-one (48)

(*E*)-3-(Anthracen-9-yl)-1-(furan-2-yl)prop-2-en-1-one was synthesised from 2-acetylfuran (5.02 mmol, 552.8 mg) and 9-anthracenecarboxaldehyde (5.02 mmol, 1.035 g), according to the general procedure (3), yellow crystals (67%)

Melting Point: 148-150 ˚C

^{1}H NMR (400 MHz, $CDCl_3$) δ ppm 6.60 (dd, *J*=3.73, 1.66 Hz, 1 H, C=CH), 7.32 - 7.36 (m, 1 H, CH=C), 7.42 (d, *J*=16.17 Hz, 1 H, CH=C), 7.47 - 7.54 (m, 4 H, ArH), 7.64 - 7.68 (m, 1 H, CH=C), 7.99 - 8.05 (m, 2 H, ArH), 8.26 - 8.32 (m, 2H, ArH), 8.46 (br.s, 1 H, ArH), 8.84 (d, *J*=15.76 Hz, 1H, CH=C)

^{13}C NMR (101 MHz, $CDCl_3$) δ ppm 112.61, 118.13, 125.28, 125.40, 126.41, 128.48, 128.88, 129.64, 129.93, 130.27, 131.28, 141.14, 146.92, 153.59, 177.39 (C=O)

IR*Vmax* (ATR): 3082, 3048.70 (Ar C-H), 1587.15 (C=O), 1622.50 (*trans* C=C), 1663.59, 1555.20, 1518.79, 1441.13 (Ar C=C), 1013.08 (C-O) cm^{-1}

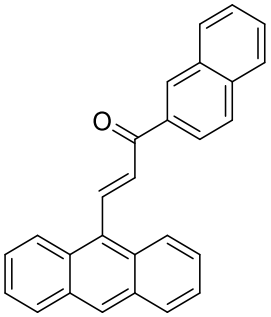

(*E*)-3-(Anthracen-9-yl)-1-(naphthalen-2-yl) prop-2-en-1-one (49)

(*E*)-3-(Anthracen-9-yl)-1-(naphthalen-2-yl)prop-2-en-1-one was synthesised from 1-(naphthalen-2-yl)ethan-1-one (5.02 mmol, 0.855 g) and 9-anthracenecarboxaldehyde (5.02 mmol, 1.035 g), according to the general procedure (3), yellow crystals (38%)

Melting point: 160-164˚C

^{1}H NMR (400 MHz, $CDCl_3$) δ ppm 7.47 - 7.56 (m, 5 H, ArH) 7.57 - 7.63 (m, 1 H, ArH) 7.72 (d, *J*=15.76 Hz, 1 H, CH=C) 7.87 - 7.98 (m, 3 H, ArH) 8.00 - 8.06 (m, 2 H, ArH) 8.19 (dd, *J*=8.71, 1.66 Hz, 1 H,ArH) 8.31 - 8.37 (m, 2 H, ArH) 8.45 - 8.50 (m, 1 H, ArH) 8.56 (br.s, 1 H, ArH) 8.85 (d, *J*=15.76 Hz, 1 H,C=CH)

^{13}C NMR (101 MHz, $CDCl_3$) δ ppm 124.48,125.00, 125.29 - 125.48, 125.89, 126.21, 126.44 ,126.84 ,127.09 ,127.83 128.03 - 128.05 128.42 128.55 128.67 - 128.76 128.83 - 128.97 129.14 129.58 129.66 130.37 131.01 - 131.12 131.32 132.56 134.54 135.07 135.21 135.60 138.95 141.80 189.41 (C=O)

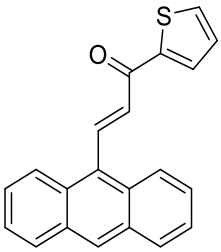

(*E*)-3-(Anthracen-9-yl)-1-(thiophen-2-yl)prop-2-en-1-one (50)

(*E*)-3-(Anthracen-9-yl)-1-(thiophen-2-yl)prop-2-en-1-one was synthesised from 2-acetylthiophene (5.02 mmol, 0.54 mL) and 9-anthracenecarboxaldehyde (5.02 mmol, 1.035 g), according to the general procedure (3), yellow crystals (86%)

Melting Point: 157-158 ˚C

^{1}H NMR (400 MHz, $CDCl_3$) δ ppm 7.18 (dd, *J*=4.98, 3.73 Hz, 1 H,C=CH), 7.42 (d, *J*=15.76 Hz, 1 H, C=CH), 7.47 - 7.54 (m, 4 H, ArH), 7.72 (dd, *J*=4.77, 1.04 Hz, 1 H,C=CH), 7.82 (dd, *J*=3.94, 1.04 Hz, 1 H,(C=CH), 8.00 - 8.06 (m, 2 H, ArH), 8.26 - 8.32 (m, 2 H, ArH), 8.47 (br.s, 1 H, ArH), 8.81 (d, *J*=15.76 Hz, 1 H,C=CH)

^{13}C NMR (101 MHz, $CDCl_3$) δ ppm 125.27, 125.43, 126.44, 128.37, 128.45, 128.89, 129.63, 129.93, 130.71, 131.28, 132.27, 134.37, 141.21, 145.41, 181.48 (C=O)

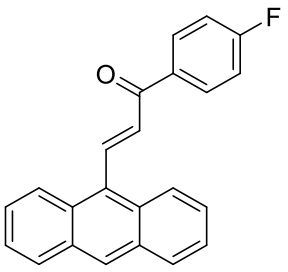

(*E*)-3-(Anthracen-9-yl)-1-(4-fluorophenyl) prop-2-en-1-one (41)

(*E*)-3-(Anthracen-9-yl)-1-(4-fluorophenyl)prop-2-en-1-one was synthesised from of 4-fluoroacetophenone (5.02mmol, 0.61 mL) and 9-anthracenecarboxaldehyde (5.02mmol, 1.035 g), according to the general procedure (3), yellow crystals (88%)

Melting Point: 142℃

^{1}H NMR (400 MHz, $CDCl_3$) δ ppm 7.15 - 7.22 (m, 2 H, ArH), 7.47 - 7.55 (m, 5 H, 4x ArH, 1x C=CH), 8.00 - 8.04 (m, 2H, ArH), 8.08 - 8.14 (m, 2H, ArH), 8.26 - 8.31 (m, 2 H, ArH), 8.46 (br.s, 1 H, ArH), 8.80 (d, *J*=16.17 Hz, 1H,C=CH)

^{13}C NMR (101 MHz, $CDCl_3$) δ ppm 115.77, 115.99, 125.20, 125.43, 126.47, 128.51, 128.93, 129.61, 130.52, 131.27, 131.28, 131.36, 134.24, 142.13, 164.50, 167.03, 187.95 (C=O)

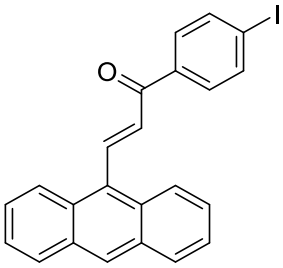

(*E*)-3-(Anthracen-9-yl)-1-(4-iodophenyl) prop-2-en-1-one (40)

(*E*)-3-(Anthracen-9-yl)-1-(4-iodophenyl)prop-2-en-1-one was synthesised from 4-iodoacetophenone (5.02 mmol, 1.235 g) and 9-anthracenecarboxaldehyde (5.02 mmol, 1.035 g), according to the general procedure (3), orange crystals (80%)

Melting Point: 167-173℃

^{1}H NMR (400 MHz, $CDCl_3$) δ ppm 7.44 - 7.54 (m, 5 H, 4x ArH, 1xC=CH), 7.75 - 7.80 (m, 2 H, ArH), 7.84 - 7.89 (m, 2 H, ArH), 7.99 - 8.05 (m, 2 H, ArH), 8.24 - 8.29 (m, 2 H, ArH), 8.46 (br.s, 1 H, ArH), 8.80 (d, *J*=16.17 Hz, 1 H, C=CH)

^{13}C NMR (101 MHz, $CDCl_3$) δ ppm 101.06, 125.17, 125.46, 126.54, 128.65, 128.96, 129.63, 130.06, 129.86, 130.33, 131.28, 137.12, 138.05, 142.46, 188.80 (C=O)

IR*Vmax* (ATR): 3045.07 (Ar C-H), 1593.90 (C=O), 1618.99 (*trans* C=C) 1658.74, 1577.36, 1515.35, 1439.81 (Ar C=C), 669.23 (C-I) cm^{-1}

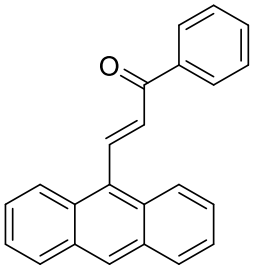

***(E)*-3-(Anthracen-9-yl)-1-phenylprop-2-en-1-one (39)**

(*E*)-3-(Anthracen-9-yl)-1-phenylprop-2-en-1-one was synthesised from acetophenone (5.02 mmol, 0.59 mL) and 1.035g of 9-anthracenecarboxaldehyde (5.02 mmol, 1.035 g) according to the general procedure (3), yellow crystals (44 %)

Melting point: 128 – 130˚C

^{1}H NMR (400 MHz, $CDCl_3$) δ ppm: 8.76 - 8.84 (m, 1 H), 8.81 (d, *J*=15.76 Hz, 1 H), 8.44 (s, 1 H,) 8.28 - 8.34 (m, 2 H), 8.08 - 8.13 (m, 2 H), 7.98 - 8.04 (m, 2 H), 7.56 - 7.65 (m, 2 H), 7.47 -7.56 (m, 6 H)

^{13}C NMR (101 MHz, $CDCl_3$) δ ppm:125.29, 125.43, 126.44, 128.45, 128.64 - 129.03, 129.63, 130.14, 131.02, 131.31, 137.91, 141.89, 189.65 (C=O)

IR*Vmax* (ATR): 3057.23 (Ar C-H), 1662.94 (Alkene C=C), 1604.17 (Ar C=C) cm^{-1}

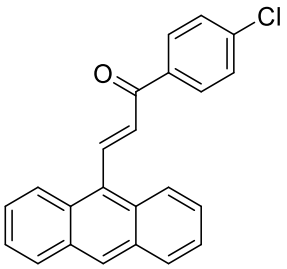

(*E*)-3-Anthracen-9-yl)-1-(4-chor ophenyl) prop-2-en-1-one (45)

(*E*)-3-Anthracen-9-yl)-1-(4-chorophenyl) prop-2-en-1-one was synthesised from of 4-chloroacetophenone (5.02 mmol, 0.65 mL) and of 9-anthracenecarboxaldehyde (5.02 mmol, 1.035 g) according to the general procedure (3), yellow crystals (65%)

Melting point: 142 – 145˚C

^{1}H NMR (400 MHz,$CDCl_3$) δ ppm: 7.46 - 7.56 (m, 7 H) 8.00 - 8.06 (m, 4 H) 8.26 -8.32 (m, 2 H) 8.48 (s, 1 H) 8.81 (d, *J*=15.76 Hz, 1 H)

^{13}C NMR (101 MHz, $CDCl_3$) δ ppm: 125.18, 125.46, 126.53, 128.63, 128.96, 129.08, 129.63, 129.88, 130.10, 130.41, 131.28, 136.17, 139.56, 142.44, 188.31 (C=O)

IR*Vmax* (ATR): 3048.63 (Ar C-H), 1660.22 (C=O), 1596.31 (Ar C=C), 731.61 (C-Cl) cm^{-1}

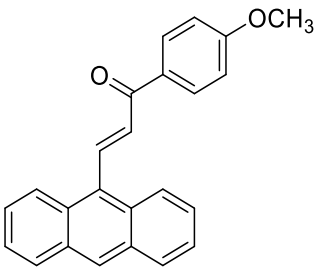

(*E*)-3-(Anthracen-9-yl)-1-(4-methoxyphenyl) prop-2-en-1-one (42)

(*E*)-3-(Anthracen-9-yl)-1-(4-methoxyphenyl)prop-2-en-1-one

was synthesised from of 4-methoxyacetophenone (5.02 mmol, 0.754 g) and 9-anthracenecarboxaldehyde (5.02 mmol, 1.035 g) according to the general procedure (3), yellow powder (58%)

Melting point: 122-125 ℃

^{1}H NMR (400 MHz, $CDCl_3$) δ ppm 3.89 (s, 3H) 7.00 (d, *J*=8.71 Hz, 2H) 7.47 -7.59 (m, 5 H) 8.01 - 8.06 (m, 2H) 8.07 - 8.12 (m, 2H) 8.29 - 8.35 (m, 2H) 8.47 (s, 1H) 8.78 (d, *J*=15.76 Hz, 1H)

^{13}C NMR (101 MHz, $CDCl_3$) δ ppm 55.50, 113.98, 125.40, 126.31, 128.19, 128.86, 129.61, 130.48, 130.73 - 131.17, 131.31, 141.01, 163.65, 187.90 (C=O)

IR*Vmax* (ATR): 3045.86 (Ar C-H), 1654.13 (C=O), 1593.97 (Ar C=C), 1254.32 (C-O) cm^{-1}

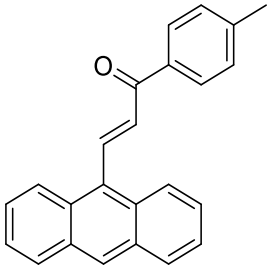

(*E*)-3-(Anthracen-9-yl)-1-(*p*-tolyl) prop-2-en-1-one (43)

(*E*)-3-(Anthracen-9-yl)-1-(*p*-tolyl) prop-2-en-1-one was synthesised from 4-methylacetophenone (5.02 mmol, 0.67 mL) and 9-anthracenecarboxaldehyde (5.02 mmol, 1.035g) according to the general procedure (3), yellow powder (61%)

Melting point: 98-103˚C

^{1}H NMR (400 MHz, $CDCl_3$) δ ppm 2.45 (s, 3H), 7.32 (d, *J*=8.29 Hz, 2H), 7.48 -7.59 (m, 5H), 7.96 - 8.09 (m, 4H), 8.29 - 8.36 (m, 2H), 8.47 (s, 1H), 8.79 (d, *J*=15.76 Hz, 1H)

^{13}C NMR (101 MHz, $CDCl_3$) δ ppm 28.34, 124.83, 125.36, 125.81 - 126.41, 126.90, 128.05 - 129.12, 129.62, 130.09 - 130.73, 131.19 - 131.90, 134.46, 135.11 - 135.51, 138.33, 139.35, 142.48, 143.98, 146.79, 188.50 (C=O)

IR*Vmax* (ATR): 3046.66 (Ar C-H), 1657.95 (C=O), 1592.79 (Ar C=C), 1441.79 (C-CH_3) cm^{-1}

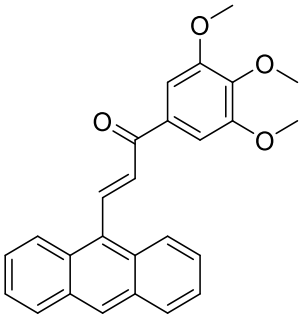

(*E*)-3-(Anthracen-9-yl)-1-(3,4,5-trimethoxyphenyl)prop-2-en-1-one (44)

(*E*)-3-(Anthracen-9-yl)-1-(3,4,5-trimethoxyphenyl)prop-2-en-1-one was synthesised from 1-(3,4,5-trimethoxyphenyl)ethan-1-one (5.02 mmol, 0.65 mL) and 9-anthracenecarboxaldehyde (5.02 mmol, 1.035 g) according to the general procedure (3), yellow crystals (86%)

Melting point: 160-164˚C

^{1}H NMR (400 MHz, $CDCl_3$) δ ppm 3.90 - 3.99 (m, 9H), 7.35 (s, 2 H), 7.49 - 7.56 (m, 5H), 8.03 - 8.08 (m, 2H), 8.28 - 8.35 (m, H), 8.50 (s, 1 H), 8.79 (d, *J*=15.76 Hz, 1H)

^{13}C NMR (101 MHz, $CDCl_3$) δ ppm 56.35, 61.00, 61.45, 62.52, 106.22, 125.38, 126.40, 128.37, 128.92, 129.62, 130.27, 130.70 - 131.49, 133.10, 141.70, 153.24, 188.33 (C=O)

IR*Vmax* (ATR): 3045.78 (Ar C-H), 1657.91 (C=O), 1592.99 (Ar C=C), 1268.62 (C-O) cm^{-1}

5.4 General Procedure (4) for synthesis of chalcone anthracene Diels–Alder products

To a solution of the appropriate chalcone anthracene analog (1.0 mmol) in toluene (2 mL) was added dienophile (1.3 mmol). The mixture was heated, with stirring at 90℃ for 48 h. The reaction was then cooled to RT and the resulting solid was isolated by filtration. The solid product was sequentially washed with toluene (2 mL) and diethyl ether (2 mL). The product was then recrystallized from toluene if necessary.

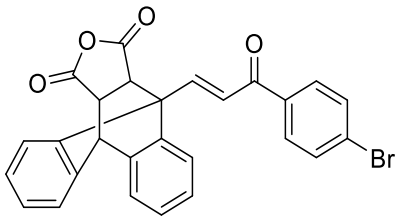

9-(*E*)-3-(4-Bromophenyl)-3-oxoprop-1-en-1-yl)-9,10-dihydro-9,10-[3,4]furanoanthracene-12,14-dione (70)

9-(*E*)-3-(4-Bromophenyl)-3-oxoprop-1-en-1-yl)-9,10-dihydro-9,10-[3,4]furanoanthracene-12,14-dione was prepared from (*E*)-3-(anthracen-9-yl)-1-(4-bromophenyl)prop-2-en-1-one (1.0 mmol, 0.3873 g) and maleic anhydride (1.3 mmol, 0.13 g) according to general procedure (4), light yellow powder (86%)

Melting point: 254°C – 256 °C

^{1}H NMR (400 MHz, $CDCl_3$) δ ppm 3.65 (dd, *J*=9.12, 3.32 Hz, 1 H,CH), 3.81 (d, *J*=9.12 Hz, 1 H,CH), 4.87 (d, *J*=3.32 Hz, 1 H,CH), 7.16 - 7.36 (m, 6 H,5 x ArH,1xC=CH), 7.39-7.44 (m, 2 H), 7.66 - 7.76 (m, 3 H, ArH), 7.95 (d, *J*=16.17 Hz, 1 H, C=CH), 8.03 (d, *J*=8.71 Hz, 2 H, ArH)

^{13}C NMR (101 MHz, $CDCl_3$) δ ppm 45.46, 48.96, 49.28, 51.93, 123.52, 123.87, 124.18, 127.12, 127.63, 130.39, 130.92, 132.16, 136.24, 137.36, 138.85, 140.22, 141.51, 168.82, 169.74, 188.80 (C=O)

IR*Vmax* (ATR): 3328.89, 3074.11 (Ar C-H), 1835.25 *trans* (C=C), 1773.04, 1665.51 (C=O), 1617.10, 1581.33, 1458.65, 1397.18 (Ar C=C), 1076.35 (C-O) cm^{-1}

LRMS (APCI) calculated for $C_{27}H_{18}BrO_4$ [M^++H]: 485.03 found: 485.04

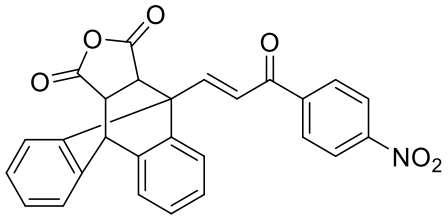

9-(*E*)-3-(4-Nitrophenyl)-3-oxoprop-1-en-1-yl)-9,10-dihydro-9,10-[3,4]furanoanthracene-12,14-dione (71)

9-(*E*)-3-(4-Nitrophenyl)-3-oxoprop-1-en-1-yl)-9,10-dihydro-9,10-[3,4]furanoanthracene-12,14-dione was prepared from (*E*)-3-(anthracen-9-yl)-1-(4-

nitrophenyl)prop-2-en-1-one (1.0 mmol, 0.3534 g) and maleic anhydride (1.3 mmol, 0.13 g) according to general procedure (4), cream powder (77%)

Melting Point: >200 °C

^{1}H NMR (400 MHz, DMSO-d_6) δ ppm 3.80 (dd, *J*=9.12, 3.32 Hz, 1 H), 4.25 (d, *J*=9.12 Hz, 1 H), 4.95 (d, *J*=3.32 Hz, 1 H), 7.16 - 7.28 (m, 3 H), 7.31 - 7.36 (m, 1 H), 7.41 (dd, *J*=5.60, 3.11 Hz, 1 H), 7.53 - 7.57 (m, 1 H), 7.55 (d, *J*=7.05 Hz, 1 H), 7.86 (s, 1 H), 8.34 - 8.44 (m, 4 H)

^{13}C NMR (400 MHz, DMSO-d_6) δ ppm 49.73, 49.78, 51.71, 56.89, 109.99, 123.47, 124.01, 124.46, 124.51, 125.00, 125.74, 125.77, 127.03, 127.53, 127.94, 130.55, 132.01, 138.92, 139.80, 141.19, 142.06, 142.92, 150.52, 170.66, 171.37, 189.02 (chalcone C=O)

IR*Vmax* (ATR): (C-H) 2972.12, (*trans* C=C) 1820.65, (C=O) 1770.72, (Ar C=C) 1667.96, 1596.43, (NO_2) 1516.78, 1346.74 (C-O) cm^{-1}

HRMS (APCI) calculated for $C_{27}H_{16}NO_6$ [M^+-H]: 450.098311 found: 450.098228. Mass accuracy (0.2 ppm).

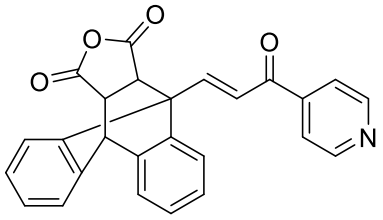

9-(*E*)-3-Oxo-3-(pyridin-4-yl)prop-1-en-1-yl)-9,10-dihydro-9,10-[3,4]furanoanthracene-12,14-dione (82)

9-(*E*)-3-Oxo-3-(pyridin-4-yl)prop-1-en-1-yl)-9,10-dihydro-9,10-[3,4]furanoanthracene-12,14-dione was prepared from (*E*)-3-(anthracen-9-yl)-1-(pyridin-4-yl)prop-2-en-1-one (1.0 mmol, 0.3094 g) and maleic anhydride (1.3 mmol, 0.13 g) according to general procedure (4), light brown solid (99%)

Melting Point: >200 °C

^{1}H NMR (400 MHz, $CDCl_3$) δ ppm 3.65 (dd, *J*=9.12, 2.90 Hz, 1H, CH), 3.80 (d, *J*=9.12 Hz, 1H, CH), 4.87 (d, *J*=2.49 Hz, 1H, CH), 7.10 - 7.23 (m, 3H, ArH), 7.25 - 7.34 (m, 3H, ArH), 7.36 - 7.46 (m, 2H, ArH), 7.70 (d, *J*=16.17 Hz, 1H, CH=C), 7.94 (d, *J*=4.98 Hz, 2 H, ArH), 8.01 (d, *J*=16.17 Hz, CH=C)

^{13}C NMR (101 MHz, $CDCl_3$) δ ppm 45.44, 48.99, 49.24, 51.99, 123.42, 123.71, 124.33, 125.70, 127.18, 127.77, 128.02, 128.28, 130.41, 140.20, 143.49, 150.40, 168.91, 169.60, 188.91 (chalcone C=O)

IR*Vmax* (ATR): 3064.92, 2969.14 **(**Ar C-H), 1860.19, 1836.15 (C=C), 1773.15 (C=O), 1638.35, 1677.99 (C=N), 1625.35, 1585.28, 1458.89 (Ar C=C), 1069.92 (C-N) cm^{-1}

HRMS (APCI) calculated for $C_{26}H_{18}NO_4$ $[M^+ + H]$: 408.123034 found: 408.123065. Mass accuracy (-0.1 ppm).

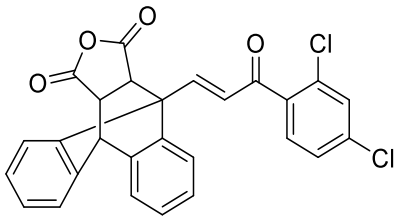

9-(*E*)-3-(2,4-Dichlorophenyl)-3-oxoprop-1-en-1-yl)-9,10-dihydro-9,10-[3,4]furanoanthracene-12,14-dione (73)

9-(*E*)-3-(2,4-Dichlorophenyl)-3-oxoprop-1-en-1-yl)-9,10-dihydro-9,10-[3,4]furanoanthracene-12,14-dione was prepared from (*E*)-3-(anthracen-9-yl)-1-(2,4-dichlorophenyl)prop-2-en-1-one (1.0 mmol, 0.3773 g) and maleic anhydride (1.3 mmol, 0.13 g) according to general procedure (4), beige powder (76%)

Melting Point: 232-236 ℃

^{1}H NMR (400 MHz, $CDCl_3$) δ ppm 3.60 (dd, *J*=9.12, 3.32 Hz, 1H), 3.72 (d, *J*=9.54 Hz, 1H), 4.84 (d, *J*=2.90 Hz, H), 7.20-7.28 (m, 5H, ArH), 7.28 - 7.34 (m, 2 H, ArH, 1, CH=C), 7.35 - 7.39 (m, 1H, ArH), 7.39 - 7.44 (m, 2H, ArH), 7.52 (d, *J*=1.66 Hz, 1H, ArH), 7.68 (d, *J*=8.29 Hz, 1H, ArH), 7.75 (d, *J*=16.59 Hz, 1H, CH=C)

^{13}C NMR (101 MHz, $CDCl_3$) δ ppm 45.49, 49.12, 51.74, 123.44, 123.73, 124.30, 125.64, 127.11, 127.63, 127.92, 128.16, 130.46, 130.95, 134.60, 140.21, 141.14, 143.00, 168.53, 169.72, 191.11 (chalcone C=O)

IR*Vmax* (ATR): 3071.19 **(**Ar C-H), 1862.79 (C=C), 1776.62, 1662.20 (C=O), 1619.95, 1580.28, 1456.96 (Ar C=C), 1212.92 (C-O) cm^{-1}

HRMS (APCI) calculated for $C_{27}H_{17}Cl_2O_4$ 475.049841 $[M^+ + H]$: 475.049099 found. Mass accuracy (-1.6 ppm).

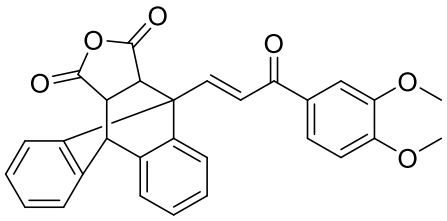

9-(*E*)-3-(3,4-Dimethoxyphenyl)-3-oxoprop-1-en-1-yl)-9,10-dihydro-9,10-[3,4]furanoanthracene-12,14-dione (74)

9-(*E*)-3-(3,4-Dimethoxyphenyl)-3-oxoprop-1-en-1-yl)-9,10-dihydro-9,10-[3,4]furanoanthracene-12,14-dione was prepared from (*E*)-3-(anthracen-9-yl)-1-(3,4-dimethoxyphenyl)prop-2-en-1-one (1.0 mmol, 0.3684 g) and maleic anhydride (1.3 mmol, 0.13 g) according to general procedure (4), cream/yellow powder (83%)

Melting Point: 243-246 ℃

^{1}H NMR (400 MHz, $CDCl_3$) δ ppm 3.63 (dd, *J*=9.33, 3.11 Hz, 1H, CH), 3.81 (d, *J*=9.54 Hz, 1H, CH), 3.97 (d, *J*=7.05 Hz, 6H, CH_3), 4.85 (d, *J*=3.32 Hz, 1H, CH), 6.96 (d, *J*=8.29 Hz, 1H, ArH), 7.19 - 7.27 (m, 4H, ArH), 7.31 - 7.37 (m, 2H, ArH), 7.37 - 7.43 (m, 2H, ArH), 7.73 - 7.76 (m, 2H, ArH, CH=C), 7.78 (s, 1 H), 7.82 (dd, *J*=8.29, 2.07 Hz, 1 H, ArH), 7.84 - 7.90 (d, *J*=16.2 Hz, 1H, CH=C)

^{13}C NMR (101 MHz, $CDCl_3$ δ ppm 45.47, 49.01, 49.33, 51.91, 56.09, 110.27, 111.02, 123.59, 123.70, 124.07, 125.53, 127.08, 127.54, 127.89, 128.04, 130.68, 131.47 , 137.43, 139.09, 139.75 , 140.26 , 141.75, 149.30, 153.67, 168.81, 169.92, 188.39 (chalcone C=O)

IR*Vmax* (ATR): 3071.19 **(**Ar C-H), 1862.79 (C=C), 1777.39, 1668.50 (C=O), 1619.46, 1580.35, 1456.83 (Ar C=C), 1213.57, 1018.24 (C-O) cm^{-1}

HRMS (ESI): calculated for $C_{29}H_{22}NaO_6$ 489.130859 [M^+-H] found:489.130483. Mass accuracy (0.8 ppm)

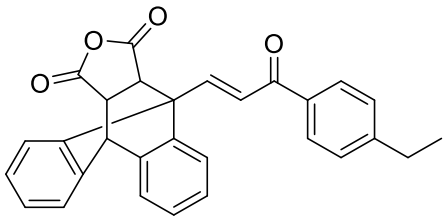

(*E*)-3-(4-ethylphenyl)-3-oxoprop-1-en-1-yl)-9,10-dihydro-9,10-[3,4]furanoanthracene-12,14-dione (72)

(*E*)-3-(4-ethylphenyl)-3-oxoprop-1-en-1-yl)-9,10-dihydro-9,10-[3,4]furanoanthracene-12,14-dione was prepared from (*E*)-3-(anthracen-9-yl)-1-(4-ethylphenyl)prop-2-en-1-

one (1.0 mmol, 0.3364 g) and maleic anhydride (1.3 mmol, 0.13 g) according to general procedure (4), cream powder (70%)

Melting Point: 195-200 ℃

^{1}H NMR (400 MHz, DMSO-d_6) δ ppm 1.16 - 1.23 (m, 3H), 2.70 (q, *J*=7.46 Hz, 7H), 3.79 (dd, *J*=9.12, 3.32 Hz, 4H), 4.25 (d, *J*=9.12 Hz, 4H), 4.94 (d, *J*=3.32 Hz, 4H), 7.16 - 7.20 (m, 8H), 7.20 - 7.23 (m, H), 7.23 - 7.27 (m, 9H), 7.28 - 7.33 (m, 1H), 7.37 - 7.42 (m, 4H), 7.43 (d, *J*=8.29 Hz, 2H), 7.54 (d, *J*=6.63 Hz, 4H), 7.74 - 7.80 (m, 4H), 7.82 - 7.88 (m, 4H), 8.09 (d, *J*=8.29 Hz, 7H)

^{13}C NMR (DMSO-d_6) δ ppm 15.65, 28.70, 44.80, 49.37, 49.60, 51.58, 123.37, 123.91, 125.77 , 127.03, 127.47, 127.79, 129.40, 132.06, 135.37, 138.95, 140.03, 140.65, 141.25, 142.31, 150.55, 170.57, 171.42, 189.00 (chalcone C=O)

IR*Vmax* (ATR): 3071.36, 2882.33 **(**Ar C-H), 1861.93 (C=C), 1778.67, 1670.45 (C=O)1619.17, 1604.57, 1580.44 (Ar C=C), 1465.80 (CH_2), 1374.93 (CH_3), 1224.51 (C-O) cm^{-1}

HRMS (APCI): calculated for $C_{29}H_{23}O_4$ 435.159086 [M^++H] found: 435.159469. Mass accuracy (0.9 ppm).

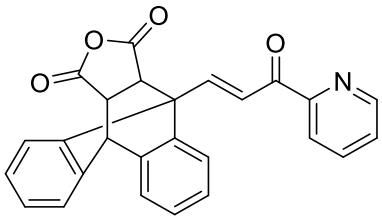

9-(*E*)-3-Oxo-3-(pyridin-2-yl)prop-1-en-1-yl)-9,10-dihydro-9,10-[3,4]furanoanthracene-12,14-dione (83 A)

9-(*E*)-3-Oxo-3-(pyridin-2-yl)prop-1-en-1-yl)-9,10-dihydro-9,10-[3,4]furanoanthracene-12,14-dione was prepared from (*E*)-3-(anthracen-9-yl)-1-(pyridin-2-yl)prop-2-en-1-one (1.0 mmol, 0.3094 g) and maleic anhydride (1.3 mmol, 0.13 g) according to general procedure (4), white powder (100%)

Melting Point: 225-227 ℃

^{1}H NMR (400 MHz, $CDCl_3$) δ ppm 3.62 (dd, *J*=9.12, 3.32 Hz, 1H, CH), 3.93 (d, *J*=9.54 Hz, 1H, CH), 4.85 (d, *J*=3.32 Hz, 1H, CH), 7.13 - 7.24 (m, 3H, ArH), 7.25 - 7.31 (m, 3 H,ArH), 7.36 - 7.45 (m, 3 H ArH), 7.51 (ddd, *J*=7.57, 4.67, 1.04 Hz, 1 ArH), 7.93 (td, *J*=7.67, 1.66 Hz, 1H, ArH), 8.13 (d, *J*=16.59 Hz, 1 H, CH=C), 8.29 (dt, *J*=7.88, 1.04 Hz, 1H, ArH), 8.42 (d, *J*=16.59 Hz, 1H, CH=C), 8.70 - 8.73 (m, 1H, ArH)

IR*Vmax* (ATR): 3087.05, 3064.46, 29685.93 **(**Ar C-H), 1862.63, 1836.60 (C=C), 1770.84 (C=O), 1676.99 (C=N), 1625.37, 1584.71, 1479.76, 1456.99 (Ar C=C), 1325.60 (C-N), 1084.30 (C-O) cm^{-1}

HRMS (APCI): calculated for $C_{26}H_{18}NO_4$ 408.123034 $[M^+ + H]$ found: 408.123728. Mass accuracy (1.7 ppm).

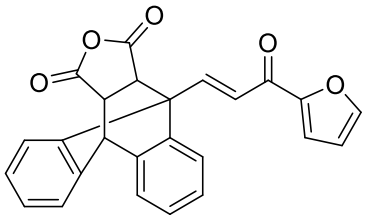

9-(*E*)-3-(Furan-2-yl)-3-oxoprop-1-en-1-yl)-9,10-dihydro-9,10-[3,4]furanoanthracene-12,14-dione (83 B)

9-(*E*)-3-(Furan-2-yl)-3-oxoprop-1-en-1-yl)-9,10-dihydro-9,10-[3,4]furanoanthracene-12,14-dione was prepared from (*E*)-3-(anthracen-9-yl)-1-(furan-2-yl)prop-2-en-1-one (1.0 mmol, 0.2983 g) and maleic anhydride (1.3 mmol, 0.13 g) according to general procedure (4), cream powder (81%)

Melting Point: 222-225 ℃

^{1}H NMR (400 MHz, $CDCl_3$) δ ppm 3.63 (dd, *J*=9.54, 3.32 Hz, 1H, CH), 3.82 (d, *J*=9.12 Hz, 1H, CH), 4.85 (d, *J*=3.32 Hz, 1H, CH), 6.63 (dd, *J*=3.73, 1.66 Hz, 1H, CH=C), 7.15 – 7.29, 5H, ArH, CH=C), 7.33 - 7.40 (m, 2H, ArH), 7.40 - 7.46 (m, 2H, ArH), 7.63 (d, *J*=16.59 Hz, 1H, CH=C), 7.69 (d, *J*=1.24 Hz, 1H, CH=C), 8.02 (d, *J*=16.17 Hz, 1H, CH=C)

^{13}C NMR (101 MHz, $CDCl_3$) δ ppm 45.50, 49.08, 49.26, 51.82, 112.78, 118.91, 123.63, 123.95, 124.15, 125.53, 127.05, 127.56, 127.91, 128.04, 130.36, 137.38, 138.96, 140.29, 140.61, 141.55, 147.26, 153.19, 168.65, 169.93, 177.01 (chalcone C=O)

IR*Vmax* (ATR): 3071.48, 2882.79 **(**Ar C-H), 1862.53 (C=C), 1776.90, 1668.01 (C=O), 1580.26, 1405.03 (Ar C=C), 1226.47, 1071.29 (C-O) cm^{-1}

HRMS (APCI): calculated for $C_{25}H_{17}O_5$ 397.107050 $[M^+ + H]$, found: 397.107371. Mass accuracy (-0.8 ppm)

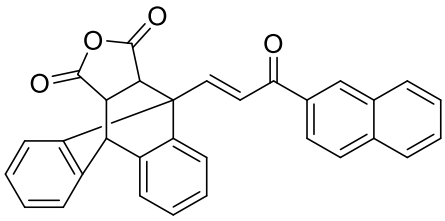

9-(*E*)-3-(Naphthalen-2-yl)-3-oxoprop-1-en-1-yl)-9,10-dihydro-9,10-[3,4]furanoanthracene-12,14-dione (84)

9-(*E*)-3-(Naphthalen-2-yl)-3-oxoprop-1-en-1-yl)-9,10-dihydro-9,10-[3,4]furanoanthracene-12,14-dione was prepared from (*E*)-3-(anthracen-9-yl)-1-(naphthalen-2-yl)prop-2-en-1-one (1.0 mmol, 0.3584 g) and maleic anhydride (1.3 mmol, 0.13 g) according to general procedure (4), green crystals (86%)

Melting Point: 226-231 ℃

^{1}H NMR (400 MHz, $CDCl_3$) δ ppm 3.66 (dd, *J*=9.12, 3.32 Hz, 1H), 3.86 (d, *J*=9.54 Hz, 1 H), 4.88 (d, *J*=3.32 Hz, 1H), 7.17 - 7.31 (m, 4H), 7.34 - 7.46 (m, 4H), 7.54 - 7.65 (m, 2H), 7.88 - 7.94 (m, 2H), 7.96 - 8.03 (m, 3H), 8.22 (dd, *J*=8.71, 1.66 Hz, 1H), 8.71 (s, 1 H)

^{13}C NMR (101 MHz, $CDCl_3$) δ ppm 55.53 - 56.38, 60.88, 69.77 - 71.12, 106.07, 106.66, 107.75, 110.78 - 111.13, 114.44, 114.76, 123.43, 126.97, 127.76, 128.45

IR*Vmax* (ATR): 3064.36, 2968.90 **(**Ar C-H), 1860.33, 1836.33 (C=C),1771.08 (C=O), 1676.62, 1625.39, 1584.75, 1458.10 (Ar C=C),1 325.74 (C-O) cm^{-1}

HRMS (APCI): calculated for $C_{31}H_{21}O_4$ $[M^+ + H]$: 457.143436, found: 457.143830. Mass accuracy (0.9 ppm)

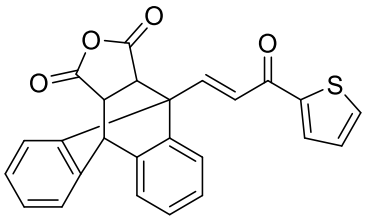

9-(*E*)-3-Oxo-3-(thiophen-2-yl)prop-1-en-1-yl)-9,10-dihydro-9,10-[3,4]furanoanthracene-12,14-dione (85)

9-(*E*)-3-Oxo-3-(thiophen-2-yl)prop-1-en-1-yl)-9,10-dihydro-9,10-[3,4]furanoanthracene-12,14-dione was prepared from (*E*)-3-(anthracen-9-yl)-1-(thiophen-2-yl)prop-2-en-1-one (1.0 mmol, 0.3144 g) and maleic anhydride (1.3 mmol, 0.13 g) according to general procedure (4), cream powder (76%)

Melting Point: 214-218 ℃

^{1}H NMR (400 MHz, $CDCl_3$) δ ppm 3.64 (dd, *J*=9.12, 2.90 Hz, 1H, CH), 3.81 (d, *J*=9.12 Hz, 1H, CH), 4.86 (d, *J*=2.90 Hz, 1H, CH), 7.11 - 7.28 (m, 5 H, ArH, CH=C), 7.28 - 7.46 (m, 4H, ArH), 7.66 (d, *J*=16.17 Hz, 1H, CH=C), 7.75 (d, *J*=4.98 Hz, 1H, CH=C), 7.91 - 8.01 (m, 2H, CH=C)

^{13}C NMR (101 MHz, $CDCl_3$) δ ppm 45.40, 48.99, 49.63, 52.01, 56.07, 110.20, 111.07, 123.48, 123.70, 123.93, 125.41, 126.70, 127.24, 127.41, 130.88, 131.48, 139.42, 140.66 - 140.97, 142.44, 149.24, 153.52, 174.93, 175.64, 188.72 (chalcone C=O)

IR*Vmax* (ATR): 3089.66, 2882.60 **(**Ar C-H), 1864.28 (C=C), 1777.72, 1664.07 (C=O) 1616.88, 1579.42, 1512.85, 1465.10, 1456.62, 1418.52 (Ar C=C), 1213.16 (C-O) cm^{-1}

LRMS (APCI): calculated for $C_{25}H_{16}O_4S$ [M^+-H]:412.08, found 411.22

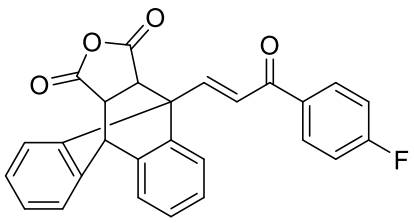

9-(*E*)-3-(4-Fluorophenyl)-3-oxoprop-1-en-1-yl)-9,10-dihydro-9,10-[3,4]furanoanthracene-12,14-dione (77)

9-(*E*)-3-(4-Fluorophenyl)-3-oxoprop-1-en-1-yl)-9,10-dihydro-9,10-[3,4]furanoanthracene-12,14-dione was prepared from (*E*)-3-(anthracen-9-yl)-1-(4-fluorophenyl)prop-2-en-1-one (1.0 mmol, 0.3264 g) and maleic anhydride (1.3 mmol, 0.13 g) according to general procedure (4), cream/yellow powder (79%)

Melting Point: 242-247 ℃

^{1}H NMR (400 MHz, $CDCl_3$) δ ppm 3.64 (dd, *J*=9.54, 3.32 Hz, 1H, CH), 3.81 (d, *J*=9.12 Hz, 1H, CH), 4.87 (d, *J*=3.32 Hz, 1H, CH), 7.18 - 7.28 (m, 6H, ArH), 7.29 - 7.36 (m, 2 H, ArH), 7.36 - 7.45 (m, 2H, ArH), 7.75 (d, *J*=16.59 Hz, 1H, CH=C), 7.93 (d, *J*=16.59 Hz, CH=C), 8.16 - 8.24 (m, 2H, ArH)

^{13}C NMR (101 MHz, $CDCl_3$) δ ppm 45.47, 48.96, 49.30, 51.91, 115.73 - 116.31, 123.54, 123.91, 124.17, 125.58, 127.12, 127.61, 128.03, 131.06, 131.59, 137.38, 140.23, 141.09 , 141.58 ,168.86, 169.78, 188.26 (chalcone C=O)

IR*Vmax* (ATR): 3064.79, 2968.92 **(**Ar C-H), 1861.53, 1835.33 (C=C), 1773.01 (C=O),1667.75 (C=N), 1625.39, 1585.13, 1481.57, 1458.78 (Ar C=C), 1292.88 (C-F), 1069.82 (C-O) cm^{-1}

LRMS (APCI): calculated for $C_{24}H_{17}FO_4$ $[M^+-H]$: 424.11, found 423.23

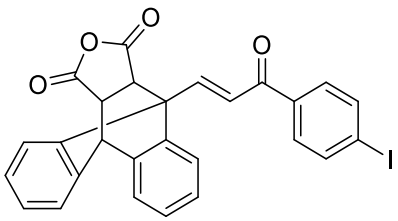

9-(*E*)-3-(4-Iodophenyl)-3-oxoprop-1-en-1-yl)-9,10-dihydro-9,10-[3,4]furanoanthracene-12,14-dione (76)

9-(*E*)-3-(4-Iodophenyl)-3-oxoprop-1-en-1-yl)-9,10-dihydro-9,10-[3,4]furanoanthracene-12,14-dione was prepared from (*E*)-3-(anthracen-9-yl)-1-(4-iodophenyl)prop-2-en-1-one (1.0 mmol, 0.4343 g) and maleic anhydride (1.3 mmol, 0.13 g) according to general procedure (4), light yellow powder (81%)

Melting Point: 228-231 ℃

^{1}H NMR (400 MHz, $CDCl_3$) δ ppm 3.63 (dd, *J*=9.12, 2.90 Hz, 1H, CH), 3.79 (d, *J*=9.12 Hz, 1H, CH), 4.86 (d, *J*=3.32 Hz, 1H, CH), 7.15 - 7.34 (m, 6H, ArH), 7.36 - 7.44 (m, 2 H, ArH), 7.70 (d, *J*=16.17 Hz, 1H, CH=C), 7.83 - 7.97 (m, 5 H, ArH, CH=C)

^{13}C NMR (101 MHz, $CDCl_3$) δ ppm 45.46, 48.97, 49.27, 51.93, 123.53, 123.88, 124.20, 125.59, 127.12, 127.63, 127.95, 128.13, 130.24, 130.88, 136.77, 137.38 , 138.17, 138.86 , 140.22 , 141.53 , 168.83, 189.12 (chalcone C=O)

IR*Vmax* (ATR): (C-H) 3016.49, 2876.80, (*trans* C=C) 1861.84, (C=O) 1771.38, (Ar C=C) 1619.73, 1579.29, 1479.43, 1456.94, (C-O) 1292.32, (C-I) 619.66 cm^{-1}

LRMS (APCI): calculated for $C_{24}H_{17}IO_4$ $[M^+-H]$: 531.02, found 531.20

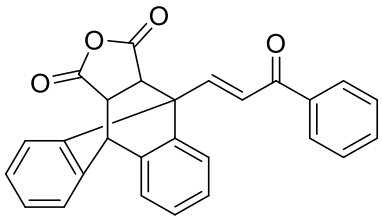

(*E*)-9-(3-Oxo-3-phenylprop-1-en-1-yl)-9,10-dihydro-9,10-[3,4]furanoanthracene-12,14-dione (75)

(*E*)-9-(3-Oxo-3-phenylprop-1-en-1-yl)-9,10-dihydro-9,10-[3,4]furanoanthracene-12,14-dione was synthesised from (*E*)-3-(anthracen-9-yl)-1-phenylprop-2-en-1-one (1.0 mmol, 0.3084 g) and maleic anhydride (1.3 mmol, 0.13 g) according to the general procedure (4), white powder (91%)

Melting point: 214-218 ℃

^{1}H NMR (400 MHz, DMSO-*d6*) δ ppm 3.81 (dd, *J*=9.12, 3.32 Hz, 1H), 4.27 (d, *J*=9.12 Hz, 1H), 4.96 (d, *J*=3.32 Hz, 1H), 7.19 - 7.29 (m, 5H), 7.30 - 7.35 (m, 1H), 7.39 - 7.45 (m, 1H) ,7.56 (d, *J*=6.63 Hz, 1H), 7.58 - 7.65 (m, 2H), 7.68 - 7.74 (m, 1H), 7.77 - 7.92 (m, 2H), 8.14 - 8.21 (m, 2H)

^{13}C NMR (101 MHz, DMSO-*d6*) δ ppm: 38.57 - 41.35, 44.84, 48.69 - 50.08, 51.64, 122.68 - 124.27,124.99, 125.48 - 125.98, 127.06, 127.40 - 128.13, 128.64, 128.91 - 129.60, 132.07, 134.01, 138.96,141.21, 142.29, 170.61, 171.43, 189.75 (chalcone C=O)

IR*Vmax* (ATR): 1774.31 (C=O), 1634.26 (C=C),1221.80 (C-O) cm^{-1}

HRMS (APCI): calculated for $C_{27}H_{18}O_4$ [M^++Na]:429.109730, found 429.110101. Mass accuracy (0.9 ppm)

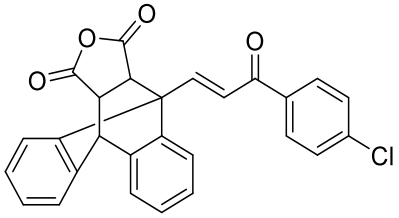

(*E*)-9-(3-(4-Cholrophenyl)-3-oxoprop-1-en-1-yl)-9,10-dihydro-9,10 [3,4]furanoanthracene-12,14-dione (81)

(*E*)-9-(3-(4-Cholrophenyl)-3-oxoprop-1-en-1-yl)-9,10-dihydro-9,10-[3,4] furanoanthracene-12,14-dione was synthesised from (*E*)-3-(anthracen-9-yl)-1-(4-

chorophenyl)prop-2-en-1-one (1.0 mmol, 0.3428 g) and maleic anhydride (1.3 mmol, 0.13 g) according to the general procedure (4), white powder (89%)

Melting point: 248-252 ℃

^{1}H NMR (400 MHz, $CDCl_3$) δ ppm 3.81 (dd, *J*=8.71, 3.32 Hz, 1H), 4.27 (d, *J*=9.12 Hz, 1H), 4.96 (d, *J*=3.32 Hz, H), 7.18 - 7.29 (m, 5H), 7.30 - 7.35 (m, 1H), 7.42 (dd, *J*=5.60, 3.11 Hz, 1H), 7.56 (d, *J*=7.05 Hz, 1H), 7.67 - 7.72 (m, 2H), 7.79 - 7.90 (m, 2H), 8.16 - 8.21 (m, 2H)

^{13}C NMR (101 MHz, $CDCl_3$) δ ppm 39.13 - 40.72, 44.90, 125.51, 128.81, 129.41 - 129.54, 130.18, 131.84, 134.30, 135.66, 142.34, 143.69, 148.97, 149.27, 150.80, 171.10, 191.34 (chalcone C=O)

IR*Vmax* (ATR): 1773.83 (C=O), 1666.32 (C=C), 1618.07 (Ar C=C), 1221.94 (C-O), 712.12 (C-Cl) cm^{-1}

HRMS (APCI): Calculated for $C_{27}H_{17}ClO_4$ [M^++H]: 439.074260, found: 439.073928**.** Mass accuracy (0.8 ppm).

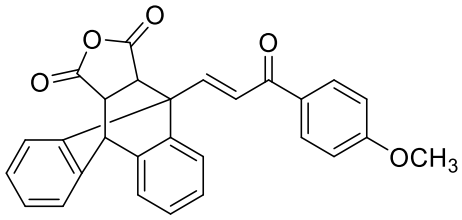

(*E*)-9-(3-(4-Methoxyphenyl)-3-oxoprop-1-en-1-yl)-9,10-dihydro-9,10- [3,4] furanoanthracene-12,14-dione (78)

(*E*)-9-(3-(4-Methoxyphenyl)-3-oxoprop-1-en-1-yl)-9,10-dihydro-9,10-[3,4] furanoanthracene-12,14-dione was synthesised from (*E*)-3-(anthracen-9-yl)-1-(4-methoxyphenyl) prop-2-en-1-one (1.0 mmol, 0.3384 g) and maleic anhydride (1.3 mmol, 0.1280 g) according to the general procedure (4), (30%)

Melting point: 200-205 ℃

^{1}H NMR (400 MHz, $CDCl_3$) δ ppm 3.81 (dd, *J*=8.92, 3.11 Hz, 1H) 3.87 (s, 3H) 4.27 (d, *J*=9.12 Hz, 1H) 4.96 (d, *J*=3.32 Hz, 1H) 7.10 - 7.16 (m, 2H) 7.20 (d, *J*=3.73 Hz, 2H) 7.21 -7.29 (m, 4H) 7.29 - 7.33 (m, 1H) 7.42 (dd, *J*=4.98, 3.73 Hz, 1H) 7.56 (d, *J*=6.63 Hz, 1H) 7.73 - 7.91 (m, 1H) 8.15 - 8.20 (m, 2H)

^{13}C NMR (101 MHz, $CDCl_3$) δ ppm 40.15 - 40.69, 44.50, 49.19 - 50.26, 51.26,

51.57, 55.08, 57.04 - 58.17, 114.72, 122.69, 127.03, 130.49, 131.59, 138.97, 140.11, 141.27, 142.39, 170.58, 171.44, 175.90, 185.10, 187.87 (chalcone C=O)

IR*Vmax* (ATR): 1670.35 (C=O), 1600.48 (Ar C=C), 1229.19 (C-O) cm^{-1}

HRMS (APCI): calculated for $C_{28}H_{19}O_5$ [M^+-H]:435.123797, found : 435.124173**.** Mass accuracy (-0.9 ppm)

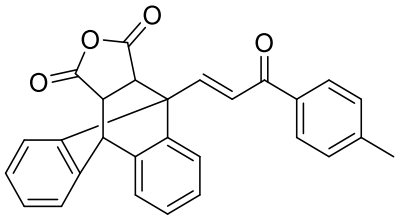

***(E)*-9-(3-Oxo-3-(*p*-tolyl) prop-1-en-1-yl)-9,10-dihydro-9,10- [3,4] furanoanthracene-12,14- dione (79)**

(E)-9-(3-Oxo-3-(*p*-tolyl)prop-1-en-1-yl)-9,10-dihydro-9,10-[3,4]furanoanthracene-12,14-dione was synthesised from (*E*)-3-(anthracen-9-yl)-1-(*p*-tolyl) prop-2-en-1-one (1.0 mmol, 0.3384 g) and maleic anhydride (1.3 mmol, 0.13 g) according to the general procedure (4), white powder (73%)

Melting point: 223-227 ℃

^{1}H NMR (400 MHz, $CDCl_3$) δ ppm 2.41 (s, 3H) 3.81 (dd, *J*=8.92, 3.11 Hz, 1H) 4.27 (d, *J*=9.12 Hz, 1H) 4.96 (d, *J*=2.90 Hz, 1H) 7.20 (d, *J*=3.73 Hz, 2H) 7.21 - 7.29 (m, 3H) 7.29 - 7.34 (m, H) 7.42 (d, *J*=7.88 Hz, 3H) 7.56 (d, *J*=6.63 Hz, 1H) 7.82 (q, *J*=16.17 Hz, 2H) 8.08 (d, *J*=7.88 Hz, 2H)

^{13}C NMR (101 MHz, $CDCl_3$) δ ppm 21.70, 44.81, 49.00 - 50.00, 123.38, 124.98, 127.04, 127.49, 127.85, 129.30, 129.99, 132.05, 135.15, 138.96, 140.06, 140.69, 142.33, 144.52, 170.59, 171.43, 189.16 (chalcone C=O)

IR*Vmax* (ATR): 1769.23 (C=O), 1603.35 (Ar C=C), 1458.64 (C-CH_3 bend), 1228.91 (C-O) cm^{-1}

LRMS (APCI): Calculated $C_{30}H_{25}O_7$ [M^++H]: 419.1362, found: 419.2967.

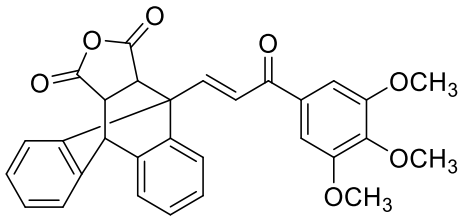

(*E*)-9-(3-Oxo-3-(3,4,5-trimethoxyphenyl)-prop-1-en-1-yl)-9,10-dihydro-9,10- [3,4] furanoanthracene-12,14-dione (80)

(*E*)-9-(3-Oxo-3-(3,4,5-trimethoxyphenyl)-prop-1-en-1-yl)-9,10-dihydro-9,10- [3,4] furanoanthracene-12,14-dione was synthesised from (*E*)-3-(anthracen-9-yl)-1-(4-chorophenyl)prop-2-en-1-one (1.0 mmol, 0.3985 g) and maleic anhydride (1.3 mmol, 0.13 g) according to the general procedure (4), white powder (78%)

Melting point: 262-266 ℃

^{1}H NMR (400 MHz, $CDCl_3$) δ ppm 3.77 (s, 3H) 3.80 (dd, *J*=9.12, 3.32 Hz, 1H), 3.87 (s, 6H) 4.27 (d, *J*=9.12 Hz, 1H), 4.96 (d, *J*=3.32 Hz, 1H) 7.20 - 7.23 (m, 2H) 7.23 - 7.28 (m, 3H) 7.32 - 7.35 (m, 1H) 7.40 - 7.43 (m, 1H) 7.48 (s, 2H) 7.56 (d, *J*=6.22 Hz, 1H) 7.72 - 7.91 (m, 2 H)

^{13}C NMR (101 MHz, $CDCl_3$) δ ppm 43.55, 44.81, 49.23 - 49.97, 56.55, 60.70, 106.84, 123.39, 123.96, 125.00, 125.78, 127.50, 132.58, 132.95, 138.99, 139.83 - 140.53, 153.45, 171.40, 188.92 (chalcone C=O)

IR*Vmax* (ATR): 1662.19 (C=O), 1571.62 (Ar C=C), 1231.78 (C-O) cm^{-1}

HRMS (APCI): Calculated $C_{30}H_{25}O_7$ [M^++H]: 495.144927, found: 495.144908**.** Mass accuracy (0 ppm)

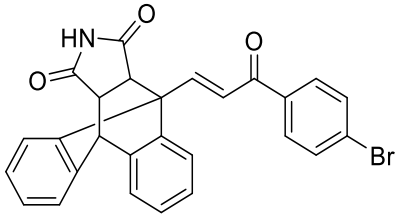

9-(*E*)-3-(4-Bromophenyl)-3-oxoprop-1-en-1-yl)-9,10-dihydro-9,10-[3,4]epipyrroloanthracene-12,14-dione (86)

9-(*E*)-3-(4-Bromophenyl)-3-oxoprop-1-en-1-yl)-9,10-dihydro-9,10-[3,4]epipyrroloanthracene-12,14-dione was prepared from (*E*)-3-(anthracen-9-yl)-1-(4-

bromophenyl)prop-2-en-1-one (1.0 mmol, 0.3873 g) and maleimide (1.3 mmol, 0.13g) according to general procedure (4), light yellow powder (91%)

Melting Point: 295-297 ℃

^{1}H NMR (400 MHz, DMSO-d_6) δ ppm 3.29 (d, *J*=3.32 Hz, 1H, CH), 3.79 (d, *J*=8.71 Hz, 1H, CH), 4.78 (d, *J*=3.32 Hz, 1H, CH), 7.11 - 7.22 (m, 5 H,ArH, CH=C), 7.23 - 7.29 (m, 1H, ArH), 7.30 - 7.35 (m, 1H, ArH), 7.51 (d, *J*=7.05 Hz, 1 H, ArH), 7.78 - 7.85 (m, 4H), 8.06 - 8.12 (m, 2H), 10.84 (s, 1H)

^{13}C NMR (101 MHz, DMSO-d_6) δ ppm 44.96, 49.09, 49.30, 51.70, 123.24, 123.66, 124.61, 126.65, 127.16, 127.28, 131.14, 131.47, 132.47, 136.76, 139.29, 140.24, 142.15, 143.10, 143.11, 177.48, 177.74, 189.08 (chalcone C=O)

IR*Vmax* (ATR): (N-H) 3341, (C-H) 3096.65, (*trans* C=C) 1776.06, (C=O) 1720, (Ar C=C) 1629.57, 1603.21, 1522.86, 1458.09, (C-N) 1311, 1165, (C-Br) 1003.06 cm^{-1}

HRMS (EI) Calculated for $C_{27}H_{17}BrNO_3$ [M^+-H]: 482.039729, found 482.039159. Mass accuracy (1.2 ppm)

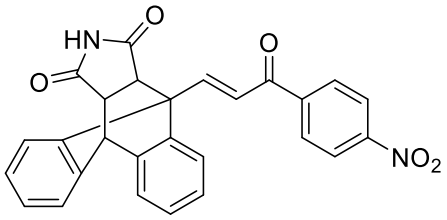

9-*(E)*-3-(4-Nitrophenyl)-3-oxoprop-1-en-1-yl)-9,10-dihydro-9,10-[3,4]epipyrroloanthracene-12,14-dione (87)

9-(*E*)-3-(4-Nitrophenyl)-3-oxoprop-1-en-1-yl)-9,10-dihydro-9,10-[3,4]epipyrroloanthracene-12,14-dione was prepared from (*E*)-3-(anthracen-9-yl)-1-(4-nitrophenyl)prop-2-en-1-one (1.0 mmol, 0.3534 g) and maleimide (1.3 mmol, 0.13 g) according to general procedure (4), beige powder (87%)

^{1}H NMR (400 MHz, DMSO-d_6) δ ppm 3.35 (d, *J*=3.32 Hz, 1H, CH), 3.82 (d, *J*=8.71 Hz, 1H, CH), 4.82 (d, *J*=2.90 Hz, 1H, CH), 7.15 - 7.23 (m, 4H, ArH), 7.28 - 7.33 (m, 1 H, ArH), 7.34 - 7.39 (m, 1H, ArH), 7.52 - 7.57 (m, 1H, ArH), 7.82 - 7.89 (d, *J*=15.8 Hz, 1 H, CH=C), 7.89 - 8.01 (d, *J*=16.2 Hz, 1H, CH=C,), 8.37 - 8.47 (m, 4H, ArH), 10.88 (s, 1H)

^{13}C NMR (101 MHz, DMSO-d_6) δ ppm 20.05, 24.86, 44.97, 49.24, 51.78, 63.44, 73.92, 78.91, 88.39, 109.61, 111.59, 118.64, 123.30, 123.71, 124.64, 125.65, 126.66, 127.25,

130.51 , 131.69, 139.28, 140.12, 142.13, 142.52, 142.96, 144.40, 150.46,177.52 , 177.70, 189.16 (chalcone C=O)

IR*Vmax* (ATR) : 3343 (N-H), 3058.45 (C-H), 1776.27 (*trans* C=C), 1719 (C=O), 1677.02, 1638.82, 1599.84, 1458.22 (Ar C=C), 1517, 1340 (NO_2), 1317, 1164 (C-N) cm^{-1}

HRMS (EI): Calculated for $C_{27}H_{17}N_2O_3$ [M^+-H] :449.114295, found : 449.114553. Mass accuracy **(**0.6 ppm)

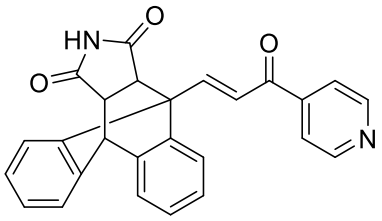

9-(*E*)-3-Oxo-3-(pyridin-4-yl)prop-1-en-1-yl)-9,10-dihydro-9,10-[3,4]epipyrroloanthracene-12,14-dione (98)

9-(*E*)-3-Oxo-3-(pyridin-4-yl)prop-1-en-1-yl)-9,10-dihydro-9,10-[3,4]epipyrroloanthracene-12,14-dione was prepared from (*E*)-3-(anthracen-9-yl)-1-(pyridin-4-yl)prop-2-en-1-one (1.0 mmol, 0.3094 g) and maleimide (1.3 mmol, 0.13g) according to general procedure (4), white powder (100%)

Melting Point: 256-258˚C

^{1}H NMR (400 MHz, $CDCl_3$) δ ppm 3.36 (dd, *J*=8.29, 3.32 Hz, 1H, CH), 3.54 (d, *J*=8.29 Hz, 1H, CH), 4.81 (d, *J*=3.32 Hz, 1H, CH), 7.12 - 7.25 (m, 6H, ArH), 7.26 - 7.31 (m, 1 H, ArH), 7.33 - 7.38 (m, 1H, ArH), 7.39 - 7.43 (m, 1H, ArH), 7.73 (d, *J*=16.17 Hz, 1 H, CH=C), 7.95 (d, *J*=5.39 Hz, 2H, ArH), 8.01 (d, *J*=16.17 Hz, 1H, CH=C), 8.86 (br.s., 1 H, NH)

^{13}C NMR (101 MHz,$CDCl_3$) δ ppm 45.37, 48.96, 49.54, 52.07, 121.87, 123.29, 123.57, 124.14, 125.55, 126.76, 127.35, 127.60 , 130.63 , 137.92 , 138.98 , 141.97, 143.80, 144.39, 150.82 , 175.03, 175.54, 189.49 (chalcone C=O)

IR*Vmax* (ATR): (N-H) 3340,(C-H) 3010.28,(*trans* C=C) 1776.21, (C=O) 1721, 1317,(Ar C=C) 1634.91,1457.77, 1407.25, (C-N) 1166 cm^{-1}

HRMS (ESI): Calculated $C_{26}H_{17}N_2O_3$ [M^+-H] 405.124466, found: 405.124727. Mass accuracy (-0.6 ppm)

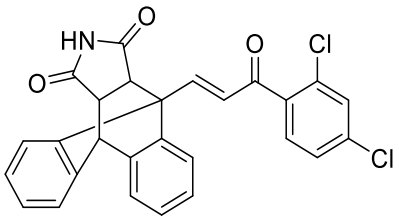

9-(*E*)-3-(2,4-Dichlorophenyl)-3-oxoprop-1-en-1-yl)-9,10-dihydro-9,10-[3,4]epipyrroloanthracene-12,14-dione (89)

9-(*E*)-3-(2,4-Dichlorophenyl)-3-oxoprop-1-en-1-yl)-9,10-dihydro-9,10-[3,4]epipyrroloanthracene-12,14-dione was prepared from (*E*)-3-(anthracen-9-yl)-1-(2,4-dichlorophenyl)prop-2-en-1-one (1.0 mmol, 0.3773 g) and maleimide (1.3 mmol, 0.13 g) according to general procedure (4), beige powder (82%)

Melting Point: 265-268 ℃

^{1}H NMR (400 MHz, DMSO-d_6) δ ppm 3.24 (dd, *J* = 8.6, 3.2 Hz, 1H), 3.61 (d, *J* = 8.6 Hz, 1H), 4.76 (d, *J* = 3.2 Hz, 1H), 7.23 – 7.10 (m, 7H), 7.31 (dq, *J* = 4.7, 2.6 Hz, 1H), 7.49 (dd, *J* = 6.6, 1.8 Hz, 1H), 7.67 – 7.53 (m, 2H), 7.86 – 7.79 (m, 2H), 10.81 (s, 1H)

^{13}C NMR (101 MHz, DMSO-d_6) δ ppm 44.92, 49.24, 51.71, 123.17, 123.47, 124.73, 125.68, 126.63, 127.12, 127.26, 127.38, 128.23, 130.31, 131.41, 131.87, 135.33, 136.45, 137.33, 139.23, 139.82, 142.09, 142.59, 146.63, 177.28, 177.68, 192.42 (chalcone C=O)

IR*Vmax* (ATR): (N-H) 3336,(C-H) 3062.21, (*trans* C=C) 1778.31, (C=O) 1720, (Ar C=C) 1601.84, 1578.57, 1521.96, 1457.78, (C-N) 1315, 1171 cm^{-1}

HRMS (ESI): Calculated for $C_{27}H_{16}Cl_2NO_3$ [M^+-H]: 472.051272, found 472.051893. Mass accuracy (1.3 ppm)

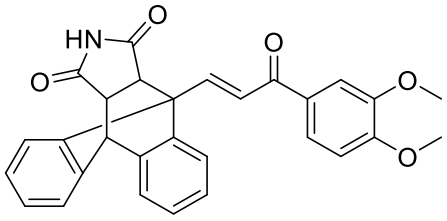

9-(*E*)-3-(3,4-Dimethoxyphenyl)-3-oxoprop-1-en-1-yl)-9,10-dihydro-9,10-[3,4]epipyrroloanthracene-12,14-dione (90)

9-(*E*)-3-(3,4-Dimethoxyphenyl)-3-oxoprop-1-en-1-yl)-9,10-dihydro-9,10-[3,4]epipyrroloanthracene-12,14-dione was prepared from (*E*)-3-(anthracen-9-yl)-1-(3,4-

dimethoxyphenyl)prop-2-en-1-one (1. mmol, 0.3684 g) and maleimide (1.3 mmol, 0.13 g) according to general procedure (4), cream/yellow powder (83%).

Melting Point: 269-271 ℃

^{1}H NMR (400 MHz, $CDCl_3$) δ ppm 3.37 (dd, *J* = 8.5, 3.2 Hz, 1H), 3.56 (d, *J* = 8.6 Hz, 1H), 3.98 (d, *J* = 9.3 Hz, 6H), 4.81 (d, *J* = 3.2 Hz, 1H), 6.97 (d, *J* = 8.4 Hz, 1H), 7.14 – 7.24 (m, 4H), 7.35 (ddd, *J* = 10.9, 6.8, 2.5 Hz, 3H), 7.38 – 7.45 (m, 1H), 7.47 (s, 1H), 7.75 – 7.84 (m, 2H), 7.85 (dd, *J* = 8.4, 2.0 Hz, 1H), 7.91 (d, *J* = 16.2 Hz, 1H)

^{13}C NMR (101 MHz, $CDCl_3$) δ ppm 45.41, 48.99, 49.63, 52.00, 56.05, 56.09, 110.20, 111.07, 123.48, 123.70, 123.90, 123.95, 125.41, 126.70, 127.20, 127.27, 127.41, 130.88, 131.48, 137.96, 139.42, 140.87, 142.44, 149.24, 153.52, 174.95, 175.67, 188.72 (chalcone C=O)

IR*Vmax* (ATR): (N-H) 3342, (C-H) 3061.45, (*trans* (C=C) 1774.72, (C=O) 1719, (Ar C=C) 1626.19, 1598.13, 1517.42, 1458.15, (C-N) 1317, 1169, (C-O) 1268.92, 1017.26 cm^{-1}

HRMS (ESI): Calculated for $C_{29}H_{22}NO_5$ $[M^+-H]$ 464.150346, found 464.150357.

Mass Accuracy (0 ppm)

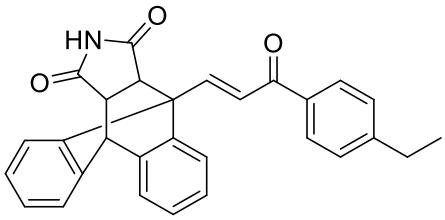

9-((*E*)-3-(4-Ethylphenyl)-3-oxoprop-1-en-1-yl)-9,10-dihydro-9,10-[3,4]epipyrroloanthracene-12,14-dione (88)

9-((*E*)-3-(4-Ethylphenyl)-3-oxoprop-1-en-1-yl)-9,10-dihydro-9,10-[3,4]epipyrroloanthracene-12,14-dione was prepared from (*E*)-3-(anthracen-9-yl)-1-(4-ethylphenyl)prop-2-en-1-one (1.0 mmol, 0.3364 g) and maleimide (1.3 mmol, 0.13 g) according to general procedure (4), white powder (82%)

Melting Point: 265-269 ℃

^{1}H NMR (400 MHz, DMSO-*d*$_6$) δ ppm 1.24 (t, *J*=7.58 Hz, 3H), 2.73 (q, *J*=7.83 Hz, 2H), 3.32 (d, *J*=3.42 Hz, 1H), 3.82 (d, *J*=8.31 Hz, 1H), 4.82 (d, *J*=3.42 Hz, 1H), 7.11 - 7.26 (m, 5H), 7.27 - 7.32 (m, 6H), 7.34 - 7.40 (m, 1 H), 7.46 (d, *J*=7.83 Hz, 1H), 7.54 (d,

J=6.85 Hz, 1H), 7.80 - 7.84 (m, 1H), 7.80 - 7.84 (m, 1H), 7.87 (d, *J*=16.14 Hz, 1H), 8.13 (d, *J*=8.31 Hz, 2H), 10.87 (br. s., 1H)

IR*Vmax* (ATR): (N-H) 3343 (C-H) 3088.25, (*trans* C=C) 1776.11, (C=O) 1720, (Ar C=C) 1626.04, 1603.36, 1522.96, 1457.88, (C-N) 1313, 1165 cm^{-1}

HRMS (EI) Calculated for $C_{29}H_{23}NNaO_3$ [M^++Na]: 456.157014, found: 456.15623. Mass accuracy (-1.7 ppm)

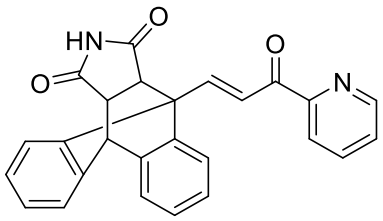

9-(*E*)-3-Oxo-3-(pyridin-2-yl)prop-1-en-1-yl)-9,10-dihydro-9,10-[3,4]epipyrroloanthracene-12,14-dione (99)

9-(*E*)-3-Oxo-3-(pyridin-2-yl)prop-1-en-1-yl)-9,10-dihydro-9,10-[3,4]epipyrroloanthracene-12,14-dione was prepared from (*E*)-3-(anthracen-9-yl)-1-(pyridin-2-yl)prop-2-en-1-one (1.0 mmol, 0.3094 g) and maleimide (1.3 mmol, 0.13 g) according to general procedure (4), brown powder (72%)

Melting Point: > 200 ℃

^{1}H NMR (400 MHz, DMSO-*d*6) δ ppm 3.33 (dd, *J*=8.50, 3.11 Hz, 1H, CH), 3.64 (d, *J*=8.29 Hz, 1H, CH), 4.78 (d, *J*=3.32 Hz, 1H, CH), 7.10 - 7.22 (m, 4H, ArH), 7.29 (d, *J*=7.46 Hz, 1H, ArH), 7.31 - 7.35 (m, 1H, ArH), 7.37 - 7.43 (m, 2H, ArH), 7.49 (ddd, *J*=7.57, 4.66, 1.04 Hz, 2H, ArH), 7.90 (td, *J*=7.67, 1.66 Hz, 1H, ArH), 8.11 - 8.19 (m, 1 H, ArH), 8.15 (d, *J*=16.59 Hz, 1H, CH=C), 8.28 (d, *J*=7.88 Hz, 1H, ArH), 8.40 (d, *J*=16.59 Hz, 1H, CH=C), 8.67 - 8.72 (m, 1H, ArH)

^{13}C NMR (DMSO-d_6) δ ppm 44.99, 49.37, 49.74 - 50.02, 51.79, 123.23, 123.29, 123.61, 124.67, 126.62, 127.12, 127.17, 127.30, 130.11, 135.68, 139.39, 140.25, 142.22, 143.03, 143.46, 149.74, 153.73, 177.39, 177.77, 188.9

IR*Vmax* (ATR): 3344 (N-H), (C-H) 2964.41,(*trans* C=C) 1776.26, 1719 (C=O), (Ar C=C) 1623.69, 1603.44, 1523.46, 1458.07, (C-N) 1323, 1170 cm^{-1}

HRMS (ESI): Calculated for $C_{26}H_{19}N_2O_3$ [M^+-H]**:** 407.139019, found: 407.139590. Mass accuracy (-1.4 ppm)

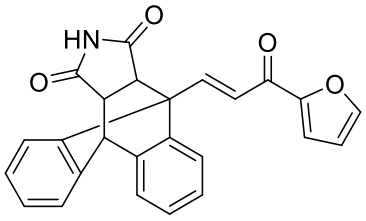

9-(*E*)-3-(Furan-2-yl)-3-oxoprop-1-en-1-yl)-9,10-dihydro-9,10-[3,4]epipyrroloanthracene-12,14-dione (100)

9-(*E*)-3-(Furan-2-yl)-3-oxoprop-1-en-1-yl)-9,10-dihydro-9,10-[3,4]epipyrroloanthracene-12,14-dione was prepared from (*E*)-3-(anthracen-9-yl)-1-(furan-2-yl)prop-2-en-1-one (1.0 mmol, 0.2934g) and maleimide (1.3 mmol, 0.13 g) according to general procedure (4), light yellow powder (81%)

Melting Point: 268-270 ℃

^{1}H NMR (400 MHz, $CDCl_3$) δ ppm 3.34 (dd, *J* = 8.6, 3.2 Hz, 1H), 3.54 (d, *J* = 8.6 Hz, 1H), 4.79 (d, *J* = 3.2 Hz, 1H), 6.61 (dd, *J* = 3.6, 1.7 Hz, 1H), 7.10 – 7.24 (m, 4H), 7.27 (dd, *J* = 6.9, 1.2 Hz, 1H), 7.34 (dd, *J* = 5.5, 3.2 Hz, 2H), 7.36 – 7.47 (m, 3H), 7.59 – 7.71 (m, 2H), 8.04 (d, *J* = 16.3 Hz, 1H)

^{13}C NMR (101 MHz, $CDCl_3$) δ ppm 45.42, 49.06, 49.55, 51.92, 67.18, 112.64, 118.71, 123.52, 123.82, 123.99, 125.41, 126.67, 127.22, 127.29, 127.43, 130.42, 137.89, 139.25, 140.95, 141.73, 142.21, 147.10, 153.32, 174.77, 175.62, 177.38

IR*Vmax* (ATR): (N-H) 3343 (C-H) 3033.42, (*trans* C=C) 1776.09, (C=O) 1719,(Ar C=C) 1626.86, 1602.84, 1522.49, 1458.42 (C-N) 1330, 1168, (C-O) 1287.87, 1010.65 cm^{-1}

HRMS (ESI): Calculated for $C_{25}H_{18}NO_4$ $[M^+ + H]$**:** 407.139019 , found: 407.139590. Mass accuracy (2.4 ppm)

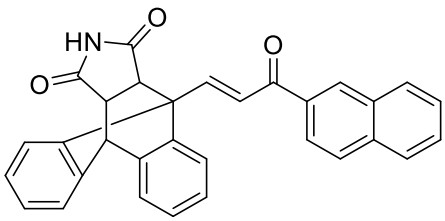

9-(*E*)-3-(Naphthalen-2-yl)-3-oxoprop-1-en-1-yl)-9,10-dihydro-9,10-[3,4]epipyrroloanthracene-12,14-dione (101)

9-(*E*)-3-(Naphthalen-2-yl)-3-oxoprop-1-en-1-yl)-9,10-dihydro-9,10-[3,4]epipyrroloanthracene-12,14-dione was prepared from (*E*)-3-(anthracen-9-yl)-1-(naphthalen-2-yl)prop-2-en-1-one (1.0 mmol, 0.3584 g) and maleimide (1.3 mmmol, 0.13 g) according to general procedure (4), cream/yellow powder (71%)

Melting Point: 209-215 ℃

^{1}H NMR (400 MHz, $CDCl_3$) δ ppm 3.42 (dd, *J* = 8.56, 3.18 Hz, 1H), 3.64 (d, *J* = 8.56 Hz, 1H), 4.86 (d, *J* = 3.18 Hz, 1H), 7.23 - 7.25 (m, 1H), 7.25 - 7.28 (m, 2H), 7.37 - 7.42 (m, 2H), 7.43 - 7.47 (m, 2H), 7.57 - 7.62 (m, 1H), 7.63 - 7.68 (m, 1H), 7.91 - 7.98 (m, 3H), 8.00 - 8.08 (m, 3H), 8.26 (dd, *J* = 8.56, 1.71 Hz, 3H), 8.76 (s, 3H)

^{13}C NMR (101 MHz, $CDCl_3$) δ ppm 45.5, 49.1, 49.6, 123.6, 123.9, 124.1, 124.6, 125.5, 126.8, 126.9, 127.3, 127.4, 127.5, 127.9, 128.6, 128.8, 129.8, 131.0, 131.6, 135.6, 142.1, 193.0

IR*ν_{max}* (ATR): (N-H) 3343, (C-H) 3062,(*trans* C=C) 1776.30, (C=O) 1719, (Ar C=C) 1625.58, 1602.54, 1522.97, 1457.95, (C-N) 1312, 1164 cm^{-1}

HRMS (APCI): calculated for $C_{31}H_{22}NO_3$ $[M^+ + H]$: 456.159420, found: 456.159925. Mass accuracy (-1.1 ppm).

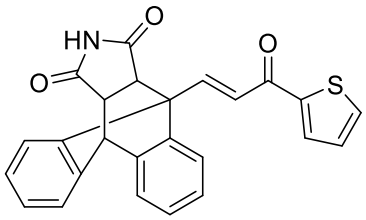

9-(*E*)-3-Oxo-3-(thiophen-2-yl)prop-1-en-1-yl)-9,10-dihydro-9,10-[3,4]epipyrroloanthracene-12,14-dione (102)

9-(*E*)-3-Oxo-3-(thiophen-2-yl)prop-1-en-1-yl)-9,10-dihydro-9,10-[3,4]epipyrroloanthracene-12,14-dione was prepared from (*E*)-3-(anthracen-9-yl)-1-(thiophen-2-yl)prop-2-en-1-one (1.0 mmol, 0.3144 g) and maleimide (1.3 mmol, 0.13 g) according to general procedure (4), beige/ yellow powder (80%)

Melting Point: 263-268 ℃

^{1}H NMR (400 MHz, $CDCl_3$) δ ppm 3.35 (ddd, *J* = 8.5, 3.2, 0.6 Hz, 1H), 3.53 (d, *J* = 8.5 Hz, 1H), 4.80 (d, *J* = 3.1 Hz, 1H), 7.12 – 7.23 (m, 5H), 7.27 – 7.31 (m, 1H), 7.34 (ddd, *J* = 7.9, 4.1, 1.9 Hz, 2H), 7.38 – 7.44 (m, 1H), 7.63 – 7.78 (m, 2H), 7.94 – 8.03 (m, 2H)

^{13}C NMR (101 MHz, $CDCl_3$) δ ppm 45.40, 49.05, 49.60, 51.95, 123.51, 123.82, 124.00, 125.42, 126.71 , 127.25, 127.31, 127.45, 128.42, 131.06, 132.95, 134.55, 137.91, 139.26, 140.93, 141.51, 142.25, 145.09, 174.85, 175.61, 181.86 (chalcone C=O)

IR*Vmax* (ATR) : (N-H) 3343,(C-H) 2963.67, (*trans* C=C) 1776.30, (Ar C=C) 1623.56, 1582.14, 1524.12, 1457.91, (C=O) 1718, (C-N) 1324, 1169, (C-S) 720.73 cm^{-1}

HRMS (APCI): calculated for $C_{25}H_{18}NO_3S$ [M^++H]: 412.100191, found: 412.100395. Mass accuracy (0.5 ppm)

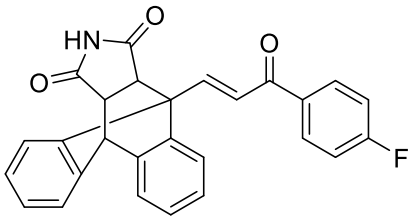

9-(*E*)-3-(4-Fluorophenyl)-3-oxoprop-1-en-1-yl)-9,10-dihydro-9,10-[3,4]epipyrroloanthracene-12,14-dione (93)

9-(*E*)-3-(4-Fluorophenyl)-3-oxoprop-1-en-1-yl)-9,10-dihydro-9,10-[3,4]epipyrroloanthracene-12,14-dione was prepared from (*E*)-3-(anthracen-9-yl)-1-(4-fluorophenyl)prop-2-en-1-one (1.0 mmol, 0.3264 g) and maleimide (1.3 mmol, 0.13 g) according to general procedure (4), cream powder (100%)

Melting Point: 260-268 ℃

^{1}H NMR (400 MHz, $CDCl_3$) δ ppm 3.36 (dd, *J* = 8.5, 3.2 Hz, 1H), 3.54 (d, *J* = 8.5 Hz, 1H), 4.80 (d, *J* = 3.2 Hz, 1H), 7.12 – 7.26 (m, 6H), 7.32 (dddd, *J* = 20.4, 8.9, 5.5, 2.2 Hz, 3H), 7.37 – 7.44 (m, 1H), 7.49 (s, 1H), 7.76 (d, *J* = 16.2 Hz, 1H), 7.94 (d, *J* = 16.2 Hz, 1H), 8.16 – 8.26 (m, 2H)

IR*Vmax* (ATR): (N-H) 3340 (C-H) 2984.37, (*trans* C=C) 1776.16, (C=O) 1718, (Ar C=C) 1630.99, 1595.20, 1457.80, (C-N) 1311, 1157, (C-F) 1224.84 cm^{-1}

HRMS (APCI): calculated for $C_{27}H_{19}FNO_3$ [M^++H]: 412.100191, found: 412.100395. Mass accuracy (-0.4 ppm)

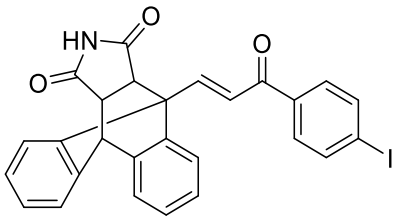

9-(*E*)-3-(4-Iodophenyl)-3-oxoprop-1-en-1-yl)-9,10-dihydro-9,10-[3,4]epipyrroloanthracene-12,14-dione (92)

9-(*E*)-3-(4-Iodophenyl)-3-oxoprop-1-en-1-yl)-9,10-dihydro-9,10-[3,4]epipyrroloanthracene-12,14-dione was prepared from (*E*)-3-(anthracen-9-yl)-1-(4-iodophenyl)prop-2-en-1-one (1.0 mmol, 0.4493 g) and maleimide (1.3 mmol, 0.13 g) according to general procedure (4), yellow powder (93%).

Melting Point: 288-293 ℃

^{1}H NMR (400 MHz, DMSO-*d6*) δ ppm 3.79 (d, J = 8.6 Hz, 1H), 3.31 – 3.29 (m,1H). 4.80 (d, J = 3.2 Hz, 1H), 7.29 – 7.24 (m,1H), 7.23 – 7.13 (m, 5H), 7.37 – 7.31 (m, 1H), 7.52 (dt, J = 7.0, 1.1 Hz, 1H), 7.82 (d, J = 6.7 Hz, 2H), 7.95 – 7.91 (m, 2H), 8.03 – 7.98 (m, 2H), 10.85 (s, 1H)

^{13}C NMR (101 MHz, DMSO-*d6*) δ ppm 44.98, 49.13, 49.32, 51.72, 102.63, 123.26 ,123.67, 124.62, 125.65, 126.66, 127.17, 127.29,130.84, 131.45, 137.06, 138.35, 139.30, 140.27, 142.17, 143.05, 143.12, 177.48, 177.74, 189.40,

IR*Vmax* (ATR): (N-H) 3339,(C-H) 2987.83, (*trans* C=C) 1688.48, (C=O) 1633, (Ar C=C) 1621.45, 1557.57 1485.56, (C-I) 687.18 cm^{-1}

HRMS (APCI): calculated $C_{27}H_{19}INO_3$ $[M^+ + H]$: 532.040418, found 532.040222. Mass accuracy (0.4 ppm).

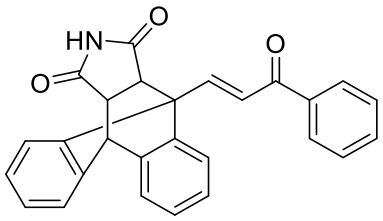

(*E*)-9-(3-oxo-3-phenylprop-1-en-yl)-9,10-dihydro-9,10- [3,4] epipyrroloanthracene-12,14-dione (91)

(*E*)-9-(3-oxo-3-phenylprop-1-en-yl)-9,10-dihydro-9,10- [3,4] epipyrroloanthracene-12,14-dione was synthesised from (*E*)-3-(anthracen-9-yl)-1-phenylprop-2-en-1-one (1.0

mmol, 0.3084 g) and maleimide (1.3 mmol, 0.13 g) according to the general procedure (4), (61%)

Melting point: 218-222 ℃

^{1}H NMR (400 MHz, DMSO-*d6*) ppm 3.80 (d, *J*=8.71 Hz, 1H) 4.79 (d, *J*=3.32 Hz, 1H) 7.10 - 7.24 (m, 6H) 7.24 - 7.29 (m, 1H) 7.32 - 7.37 (m, 1H) 7.52 (d, *J*=6.63 Hz, 1H) 7.57 - 7.65 (m, 2H) 7.67 -7.74 (m, 1H) 7.84 (dd, *J*=16.60 Hz, 2H) 8.12 - 8.21 (m, 2H) 10.84 (s, 1H)

^{13}C NMR (101 MHz, DMSO-d6) δ ppm 123.23, 123.64, 124.62, 125.66, 125.76, 126.67 127.24, 128.64, 129.15, 129.30 - 129.46 131.65 - 131.81, 133.89, 137.78, 139.32, 140.34, 142.55, 143.20, 177.31 - 177.97, 189.92 (chalcone C=O)

IR*Vmax* (ATR): 3347.06 (N-H), 1720.18 (C=O), 1674.84, 1628.01 (C=C), 1000.09 (CN) cm^{-1}

HRMS (APCI): calculated for $C_{27}H_{20}NO_3$ [M^++H]: 406.14377, found: 406.144966. Mass accuracy (-2.9 ppm)

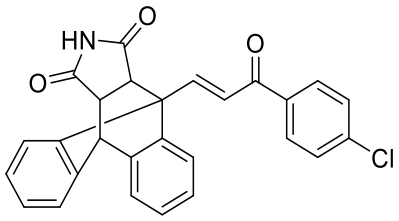

(*E*)-9-(3-(4-Chlorophenyl)-3-oxoprop-1-en-1-yl)-9,10-dihydro-9,10- [3,4] epipyrroloanthracene-12,14-dione (97)

(*E*)-9-(3-(4-Chlorophenyl)-3-oxoprop-1-en-1-yl)-9,10-dihydro-9,10-[3,4] epipyrroloanthracene-12,14-dione was synthesised from (*E*)-3-(anthracen-9-yl)-1-(4-chorophenyl) prop-2-en-1-one (1.0 mmol, 0.3430 g) and maleimide (1.3 mmol, 0.13 g) according to the general procedure (4), white solid (65%)

Melting point: 280 – 285 ℃

^{1}H NMR (400 MHz, $CDCl_3$) δ ppm: 3.80 (d, *J*=8.71 Hz, 1H) 4.80 (d, *J*=2.90 Hz, 1H) 7.09 - 7.39 (m, 8H) 7.52 (d, *J*=7.05 Hz, 1H) 7.68 (d, *J*=8.29 Hz, H) 7.85 (s, 2 H) 8.19 (d, *J*=8.29Hz, 2H) 10.85 (s, 1H)

^{13}C NMR (101 MHz, $CDCl_3$) δ ppm: 44.98, 49.11, 49.32, 51.71, 123.26, 123.67,124.13, 124.62, 125.65, 125.75, 126.66, 127.18, 127.29, 128.64, 129.34, 129.54, 136.45, 140.28, 142.17, 143.11, 177.12 - 178.10, 198.62 (chalcone C=O)

IR*Vmax* (ATR): 1717.64 (C=O), 754.55 (C-Cl) cm^{-1}

LRMS (APCI): calculated $C_{27}H_{17}ClNO_3$ [M^+-H]: 438.0975, found: 438.2284

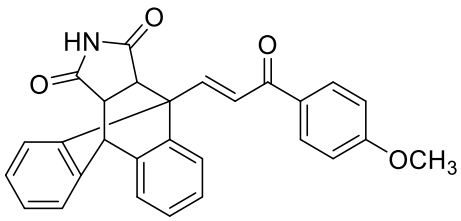

***(E)*-9-(3-(4-Methoxyphenyl)-3-oxoprop-1-en-1-yl)-9,10-dihydro-9,10-[3,4] epipyrroloanthracene-12,14-dione (94)**

(E)-9-(3-(4-Methoxyphenyl)-3-oxoprop-1-en-1-yl)-9,10-dihydro-9,10-[3,4] epipyrroloanthracene-12,14-dione was synthesised from (*E*)-3-(anthracen-9-yl)-1-(4-methoxyphenyl) prop-2-en-1-one (1.0 mmol, 0.3384g) and maleimide (1.3 mmol, 0.13 g) according to the general procedure (4), white solid (70%)

Melting point: 281-284 ℃

^{1}H NMR (400 MHz, $CDCl_3$)δ ppm 3.80 (d, *J*=8.29 Hz, 1H) 3.87 (s, 3H) 4.79 (d, *J*=2.90 Hz, 1H) 7.10 - 7.19 (m, 5H) 7.19 - 7.23 (m, 3H) 7.25 (t, *J*=5.39 Hz, 2H) 7.32 - 7.36 (m, 1H) 7.52 (d, *J*=6.63 Hz, 1H) 7.74 - 7.88 (m, 2H) 8.17 (d, *J*=9.12 Hz, 2H)

^{13}C NMR (101 MHz, $CDCl_3$) δ ppm 39.15 - 40.72, 44.97, 49.37, 56.07, 123.21, 124.60, 125.65, 127.01 - 127.38, 130.62, 131.37 - 132.01, 140.43, 141.47, 143.30, 177.79, 188.12 (C=O chalcone)

IR*Vmax* (ATR): 3343.73 (N-H), 1670.36 (C=O), 1601.24 (Ar C=C), 1230.33 (C-O), 1019.60 (C-N) cm^{-1}

LRMS (APCI): calculated $C_{28}H_{20}NO_4$ [M^+-H]: 434.1471, found: 434.2974

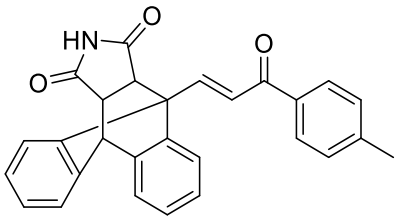

***(E)*-9-(3-Oxo-3-(*p*-tolyl)prop-1-en-1-yl)-9,10-dihydro-9,10-[3,4]epipyrroloanthracene- 12,14-dione (95)**

(E)-9-(3-Oxo-3-(*p*-tolyl) prop-1-en-1-yl)-9,10-dihydro-9,10-[3,4] epipyrroloanthracene-12,14- dione was synthesised from (*E*)-3-(anthracen-9-yl)-1-(*p*-tolyl) prop-2-en-1-one (1.0 mmol, 0.3384 g) and maleimide (1.3 mmol, 0.13 g) according to the general procedure (4), white powder (46%)

Melting point: 129-134 ℃

^{1}H NMR (400 MHz, $CDCl_3$) δ ppm 2.41 (s, 3H) 3.80 (d, *J*=8.71 Hz, 1H) 4.79 (br.s., 1H) 7.10 - 7.30 (m, 7H) 7.30 - 7.45 (m, 3H) 7.52 (d, *J*=6.63 Hz, 1H) 7.75 - 7.89 (m, 2H) 8.03 - 8.04 (m, 1H) 8.04 - 8.13 (m, 2H)

^{13}C NMR (101 MHz, $CDCl_3$) δ ppm 21.69, 39.07 - 40.73, 44.99, 48.86 - 49.53, 55.35, 123.23, 123.64, 126.93 - 127.51, 129.04 - 129.58, 129.96, 135.30, 140.39, 141.79 - 142.33, 144.37, 177.47, 189.36 (chalcone C=O)

IR*Vmax* (ATR): 1710.75 (C=O), 1625.28 (Ar C=C), 1458.68 (C-CH3 bend), 1231.30 (C-O), 1072.28 (C-N) cm^{-1}

HRMS (APCI): calculated $C_{28}H_{22}NO_3$ [M^+-H]: 420.159420, found: 420.160642. Mass accuracy **(**2.9 ppm)

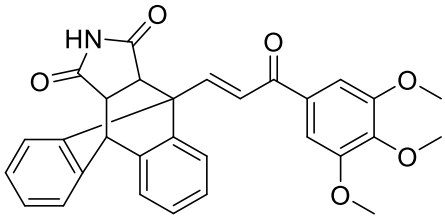

(*E*)-9-(3-Oxo-3-(3,4,5-trimethoxyphenyl)-prop-1-en-1-yl)-9,10-dihydro-9,10- [3,4] epipyrroloanthracene-12,14-dione (96)

(*E*)-9-(3-Oxo-3-(3,4,5-trimethoxyphenyl)-prop-1-en-1-yl)-9,10-dihydro-9,10-[3,4]epipyrroloanthracene-12,14-dione was synthesised from (*E*)-3-(anthracen-9-yl)-1-

(4-chorophenyl) prop-2-en-1-one (1.0 mmol, 0.3985 g) and maleimide (1.3 mmol, 0.13 g) according to the general procedure (4), white powder (53%)

Melting point: 257-260 ℃

^{1}H NMR (400 MHz, $CDCl_3$) δ ppm 3.30 (d, *J*=2.90 Hz, 1H) 3.76 - 3.79 (m, 3H), 3.81 (s, 1H) 3.87 (s, 6H) 4.79 (d, *J*=3.32 Hz, 1H) 7.16 - 7.25 (m, 5H) 7.28 (d, *J*=4.98 Hz, 1H) 7.32 -7.36 (m, 1H) 7.47 - 7.54 (m, 3H) 7.72 - 7.87 (m, 2H) 10.85 (s, 1H)

^{13}C NMR (101 MHz, $CDCl_3$) δ ppm 41.66, 43.00, 46.27, 49.08 - 49.42, 51.67, 56.51, 65.87, 106.82, 123.23, 123.67, 124.66, 125.66, 126.63,127.39, 132.39, 133.09, 139.33, 141.76, 142.56, 143.27,177.96, 189.32 (C=O chalcone)

IR*Vmax* (ATR): 1670.40 (C=O), 1600.25 (Ar C=C), 1229.98 (C-O), 1017.32 (C-N) cm^{-1}

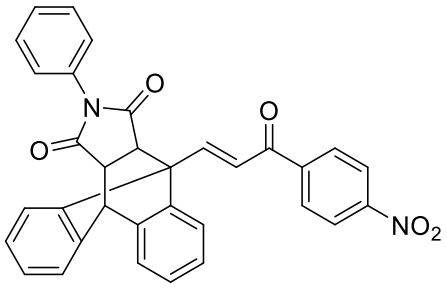

9-(*E*)-3-(4-Nitrophenyl)-3-oxoprop-1-en-1-yl)-13-phenyl-9,10-dihydro-9,10-[3,4]epipyrroloanthracene-12,14-dione (104)

9-(*E*)-3-(4-Nitrophenyl)-3-oxoprop-1-en-1-yl)-13-phenyl-9,10-dihydro-9,10-[3,4]epipyrroloanthracene-12,14-dione was prepared from (*E*)-3-(anthracen-9-yl)-1-(4-nitrophenyl)prop-2-en-1-one (1.0 mmol, 0.3534 g) and *N*-phenylmaleimide (1.3 mmol, 0.23 g) according to general procedure (4), cream powder (86%)

Melting Point: 242-246 ℃

^{1}H NMR (400 MHz, $CDCl_3$) δ ppm, 3.50 (dd, *J* = 8.4, 3.2 Hz, 1H) , 3.67 (d, *J* = 8.5 Hz, 1H), 4.94 (d, *J* = 3.2 Hz, 1H), 6.54 – 6.45 (m, 2H), 7.40 – 7.17 (m, 9H), 7.46 – 7.37 (m, 1H), 7.51 – 7.43 (m, 1H), 7.85 (d, *J* = 16.2 Hz, 1H), 8.06 (d, *J* = 16.2 Hz, 1H), 8.38 – 8.26 (m, 4H),]

^{13}C NMR (101 MHz, $CDCl_3$) δ ppm 45.92, 47.95, 48.43, 52.55, 123.39, 123.77, 123.95, 124.28, 125.65, 126.42, 126.87, 127.42, 127.51, 127.67, 128.99, 129.16, 129.96, 131.04, 131.17, 138.16, 139.18, 140.77, 141.95, 144.32, 174.72, 175.20 (chalcone C=O)

IR*Vmax* (ATR): 3335.77 (Ar C-H), 1771.68 (*trans* C=C), 1700.63, 1671.17 (C=O), 1519, 1383 (NO_2), 1179 (C-N) cm^{-1}

LRMS (APCI): calculated $C_{33}H_{23}N_2O_5$ [M^++H] 527.15, found: 527.14

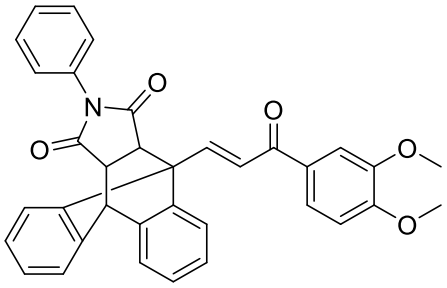

9-(*E*)-3-(3,4-Dimethoxyphenyl)-3-oxoprop-1-en-1-yl)-13-phenyl-9,10-dihydro-9,10-[3,4]epipyrroloanthracene-12,14-dione (107)

9-(*E*)-3-(3,4-Dimethoxyphenyl)-3-oxoprop-1-en-1-yl)-13-phenyl-9,10-dihydro-9,10-[3,4]epipyrroloanthracene-12,14-dione was prepared from (*E*)-3-(anthracen-9-yl)-1-(3,4-dimethoxyphenyl)prop-2-en-1-one (1.0 mmol, 0.3684 g) and *N*-phenylmaleimide (1.3 mmol, 0.23 g) according to general procedure (4), white powder (93%)

Melting Point: 242-244 ℃

^{1}H NMR (400 MHz, $CDCl_3$) δ ppm 3.47 (dd, *J* = 8.4, 3.3 Hz, 1H), 3.65 (d, *J* = 8.4 Hz, 1H), 3.94 (d, *J* = 9.4 Hz, 6H), 4.92 (d, *J* = 3.2 Hz, 1H), 6.45 – 6.54 (m, 2H), 6.91 (d, *J* = 8.4 Hz, 1H), 7.20 (td, *J* = 7.5, 1.6 Hz, 1H), 7.20 – 7.28 (m, 3H), 7.24 – 7.32 (m, 3H), 7.34 – 7.44 (m, 3H), 7.42 – 7.48 (m, 1H), 7.75 (d, *J* = 2.0 Hz, 1H), 7.80 – 7.89 (m, 2H), 7.95 (d, *J* = 16.1 Hz, 1H)

^{13}C NMR (101 MHz, $CDCl_3$) δ ppm 45.96, 47.99, 48.51, 52.48, 56.02, 56.08, 110.18, 110.99, 123.60, 123.84, 124.08, 125.49, 126.43, 126.79, 127.30, 127.33, 127.47, 128.82, 129.05, 130.89, 131.54, 138.21, 139.62, 140.83, 141.01, 142.42, 153.49, 188.72 (chalcone C=O)

IR*Vmax* (ATR): 3011.75 (Ar C-H), 1775.53 (*trans* C=C), 1708.96, 1676.49 (C=O), 1379.80 (C-N), 1181.33 (C-O) cm^{-1}

LRMS (APCI): calculated $C_{35}H_{28}NO_5$ [M^++H]: 542.19, found: 542.28

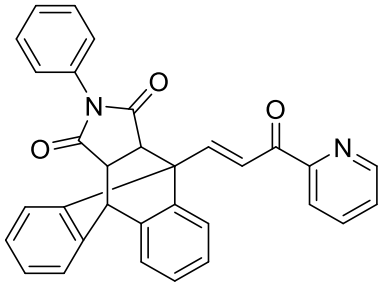

9-(*E*)-3-Oxo-3-(pyridin-2-yl)prop-1-en-1-yl)-13-phenyl-9,10-dihydro-9,10-[3,4]epipyrroloanthracene-12,14-dione (116)

9-(*E*)-3-Oxo-3-(pyridin-2-yl)prop-1-en-1-yl)-13-phenyl-9,10-dihydro-9,10-[3,4]epipyrroloanthracene-12,14-dione was prepared from (*E*)-3-(anthracen-9-yl)-1-(pyridin-2-yl)prop-2-en-1-one (1.0 mmol, 0.3094 g) and *N*-phenylmaleimide (1.3 mmol, 0.23 g) according to general procedure (4), grey powder (91%)

^{1}H NMR (400 MHz, $CDCl_3$) δ ppm 3.47 (dd, *J* = 8.4, 3.2 Hz, 1H), 3.75 (d, *J* = 8.4 Hz, 1H), 4.92 (d, *J* = 3.2 Hz, 1H), 6.44 – 6.53 (m, 2H), 7.14 – 7.30 (m, 7H), 7.31 – 7.42 (m, 2H), 7.46 (ddt, *J* = 7.2, 6.1, 1.1 Hz, 3H), 7.88 (td, *J* = 7.7, 1.8 Hz, 1H), 8.21 (d, *J* = 16.6 Hz, 1H), 8.26 (dt, *J* = 7.9, 1.1 Hz, 1H), 8.49 (d, *J* = 16.5 Hz, 1H), 8.69 (ddd, *J* = 4.8, 1.8, 1.0 Hz, 1H).

^{13}C NMR (101 MHz, $CDCl_3$) δ ppm 46.06, 48.18, 48.39, 52.51, 123.15, 123.74, 124.07, 124.15, 125.42, 126.41, 126.70, 127.00, 127.21, 127.31, 127.38, 128.69, 128.94, 130.07, 131.31, 137.00, 138.22, 139.70, 140.93, 142.30, 142.60, 149.08, 174.40, 175.50, 188.99 (chalcone C=O)

IR*Vmax* (ATR): 3054.46 (Ar C-H), 1779.59 (*trans* C=C), 1713.79, 1674.55 (C=O), 1201.95 (C-N), 1181.33 (C-O) cm^{-1}

LRMS (APCI) calculated for $C_{32}H_{23}N_2O_3$ $[M^+ + H]$: 483.16, found: 483.23

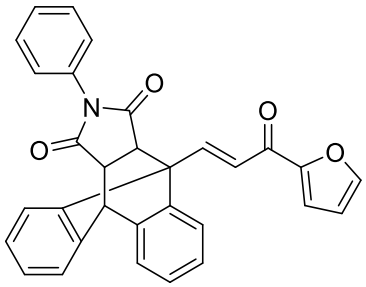

9-(*E*)-3-(Furan-2-yl)-3-oxoprop-1-en-1-yl)-13-phenyl-9,10-dihydro-9,10-[3,4]epipyrroloanthracene-12,14-dione (117)

9-(*E*)-3-(Furan-2-yl)-3-oxoprop-1-en-1-yl)-13-phenyl-9,10-dihydro-9,10-[3,4]epipyrroloanthracene-12,14-dione was prepared from (*E*)-3-(anthracen-9-yl)-1-(furan-2-yl)prop-2-en-1-one (1.0 mmol, 0.2983 g) and *N*-phenylmaleimide according to general procedure (4), cream powder (87%)

^{1}H NMR (400 MHz, $CDCl_3$) δ ppm 3.47 (dd, *J* = 8.4, 3.2 Hz, 1H), 3.65 (d, *J* = 8.4 Hz, 1H), 4.92 (d, *J* = 3.2 Hz, 1H), 6.43 – 6.53 (m, 2H), 6.58 (dd, *J* = 3.6, 1.7 Hz, 1H), 7.13 – 7.29 (m, 5H), 7.25 – 7.31 (m, 2H), 7.33 (dd, *J* = 7.4, 1.5 Hz, 1H), 7.36 – 7.44 (m, 2H), 7.41 – 7.49 (m, 2H), 7.66 (dd, *J* = 1.7, 0.8 Hz, 1H), 7.71 (d, *J* = 16.3 Hz, 1H), 8.09 (d, *J* = 16.3 Hz, 1H)

^{13}C NMR (101 MHz, $CDCl_3$) δ ppm 45.96, 48.07, 48.46, 52.41, 112.61, 118.83, 123.63, 123.99, 124.13, 125.49, 126.40, 126.78, 127.34, 127.50, 128.81, 129.04, 130.61, 131.25, 138.15, 139.45, 140.83, 141.76, 142.19, 147.13, 175.35

LRMS (APCI) calculated for $C_{31}H_{22}NO_4$ [M^++H]: 472.1471, found: 472.1907

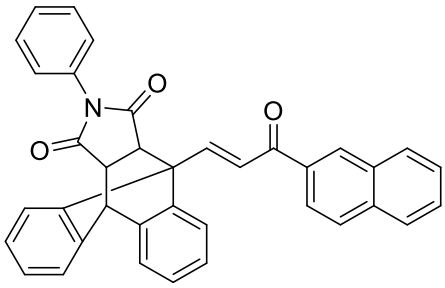

9-(*E*)-3-(Naphthalen-2-yl)-3-oxoprop-1-en-1-yl)-13-phenyl-9,10-dihydro-9,10-[3,4]epipyrroloanthracene-12,14-dione (118)

9-(*E*)-3-(Naphthalen-2-yl)-3-oxoprop-1-en-1-yl)-13-phenyl-9,10-dihydro-9,10-[3,4]epipyrroloanthracene-12,14-dione was prepared from (*E*)-3-(anthracen-9-yl)-1-(naphthalen-2-yl)prop-2-en-1-one (1.0 mmol, 0.3584 g) and *N*-phenylmaleimide (1.3 mmol, 0.23g) according to general procedure (4), light green powder (65%)

Melting Point: 202-206 ℃

^{1}H NMR (400 MHz, $CDCl_3$) δ ppm 3.52 (dd, *J* = 8.4, 3.2 Hz, 1H), 3.69 (d, *J* = 8.5 Hz, 1H), 4.94 (d, *J* = 3.2 Hz, 1H), 6.64 – 6.71 (m, 2H), 7.10 – 7.22 (m, 2H), 7.19 – 7.25 (m, 1H), 7.22 – 7.31 (m, 3H), 7.33 – 7.42 (m, 2H), 7.38 – 7.48 (m, 3H), 7.44 – 7.64 (m, 2H), 7.67 – 7.75 (m, 4H), 7.77 (s, 1H), 7.97 (dd, *J* = 3.8, 1.1 Hz, 1H), 8.05 (d, *J* = 16.1 Hz, 1H).

IR*Vmax* (ATR): 3068.21 (Ar C-H), 1773.41 (*trans* C=C), 1710.67, 1675.13 (C=O), 1380.71 (C-N), 1195.89 (C-O) cm^{-1}

LRMS (APCI) calculated for $C_{31}H_{21}NO_3SNa$ $[M^+-H]$: 530.1834, found: 530.3089

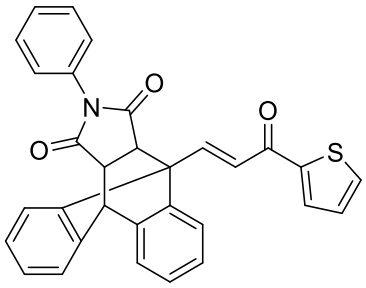

9-(*E*)-3-Oxo-3-(thiophen-2-yl)prop-1-en-1-yl)-13-phenyl-9,10-dihydro-9,10-[3,4]epipyrroloanthracene-12,14-dione (119)

9-(*E*)-3-Oxo-3-(thiophen-2-yl)prop-1-en-1-yl)-13-phenyl-9,10-dihydro-9,10-[3,4]epipyrroloanthracene-12,14-dione was prepared from (*E*)-3-(anthracen-9-yl)-1-(thiophen-2-yl)prop-2-en-1-one (1.0 mmol, 0.3144 g) and *N*-phenylmaleimide (1.3 mmol, 0.23 g) according to general procedure (4), cream powder (81%)

^{1}H NMR (400 MHz, $CDCl_3$) δ ppm 3.48 (dd, *J* = 8.4, 3.2 Hz, 1H), 3.65 (d, *J* = 8.4 Hz, 1H), 4.93 (d, *J* = 3.2 Hz, 1H), 6.45 – 6.54 (m, 2H), 7.14 – 7.19 (m, 1H), 7.19 – 7.24 (m, 1H), 7.24 – 7.31 (m, 6H), 7.38 (ddd, *J* = 13.1, 6.4, 2.5 Hz, 3H), 7.44 – 7.49 (m, 1H), 7.70 (dd, *J* = 4.9, 1.1 Hz, 1H), 7.77 (d, *J* = 16.1 Hz, 1H), 7.98 (dd, *J* = 3.8, 1.1 Hz, 1H), 8.04 (d, *J* = 16.1 Hz, 1H)

^{13}C NMR (101 MHz, $CDCl_3$) δ ppm 45.96, 48.06, 48.51, 52.44, 123.63, 124.01, 124.14, 125.51, 126.43, 126.82, 127.36, 127.52, 128.43, 128.85, 129.08, 131.20, 133.10, 134.54, 138.17, 139.46, 140.82, 141.60, 142.24, 174.57

LRMS (APCI) calculated for $C_{31}H_{21}NO_3SNa$ $[M^+$+Na]: 510.1242, found: 510.2953

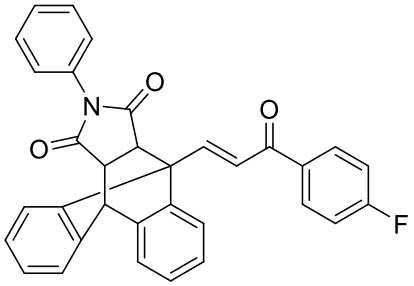

9-(*E*)-3-(4-Fluorophenyl)-3-oxoprop-1-en-1-yl)-13-phenyl-9,10-dihydro-9,10-[3,4]epipyrroloanthracene-12,14-dione (110)

9-(*E*)-3-(4-Fluorophenyl)-3-oxoprop-1-en-1-yl)-13-phenyl-9,10-dihydro-9,10-[3,4]epipyrroloanthracene-12,14-dione was prepared from (*E*)-3-(anthracen-9-yl)-1-(4-fluorophenyl)prop-2-en-1-one (1.0 mmol, 0.4343 g) and *N*-phenylmaleimide (1.3 mmol, 0.23 g) according to general procedure (4), green solid (88%)

Melting point: 79 ℃

^{1}H NMR (400 MHz, CDCl3) δ ppm 3.48 (dd, *J* = 8.4, 3.2 Hz, 1H), 3.66 (d, *J* = 8.4 Hz, 1H), 4.93 (d, *J* = 3.2 Hz, 1H), 6.44 – 6.54 (m, 2H), 7.13 – 7.21 (m, 2H), 7.22 (dd, *J* = 3.5, 1.6 Hz, 1H), 7.25 – 7.31 (m, 5H), 7.31 – 7.42 (m, 4H), 7.43 – 7.49 (m, 1H), 7.83 (d, *J* = 16.1 Hz, 1H), 8.00 (d, *J* = 16.1 Hz, 1H), 8.15 – 8.24 (m, 2H)

^{13}C NMR (101 MHz, $CDCl_3$) δ ppm 45.39, 48.93, 49.61, 52.01, 115.81, 116.03, 123.41, 123.79, 124.03, 125.47, 126.74, 127.28, 127.32, 127.49, 131.19, 131.58, 131.67, 134.09, 134.12, 137.94, 139.26, 140.92, 142.18, 142.28, 175.17, 175.73, 188.70 (chalcone C=O)

LRMS (APCI) calculated for $C_{33}H_{22}FNO_3$ [M^++H]: 500.16, found: 500.20

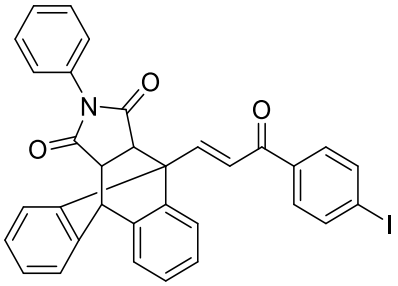

9-(*E*)-3-(4-Iodophenyl)-3-oxoprop-1-en-1-yl)-13-phenyl-9,10-dihydro-9,10-[3,4]epipyrroloanthracene-12,14-dione (109)

9-(*E*)-3-(4-Iodophenyl)-3-oxoprop-1-en-1-yl)-13-phenyl-9,10-dihydro-9,10-[3,4]epipyrroloanthracene-12,14-dione was prepared from (*E*)-3-(anthracen-9-yl)-1-(4-

iodophenyl)prop-2-en-1-one (1.0 mmol, 0.4343 g) and *N*-phenylmaleimide (1.3 mmol, 0.23 g) according to general procedure (4), white crystals (20%)

Melting Point: 214 ℃

^{1}H NMR (400 MHz, DMSO-*d*$_6$) δ ppm 3.51 (dd, *J* = 8.3, 3.2 Hz, 1H), 3.97 (d, *J* = 8.4 Hz, 1H), 4.92 (d, *J* = 3.2 Hz, 1H), 6.34 – 6.43 (m, 2H), 7.09 – 7.16 (m, 1H), 7.18 – 7.23 (m, 3H), 7.25 – 7.33 (m, 7H), 7.33 – 7.39 (m, 1H), 7.41 – 7.50 (m, 1H), 7.57 (dt, *J* = 7.1, 1.2 Hz, 1H), 7.78 – 7.85 (m, 2H), 7.86 – 7.91 (m, 2H), 7.94 – 8.01 (m, 2H)

^{13}C NMR (101 MHz, DMSO-*d6*) δ ppm 44.98, 49.13, 49.32, 51.72, 102.63, 123.26, 123.67, 124.62,125.65, 126.66, 127.17, 127.29, 130.84,131.45, 137.06, 138.35, 139.30, 140.27, 142.17, 143.05, 143.12, 177.48, 177.74, 189.40 (chalcone C=O)

IR*Vmax* (ATR): (C-H) 3088.53, (*trans* C=C) 1772.98, 1705 (C=O), (Ar C=C) 1633.80, 1587.05, 1499.05, (C-N) 1467.03, 1381, 1180, (C-I) 691.17 cm^{-1}

LRMS (APCI) calculated for $C_{33}H_{23}INO_3$ [M$^+$+H]: 608.06, found: 608.03

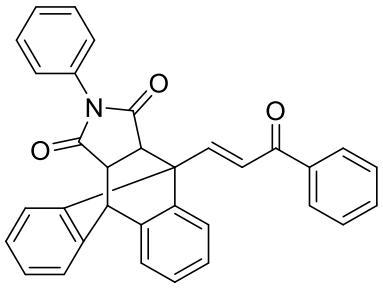

(*E*)-9-(3-Oxo-3-phenylprop-1-en-yl)-13-phenyl-9,10-dihydro-9,10- [3,4] epipyrroloanthracene-12,14-dione (108)

(*E*)-9-(3-Oxo-3-phenylprop-1-en-yl)-13-phenyl-9,10-dihydro-9,10-[3,4]epipyrroloanthracene-12,14-dione was synthesised from (*E*)-3-(anthracen-9-yl)-1-phenylprop-2-en-1-one (1.0 mmol, 0.3084 g) and *N*-phenyl maleimide (1.3 mmol, 0.23 g) according to the general procedure (4), white powder (42%)

Melting point: 103-105℃

^{1}H NMR (400 MHz, DMSO-*d6*) δ ppm 3.54 (dd, *J*=8.29, 3.32 Hz, 1H) 4.00 (d, *J*=8.29 Hz, 1H) 4.94 (d, *J*=3.32 Hz, H) 6.39 - 6.43 (m, 2H) 7.19 - 7.27 (m, 3H) 7.27 - 7.34 (m, 6H) 7.36 - 7.41 (m, 1H) 7.57 - 7.62 (m, 3H) 7.66 - 7.71 (m, 1H) 7.88 (d, *J*=1.66 Hz, 2H) 8.13 - 8.17 (m, 2H)

^{13}C NMR (101 MHz, DMSO-*d6*) δ ppm 45.41, 48.33, 52.15, 122.71, 123.42, 123.90, 124.86, 125.72, 126.88, 127.06, 127.44, 128.95, 129.20, 129.36, 132.01, 132.18, 133.88, 137.74, 139.24, 140.16, 141.70, 142.35, 142.82, 175.35, 175.76, 189.96 (chalcone C=O)

IR*Vmax* (ATR): 1707.50 (C=O), 1673.57 (C=C), 1636.62 (Ar C=C),1332.23 (C-N) cm^{-1}

LRMS (APCI) calculated for $C_{33}H_{24}NO_3$ [M^++H] 482.17, found 482.20

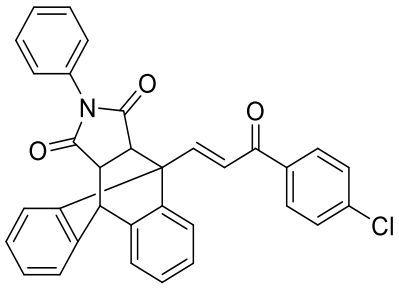

(*E*)-9-(3-(4-Chlorophenyl)-3-oxoprop-1-en-1-yl)-13-phenyl-9,10-dihydro-9,10- [3,4] epipyrroloanthracene-12,14-dione (114)

(*E*)-9-(3-(4-Chlorophenyl)-3-oxoprop-1-en-1-yl)-13-phenyl-9,10-dihydro-9,10- [3,4] epipyrroloanthracene-12,14-dione was synthesised from (*E*)-3-(anthracen-9-yl)-1-(4-chorophenyl) prop-2-en-1-one (1.0 mmol, 0.3430 g) and *N*-phenyl maleimide (1.3 mmol, 0.23 g) according to the general procedure (4), white powder (20%)

Melting point: 207-211℃

^{1}H NMR (400 MHz, $CDCl_3$) δ ppm 3.53 (dd, *J*=8.29, 3.32 Hz, 1H) 3.99 (d, *J*=8.29Hz, 1H) 4.94 (d, *J*=3.32 Hz, 1H) 6.37 - 6.44 (m, 2H) 7.23 (d, *J*=0.83 Hz, 3H) 7.27 - 7.35 (m, 6H) 7.35- 7.40 (m, 1H) 7.59 (d, *J*=6.63 Hz, 1H) 7.67 (d, *J*=8.29 Hz, 2H) 7.87 (s, 2H) 8.16 (d, *J*=8.29 Hz, 2H)

^{13}C NMR (101 MHz, $CDCl_3$) δ ppm 39.12 - 40.77, 45.42, 52.17, 123.44, 123.92, 124.86, 125.72, 126.72 -127.66, 129.24 - 129.66, 131.03, 131.75, 132.16, 135.09, 138.84, 139.21, 141.68, 142.74, 142.92, 175.37, 175.76, 188.95 (chalcone C=O)

IR*Vmax* (ATR): 3058.71 (Ar C-H), 1708.71(C=O), 1674.04 (C=C), 1591.39 (Ar C=C), 1455.69 (C-CH3), 1015.46 (C-N), 743.22 (C-Cl) cm^{-1}

LRMS (APCI) calculated for $C_{33}H_{23}ClNO_3$ [M^++H] 516.13, found 516.13

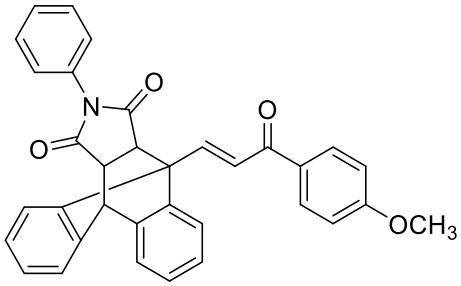

(*E*)-9-(3-(4-Methoxyphenyl)-3-oxoprop-1-en-1-yl)-13-phenyl-9,10-dihydro-9,10-[3,4]epipyrroloanthracene-12,14-dione (111)

(*E*)-9-(3-(4-Methoxyphenyl)-3-oxoprop-1-en-1-yl)-13-phenyl-9,10-dihydro-9,10- [3,4] epipyrroloanthracene-12,14-dione was synthesised from (*E*)-3-(anthracen-9-yl)-1-(4-methoxyphenyl)prop-2-en-1-one (1.0 mmol, 0.3384 g) and *N*-phenyl maleimide (1.3 mmol, 0.23 g) according to the general procedure (4), white powder (56%)

Melting point: 207-212 ℃

^{1}H NMR (400 MHz, $CDCl_3$) δ ppm 3.53 (dd, *J*=8.29, 3.32 Hz, 1H) 3.85 (s, 3H) 3.99 (d, *J*=8.29 Hz, 1H) 7.09 - 7.18 (m, 5H) 7.20 - 7.34 (m, 11H) 7.78 - 7.93 (m, 2H) 8.16 (d, *J*=9.12Hz, 2H)

^{13}C NMR (101 MHz, $CDCl_3$) δ ppm 40.17 - 40.89, 45.42, 48.33, 52.11, 55.35, 56.07, 114.67, 122.22, 123.41, 123.90, 124.83, 125.71, 126.85, 127.07, 127.26 - 127.55, 128.64, 129.00, 129.32, 130.59, 131.53, 131.92, 132.19, 139.24, 140.28, 141.20, 141.72, 142.95, 163.88, 175.34, 175.76, 177.93, 188.14 (chalcone C=O)

IR*Vmax* (ATR): 3343.74 (N-H), 1670.84 (C=O), 1600.33 (Ar C=C), 1380.68 (C-CH3), 1230.69 (C-O), 1024.50 (C-N) cm^{-1}

LRMS (APCI) calculated for $C_{34}H_{26}NO_4$ [M^++H]: 512.18, found: 512.19

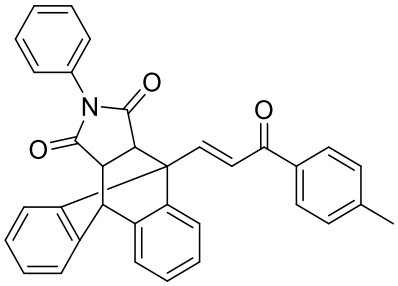

_(E)_-9-(3-Oxo-3-(p-tolyl)prop-1-en-1-yl)-13-phenyl-9,10-dihydro-9,10-[3,4] epipyrroloanthracene-12,14-dione (112)

_(E)_-9-(3-Oxo-3-(_p_-tolyl)prop-1-en-1-yl)-13-phenyl-9,10-dihydro-9,10-[3,4] epipyrroloanthracene-12,14-dione was synthesised from (_E_)-3-(anthracen-9-yl)-1-(_p_-tolyl)prop-2-en-1-one (1.0 mmol, 0.3384 g) and _N_-phenyl maleimide (1.3 mmol, 0.23 g) according to the general procedure (4), white powder (51%)

Melting point: 185-190 ℃

^{1}H NMR (400 MHz, $CDCl_3$) δ ppm 2.39 (s, 3H) 3.53 (dd, _J_=8.50, 3.11 Hz, 1H) 3.99 (d, _J_=8.71 Hz, 1H) 4.94 (d, _J_=2.90 Hz, 1H) 6.38 - 6.44 (m, 2H) 7.19 - 7.26 (m, 3H) 7.26 - 7.34 (m, 6H) 7.36 - 7.42 (m, 3H) 7.59 (d, _J_=6.63 Hz, 1H) 7.86 (d, _J_=3.32 Hz, 2H) 8.06 (d, _J_=8.29 Hz, 2H)

^{13}C NMR (101 MHz, $CDCl_3$) δ ppm 21.69, 39.22 - 40.74, 48.34, 52.13, 123.89, 125.38 -125.98, 126.76-127.19, 127.26 - 127.61, 128.92-129.49, 129.95, 131.97, 135.25, 140.21, 141.91, 144.37, 175.34, 189.38 (chalcone C=O)

IR$_{Vmax}$ (ATR): 2917.28 (Ar C-H), 1772.13 (C=O), 1624.76 (Ar C=C), 1458.34 (C-CH_3), 1230.53 (C-O), 1072.21 (C-N) cm^{-1}

LRMS (APCI) calculated for $C_{34}H_{26}NO_3$ [M^++H]: 496.18, found: 496.19.

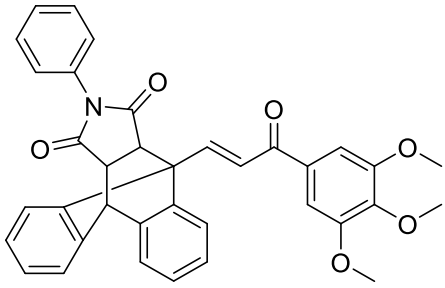

***(E)*-9-(3-Oxo-3-(3,4,5-trimethoxyphenyl)-prop-1-en-1-yl)-13-phenyl-9,10-dihydro-9,10- [3,4] epipyrroloanthracene-12,14-dione (113)**

(E)-9-(3-Oxo-3-(3,4,5-trimethoxyphenyl)-prop-1-en-1-yl)-13-phenyl-9,10-dihydro-9,10-[3,4] epipyrroloanthracene-12,14-dione was synthesised from (*E*)-3-(anthracen-9-yl)-1-(4- chorophenyl)prop-2-en-1-one (1.0 mmol, 0.3985 g) and *N*-phenyl maleimide (1.3 mmol, 0.23 g) according to the general procedure (4), white powder (62%)

Melting point: 242-246 ℃

^{1}H NMR (400 MHz, $CDCl_3$) δ ppm 3.53 (dd, *J*=8.50, 3.11 Hz, 1H) 3.76 (s, 3H) 3.68 (s, 6H) 4.00 (d, *J*=8.29 Hz, 1H) 4.94 (d, *J*=3.32 Hz, 1H) 6.42 (dd, *J*=7.46, 2.07 Hz, 2H) 7.23 - 7.26 (m, 2H) 7.26 - 7.33 (m, 6H) 7.34 (s, 1H) 7.37 - 7.40 (m, H) 7.47 (s, 2H) 7.58 - 7.61 (m, 1H) 7.78 - 7.91 (m, 2H)

^{13}C NMR (101 MHz, $CDCl_3$) δ ppm 39.30-40.78, 45.43, 48.1-48.62, 56.54, 60.67, 106.88, 123.42, 123.95, 124.88, 125.71, 126.75 -126.96, 127.29-127.48, 128.94, 129.26, 132.13, 132.50, 133.05, 140.18, 141.65, 153.41, 175.39, 175.73, 189.11 (chalcone C=O)

IRν_{max} (ATR) 1702.71 (C=O), 1123.37 (C-O) cm^{-1}

LRMS (APCI) calculated for $C_{36}H_{30}NO_6$ [M^++H] 572.199, found: 572.192

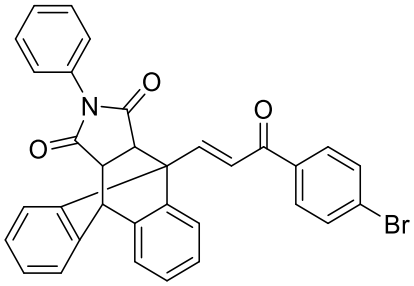

(*E*)-3-(4-Bromophenyl)-3-oxoprop-1-en-1-yl)-13-phenyl-9,10-dihydro-9,10-[3,4]epipyrroloanthracene-12,14-dione (103)

(*E*)-3-(4-Bromophenyl)-3-oxoprop-1-en-1-yl)-13-phenyl-9,10-dihydro-9,10-[3,4]epipyrroloanthracene-12,14-dione was synthesised from (*E*)-3-(anthracen-9-yl)-1-(4-bromophenyl)prop-2-en-1-one (1.0 mmol, 0.3873 g) and *N*-phenyl maleimide (1.3 mmol, 0.23 g) according to the general procedure (4), white powder (84%)

Melting Point: 218 ℃

^{1}H NMR (400 MHz, $CDCl_3$) δ ppm 3.47 (dd, *J*=8.29, 3.32 Hz, 2H), 3.64 (d, *J*=8.29 Hz, 2H), 4.92 (d, *J*=2.90 Hz, 2H), 6.46 - 6.53 (m, 3H), 7.19 - 7.23 (m, 2H), 7.25 - 7.30 (m, 8H), 7.30 - 7.35 (m, 3H), 7.35 - 7.43 (m, 4H), 7.45 (dd, *J*=7.05, 1.24 Hz, 2H), 7.61 - 7.65 (m, 3H), 7.80 (d, *J*=16.17 Hz, 1H), 7.97 - 8.05 (m, 3H)

^{13}C NMR (101 MHz, $CDCl_3$) δ ppm 45.94, 47.95, 48.48, 52.49, 123.51, 123.92, 124.17, 125.55, 126.05, 126.44, 126.82, 127.38, 127.55, 127.94, 128.36, 128.91, 129.11, 129.13, 130.49, 131.14, 131.25, 132.06, 134.17, 136.45, 138.17, 139.39, 140.80, 142.17, 142.81, 169.49, 174.63, 175.29, 189.25 (chalcone C=O)

IR*Vmax* (ATR): 3057 (C-H), 1773.49 (*trans* C=C),1706 (C=O), 1635, 1490, 1455 (Ar C=C), 1380.41 (C-N), 1180 (C-O), 691.05 (C-Br) cm^{-1}

LRMS (APCI) calculated for $C_{33}H_{22}BrNO_3$ [M^++H]: 560.08, found: 560.20

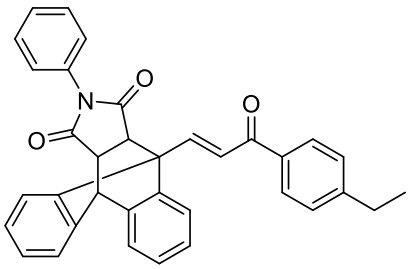

(*E*)-9-(3-(4-Ethylphenyl)-3-oxoprop-1-en-1-yl)-13-phenyl-9,10-dihydro-9,10-[3,4]epipyrroloanthracene-12,14-dione (105)

(*E*)-9-(3-(4-Ethylphenyl)-3-oxoprop-1-en-1-yl)-13-phenyl-9,10-dihydro-9,10-[3,4]epipyrroloanthracene-12,14-dione was synthesised from (*E*)-3-(anthracen-9-yl)-1-(4-ethylphenyl)prop-2-en-1-one (1.0 mmol, 0.3364 g) and *N*-phenyl maleimide (1.3 mmol, 0.23 g) according to the general procedure (4), light green powder (90%)

Melting Point: 207 ℃

^{1}H NMR (400 MHz, DMSO-*d*$_6$) δ ppm 3.57 (dd, *J*=8.31, 3.42 Hz, 3H), 4.01 (d, *J*=8.31 Hz, H), 4.97 (d, *J*=2.93 Hz, 3H), 6.38 - 6.46 (m, 6H), 7.26 - 7.36 (m,2H), 7.36 - 7.39 (m,

3H), 7.40 - 7.43 (m, 1H), 7.59 - 7.65 (m, 1 H), 7.83 (d, *J*=17.12 Hz, 1 H), 7.96 (d, *J*=16.63 Hz, 1H), 8.01 (d, *J*=5.87 Hz, 2 H), 8.89 (d, *J*=5.87 Hz, 2H)

^{13}C NMR (101 MHz, DMSO-*d*$_6$) δ ppm 15.6, 25.9, 28.7, 45.4, 48.3, 52.1, 123.4, 123.9, 124.8, 125.7, 126.9, 127.0, 127.2, 127.3, 127.4, 127.5, 128.2, 128.6, 128.8, 129.0, 129.3, 129.4, 132.0, 132.2, 135.1, 135.5, 139.2, 140.2, 141.7, 141.9, 142.9, 150.4, 170.4, 175.3, 175.7, 189.4 (chalcone C=O)

LRMS (APCI) calculated for $C_{35}H_{28}NO_3$ [M^+-H]: 510.20, found: 510.24

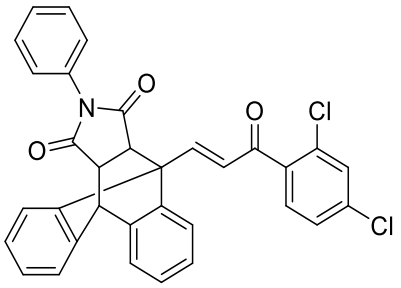

(*E*)-9-(3-(2,4-Dichlorophenyl)-3-oxoprop-1-en-1-yl)-13-phenyl-9,10-dihydro-9,10-[3,4]epipyrroloanthracene-12,14-dione (106)

(*E*)-9-(3-(2,4-Dichlorophenyl)-3-oxoprop-1-en-1-yl)-13-phenyl-9,10-dihydro-9,10-[3,4]epipyrroloanthracene-12,14-dione was synthesised from (*E*)-3-(anthracen-9-yl)-1-(2,4-dichlorophenyl)prop-2-en-1-one (1.0 mmol, 0.3773 g) and *N*-phenyl maleimide (1.3 mmol, 0.23 g) according to the general procedure (4), white powder (75%)

Melting Point: 208-210 ℃

^{1}H NMR (400 MHz,CDCl$_3$) δ ppm 3.44 (dd, *J*=8.29, 3.32 Hz, 1H), 3.55 (d, *J*=8.29 Hz, 1H), 4.91 (d, *J*=3.32 Hz, 1H), 6.46 (m, 2H), 7.24 (m, 7H), 7.35 (m, 5H), 7.46 (m, 1H), 7.50 (d, *J*=1.66 Hz, H), 7.66 (d, *J*=8.29 Hz, 1 H), 7.83 (d, *J*=17.00 Hz, 1H), 7.79 (d, *J*=17.00 Hz, 1H)

^{13}C NMR (101 MHz, CDCl$_3$) δ ppm 45.97, 48.23, 48.34, 52.30, 123.43, 123.76, 124.28, 125.57, 126.38, 126.81, 127.33, 127.43, 127.45, 127.57, 128.88, 129.08, 130.87, 131.16, 132.66, 134.88, 136.80, 138.15, 139.07, 140.78, 141.69, 144.77, 174.43, 175.25, 191.55 (chalcone C=O)

IR*Vmax* (ATR): 3067.32 (C-H), 1776.64 (*trans* C=C), 1710.54, 1630.86 (C=O), 1381.66 (C-N), 1183.14 (C-O) cm^{-1}

HRMS (ESI) calculated for $C_{33}H_{20}Cl_2NO_3$ [M^+-H]: 548.082572, found: 548.082538. Mass accuracy (0.1 ppm).

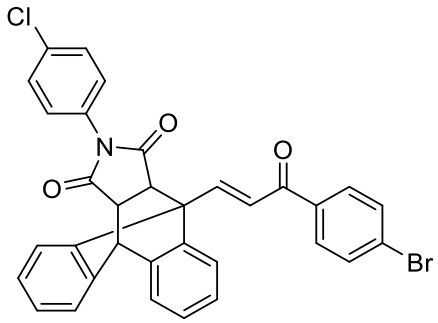

(*E*)-9-(3-(4-Bromophenyl)-3-oxoprop-1-en-1-yl)-13-(4-chlorophenyl)-9,10-dihydro-9,10-[3,4]epipyrroloanthracene-12,14-dione (120)

(*E*)-9-(3-(4-Bromophenyl)-3-oxoprop-1-en-1-yl)-13-(4-chlorophenyl)-9,10-dihydro-9,10-[3,4]epipyrroloanthracene-12,14-dione was synthesised (*E*)-3-(anthracen-9-yl)-1-(4-bromophenyl)prop-2-en-1-one (1.0 mmol, 0.3873 g) and *p*-chloromaleimide (1.3 mmol, 0.27 g) according to the general procedure (4), white powder (95%)

^{1}H NMR (400 MHz, $CDCl_3$) δ ppm δ 3.52 (dd, J = 8.32, 3.15 Hz, 1H), 4.01 (d, *J* = 8.33 Hz, 1H), 4.94 (d, *J* = 3.22 Hz, 1H), 6.47 (d,*J*=8.28 Hz, 2H), 7.14-7.32 (m, 9H), 7.45-7.56 (m, 1H), 7.60 (d, *J* = 6.3 Hz, 1H), 7.82 (m, 2H), 7.85 (d, J=16.12 Hz, 1 H),7.97 (d, *J* = 8.4 Hz, 2H)

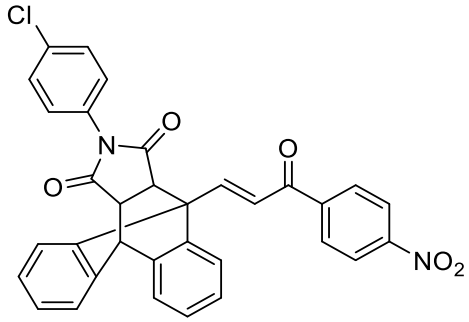

(*E*)-13-(4-Chlorophenyl)-9-(3-(4-nitrophenyl)-3-oxoprop-1-en-1-yl)-9,10-dihydro-9,10-[3,4]epipyrroloanthracene-12,14-dione (121)

(*E*)-13-(4-Chlorophenyl)-9-(3-(4-nitrophenyl)-3-oxoprop-1-en-1-yl)-9,10-dihydro-9,10-[3,4]epipyrroloanthracene-12,14-dione was synthesised from (*E*)-3-(anthracen-9-yl)-1-(4-nitrophenyl)prop-2-en-1-one (1.0 mmol, 0.3534 g) and *p*-chloromaleimide (1.3 mmol, 0.27 g) according to the general procedure (4), white powder (82%)

^{1}H NMR (400 MHz,$CDCl_3$) δ ppm 3.51 (dd, *J*=8.50, 3.11 Hz, 4 H), 3.67 (d, *J*=8.29 Hz, 1 H), 4.94 (d, *J*=3.32 Hz, 1 H), 6.47 (d, *J*=9.12 Hz, 2 H), 7.20 - 7.31 (m, 6 H), 7.31 - 7.38 (m, 2 H), 7.39 - 7.45 (m, 1 H), 7.46 - 7.51 (m, 1 H), 7.84 (d, *J*=16.17 Hz, 1 H), 8.06 (d, *J*=16.17 Hz, 1 H), 8.32 (d, *J*=8.71 Hz, 2 H), 8.37 (d, *J*=8.71 Hz, 2 H)

HRMS (ESI) calculated for $C_{33}H_{21}Cl_2N_2O_5$ [M^++Cl]: 595.083301, found: 595.082000. Mass accuracy (2.2 ppm)

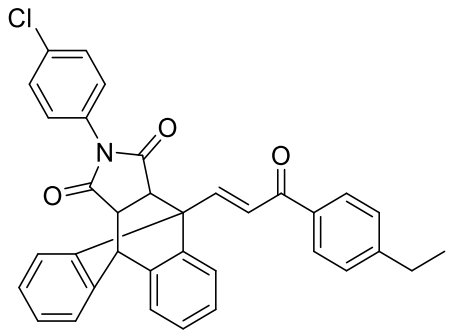

(*E*)-13-(4-Chlorophenyl)-9-(3-(4-ethylphenyl)-3-oxoprop-1-en-1-yl)-9,10-dihydro-9,10-[3,4]epipyrroloanthracene-12,14-dione (122)

(*E*)-13-(4-Chlorophenyl)-9-(3-(4-ethylphenyl)-3-oxoprop-1-en-1-yl)-9,10-dihydro-9,10-[3,4]epipyrroloanthracene-12,14-dione was synthesised from (*E*)-3-(anthracen-9-yl)-1-(4-ethylphenyl)prop-2-en-1-one (1 mmol, 0.3364 g) and *p*-chloro maleimide (1.3 mmol, 0.27 g) according to the general procedure (4), white powder (3%)

^{1}H NMR (400 MHz,$CDCl_3$) δ ppm 1.19-1.25 (m, 3H), 2.37 (m, 2H), 3.54 (dd, *J*=8.27, 3.39 Hz, 1H), 3.98 (d, *J*=8.27 Hz, 1 H), 4.97 (d, *J*=2.91 Hz, 1 H), 6.39-6.47 (m, 2H), 7.23-7.32 (m, 5H), 7.34 - 7.36 (m, 1 H), 7.37 - 7.43 (m, 3H), 7.47 - 7.59 (m, 2 H), 7.78 (d, *J*=16.2 Hz, 1 H), 7.83 (d, *J*=5.87 Hz, 2 H), 7.98 (d, *J*=5.87 Hz, 2 H)

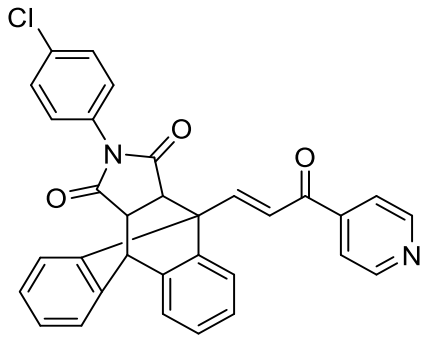

(*E*)-13-(4-Chlorophenyl)-9-(3-oxo-3-(pyridin-4-yl)prop-1-en-1-yl)-9,10-dihydro-9,10-[3,4]epipyrroloanthracene-12,14-dione (132)

(*E*)-13-(4-Chlorophenyl)-9-(3-oxo-3-(pyridin-2-yl)prop-1-en-1-yl)-9,10-dihydro-9,10-[3,4]epipyrroloanthracene-12,14-dione was synthesised from (*E*)-3-(anthracen-9-yl)-1-(pyridin-2-yl)prop-2-en-1-one (1.0 mmol, 0.3094 g) and *p*-chloromaleimide (1.3 mmol, 0.27 g) according to the general procedure (4), (92%)

^{1}H NMR (400 MHz, DMSO-*d*$_6$) δ ppm 3.52 (dd, *J*=8.29, 3.32 Hz, 1H), 3.97 (d, *J*=8.71 Hz, 1H), 4.93 (d, *J*=2.90 Hz, 1H), 6.44 (d, *J*=8.71 Hz, 2H), 7.24 - 7.29 (m, 4H), 7.30 - 7.35 (m, 1H), 7.35 - 7.42 (m, 3H), 7.54 - 7.60 (m, 2H), 7.78 (d, *J*=16.17 Hz, 1H), 7.91 (d, *J*=15.76 Hz, 1H), 7.97 (d, *J*=6.63 Hz, 2H), 8.85 (d, *J*=6.22 Hz, 2H)

HRMS (ESI) calculated for $C_{32}H_{22}Cl_2NO_3$ [M^++H]: 551.093471, found:551.092384. Mass accuracy (-2.0 ppm)

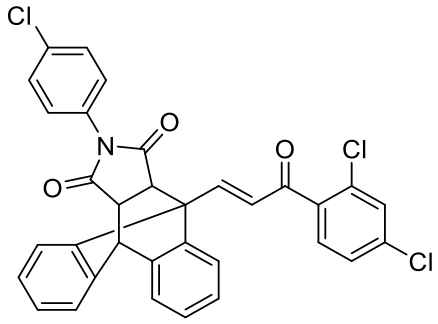

(*E*)-13-(4-Chlorophenyl)-9-(3-(2,4-dichlorophenyl)-3-oxoprop-1-en-1-yl)-9,10-dihydro-9,10-[3,4]epipyrroloanthracene-12,14-dione (123)

(*E*)-13-(4-Chlorophenyl)-9-(3-oxo-3-(pyridin-2-yl)prop-1-en-1-yl)-9,10-dihydro-9,10-[3,4]epipyrroloanthracene-12,14-dione was synthesised from (*E*)-3-(anthracen-9-yl)-1-

(pyridin-2-yl)prop-2-en-1-one (1.0 mmol, 0.3094 g) and *p*-chloromaleimide (1.3 mmol, 0.27 g) according to the general procedure (4), white powder (87%)

^{1}H NMR (400 MHz, $CDCl_3$) δ ppm 3.45 (dd, *J*=8.50, 3.11 Hz, 3H), 3.56 (d, *J*=8.29 Hz, 2H), 4.91 (d, *J*=3.32 Hz, 2H), 6.43 (d, *J*=9.12 Hz, 2H), 7.19 - 7.23 (m, 1H), 7.25 -7.30 (m, 4H), 7.30 - 7.37 (m, 3H), 7.41 (d, *J*=2.07 Hz, 1H), 7.43 -7.48 (m, 1H), 7.52 (d, *J*=1.66 Hz, 1H), 7.67 (d, *J*=8.29 Hz, 1H), 7.81 (d, *J*=16.59 Hz, 1H)

HRMS (ESI) calculated for $C_{32}H_{20}Cl_4NO_3$ [M^++Cl]: 618.020278, found: 618.019336 Mass accuracy (1.5 ppm).

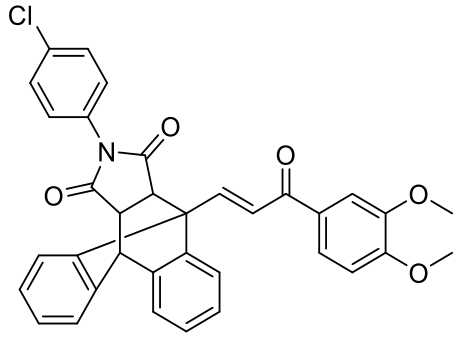

(*E*)-13-(4-Chlorophenyl)-9-(3-(3,4-dimethoxyphenyl)-3-oxoprop-1-en-1-yl)-9,10-dihydro-9,10-[3,4]epipyrroloanthracene-12,14-dione (124)

(*E*)-13-(4-Chlorophenyl)-9-(3-(3,4-dimethoxyphenyl)-3-oxoprop-1-en-1-yl)-9,10-dihydro-9,10-[3,4]epipyrroloanthracene-12,14-dione was synthesised from (*E*)-3-(anthracen-9-yl)-1-(3,4-dimethoxyphenyl)prop-2-en-1-one (1.0 mmol, 0.3684 g) and *p*-chloromaleimide (1.3 mmol, 0.27 g) according to the general procedure (4), white powder (4%)

^{1}H NMR (400 MHz, $CDCl_3$) δ ppm 2.83 (d, *J*=4.98 Hz, 1H), 2.88 (d, *J*=4.98 Hz, 1H), 3.49 (dd, *J*=8.09, 3.11 Hz, 1H), 3.71 (d, *J*=9.12 Hz, 1H), 4.93 (d, *J*=3.73 Hz, 1H), 6.48 (d, *J*=9.12 Hz, 1H), 7.50 - 7.67 (m, 5H), 7.87 - 7.91 (m, 1H), 7.93 - 7.99 (m, 1H), 8.06 (d, *J*=15.76 Hz, 1H), 8.21 (d, *J*=9.54 Hz, 1H)

LRMS (APCI) calculated for $C_{33}H_{22}ClNO_3$ [M^+-$(OCH_3)_2$]: 514.12, found: 514.20

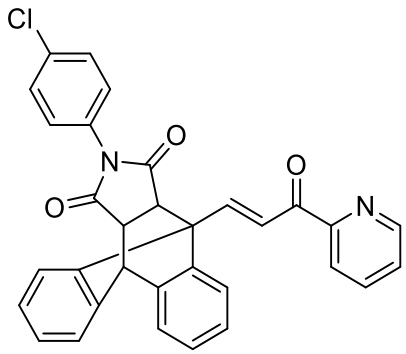

(*E*)-13-(4-Chlorophenyl)-9-(3-oxo-3-(pyridin-2-yl)prop-1-en-1-yl)-9,10-dihydro-9,10-[3,4]epipyrroloanthracene-12,14-dione (133)

(*E*)-13-(4-Chlorophenyl)-9-(3-oxo-3-(pyridin-2-yl)prop-1-en-1-yl)-9,10-dihydro-9,10-[3,4]epipyrroloanthracene-12,14-dione was synthesised from (*E*)-3-(anthracen-9-yl)-1-(pyridin-2-yl)prop-2-en-1-one (1.0 mmol, 0.3094 g) and *p*-chloromaleimide (1.3 mmol, 0.27 g) according to the general procedure (4), white powder (57%)

^{1}H NMR (400 MHz, DMSO-d_6) δ ppm 3.50 (dd, *J*=8.29, 3.32 Hz, 3H), 3.84 (d, *J*=8.71 Hz, H), 4.94 (d, *J*=2.90 Hz, 3 H), 6.45 (d, *J*=8.29 Hz, H), 7.11 - 7.22 (m, 1 H), 7.22 - 7.30 (m, 4H), 7.30 - 7.35 (m, 1H), 7.36 - 7.42 (m, 3H), 7.59 (d, *J*=7.05 Hz, 1H), 7.70 (dd, *J*=7.46, 4.98 Hz, 1H), 8.04 (d, *J*=17.00 Hz, 1H), 8.07 - 8.12 (m, 1H), 8.21 (d, *J*=7.88 Hz, 1H), 8.27 (d, *J*=16.59 Hz, 1H), 8.76 (d, *J*=4.98 Hz, 1H)

^{13}C NMR (101 MHz, DMSO-d_6) δ ppm 45.41, 48.40, 48.96, 52.25, 127.37, 127.41, 127.54, 128.31, 128.64, 129.4 , 130.28, 130.89, 133.51, 138.34, 139.29, 140.07, 141.66, 142.60, 143.09, 149.75, 153.68, 174.99, 175.58, 188.85

HRMS (ESI) calculated for $C_{23}H_{22}ClN_2O_3$ [M^++H]: 517.131347, found: 517.103235. Mass accuracy (2.1 ppm)

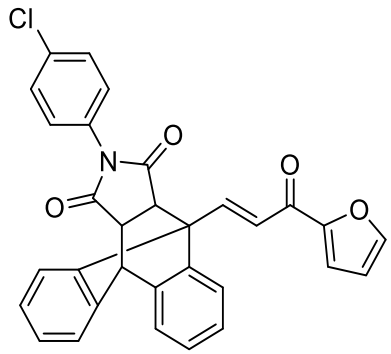

(*E*)-13-(4-Chlorophenyl)-9-(3-(furan-2-yl)-3-oxoprop-1-en-1-yl)-9,10-dihydro-9,10-[3,4]epipyrroloanthracene-12,14-dione (134)

(*E*)-13-(4-Chlorophenyl)-9-(3-(furan-2-yl)-3-oxoprop-1-en-1-yl)-9,10-dihydro-9,10-[3,4]epipyrroloanthracene-12,14-dione was synthesised from (*E*)-3-(anthracen-9-yl)-1-(furan-2-yl)prop-2-en-1-one (1.0 mmol, 0.2983 g) and *p*-chloro maleimide (1.3 mmol, 0.27 g) according to the general procedure (4), white powder (46%)

^{1}H NMR (400 MHz, $CDCl_3$) δ ppm 3.54 (dd, *J* = 8.33, 3.18 Hz, 1H), 4.03 (d, *J* = 8.21 Hz, 1H), 4.94 (d, *J* = 3.3 Hz, 1H), 6.61 (m, 2H), 7.12-7.32 (m, 6H), 7.35-7.43 (m, 2H), 7.45 – 7.49 (m, 2H), 7.55 – 7.63 (m, 2H), 7.66 (m, 1H), 7.75 (d, *J* = 16.18 Hz, 1H), 8.13 (d, *J* = 16.18 Hz, 1H)

^{13}C NMR (101 MHz, $CDCl_3$) δ ppm 45.4, 48.3, 48.8, 52.0, 113.4, 120.6, 123.4, 123.9, 124.9, 125.7, 125.7, 126.9, 127.4, 127.5, 128.6, 129.3, 129.4, 130.9, 131.4, 133.5, 139.2, 140.0, 141.5, 141.6, 142.6, 149.2, 153.1, 167.3, 175.1, 175.5, 176.8

LRMS (APCI): calculated for $C_{31}H_{21}ClNO_4$ $[M^+ + H]$: 506.11, found: 506.14

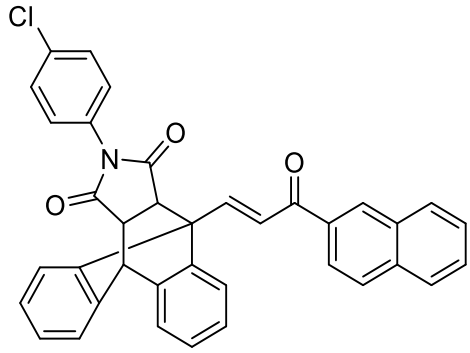

(*E*)-13-(4-Chlorophenyl)-9-(3-(naphthalen-2-yl)-3-oxoprop-1-en-1-yl)-9,10-dihydro-9,10-[3,4]epipyrroloanthracene-12,14-dione (135)

(*E*)-13-(4-Chlorophenyl)-9-(3-(naphthalen-2-yl)-3-oxoprop-1-en-1-yl)-9,10-dihydro-9,10-[3,4]epipyrroloanthracene-12,14-dione was synthesised from (*E*)-3-(anthracen-9-yl)-1-(naphthalen-2-yl)prop-2-en-1-one (1.0 mmol, 0.3584 g) and *p*-chloromaleimide (1.3 mmol, 0.27 g) according to the general procedure (4), grey powder (88%)

^{1}H NMR (400 MHz,$CDCl_3$) δ ppm 3.51 (dd, *J*=8.50, 3.11 Hz, 3H), 3.72 (d, *J*=8.29 Hz, 3H), 4.95 (d, *J*=3.32 Hz, 1H), 6.51 (d, *J*=8.71 Hz, 2H), 7.24 - 7.32 (m, 6H), 7.38 - 7.43 (m, 2H), 7.43 - 7.50 (m, 2H), 7.52 - 7.58 (m, 1H), 7.58 - 7.64 (m, 1H), 7.91 (d, *J*=7.88 Hz, 1H), 7.94 - 8.02 (m, H), 8.05 - 8.11 (m, 1H), 8.23 (dd, *J*=8.50, 1.45 Hz, 1H), 8.71 (s, 1H)

^{13}C NMR (101 MHz, $CDCl_3$) δ ppm 46.00, 48.1 , 48.47, 52.5 , 123.63, 124.08, 124.16, 124.57, 125.50, 126.78, 126.89, 127.40, 127.54, 127.70, 127.82, 128.57, 128.71, 129.31, 129.48, 129.71, 129.74, 130.81, 131.62, 132.59, 134.74, 135.05, 135.68, 138.16, 140.69, 142.05, 142.19, 174.34, 175.15, 189.99

LRMS (APCI): calculated for $C_{37}H_{24}Cl_2NO_3$ [M^++Cl]: 602.15, found: 602.31

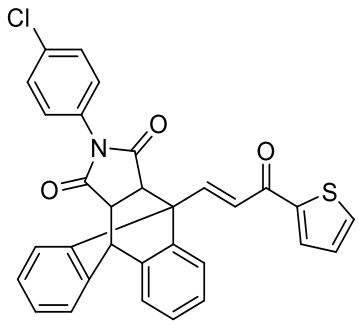

(*E*)-13-(4-Chlorophenyl)-9-(3-oxo-3-(thiophen-2-yl)prop-1-en-1-yl)-9,10-dihydro-9,10-[3,4]epipyrroloanthracene-12,14-dione (136)

(*E*)-13-(4-Chlorophenyl)-9-(3-oxo-3-(thiophen-2-yl)prop-1-en-1-yl)-9,10-dihydro-9,10-[3,4]epipyrroloanthracene-12,14-dione was synthesised from (*E*)-3-(anthracen-9-yl)-1-(thiophen-2-yl)prop-2-en-1-one (1.0 mmol, 0.3144 g) and *p*-chloromaleimide (1.3 mmol, 0.27 g) according to the general procedure (4), white powder (70%)

^{1}H NMR (400 MHz, DMSO-d_6) δ ppm 3.56 (dd, *J*=8.29, 3.32 Hz, 1H), 3.99 (d, *J*=8.29 Hz, 1H), 4.95 (d, *J*=2.90 Hz, 1H), 6.48 (d, *J*=8.71 Hz, 2H), 7.09 - 7.17 (m, 2H), 7.18 - 7.32 (m, H), 7.32 - 7.36 (m, 1 H), 7.36 - 7.43 (m, 3H), 7.59 (d, *J*=6.63 Hz, 1H), 7.84 (d, *J*=15.76 Hz, H), 7.93 (d, *J*=16.59 Hz, 1H), 8.10 (d, *J*=4.56 Hz, 1H), 8.21 (d, *J*=3.32 Hz, 1H)

^{13}C NMR (101 MHz, DMSO-d_6) δ ppm 45.45, 48.35, 48.68, 52.08, 123.42, 123.9 , 124.88, 125.7, 125.74, 126.88, 127.3, 127.5, 129.33, 129.44, 129.4, 130.90, 131.70, 133.58, 134.6, 136.50, 137.79, 139.18, 140.05, 141.60, 142.67, 145.27

LRMS (APCI): calculated for $C_{31}H_{19}ClNO_3S$ [M^+-H]: 520.09, found: 520.30

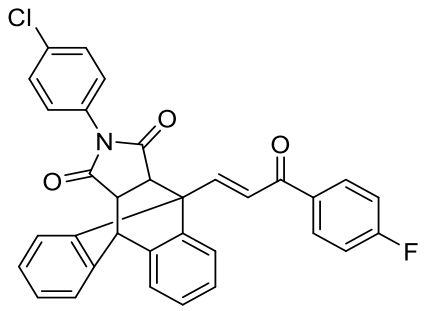

(*E*)-13-(4-Chlorophenyl)-9-(3-(4-fluorophenyl)-3-oxoprop-1-en-1-yl)-9,10-dihydro-9,10-[3,4]epipyrroloanthracene-12,14-dione (127)

(*E*)-13-(4-Chlorophenyl)-9-(3-(4-fluorophenyl)-3-oxoprop-1-en-1-yl)-9,10-dihydro-9,10-[3,4]epipyrroloanthracene-12,14-dione was synthesised (*E*)-3-(anthracen-9-yl)-1-(4-fluorophenyl)prop-2-en-1-one (1.0 mmol, 0.3264 g) and *p*-chloro maleimide (1.3 mmol, 0.27 g) according to the general procedure (4), white powder (88%)

^{1}H NMR (400 MHz, $CDCl_3$) δ ppm 3.49 (dd, *J*=8.50, 3.11 Hz, 4 H), 3.67 (d, *J*=8.29 Hz, 5 H), 4.93 (d, *J*=3.32 Hz, 1 H), 6.47 (d, *J*=8.71 Hz, 2 H), 7.16 - 7.23 (m, 3 H), 7.23 - 7.31 (m, 6 H), 7.34 - 7.43 (m, 4 H), 7.47 (d, *J*=6.63 Hz, 1 H), 7.83 (d, *J*=15.76 Hz, 1 H), 8.00 (d, *J*=15.76 Hz, 1 H), 8.21 (dd, *J*=8.71, 5.39 Hz, 5 H)

^{13}C NMR (101 MHz, DMSO-d_6) δ ppm 45.4, 48.4, 48.4, 52.1, 116.4, 116.6, 123.4, 123.9, 124.9, 125.7, 126.9, 127.4, 127.4, 127.5, 128.7, 129.5, 130.9, 131.9, 132.1, 132.2, 133.6, 134.4, 134.5, 139.2, 140.1, 141.6, 142.4, 142.7, 175.2, 175.5, 188.5

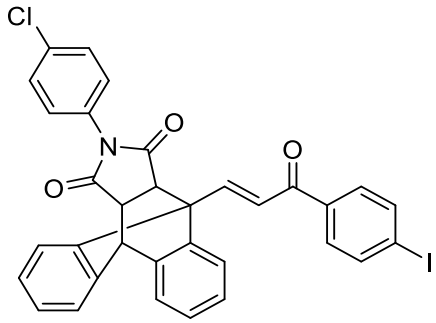

(*E*)-13-(4-Chlorophenyl)-9-(3-(4-iodophenyl)-3-oxoprop-1-en-1-yl)-9,10-dihydro-9,10-[3,4]epipyrroloanthracene-12,14-dione (126)

(*E*)-13-(4-Chlorophenyl)-9-(3-(4-iodophenyl)-3-oxoprop-1-en-1-yl)-9,10-dihydro-9,10-[3,4]epipyrroloanthracene-12,14-dione was synthesised (*E*)-3-(anthracen-9-yl)-1-(4-iodophenyl)prop-2-en-1-one (1.0 mmol, 0.4493 g) and *p*-chloromaleimide (1.3 mmol, 0.27 g) according to the general procedure (4), white powder (92%)

^{1}H NMR (400 MHz, DMSO-*d*$_6$) δ ppm 3.52 (dd, *J*=8.29, 3.32 Hz, H), 3.98 (d, *J*=8.29 Hz, 2H), 4.93 (d, *J*=3.32 Hz, 2H), 6.45 (d, *J*=8.29 Hz, 2H), 7.16 - 7.23 (m, 2H), 7.23 - 7.28 (m, 2H), 7.29 - 7.34 (m, 1H), 7.36 (d, *J*=3.73 Hz, H), 7.37 - 7.41 (m, H), 7.54 - 7.59 (m, 1H), 7.81 (d, *J*=16.59 Hz, 1H), 7.84 - 7.92 (m, H), 7.97 (d, *J*=8.29 Hz, 2H)

LRMS (APCI) calculated for $C_{33}H_{22}ClINO_3$ [M^++H]: 642.03, found: 642.04.

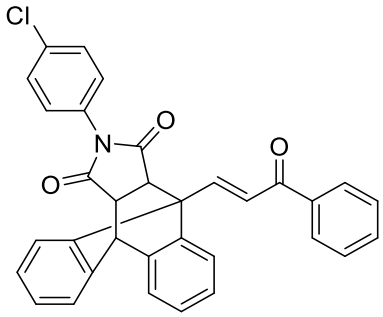

***(E)*-13-(4-Chlorophenyl)-9-(3-oxo-3-phenylprop-1-en-1-yl)-9,10-dihydro-9,10-[3,4] epipyrroloanthracene-12,14-dione (125)**

(*E*)-13-(4-Chlorophenyl)-9-(3-oxo-3-phenylprop-1-en-1-yl)-9,10-dihydro-9,10-[3,4] epipyrroloanthracene-12,14-dione was synthesised from (*E*)-3-(anthracen-9-yl)-1-phenylprop-2-en-1-one (1.0 mmol, 0.3084g) and *p*-chloro maleimide (1.3 mmol, 0.27 g) according to the general procedure (4), white powder (48%)

Melting point: 205-210 ℃

^{1}H NMR (400 MHz, DMSO-*d*6) δ ppm 3.53 (dd, *J*=8.50, 3.11 Hz, 1H) 4.00 (d, *J*=8.71 Hz, 1H) 4.94 (d, *J*=3.32 Hz, 1H) 6.43 - 6.49 (m, 2H) 7.20 - 7.29 (m, 5H) 7.29 - 7.35 (m, 1H) 7.36 - 7.44 (m, 3H) 7.55 - 7.62 (m, 3H) 7.68 (d, *J*=7.46 Hz, 1H) 7.86 (d, *J*=1.24 Hz, 2H) 8.13 - 8.18 (m, 2H)

^{13}C NMR (101 MHz, DMSO-*d*6) δ ppm 39.13 - 40.81, 48.39, 52.14, 123.39, 123.92, 124.88, 125.69, 127.46, 129.11, 129.44, 130.91, 132.03, 133.89, 137.73, 139.18, 140.10, 141.60, 142.26, 142.73, 175.14, 175.56, 189.95 (chalcone C=O)

IR*Vmax* (ATR): 3059.03 (Ar C-H), 1707.71 (C=O), 1673.57 (C=C), 1637.61 (Ar C=C), 1327.46 (C-N), 767.80 (C-Cl) cm^{-1}

LRMS (APCI) calculated for $C_{39}H_{27}N_2O_4$ [M^+-H]: 514.1288, found: 514.2120

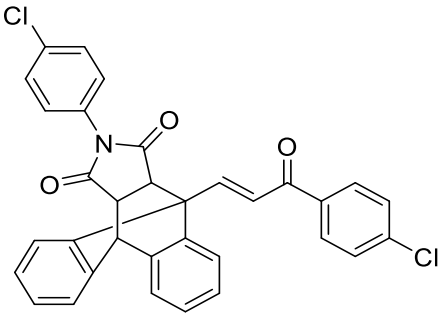

***(E)*-13-(4-Chlorophenyl)-9-(3-(4-cholrophenyl)-3-oxoprop-1-en-1-yl)-9,10-dihydro-9,10- [3,4] epipyrroloanthracene-12,14-dione (131)**

(E)-13-(4-Chlorophenyl)-9-(3-(4-cholrophenyl)-3-oxoprop-1-en-1-yl)-9,10-dihydro-9,10- [3,4] epipyrroloanthracene-12,14-dione was synthesised from (*E*)-3-(anthracen-9-yl)-1-(4-chlorophenyl) prop-2-en-1-one (1.0 mmol, 0.3430 g) and *p*-chloro maleimide (1.3 mmol, 0.27 g) according to the general procedure (4), white powder (39%)

Melting point: 268-271℃

^{1}H NMR (400 MHz, $CDCl_3$) δ ppm 3.53 (dd, *J*=8.29, 3.32 Hz, 1H) 4.00 (d, *J*=8.29 Hz, 1H) 4.94 (d, *J*=3.32 Hz, 1H) 6.42 - 6.48 (m, 2H) 7.20 - 7.31 (m, 6H) 7.32 (s, H) 7.36 - 7.43 (m, 3H) 7.59 (d, *J*=7.05 Hz, 1H) 7.65 - 7.70 (m, 2H) 7.87 (s, 2H) 8.14 - 8.19 (m, 2H)

^{13}C NMR (101 MHz, $CDCl_3$) δ ppm 39.07 - 40.76, 45.39, 48.39, 52.16, 123.42, 123.94, 124.89, 125.72, 127.46, 128.68, 129.32 - 129.73, 130.69 - 131.19, 131.78, 133.58, 138.84, 139.17, 140.04, 141.59, 142.74, 175.16, 175.55, 188.92 (chalcone C=O)

IR*Vmax* (ATR) 1707.42 (C=O), 1673.82 (C=C), 1589.01 (Ar C=C), 1015.71 (C-N), 746.57 (C-Cl) cm^{-1}

LRMS (APCI) calculated for $C_{33}H_{21}Cl_2NO_3$ [M^+-H]: 548.24, found: 548.09

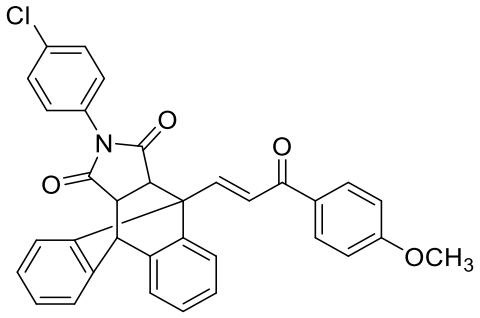

***(E)*-13-(4-Chlorophenyl)-9-(3-(4-methoxyphenyl)-3-oxoprop-1-en-1-yl)-9,10-dihydro-9,10- [3,4] epipyrroloanthracene-12,14-dione (128)**

(E)-13-(4-Chlorophenyl)-9-(3-(4-methoxyphenyl)-3-oxoprop-1-en-1-yl)-9,10-dihydro-9,10-[3,4] epipyrroloanthracene-12,14-dione was synthesised from (*E*)-3-(anthracen-9-yl)-1-(4- methoxyphenyl) prop-2-en-1-one (1.0 mmol, 0.3384 g) and *p*-chloromaleimide (1.3 mmol, 0.27 g) according to the general procedure (4), white powder (63%)

Melting point: 220-225 °C

^{1}H NMR (400 MHz, $CDCl_3$) δ ppm 3.53 (dd, *J*=8.50, 3.11 Hz, 1H) 3.85 (s, 3H) 3.99 (d, *J*=8.29 Hz, 1H) 4.94 (d, *J*=3.32 Hz, 1H) 6.44 - 6.48 (m, 2H) 7.11 (d, *J*=8.71 Hz, 2H) 7.19 - 7.34 (m, 6H) 7.35 - 7.40 (m, 1H) 7.39 - 7.43 (m, 2H) 7.59 (d, *J*=7.05 Hz, 1H), 7.77 - 7.91 (m, 2H) 8.15 (d, *J*=9.12 Hz, 2H)

^{13}C NMR (101 MHz, $CDCl_3$) δ ppm 39.21 - 40.74, 45.39, 48.40, 56.07, 123.39, 123.92, 124.86, 125.68, 126.88, 127.23 - 127.57, 128.72, 129.46, 131.53, 131.94, 140.21, 141.11, 142.86, 175.13, 175.56, 188.11 (chalcone C=O)

IR*Vmax* (ATR) 3344.59 (N-H), 1669.34 (C=O), 1599.27 (Ar C=C), 1230.74 (C-O), 1021.65 (C-N), 766.69 (C-Cl) cm^{-1}

LRMS (APCI) calculated for $C_{34}H_{23}ClNO_4$ [M^+-H]: 544.14, found: 544.24.

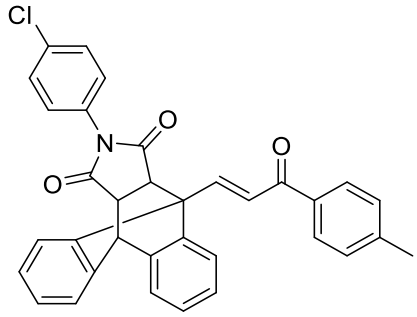

***(E)*-13-(4-Chlorophenyl)-9-(3-oxo-3-(*p*-tolyl)prop-1-en-1-yl)-9,10-dihydro-9,10-[3,4] epipyrroloanthracene-12,14-dione (129)**

(E)-13-(4-Chlorophenyl)-9-(3-oxo-3-(*p*-tolyl)prop-1-en-1-yl)-9,10-dihydro-9,10-[3,4] epipyrroloanthracene-12,14-dione was synthesised from (*E*)-3-(anthracen-9-yl)-1-(*p*-tolyl) prop-2-en-1-one (1.0 mmol, 0.3384 g) and *p*-chloromaleimide (1.3 mmol, 0.27 g) according to the general procedure (4), white powder (60%)

Melting point: 215-220 ℃

^{1}H NMR (400 MHz, $CDCl_3$) δ ppm 2.39 (s, 3H) 3.53 (dd, *J*=8.29, 3.32 Hz, 1H) 3.99 (d, *J*=8.29 Hz, 1H) 4.94 (d, *J*=2.90 Hz, 1H) 6.43 - 6.49 (m, 2H) 7.20 - 7.29 (m, 5H) 7.29 - 7.34 (m, 1H) 7.35 - 7.43 (m, 5H) 7.55 - 7.61 (m, 1H) 7.85 (d, *J*=2.49 Hz, 2H) 8.06 (d, *J*=7.88 Hz, 2H)

^{13}C NMR (101 MHz, $CDCl_3$) δ ppm 21.69, 39.15 - 40.74, 48.40, 52.13, 123.39, 123.92, 124.87, 125.72, 126.88, 127.18 - 127.58, 128.44 - 128.84, 129.05 -129.59, 129.95, 132.00, 135.24, 140.15, 141.53 - 141.91, 142.78, 175.13, 189.36 (chalcone C=O)

IR*ν_{max}* (ATR) 3340.19 (N-H), 2970.43 (O-H), 1709.33 (C=O), 1623.92 (Ar C=C), 1464.76 (C-CH_3), 1224.81 (C-O), 1014.05 (C-N), 728.59 (C-Cl) cm^{-1}

LRMS (APCI) calculated for $C_{34}H_{23}ClNO_3$ [M^+-H]: 528.14 found: 528.33.

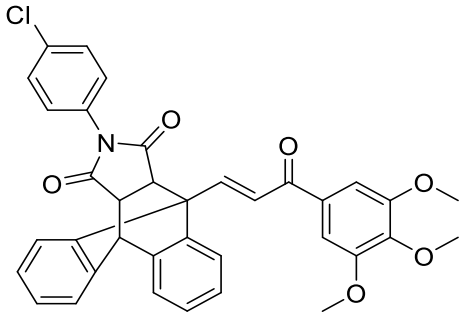

***(E)*-13-(4-Chlorophenyl)-9-(3-oxo-3-(3,4,5-trimethoxyphenyl)-prop-1-en-1-yl)-9,10-dihydro- 9,10- [3,4] epipyrroloanthracene-12,14-dione (130)**

(E)-13-(4-Chlorophenyl)-9-(3-oxo-3-(3,4,5-trimethoxyphenyl)-prop-1-en-1-yl)-9,10-dihydro-9,10-[3,4] epipyrroloanthracene-12,14-dione was synthesised from (*E*)-3-(anthracen-9-yl)-1-(3,4,5-trimethoxyphenyl)prop-2-en-1-one (1.0 mmol, 0.3985 g) and *p*-chloromaleimide (1.3 mmol, 0.27 g) according to the general procedure (4),white powder (35%)

Melting point: 160-163 ℃

^{1}H NMR (400 MHz, $CDCl_3$) δ ppm 3.53 (dd, *J*=8.29, 3.32 Hz, 1H) 3.76 (s, H) 3.85 (s, 6H) 4.00 (d, *J*=8.29 Hz, 1H) 4.94 (d, *J*=3.32 Hz, 1H) 6.45 - 6.49 (m, 2H) 7.20 - 7.31 (m, 5H) 7.31 - 7.43 (m, 4H) 7.47 (s, 2H) 7.57 - 7.61 (m, 1H) 7.78 - 7.91 (m, 2H)

^{13}C NMR (101 MHz, $CDCl_3$) δ ppm 39.23 - 40.69, 45.41, 52.11, 56.54, 60.67, 106.87, 124.90, 125.68, 126.85, 127.24 - 127.60, 128.55, 129.30-129.66, 132.54, 141.50, 142.60, 142.78, 153.42, 175.19, 189.10 (chalcone C=O)

IR*Vmax* (ATR) 2940.25 (O-H), 1707.34 (C=O), 1579.08 (Ar C=C), 1234.05 (C-O), 1090.23 (C-N), 766.71 (C-Cl) cm^{-1}

LRMS (APCI): calculated for $C_{36}H_{29}ClNO_6$ [M^++H]: 606.16, found: 606.21

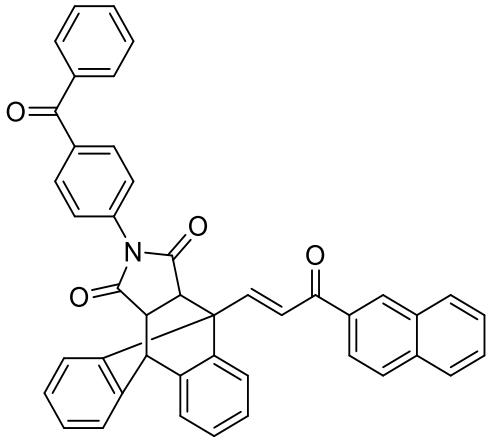

(*E*)-13-(4-Benzoylphenyl)-9-(3-(naphthalen-2-yl)-3-oxoprop-1-en-1-yl)-9,10-dihydro-9,10-[3,4]epipyrroloanthracene-12,14-dione (152)

(*E*)-13-(4-Benzoylphenyl)-9-(3-(naphthalen-2-yl)-3-oxoprop-1-en-1-yl)-9,10-dihydro-9,10-[3,4]epipyrroloanthracene-12,14-dione was synthesised from (*E*)-3-(anthracen-9-yl)-1-(naphthalen-2-yl)prop-2-en-1-one (1.0 mmol, 0.3584 g) and 4-aminobenzophenyl maleimide (1.3 mmol, 0.3610 g) according to the general procedure (4), grey powder (88%)

^{1}H NMR (400 MHz, DMSO-d_6) δ ppm 3.58 (dd, *J*=8.31, 3.42 Hz, 1H), 3.91 (d, *J*=8.80 Hz, 1H), 5.00 (d, *J*=3.42 Hz, 1H), 6.69 (d, *J*=8.31 Hz, 2H), 7.19 - 7.34 (m, 5H), 7.38 (d, *J*=4.89 Hz, 1H), 7.41 - 7.45 (m, H), 7.51 - 7.58 (m, 2 H), 7.60 - 7.67 (m, 1H), 7.67 - 7.77 (m, 5H), 8.11 (d, *J*=16.14 Hz, H), 8.24 (d, *J*=7.83 Hz, 1H), 8.32 (d, *J*=16.63 Hz, 1H), 8.79 (d, *J*=4.40 Hz, 1H)

LRMS (APCI): calculated for $C_{44}H_{30}NO_4$ [M^++H]: 636.21, found: 636.24

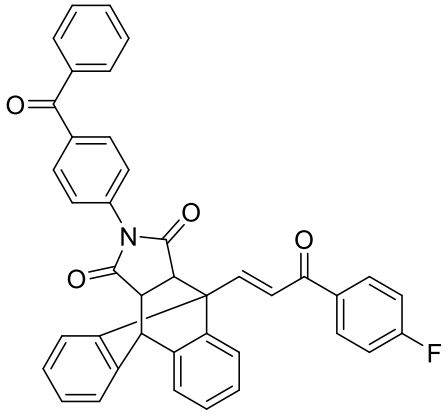

(*E*)-13-(4-Benzoylphenyl)-9-(3-(4-fluorophenyl)-3-oxoprop-1-en-1-yl)-9,10-dihydro-9,10-[3,4]epipyrroloanthracene-12,14-dione (144)

(*E*)-13-(4-Benzoylphenyl)-9-(3-(4-fluorophenyl)-3-oxoprop-1-en-1-yl)-9,10-dihydro-9,10-[3,4]epipyrroloanthracene-12,14-dione was synthesised from (*E*)-3-(anthracen-9-yl)-1-(4-fluorophenyl)prop-2-en-1-one (1.0 mmol, 0.3873 g) and 4-aminobenzophenylmaleimide (1.3 mmol, 0.3264 g) according to the general procedure (4), white powder (77%)

^{1}H NMR (400 MHz, DMSO-d_6) δ ppm 3.51 (dd, *J* = 8.22, 3.17 Hz, 1H), 4.02 (d, *J* = 8.4 Hz, 1H), 4.98 (d, *J* = 3.28 Hz, 1H), 6.49 – 6.54 (m, 2H), 7.15 – 7.32 (m, 5H), 7.35 (m, 1H), 7.36-7.40 (m, 4H), 7.41 – 7.46 (m, 4H), 7.47 – 7.49 (m, 1H), 7.83 (m, 3H), 8.02 (d, *J* = 16.18 Hz, 1H), 8.13 – 8.23 (m, 2H)

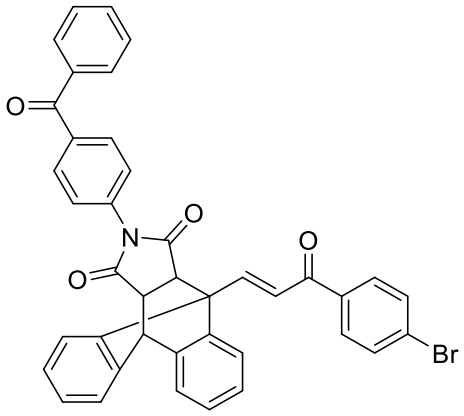

(*E*)-13-(4-Benzoylphenyl)-9-(3-(4-bromophenyl)-3-oxoprop-1-en-1-yl)-9,10-dihydro-9,10-[3,4]epipyrroloanthracene-12,14-dione (137)

(*E*)-13-(4-Benzoylphenyl)-9-(3-(4-bromophenyl)-3-oxoprop-1-en-1-yl)-9,10-dihydro-9,10-[3,4]epipyrroloanthracene-12,14-dione was synthesised from (*E*)-3-(anthracen-9-yl)-1-(4-bromophenyl)prop-2-en-1-one (1.0 mmol, 0.3873 g) and 4-aminobenzophenylmaleimide (1.3 mmol, 0.3610 g) according to the general procedure (4), white powder (71%)

^{1}H NMR (400 MHz, DMSO-*d*$_6$) δ ppm 3.57 (dd, *J*=8.29, 2.90 Hz, 3H), 4.03 (d, *J*=8.71 Hz, 3H), 4.96 (d, *J*=2.90 Hz, 3H), 6.65 (d, *J*=8.29 Hz, 6H), 7.20 - 7.30 (m, 15H), 7.32 - 7.36 (m, 3H), 7.36 - 7.41 (m, 3H), 7.48 - 7.54 (m, 6H), 7.56 - 7.61 (m, 3H), 7.61 - 7.69 (m, 15H), 7.80 (d, *J*=8.71 Hz, 6H), 7.83 - 7.87 (m, 2H), 7.88 - 7.93 (m, 1H), 8.08 (d, *J*=8.71 Hz, 2H)

^{13}C NMR (101 MHz DMSO-*d*$_6$) δ ppm 45.4, 48.4, 48.5, 52.2, 123.4, 124.0, 124.9, 125.7, 126.9, 127.0, 127.4, 127.5, 127.6, 128.0, 129.1, 130.1, 130.6, 131.1, 131.8, 132.5, 133.4, 135.5, 136.7, 137.0, 137.4, 139.2, 140.0, 141.6, 142.7, 142.8, 175.1, 175.5, 189.1, 195.3

LRMS (APCI) calculated for $C_{40}H_{27}BrNO_4$ [M^++H]: 664.1045 found: 664.1618

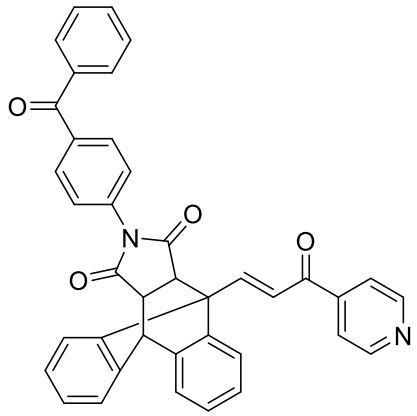

(*E*)-13-(4-Benzoylphenyl)-9-(3-oxo-3-(pyridin-4-yl)prop-1-en-1-yl)-9,10-dihydro-9,10-[3,4]epipyrroloanthracene-12,14-dione (149)

(*E*)-13-(4-Benzoylphenyl)-9-(3-oxo-3-(pyridin-4-yl)prop-1-en-1-yl)-9,10-dihydro-9,10-[3,4]epipyrroloanthracene-12,14-dione was synthesised from (*E*)-3-(anthracen-9-yl)-1-(pyridin-4-yl)prop-2-en-1-one (1.0 mmol, 0.3094 g) and 4-aminobenzophenyl maleimide (1.3 mmol, 0.3610 g) according to the general procedure (4), white powder (62%)

^{1}H NMR (400 MHz, DMSO-*d*6) δ ppm 3.58 (dd, *J*=8.29, 3.32 Hz, 2H), 4.02 (d, *J*=8.29 Hz, 2H), 4.97 (d, *J*=3.32 Hz, 2H), 6.66 (d, *J*=8.71 Hz, 4H), 7.19 - 7.32 (m, 10H), 7.33 - 7.38 (m, 2 H), 7.38 - 7.42 (m, 2 H), 7.49 - 7.56 (m, 4H), 7.59 - 7.64 (m, 3H), 7.64 - 7.69 (m, 9H), 7.78 - 7.85 (m, 2H), 7.81 (d, *J*=16.17 Hz, 1H), 7.91 - 7.97 (m, 2H), 7.94 (d, *J*=16.17 Hz, 3H), 7.99 (d, *J*=5.81 Hz, 4H)

^{13}C NMR (101 MHz, DMSO-*d*6) δ ppm: 45.41, 48.40, 48.67, 52.27, 122.20, 123.48, 123.99, 124.94, 125.73, 126.93, 127.02, 127.48, 127.63, 129.08, 130.08, 130.61, 131.80, 133.38, 135.51, 136.96, 137.40, 139.14, 139.85, 141.57, 142.48, 143.77, 144.35, 151.35, 175.14, 175.51, 190.04 (chalcone C=O), 195.32 (benzophenone C=O)

LRMS (APCI) calculated for $C_{39}H_{27}N_2O_4$ [M^++H]: 587.1895, found: 587.3651

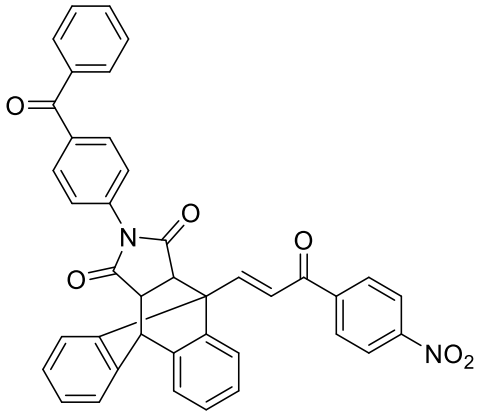

(*E*)-13-(4-Benzoylphenyl)-9-(3-(4-nitrophenyl)-3-oxoprop-1-en-1-yl)-9,10-dihydro-9,10-[3,4]epipyrroloanthracene-12,14-dione (138)

(*E*)-13-(4-Benzoylphenyl)-9-(3-(4-nitrophenyl)-3-oxoprop-1-en-1-yl)-9,10-dihydro-9,10-[3,4]epipyrroloanthracene-12,14-dione was synthesised from (*E*)-3-(anthracen-9-yl)-1-(4-nitrophenyl)prop-2-en-1-one (1.0 mmol, 0.3534 g) and 4-aminobenzophenyl maleimide (1.3 mmol, 0.3610 g) according to the general procedure (4), white powder (75%)

^{1}H NMR (400 MHz, DMSO-*d*$_6$) δ ppm 3.59 (dd, *J*=8.50, 3.11 Hz, 2H), 4.04 (d, *J*=8.71 Hz, 2H), 4.98 (d, *J*=3.32 Hz, 2H), 6.66 (d, *J*=8.29 Hz, 3H), 7.09 - 7.17 (m, 4H), 7.19 - 7.26 (m, 5H), 7.26 - 7.32 (m, 6H), 7.34 - 7.42 (m, 4H), 7.50 - 7.55 (m, 4H), 7.58 - 7.64 (m, 2H), 7.65 - 7.70 (m, 8H), 7.92 (dd, *J*=16.60 Hz, 2H), 8.34 - 8.43 (m, 4H)

^{13}C NMR (101 MHz, DMSO-*d*$_6$) δ ppm 45.45, 48.43 , 48.66, 52.30, 123.51, 124.02, 124.49, 124.94, 125.75, 126.91, 127.01, 127.48, 127.63, 128.6 , 129.07, 129.34, 130.08,

130.50, 130.61, 132.03, 133.36, 135.54, 136.98, 137.40, 137.79 , 139.17, 139.91, 141.60, 142.52, 142.54, 144.14, 150.47, 175.15, 175.51, 189.23 (chalcone C=O), 195.28 (benzophenone C=O)

LRMS (APCI): calculated for $C_{40}H_{27}N_2O_6$ [M^++H]: 631.18, found: 631.19

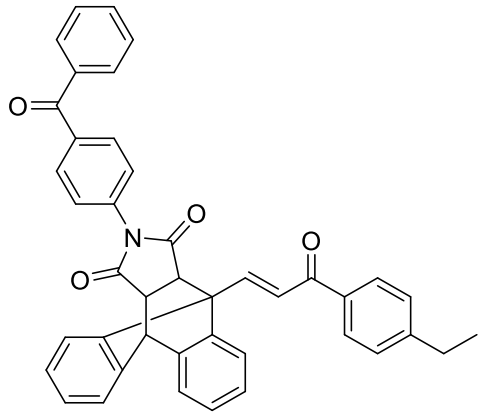

(*E*)-13-(4-Benzoylphenyl)-9-(3-(4-ethylphenyl)-3-oxoprop-1-en-1-yl)-9,10-dihydro-9,10-[3,4]epipyrroloanthracene-12,14-dione (139)

(*E*)-13-(4-Benzoylphenyl)-9-(3-(4-ethylphenyl)-3-oxoprop-1-en-1-yl)-9,10-dihydro-9,10-[3,4]epipyrroloanthracene-12,14-dione was synthesised from (*E*)-3-(anthracen-9-yl)-1-(4-ethylphenyl)prop-2-en-1-one (1.0 mmol, 0.3364 g) and 4-aminobenzophenyl maleimide (1.3 mmol, 0.3610 g) according to the general procedure (4), white powder (76%)

^{1}H NMR (400 MHz, DMSO-*d*$_6$) δ ppm 3.58 (dd, *J*=8.50, 3.11 Hz, 1H), 3.84 (s, 2H), 3.85 (s, 3H), 4.04 (d, *J*=8.71 Hz, 1H), 4.97 (d, *J*=3.32 Hz, 1H), 6.67 (d, *J*=8.29 Hz, 2H), 7.13 (d, *J*=8.29 Hz, H), 7.19 - 7.32 (m, 5), 7.32 - 7.36 (m, 1H), 7.37 - 7.42 (m, 1H), 7.49 - 7.56 (m, 2H), 7.60 (d, *J*=6.63 Hz, 1H), 7.63 - 7.72 (m, 5H), 7.81 (d, *J*=16.17 Hz, 1H), 7.78 - 7.84 (m, 1H), 7.87 (dd, *J*=8.71, 2.07 Hz, 1H), 7.91 (d, *J*=16.17 Hz, 1H)

^{13}C NMR (101 MHz, DMSO-*d*$_6$) δ ppm 45.43,48.47, 48.55, 52.14, 56.01, 56.29, 111.31, 111.51,123.39, 123.93, 124.08, 124.89, 125.71, 126.88, 126.97, 127.37, 127.45, 127.55, 129.08, 130.08, 130.60, 132.11, 133.36, 135.56, 136.97, 137.35, 139.20, 140.21, 141.65, 149.34, 175.10, 175.52, 188.25 (chalcone C=O), 195.30 (benzophenone C=O)

LRMS (APCI) calculated for $C_{42}H_{32}NO_4$ [M^++H]: 614.23, found: 614.14

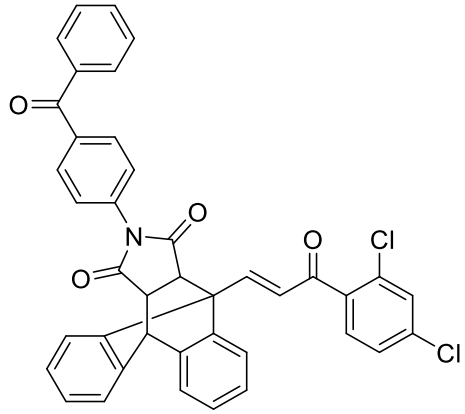

(*E*)-13-(4-Benzoylphenyl)-9-(3-(2,4-dichlorophenyl)-3-oxoprop-1-en-1-yl)-9,10-dihydro-9,10-[3,4]epipyrroloanthracene-12,14-dione (140)

(*E*)-13-(4-Benzoylphenyl)-9-(3-(2,4-dichlorophenyl)-3-oxoprop-1-en-1-yl)-9,10-dihydro-9,10-[3,4]epipyrroloanthracene-12,14-dione was synthesised from (*E*)-3-(anthracen-9-yl)-1-(2,4-dichlorophenyl)prop-2-en-1-one (1.0 mmol, 0.3773 g) and 4-aminobenzophenone maleimide (1.3 mmol, 0.3610 g) according to the general procedure (4), white powder (63%)

^{1}H NMR (400 MHz, DMSO-*d*$_6$) δ ppm 3.58 (dd, *J*=8.29, 3.32 Hz, 1H), 4.04 (d, *J*=8.29 Hz, 1H), 4.97 (d, *J*=2.90 Hz, 1H), 6.67 (d, *J*=8.29 Hz, 2H), 7.09 - 7.16 (m, 1H), 7.19 - 7.32 (m, 5H), 7.32 - 7.36 (m, 1H), 7.37 - 7.43 (m, 1H), 7.50 - 7.56 (m, 2H), 7.60 (d, *J*=6.22 Hz, 1H), 7.63 - 7.71 (m, 6H), 7.81 (d, *J*=16.17 Hz, 1H), 7.86 (d, *J*=1.66 Hz, 1H), 7.91 (d, *J*=16.17 Hz, 1H)

^{13}C NMR (101 MHz, DMSO-*d6*) δ ppm 48.5, 52.1, 56.0, 56.3, 111.3, 111.5, 123.9, 124.1, 124.9, 126.9, 127.0, 127.5, 129.1, 130.1, 130.6, 132.1, 133.4, 135.6, 137.0, 137.4, 139.2, 140.2, 140.9, 141.7, 142.9, 144.5, 145.7, 149.3, 153.9, 175.1, 175.5, 188.2 (chalcone C=O), 195.3 (benzophenone C=O)

LRMS (APCI): calculated for $C_{37}H_{22}Cl_2NO_4$ [M^+-(C_3H_3)]: 614.12, found: 614.15

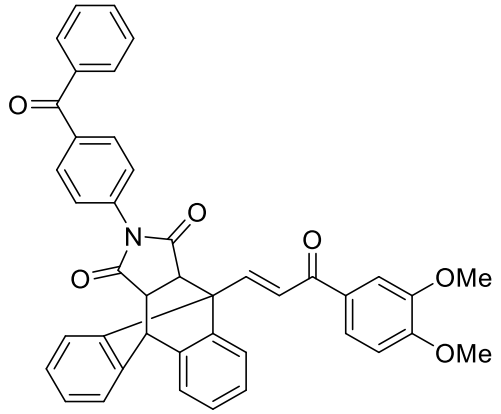

(*E*)-13-(4-Benzoylphenyl)-9-(3-(3,4-dimethoxyphenyl)-3-oxoprop-1-en-1-yl)-9,10-dihydro-9,10-[3,4]epipyrroloanthracene-12,14-dione (141)

(*E*)-13-(4-Benzoylphenyl)-9-(3-(3,4-dimethoxyphenyl)-3-oxoprop-1-en-1-yl)-9,10-dihydro-9,10-[3,4]epipyrroloanthracene-12,14-dione was synthesised from (*E*)-3-(anthracen-9-yl)-1-(3,4-dimethoxyphenyl)prop-2-en-1-one (1.0 mmol, 0.3684 g) and 4-aminobenzophenyl maleimide (1.3 mmol, 0.3610 g) according to the general procedure (4), white powder (72%)

^{1}H NMR (400 MHz, DMSO-*d*$_6$) δ ppm 1.20 (t, *J*=7.46 Hz, 2H), 2.28 (s, 2H), 3.58 (dd, *J*=8.50, 3.11 Hz, 1H), 4.03 (d, *J*=8.29 Hz, 1H), 4.97 (d, *J*=3.32 Hz, 1H), 6.67 (d, *J*=8.29 Hz, 1H), 7.09 - 7.18 (m, 2H), 7.19 - 7.25 (m, 3H), 7.26 - 7.32 (m, 2H), 7.32 - 7.36 (m, H), 7.38 - 7.45 (m, 2H), 7.50 - 7.55 (m, 2H), 7.58 - 7.63 (m, 1H), 7.63 - 7.71 (m, 4H), 7.82 - 7.93 (m, 2H), 7.87 (dd, *J*=16.20 Hz, 2H), 8.10 (d, *J*=7.88 Hz, 1H)

^{13}C NMR (101 MHz, DMSO-*d*$_6$) δ ppm 21.49, 28.70, 45.4, 48.47, 48.52, 52.18, 123.41, 123.93, 124.89, 126.90, 127.02, 127.38, 127.48, 127.57, 128.64, 128.80, 129.07, 129.34, 129.39, 130.08, 130.60, 132.09, 133.36, 135.50, 135.56, 136.97, 137.38, 137.78, 139.18, 140.14, 141.63, 141.76, 142.80, 150.41, 175.09, 175.51, 189.38 (chalcone C=O), 195.29 (benzophenone C=O)

LRMS (APCI) calculated for $C_{41}H_{19}NO_6$ [M^+-(OCH_3)]: 614.22, found: 614.19

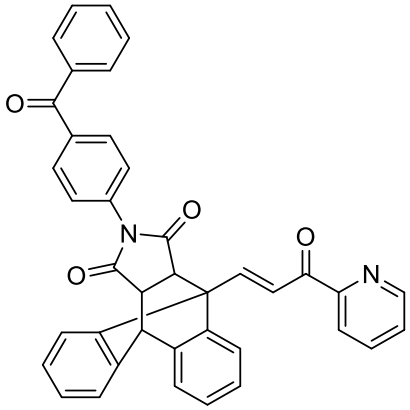

(*E*)-13-(4-Benzoylphenyl)-9-(3-oxo-3-(pyridin-2-yl)prop-1-en-1-yl)-9,10-dihydro-9,10-[3,4]epipyrroloanthracene-12,14-dione (150)

(*E*)-13-(4-Benzoylphenyl)-9-(3-oxo-3-(pyridin-2-yl)prop-1-en-1-yl)-9,10-dihydro-9,10-[3,4]epipyrroloanthracene-12,14-dione was synthesised from (*E*)-3-(anthracen-9-yl)-1-(pyridin-2-yl)prop-2-en-1-one (1.0 mmol, 0.3094 g) and 4-aminobenzophenyl maleimide (1.3 mmol, 0.3610 g) according to the general procedure (4), grey powder (75%)

^{1}H NMR (400 MHz, DMSO-*d*$_6$) δ ppm 3.54 (dd, *J*=4.98, 3.32 Hz, 1H), 3.86 - 3.91 (m, 1H), 4.96 (d, *J*=3.32 Hz, 1H), 6.66 (d, *J*=8.71 Hz, 2H), 7.19 - 7.31 (m, 6H), 7.32 - 7.38 (m, 1H), 7.38 - 7.42 (m, 1H), 7.52 (s, 2H), 7.58 - 7.64 (m, 2H), 7.64 - 7.73 (m, H), 8.08 (d, *J*=16.59 Hz, 1H), 8.09 - 8.12 (m, H), 8.20 - 8.23 (m, 1H), 8.27 (d, *J*=16.59 Hz, 1H)

^{13}C NMR (101 MHz, DMSO-*d*$_6$) δ ppm 45.44, 48.50, 49.04, 52.29, 123.30, 123.42, 123.89, 124.96, 125.75, 126.89, 126.95, 127.44, 128.31, 128.64, 129.07, 129.33, 130.06, 130.32, 130.56, 133.36, 135.53, 136.97, 137.33, 137.79, 138.34, 139.23, 140.06, 141.67, 142.62, 143.08, 149.7, 153.68, 174.9, 175.54, 188.8 (chalcone C=O), 195.32 (benzophenone C=O)

LRMS (APCI) calculated for $C_{39}H_{27}N_2O_4$ [M^++H]: 587.1893, found: 587.4890

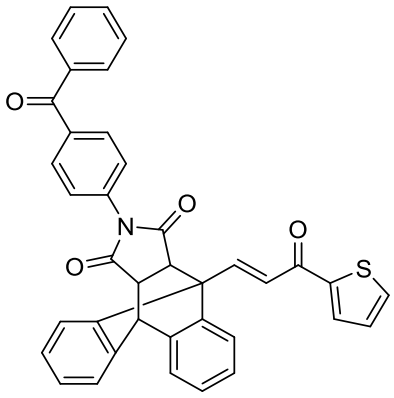

(*E*)-13-(4-Benzoylphenyl)-9-(3-oxo-3-(thiophen-2-yl)prop-1-en-1-yl)-9,10-dihydro-9,10-[3,4]epipyrroloanthracene-12,14-dione (153)

(*E*)-13-(4-Benzoylphenyl)-9-(3-oxo-3-(thiophen-2-yl)prop-1-en-1-yl)-9,10-dihydro-9,10-[3,4]epipyrroloanthracene-12,14-dione was synthesised from (*E*)-3-(anthracen-9-yl)-1-(thiophen-2-yl)prop-2-en-1-one (1.0 mmol, 0.3144 g) and 4-aminobenzophenyl maleimide (1.3 mmol, 0.3610 g) according to the general procedure (4), white solid (51%).

^{1}H NMR (400 MHz, DMSO-*d*$_6$) δ ppm 3.59 (dd, *J*=5.39, 3.73 Hz, 1H), 4.02 (d, *J*=8.71 Hz, 1H), 4.97 (d, *J*=3.32 Hz, 1H), 6.66 (d, *J*=8.29 Hz, 2H), 7.19 - 7.32 (m, 6H), 7.34 (s, 1H), 7.38 - 7.42 (m, 1H), 7.54 (d, *J*=7.46 Hz, 2H), 7.60 (s, 1H), 7.65 - 7.71 (m, 5H), 7.85 (d, *J*=15.76 Hz, 1H), 7.89 (d, *J*=16.59 Hz, 1H), 8.12 (dd, *J*=4.98, 0.83 Hz, 1H), 8.21 (dd, *J*=3.73, 0.83 Hz, 1H)

^{13}C NMR (101 MHz, DMSO-*d*$_6$) δ ppm 45.4, 48.4, 48.8, 52.1, 123.4, 124.0, 124.9, 125.7, 127.0, 127.4, 127.5, 127.6, 128.6, 129.1, 129.3, 129.5, 130.1, 130.6, 131.7, 133.3, 134.6, 135.5, 136.5, 137.0, 137.4, 139.2, 140.0, 141.5, 141.6, 142.7, 145.2, 175.1, 175.5, 182.0, 195.3

LRMS (APCI) calculated for $C_{38}H_{24}NO_4S$ [M^+-H]: 590.1504, found: 590.5366

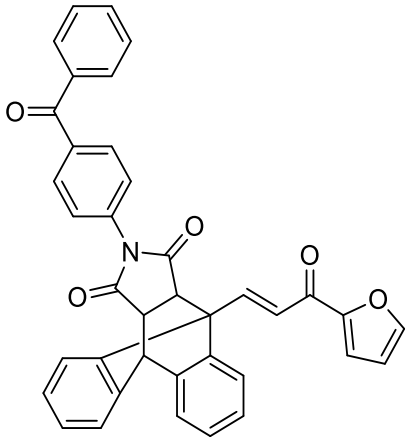

(*E*)-13-(4-Benzoylphenyl)-9-(3-(furan-2-yl)-3-oxoprop-1-en-1-yl)-9,10-dihydro-9,10-[3,4]epipyrroloanthracene-12,14-dione (151)

(*E*)-13-(4-Benzoylphenyl)-9-(3-(furan-2-yl)-3-oxoprop-1-en-1-yl)-9,10-dihydro-9,10-[3,4]epipyrroloanthracene-12,14-dione was synthesised from (*E*)-3-(anthracen-9-yl)-1-(furan-2-yl)prop-2-en-1-one (1.0 mmol, 0.2983 g) and 4-aminobenzophenyl maleimide (1.3 mmol, 0.3610 g) according to the general procedure (4), white powder (60%)

^{1}H NMR (400 MHz, DMSO-*d*$_6$) δ ppm 3.60 (dd, *J*=8.56, 3.18 Hz, 1H), 3.98 (d, *J*=8.31 Hz, 1H), 4.99 (d, *J*=3.42 Hz, 3H), 6.68 (d, *J*=8.31 Hz, 2H), 7.21 - 7.28 (m, 2H), 7.28 - 7.33 (m, 2 H), 7.33 - 7.38 (m, 1H), 7.39 - 7.44 (m, 1H), 7.52 - 7.60 (m, 2H), 7.60 - 7.64 (m, 1H), 7.65 - 7.74 (m, 6H), 7.75 - 7.80 (m, 1H), 7.95 (d, *J*=16.63 Hz, 1H), 8.14 (d, *J*=1.47 Hz, 1H)

LRMS (APCI) calculated for $C_{38}H_{26}NO_5$ [M^++H]: 576.1733, found: 576.1141

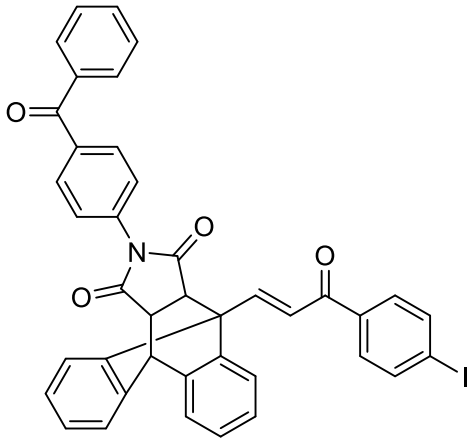

(*E*)-13-(4-Benzoylphenyl)-9-(3-(4-iodophenyl)-3-oxoprop-1-en-1-yl)-9,10-dihydro-9,10-[3,4]epipyrroloanthracene-12,14-dione (143)

(*E*)-13-(4-Benzoylphenyl)-9-(3-(4-iodophenyl)-3-oxoprop-1-en-1-yl)-9,10-dihydro-9,10-[3,4]epipyrroloanthracene-12,14-dione was synthesised from (*E*)-3-(anthracen-9-

yl)-1-(4-methoxyphenyl)prop-2-en-1-one (1.0 mmol, 0.3384 g) and 4-aminobenzophenyl maleimide (1.3 mmol, 0.3610 g) according to the general procedure (4), white powder (85%)

^{1}H NMR (400 MHz, DMSO-*d*$_6$) δ ppm 3.59 (dd, *J*=8.29, 2.90 Hz, 1H), 4.04 (d, *J*=8.71 Hz, 1H), 4.98 (d, *J*=3.32 Hz, 1H), 6.67 (d, *J*=8.29 Hz, 2H), 7.10 - 7.17 (m, 2H), 7.19 - 7.32 (m, 6H), 7.33 - 7.37 (m, 1H), 7.38 - 7.43 (m, 1H), 7.50 - 7.56 (m, 2H), 7.61 (d, *J*=7.05 Hz, 1H), 7.63 - 7.71 (m, 5H), 7.86 (d, *J*=16.59 Hz, 1H), 7.89 - 7.95 (m, 3H), 7.96 - 8.03 (m, 2H)

^{13}C NMR (101 MHz, DMSO-*d*$_6$) δ ppm 45.45, 48.4 , 48.55, 52.23, 102.63 , 123.45, 123.97, 124.90, 125.72, 125.7, 126.91, 127.03, 127.40, 127.48, 127.59, 128.64, 129.07, 129.34, 130.09, 130.61, 130.82, 131.76, 133.35, 135.56, 136.98, 137.04, 137.39, 137.79, 138.36, 139.17, 140.04, 141.61, 142.69, 142.77, 175.11, 175.50, 189.44, 195.28

LRMS (APCI) calculated for $C_{40}H_{25}INO_4$ [M^+-H]: 710.0907, found: 710.1320

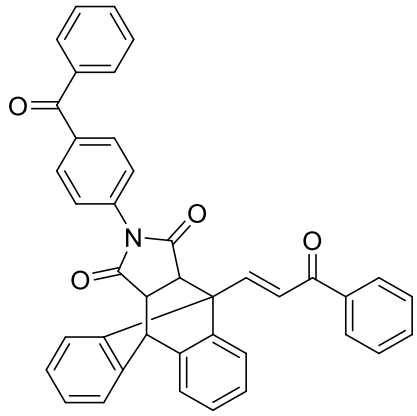

(*E*)-13-(4-Benzoylphenyl)-9-(3-oxo-3-phenylprop-1-en-1-yl)-9,10-dihydro-9,10-[3,4] epipyrroloanthracene-12,14-dione (142)

(*E*)-13-(4-Benzoylphenyl)-9-(3-oxo-3-phenylprop-1-en-1-yl)-9,10-dihydro-9,10-[3,4] epipyrroloanthracene-12,14-dione was synthesised from (*E*)-3-(anthracen-9-yl)-1-phenylprop-2-en-1-one (1.0 mmol, 0.3084 g) and 4-aminobenzophenyl maleimide (1.3 mmol, 0.3610 g) according to the general procedure (4), white powder (49%)

Melting point: 226-228 ℃

^{1}H NMR (400 MHz, DMSO-*d*6) δ ppm 3.58 (dd, *J*=8.50, 3.11 Hz, 1H) 4.04 (d, *J*=8.29 Hz, 1H) 4.97 (d, *J*=2.90 Hz, 1H) 6.67 (d, *J*=8.29 Hz, 2H) 7.19 - 7.32 (m, 6H) 7.34 (s, 1H) 7.37 - 7.42 (m, 1H) 7.49 - 7.56 (m, 2H) 7.57 - 7.64 (m, 4H) 7.64 - 7.72 (m, 6H) 7.89 (s, 2H) 8.16 (d, *J*=7.05 Hz, 2H)

^{13}C NMR (101 MHz, DMSO-*d*6) δ ppm 39.21 - 40.63, 48.48, 52.20, 55.34, 125.75, 127.03, 127.48, 128.94 - 129.60, 130.08, 130.61, 131.99, 136.97, 137.39, 139.17, 142.75, 174.93 - 175.59, 176.01, 189.96 (chalcone C=O), 195.31 (benzophenone C=O)

IR*Vmax* (ATR) 1708.57 (C=O), 1670.41 (C=C), 1603.92 (Ar C=C), 1308.22 (C-N) cm^{-1}

HRMS (APCI) calculated for $C_{40}H_{27}NNaO_4$ [M^++Na]: 608.183229, found : 608.182989. Mass accuracy (-0.4 ppm)

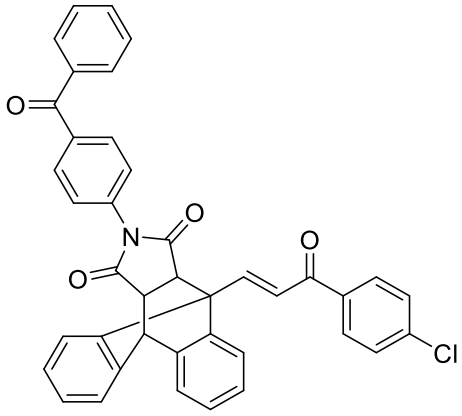

***(E)*-13-(4-Benzoylphenyl)-9-(3-(4-cholrophenyl)-3-oxoprop-1-en-1-yl)-9,10-dihydro-9,10- [3,4] epipyrroloanthracene-12,14-dione (148)**

(E)-13-(4-Benzoylphenyl)-9-(3-(4-cholrophenyl)-3-oxoprop-1-en-1-yl)-9,10-dihydro-9,10- [3,4]epipyrroloanthracene-12,14-dione was synthesised from (*E*)-3-(anthracen-9-yl)-1-(4-chorophenyl)prop-2-en-1-one (1.0 mmol, 0.3430 g) and 4-aminobenzophenyl maleimide (1.3 mmol, 0.3610 g) according to the general procedure (4), white powder (30%)

Melting point: 217-220 ℃

^{1}H NMR (400 MHz, $CDCl_3$) δ ppm 3.59 (d, *J*=3.32 Hz, 1H) 4.04 (d, *J*=8.71 Hz, 1H) 4.97 (d, *J*=3.32 Hz, 1H) 6.66 (d, *J*=8.71 Hz, 2H) 7.20 - 7.31 (m, 6H) 7.34 (s, 1H) 7.39 (s, 1H) 7.50 - 7.56 (m, 2H) 7.60 (d, *J*=6.63 Hz, 1H) 7.65 - 7.70 (m, 6H) 7.89 (s, 2H) 8.14 - 8.20 (m, 2H)

^{13}C NMR (101 MHz, $CDCl_3$) δ ppm 39.23 - 40.72, 42.31, 45.42, 48.48, 52.20, 123.44, 123.95, 124.90, 125.64, 125.78, 126.85, 127.14, 127.35, 127.66, 128.64, 129.08, 129.55, 130.08, 130.61, 131.03, 131.81, 136.41, 138.85, 139.16, 142.68, 142.81, 175.12, 175.51, 195.31 (chalcone C=O), 197.42 (benzophenone C=O)

IR*Vmax* (ATR) 3024.65 (Ar C-H), 1712.90 (C=O), 1672.35 (C=C), 1603.46 (Ar C=C), 1013.52 (C-N), 769.64 (C-Cl) cm^{-1}

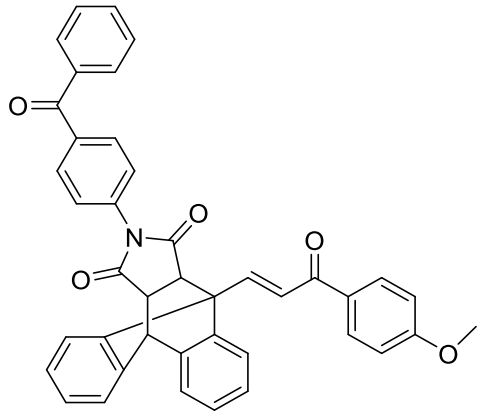

***(E)*-13-(4-Benzoylphenyl)-9-(3-(4-methoxyphenyl)-3-oxoprop-1-en-1-yl)-9,10-dihydro-9,10- [3,4] epipyrroloanthracene-12,14-dione (145)**

(E)-13-(4-Benzoylphenyl)-9-(3-(4-methoxyphenyl)-3-oxoprop-1-en-1-yl)-9,10-dihydro-9,10- [3,4] epipyrroloanthracene-12,14-dione was synthesised from (*E*)-3-(anthracen-9-yl)-1-(4-methoxyphenyl)prop-2-en-1-one (1.0 mmol, 0.3384 g) and 4-aminobenzophenone maleimide (1.3 mmol, 0.3610 g) according to the general procedure (4), white powder (50%)

Melting point: 224-228 ℃

^{1}H NMR (400 MHz, $CDCl_3$) δ ppm 3.58 (dd, *J*=8.29, 3.32 Hz, 1H) 3.86 (s, 3H) 4.04 (d, *J*=8.29 Hz, 1H) 4.97 (d, *J*=3.32 Hz, H) 6.66 (d, *J*=8.29 Hz, 2 H) 7.12 (d, *J*=8.71 Hz, 2H) 7.20 - 7.31 (m, 5H) 7.31 - 7.35 (m, 1H) 7.38 - 7.41 (m, 1H) 7.51 - 7.56 (m, 2H) 7.60 (d, *J*=6.63 Hz, 1H) 7.64 - 7.71 (m, 5H) 7.79 - 7.93 (m, 2H) 8.16 (d, *J*=8.71 Hz, 2H)

^{13}C NMR (101 MHz, $CDCl_3$) δ ppm 39.26, 40.72, 48.48, 52.15, 56.07, 114.67, 123.42, 123.93, 124.87, 125.71, 126.76, 127.69, 130.08, 131.53, 133.36, 136.97, 139.18, 141.10, 141.64, 142.88, 163.89, 175.09, 175.52, 188.12 (chalcone C=O), 195.29 (benzophenone C=O)

IR*Vmax* (ATR) 3344.36 (N-H), 1659.32 (C=O), 1599.79 (Ar C=C), 1231.15 (C-O), 1020.42 (C-N) cm^{-1}

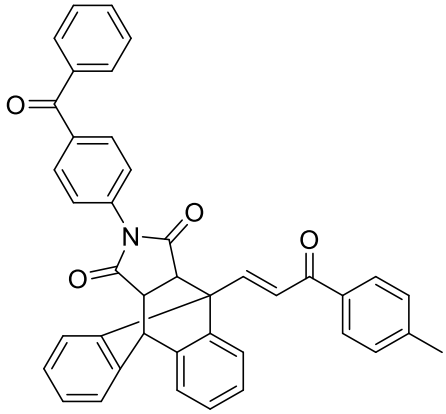

***(E)*-13-(4-Benzoylphenyl)-9-(3-oxo-3-(*p*-tolyl)prop-1-en-1-yl)-9,10-dihydro-9,10-[3,4] epipyrroloanthracene-12,14-dione (146)**

(E)-13-(4-Benzoylphenyl)-9-(3-oxo-3-(*p*-tolyl)prop-1-en-1-yl)-9,10-dihydro-9,10-[3,4] epipyrroloanthracene-12,14-dione was synthesised from (*E*)-3-(anthracen-9-yl)-1-(*p*-tolyl)prop-2-en-1-one (1.0 mmol, 0.3384 g) and 4-aminobenzophenone maleimide (1.3 mmol, 0.3610 g) according to the general procedure (4), white powder (59%)

Melting point: 256-260 ℃

^{1}H NMR (400 MHz, $CDCl_3$) δ ppm 2.40 (s, 3H) 3.57 (dd, *J*=8.29, 2.90 Hz, 1H) 4.03 (d, *J*=8.29 Hz, 1H) 4.96 (d, *J*=2.90 Hz, 1H) 6.66 (d, *J*=8.29 Hz, 2H) 7.20 - 7.31 (m, 5H) 7.31 - 7.36 (m, 1H) 7.40 (d, *J*=7.88 Hz, 3H) 7.50 - 7.56 (m, 2H) 7.56 - 7.71 (m, 6H) 7.86 (d, *J*=3.32 Hz, 2H) 8.06 (d, *J*=7.88 Hz, 2H)

^{13}C NMR (101 MHz, $CDCl_3$) δ ppm 21.69, 39.21 - 40.78, 48.49, 55.35, 123.41, 127.03, 128.83 - 129.51, 130.02, 136.97, 137.38, 139.18, 142.80, 144.38, 175.51 (chalcone C=O), 189.37 (benzophenone C=O)

IR*Vmax* (ATR) 2965 (O-H), 1712.89 (C=O), 1626.70 (Ar C=C), 1458.41 (C-CH_3), 1231.54 (C-O), 1128.77 (C-N) cm^{-1}

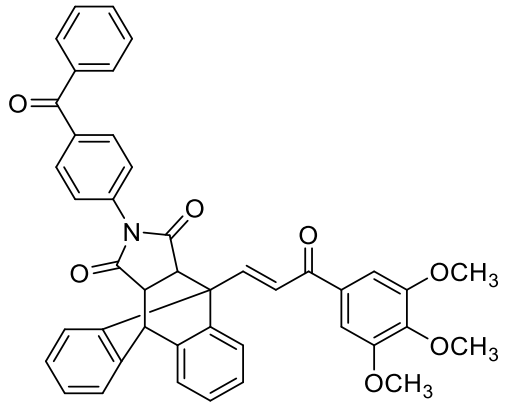

***(E)*-13-(4-Benzoylphenyl)-9-(3-oxo-3-(3,4,5-trimethoxyphenyl)-prop-1-en-1-yl)-9,10- dihydro-9,10- [3,4] epipyrroloanthracene-12,14-dione (147)**

(E)-13-(4-Benzoylphenyl)-9-(3-oxo-3-(3,4,5-trimethoxyphenyl)-prop-1-en-1-yl)-9,10-dihydro-9,10-[3,4]epipyrroloanthracene-12,14-dione was synthesised from (*E*)-3-(anthracen-9-yl)-1-(3,4,5-trimethoxyphenyl)prop-2-en-1-one (1 mmol, 0.3985 g) and 4-aminobenzo phenone maleimide (1.3 mmol, 0.3610 g) according to the general procedure (4), white powder (44%)

Melting point: 210-216˚C

^{1}H NMR (400 MHz, $CDCl_3$) δ ppm 3.58 (dd, *J*=8.50, 3.11 Hz, 1H) 3.76 (s, 3H) 3.85 (s, 6 H) 4.04 (d, *J*=8.71 Hz, 1H) 4.97 (d, *J*=3.32 Hz, 1H) 6.65 - 6.70 (m, 2H) 7.21 - 7.31 (m, 5H) 7.35 - 7.38 (m, 1H) 7.38 - 7.42 (m, 1H) 7.48 (s, 2H) 7.51 - 7.56 (m, 2H) 7.59 - 7.62 (m, 1H) 7.63 - 7.70 (m, 5H) 7.80 - 7.93 (m, 2H)

^{13}C NMR (101 MHz, $CDCl_3$) δ ppm 39.24, 40.78, 48.40, 52.16, 56.56, 60.68, 106.89, 125.53, 125.91, 126.85, 127.40, 128.64, 129.07, 129.33, 130.07, 130.56, 132.54, 133.05, 133.34, 137.00, 140.12, 141.56, 153.43, 175.03 , 175.61, 189.07 (chalcone C=O), 195.29 (benzophenone C=O)

IR*Vmax* (ATR) 2941.10 (O-H), 1708.03 (C=O), 1579.54 (Ar C=C), 1234.15 (C-O), 1091.54 (C-N) cm^{-1}

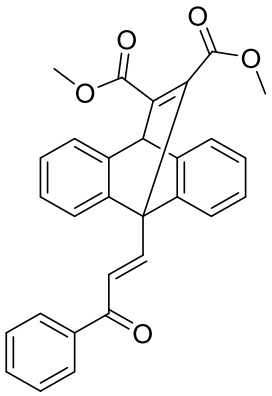

Dimethyl(*E*)-9-(3-oxo-3-phenylprop-1-en-1-yl)-9,10-dihydro-9,10-ethenoanthracene-11,12-dicarboxylate (154)

Dimethyl (*E*)-9-(3-oxo-3-phenylprop-1-en-1-yl)-9,10-dihydro-9,10-ethenoanthracene-11,12-dicarboxylate was synthesised from (*E*)-3-(anthracen-9-yl)-1-phenylprop-2-en-1-one (1 mmol, 0.3084 g) and dimethyl acetylenedicarboxylate (1.3 mmol, 0.16 mL) according to the general procedure (4), orange/yellow crystalline solid (62%)

^{1}H NMR (400 MHz, DMSO-*d*$_6$) δ ppm 3.64 (s, 3H), 3.72 (s, 3H), 5.80 (s, 1H), 7.07 - 7.15 (m, 4H), 7.45 - 7.50 (m, 2H), 7.52 - 7.58 (m, 3H), 7.61 (t, *J*=7.72 Hz, 2H), 7.73 (d, *J*=16.12 Hz, 2H), 8.08 (d, *J*=7.77 Hz, 2H)

^{13}C NMR (101 MHz, DMSO-*d*$_6$) δ ppm 49.98, 52.95, 53.2, 57.83, 122.94, 124.84, 125.77, 126.31, 129.13, 129.56, 133.42, 134.17, 137.31, 137.80, 142.62, 143.97, 145.09, 154.91, 163.57, 167.01, 189.21

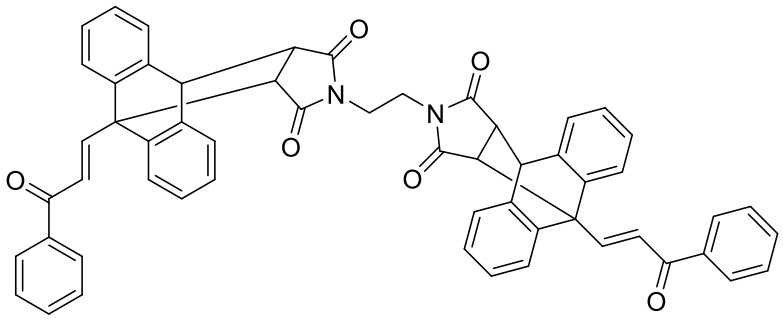

13,13'-(Ethane-1,2-diyl)bis(9-((*E*)-3-oxo-3-phenylprop-1-en-1-yl)-9,10-dihydro-9,10-[3,4]epipyrroloanthracene-12,14-dione) (155)

13,13'-(Ethane-1,2-diyl)bis(9-((*E*)-3-oxo-3-phenylprop-1-en-1-yl)-9,10-dihydro-9,10-[3,4]epipyrroloanthracene-12,14-dione) was synthesised from (*E*)-3-(anthracen-9-yl)-1-

phenylprop-2-en-1-one (1.0 mmol, 0.3084 g) and 1,1'-(ethane-1,2-diyl)bis(1H-pyrrole-2,5-dione) (2.0 mmol, 0.44 g) in toluene (2 mL). The mixture was heated, with stirring at 90 °C for 48 h. The reaction was then cooled to RT and the resulting solid was isolated by filtration. The solid product was washed with toluene (2 mL) and diethyl ether (2 mL) on isolation with no further purificaiton needed, white powder (76%)

^{1}H NMR (600 MHz, $CDCl_3$) δ ppm 3.22 - 3.27 (m, 2H), 3.43 (d, *J*=8.80 Hz, 2H), 4.72 (dd, *J*=6.79, 3.12 Hz, 2H), 7.09 - 7.22 (m, 9H), 7.24 - 7.30 (m, 9H), 7.39 (q, *J*=8.07 Hz, 4H), 7.36 - 7.43 (m, 1H), 7.46 (t, *J*=7.52 Hz, 2H), 7.51 - 7.59 (m, 2H), 7.75 (dd, *J*=16.14, 9.17 Hz, 2H), 7.92 (d, *J*=16.14 Hz, 2H), 8.12 (dd, *J*=12.10, 7.34 Hz, 4H)

^{13}C NMR (151 MHz, $CDCl_3$) δ ppm 45.55, 48.36, 48.39, 52.08, 123.37, 123.40, 123.90, 124.03, 124.07, 125.27, 126.73, 126.76, 127.14, 127.16, 127.26, 127.29, 128.68, 128.74, 128.87, 128.91, 131.39, 131.41, 133.20, 137.77, 137.79, 137.95, 137.96, 139.30, 140.81, 140.85, 142.20, 142.30, 174.95, 175.16, 175.9 , 176.02, 190.02, 190.11

HRMS (MALDI) calculated to be $C_{56}H_{40}N_2O_6Na$ [M^++Na]: 859.2784, found: 859.2796

5.5 General Procedure (5) for synthesis of phenyl and benzyl maleimides

To a solution of maleic anhydride (20 mmol) dissolved in diethyl ether (25 mL) was added the appropriately substituted amine (20 mmol) dissolved in diethyl ether (10 mL).The reaction was stirred under a reflux condenser at RT for 1 hour.The precipitated solid was isolated by filtration and washed with diethyl ether.This solid was immediately used in the next step and placed in a conical flask containing 0.7 g of sodium acetate and 10 mL acetic anhydride.This mixture was heated to 90 °C for 0.5 hours, after which the mixture was poured over ice water 100 mL.The precipitated solid was isolated by filtration and recrystallized from ethanol.

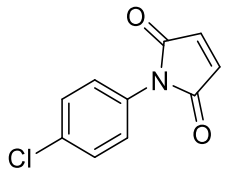

1-(4-chlorophenyl)-1*H*-pyrrole-2, 5-dione (22)

1-(4-chlorophenyl)-1*H*-pyrrole-2,5-dione was prepared from maleic anhydride and *p*-chloroaniline according to general procedure (5). The precipitated solid was isolated by filtration and recrystallized from ethanol, light green solid (55 %)

Melting Point: 118-124 ℃

^{1}H NMR (400 MHz, $CDCl_3$) δ ppm 6.81 (s, 2 H, HC=CH) 7.30 (d, *J*=8.54 Hz, 2H, ArH) 7.43 (d, *J*=8.54 Hz, 2H, ArH)

^{13}C NMR (101 MHz, $CDCl_3$) δ ppm 127.03 (CH), 129.23 (CH), 129.70, 133.51, 134.20 (HC=CH), 169.06 (O=C)

IR*Vmax* (KBr): 3165.48, 3116.48, 3084.49(Ar C-H), 1583.14 (C=C), 1497.64, 1452.35, 1402.46, 1420.91, 1386.98 (Ar C=C), 1712.44(C=O) cm^{-1}

HRMS (APCI) calculated for $C_{10}H_7ClNO_2$ [M^++H] 208.0165: found 208.0165. Mass accuracy (0 ppm).

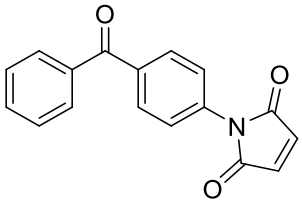

1-(4-Benzoylphenyl)-1*H*-pyrrole-2,5-dione (23)

1-(4-Benzoylphenyl)-1*H*-pyrrole-2,5-dione was prepared from maleic anhydride and (4-aminophenyl)(phenyl)methanone according to general procedure (5), white crystaline solid (29%)

Melting Point: 156-160 ℃ (lit.M.p.162-164 ℃)[297]

^{1}H NMR (400 MHz, DMSO-*d*6) δ ppm7.21 (s, 2H, C=CH), 7.53 - 7.58 (m, 4H, ArH), 7.69 (d, *J* = 7.33 Hz, 1H, ArH), 7.75 (d, *J* = 7.32 Hz, 2H, ArH), 7.94 (d, *J* = 8.55 Hz, 2 H, ArH)

^{13}C NMR (101 MHz, DMSO-*d*6) δ ppm 126.1, 128.6, 129.7, 129.7, 130.3, 132.8, 134.9, 135.3, 135.7, 136.8, 169.6 195.0 (C=O)

IR*Vmax* (KBr): 3093, 2988 (C-H), 1711 (C=O), 1592, 1510 (C=C) cm^{-1}

HRMS (APCI) calculated for $C_{17}H_{12}NO_3$ [M^++H]: 278.0817 found: 278.0817. Mass accuracy (0 ppm).

5.6 General Procedure (6) for synthesis of pyrazolines

To a solution of the appropriate chalcone anthracene analog (1 mmol) in ethanol (10 mL), 3 drops of conc HCl were added, followed by hydrazine hydrate (3 mL). The resultant mixture was refluxed for 6 h. The mixture was then cooled in a cold water bath before

product isolation, washing subsequently with distilled water (3 x 10 mL) and ethanol (5mL). The product required no further purification.

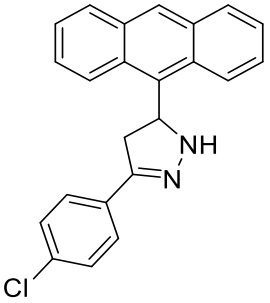

5-(anthracen-9-yl)-3-(4-chlorophenyl)-4,5-dihydro-1*H*-pyrazole

5-(anthracen-9-yl)-3-(4-chlorophenyl)-4,5-dihydro-1*H*-pyrazole was synthesised from (*E*)-3-(anthracen-9-yl)-1-(4-chlorophenyl)prop-2-en-1-one (1 mmol, 0.3482 g) and hydrazine hydrate (3 mL) according to general method (6), brown solid (30%)

^{1}H NMR (400 MHz, $CDCl_3$) δ ppm 3.61 (dd, *J*=13.06, 5.60 Hz, 4H), 3.72 (dd, *J*=7.00 Hz, 2H), 6.50 (t, *J*=12.85 Hz, 2H), 7.39 (d, *J*=8.29 Hz, 4H), 7.44 - 7.52 (m, 4H), 7.69 (d, *J*=8.29 Hz, 2H), 8.04 (dd, *J*=6.43, 2.70 Hz, 2H), 8.38 - 8.44 (m, 2H), 8.46 (s, 1H)

^{13}C NMR (101 MHz, $CDCl_3$) δ ppm 127.22, 127.28, 128.05, 131.47, 133.59, 134.10, 144.14

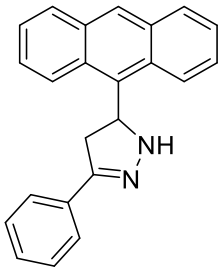

5-(anthracen-9-yl)-3-phenyl-4,5-dihydro-1*H*-pyrazole

5-(anthracen-9-yl)-3-phenyl-4,5-dihydro-1*H*-pyrazole was synthesised from (*E*)-3-(anthracen-9-yl)-1-phenylprop-2-en-1-one (1 mmol, 0.3084 g) and hydrazine hydrate (3 mL) according to general method (6), brown/yellow solid (21%)

^{1}H NMR (400 MHz, $CDCl_3$) δ ppm 3.12-3.21(dd, 1H),3.54-3.63 (dd, 1H), 5.22–5.30 (t, 1H), 6.39 (s, 1H), 7.35–7.39 (d, *J* = 7.25 Hz, 1H), 7.44–7.49 (m, 6H), 7.56–7.61 (d, J = 7.38 Hz, 2H) 8.00–8.03 (t, 4H), 8.49 (s, 1H)

^{13}C NMR (101 MHz, $CDCl_3$) δ ppm 48.12, 65.30, 125.30, 126.43, 128.42, 128.72, 128.76, 128.92, 131.06, 131.32, 141.89, 154.21

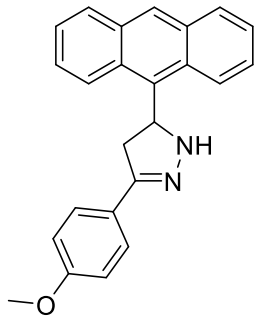

5-(anthracen-9-yl)-3-(4-methoxyphenyl)-4,5-dihydro-1*H*-pyrazole

5-(anthracen-9-yl)-3-(4-methoxyphenyl)-4,5-dihydro-1H-pyrazole was synthesised from (*E*)-3-(anthracen-9-yl)-1-(4-methoxyphenyl)prop-2-en-1-one (1 mmol, 0.3384 g) and hydrazine hydrate (3 mL) according to general method (6), dark yellow solid (3%)

^{1}H NMR (400 MHz, $CDCl_3$) δ ppm 3.09-3.19 (dd, 1H), 3.47-3.52 (dd, 1H), 3.83 (s, 3H), 5.12-5.21 (t, 1H), 6.96-7.02 (d, *J* = 8.48 Hz, 2H), 7.47-7.55 (m, 6H), 7.94-8.06 (m, 4H), 8.34 (s, 1H)

^{13}C NMR (101 MHz, $CDCl_3$) δ ppm 48.71, 55.44, 114.32, 125.28, 125.39, 125.51, 127.20, 127.38, 128.86, 130.33, 131.31, 134.09, 150.76, 159.27

5.7 General Procedure (7) for synthesis of alcohols

To a solution of the appropriate chalcone analog (1 mmol) and cerium (III) chloride (1 mmol) in MeOH:THF (1:1) (20 mL) $NaBH_4$ (2 mmol) was slowly added The solution was then left to stir in an ice-bath at 0˚C for 10 minutes. Water (10mL) was added when the reaction came to completion and the resulting mixture wasput under reduced pressure to remove MeOH. The mixture was diluted with water before undergoing extraction using EtOAc (3 x 20 mL), water (3 x 20 mL) and brine (3 x 10 mL).The organic layers were combined and dried using Na_2SO_4 , filtered and put under reduced pressure to afford the pure product.

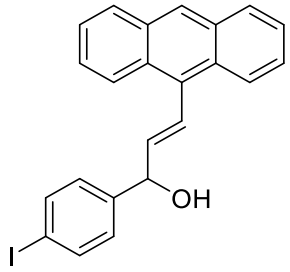

(*E*)-3-(anthracen-9-yl)-1-(4-iodophenyl)prop-2-en-1-ol (53)

(*E*)-3-(anthracen-9-yl)-1-(4-iodophenyl)prop-2-en-1-ol was synthesised from (*E*)-3-(anthracen-9-yl)-1-(4-iodophenyl)prop-2-en-1-one (1 mmol, 0.4343 g) according to general procedure (7), brown solid (96%)

^{1}H NMR (400 MHz,CDCl$_3$) δ ppm 2.20 (d, *J*=3.73 Hz, 1H), 5.59 - 5.65 (m, 1H), 6.21 (dd, *J*=16.17, 6.22 Hz, 1H), 7.33 (d, *J*=8.29 Hz, 3 H), 7.41 - 7.48 (m, 6H), 7.75 (d, *J*=8.71 Hz, 2H), 7.95 - 8.00 (m, 2H), 8.16 - 8.21 (m, 2H), 8.37 (s, 1H)

^{13}C NMR (101 MHz, CDCl$_3$) δ ppm 74.90, 124.84, 125.56, 126.69, 126.92, 128.35, 128.67, 129.39, 131.34, 131.52, 137.82, 139.51, 142.41

LRMS (APCI) calculated for $C_{23}H_{17}IO$ [$M^{+\bullet}$]: 436.03, found: 436.30.

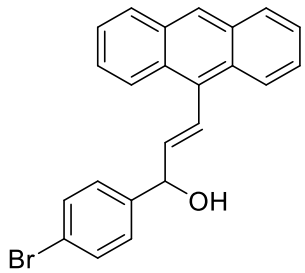

(*E*)-3-(anthracen-9-yl)-1-(4-bromophenyl)prop-2-en-1-ol (51)

(*E*)-3-(anthracen-9-yl)-1-(4-bromophenyl)prop-2-en-1-ol was synthesised from (*E*)-3-(anthracen-9-yl)-1-(4-bromophenyl)prop-2-en-1-one (1 mmol, 0.3873 g) according to general procedure (7)**,** brown solid (78%)

^{1}H NMR (400 MHz, CDCl$_3$) δ ppm 5.63 (d, J = 6.2 Hz, 1H), 6.21 (dd, J = 16.1, 6.2 Hz, 1H), 7.48 – 7.42 (m, 7H), 7.55 (d, J = 8.5 Hz, 2H), 8.00 – 7.94 (m, 2H), 8.21 – 8.16 (m, 2H), 8.37 (s, 1H)

^{13}C NMR (400 MHz, CDCl$_3$) δ ppm 75.32, 122.28, 125.62, 126.08, 127.13, 127.38, 128.62, 129.19, 129.90, 131.84, 132.02, 132.36, 140.05, 142.24

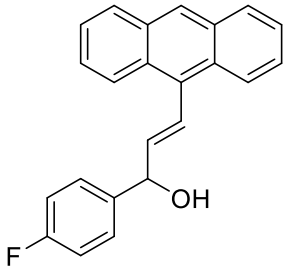

(*E*)-3-(anthracen-9-yl)-1-(4-fluorophenyl)prop-2-en-1-ol (52)

(*E*)-3-(anthracen-9-yl)-1-(4-fluorophenyl)prop-2-en-1-ol was synthesised from (*E*)-3-(anthracen-9-yl)-1-(4-fluorophenyl)prop-2-en-1-one (1 mmol, 0.3264 g) according to general procedure (7)**,** orange solid (96%)

^{1}H NMR (400 MHz, $CDCl_3$) δ ppm 8.36 (s, 1H), 8.20 (d, *J* = 9.4 Hz, 2H), 7.97 (d, *J* = 9.5 Hz, 2H), 7.57 – 7.49 (m, 2H), 7.48 – 7.39 (m, 5H), 7.11 (t, *J* = 8.6 Hz, 2H), 6.22 (dd, *J* = 16.1, 6.1 Hz, 1H), 5.63 (d, *J* = 6.0 Hz, 1H).
^{13}C NMR (400 MHz, $CDCl_3$) δ ppm 74.75, 115.51, 115.72, 125.51, 125.60, 126.55, 128.09, 128.17, 128.66, 129.41, 131.34, 131.66, 138.57, 139.89, 163.62

X-ray crystallography analysis

X-ray crystallography data was collected using a Rigaku Saturn 724 and Bruker APEX DUO diffractometer at 90(2) and 100(2)K using Mo Kα and Cu Kα wavelength radiation (λ = 0.71073 and 1.54178 Å) respectively. Data was collected using CrystalClear and APEX2 software.Absorption corrections were performed using REQAB and SADABS respectively. Space group determinations, structure solutions and refinements were performed with Bruker SHELXTL and APEX2 software. All non-hydrogen atoms were refined anisotropically. Hydrogen atoms were assigned to calculated positions using a riding model with appropriately fixed isotropic thermal parameters.

Molecular Operating Environment (MOE)

Using MOE (Molecular Operating Environment) 2016.V8, molecular structures of interest were processed using the MMFF94s force field, commonly used for small molecule modelling. Flexible alignment was conducted on each compound at 1000 iterations per run. The chirality of the stereogenic centres of the compounds was not

defined. Default parameters were utilised for other settings. The proposed alignments featured as the top ranked alignment of generated poses, ranked in order of ascending S score (flexible alignment score comprising of both molecular strain energy and configuration similarity inputs).

Chapter 6: References

1. World Health Organization. Cancer-Fact Sheet, WHO Newsroom, 2018. https://www.who.int/en/news-room/fact-sheets/detail/cancer (accessed 19/06/19).
2. World Health Organization, GLOBOCAN 2018: Estimated cancer incidence, mortality and prevalence worldwide, Cancer Tomorrow-International Ageny for Cancer Research. http://gco.iarc.fr/tomorrow/home (accessed 16/08/19).
3. National Cancer Registry. Cancer Factsheet-Overview & most common cancers. https://www.ncri.ie/sites/ncri/files/factsheets/Factsheet%20all%20cancers.pdf.
4. Bray, F.; Ferlay, J.; Soerjomataram, I.; Siegel, R. L.; Torre, L. A.; Jemal, A., Global cancer statistics 2018: GLOBOCAN estimates of incidence and mortality worldwide for 36 cancers in 185 countries. *CA: a cancer journal for clinicians* **2018,** *68* (6), 394-424.
5. Forouzanfar, M. H.; Afshin, A.; Alexander, L. T.; Anderson, H. R.; Bhutta, Z. A.; Biryukov, S.; Brauer, M.; Burnett, R.; Cercy, K.; Charlson, F. J., Global, regional, and national comparative risk assessment of 79 behavioural, environmental and occupational, and metabolic risks or clusters of risks, 1990-2015: a systematic analysis for the Global Burden of Disease Study 2015. *The Lancet* **2016,** *388* (10053), 1659.
6. National Cancer Registry *Cancer projections for Ireland 2015-2040.* ; Cork, Ireland, 2014.
7. National Cancer Registry *Cancer in Ireland 1994-2014: Annual Report of the National Cancer Registry.*; Cork, Ireland, 2016.
8. World Health Organization, Cancer prevention, WHO Cancer. https://www.who.int/cancer/prevention/en/ (accessed 20/05/19).
9. World Health Organization *Global action plan for the prevention and control of noncommunicable diseases 2013-2020*; Geneva, Switzerland, 2013.
10. World Health Organization *Cancer control- Knowledge into action, WHO guide for effective programmes: Prevention*; Geneva, 2007.
11. World Health Organization *Cancer control-Knowledge into action, WHO Guide for Effective Programmes: Early detection*; Geneva, 2007.
12. World Health Organization *Cancer control- Knowledge into action, WHO guide for effective programmes: Diagnosis and treatment*; Geneva, 2008.
13. World Health Organization *Cancer control-Knowledge into action, WHO guide for effective programmes: Palliative care*; Geneva, 2007.
14. World Health Organization *Cancer control-Knowledge into action, WHO guide for effective programmes: Planning*; Geneva, 2007.
15. American Cancer Society The History of Cancer, Cancer A-Z, Cancer Basics. http://www.cancer.org/cancer/cancerbasics/thehistoryofcancer/the-history-of-cancer-what-is-cancer (accessed 5/10/13).
16. Fiorillo, T. R.; Collins, A. G.; Waggoner, B. M.; Speer, B. R.; Rieboldt, S.; Smith, D. The Paleozoic Era. http://www.ucmp.berkeley.edu/paleozoic/paleozoic.php (accessed 5/10/2013).
17. Capasso, L. L., Antiquity of cancer. *International Journal of Cancer* **2005,** *113* (1), 2-13.
18. Stadtman, K., News from Members. *Soc Vert Paleontol* **1992,** *155*, 45.
19. Cao, Y.; DePinho, R. A.; Ernst, M.; Vousden, K., Cancer research: past, present and future. *Nature Reviews Cancer* **2011,** *11* (10), 749-754.
20. Lilienfeld, A. M.; Pedersen, E.; Dowd, J. E., *Cancer epidemiology: methods of study*. Oxford University Press: London, 1968.

21. Boylan, M. Hippocrates (c.450-c.380 B.C.E.). https://www.iep.utm.edu/hippocra/ (accessed 12/05/19).
22. Köckerling, F.; Köckerling, D.; Lomas, C., Cornelius Celsus--ancient encyclopedist, surgeon-scientist, or master of surgery? *Langenbecks Arch Surg* **2013,** *398* (4), 609-616.
23. Mukherjee, S., *The Emperor of All Maladies: A Biography of Cancer*. Simon and Schuster: New York, 2010.
24. Kumar, P. J.; Clark, M. L., *Kumar & Clark's clinical medicine*. 8th ed.; Saunders Elsevier, : Edinburgh, 2012.
25. Patrick, G. L., *An Introduction to Medicinal Chemistry*. 4th ed.; Oxford University Press: New York, 2009.
26. Alberts, B.; Johnson, A.; Lewis, J.; Morgan, D.; Raff, M.; Roberts, P. W. K., *Molecular biology of the cell*. 5th ed.; Garland Science: New York, 2008.
27. Ruddon, R. W., *Cancer Biology*. 4th ed.; Oxford University Press: New York, 2007.
28. National Institutes of Health (NIH), Medline Plus-Benign Tumours, Health Topics. http://www.nlm.nih.gov/medlineplus/benigntumors.html (accessed 05/10/13).
29. Fidler, I. J., The pathogenesis of cancer metastasis: the 'seed and soil' hypothesis revisited. *Nature Reviews Cancer* **2003,** *3* (6), 453-458.
30. American Cancer Society, What causes cancer?, Genetics and Cancer-Family Cancer Syndromes. https://www.cancer.org/cancer/cancer-causes/genetics/family-cancer-syndromes.html (accessed 23/06/19).
31. WHO Expert Committee on the Prevention of Cancer & World Health Organization *Prevention of Cancer: Report of a WHO Expert Committee*; Geneva, 1964.
32. Doll, R.; Peto, R., The causes of cancer: quantitative estimates of avoidable risks of cancer in the United States today. *Journal of the National Cancer Institute* **1981,** *66* (6), 1192-1308.
33. World Health Organization, Cancer Fact sheet No. 297, WHO Newsroom. http://www.who.int/mediacentre/factsheets/fs297/en/index.html (accessed 01/10/18).
34. World Health Organization, Tobacco Fact sheet, WHO Newsroom. https://www.who.int/news-room/fact-sheets/detail/tobacco (accessed 23/06/19).
35. Brennan, P.; Hainaut, P.; Boffetta, P., Genetics of lung-cancer susceptibility. *The Lancet Oncology* **2011,** *12* (4), 399-408.
36. World Health Organizaiton *World cancer report 2014*; International Agency for Research on Cancer: Lyon, 2014.
37. Peto, R.; Darby, S.; Deo, H.; Silcocks, P.; Whitley, E.; Doll, R., Smoking, smoking cessation, and lung cancer in the UK since 1950: combination of national statistics with two case-control studies. *BMJ* **2000,** *321* (7257), 323-329.
38. World Health Organization, Tobacco: Health benefits of smoking cessation, WHO Newsroom, Q&A Detail. https://www.who.int/tobacco/quitting/benefits/en/ (accessed 15/04/19).
39. Brugha, R.; Tully, N.; Dicker, P.; Shelley, E.; Ward, M.; McGee, H. *SLAN 2007: Smoking Patterns in Ireland*; Department of Health and Children: Dublin, 2007.
40. Kavanagh, P.; Sheridan, A. *The State of Tobacco Control in Ireland: HSE Tobacco Free Ireland Programme*; Health Service Executive: Dublin, 2018.
41. Drope J; Schluger N; Cahn Z; Drope J; Hamill S; Islami F; Liber A; Nargis N; M., S. *The Tobacco Atlas*; 1604430133; American Cancer Society and Vital Strategies: Atlanta 2018.

42. Department of Health *National Cancer Strategy 2017 - 2026*; Department of Health (DoH) & National Patient Safety Office: Dublin, 2017.
43. World Health Organization, Obesity and overweight-Fact sheet, WHO Newsroom. http://www.who.int/mediacentre/factsheets/fs311/en/ (accessed 08/12/19).
44. International Agency for Research on Cancer, Absence of Excess Body Fatness. *IARC Handb Cancer Prev.* **2018,** *16*, 1-646.
45. Key, T. J.; Schatzkin, A.; Willett, W. C.; Allen, N. E.; Spencer, E. A.; Travis, R. C., Diet, nutrition and the prevention of cancer. *Public health nutrition* **2004,** *7* (1A; SPI), 187-200.
46. World Health Organization *Diet, nutrition and the prevention of chronic diseases: report of a joint WHO/FAO expert consultation*; 2003.
47. Moore, P. S.; Chang, Y., Why do viruses cause cancer? Highlights of the first century of human tumour virology. *Nature Reviews Cancer* **2010,** *10* (12), 878-889.
48. Rawla, P.; Barsouk, A., Epidemiology of gastric cancer: global trends, risk factors and prevention. *Prz Gastroenterol* **2019,** *14* (1), 26-38.
49. National Institutes of Health (NIH), Medline Plus-Cervical Dysplasia, Health Topics. http://www.nlm.nih.gov/medlineplus/ency/article/001491.htm.
50. Krump, N. A.; You, J., Molecular mechanisms of viral oncogenesis in humans. *Nature Reviews Microbiology* **2018,** *16* (11), 684-698.
51. Torre, L. A.; Bray, F.; Siegel, R. L.; Ferlay, J.; Lortet-Tieulent, J.; Jemal, A., Global cancer statistics, 2012. *CA: a cancer journal for clinicians* **2015,** *65* (2), 87-108.
52. Colditz, G. A.; Sellers, T. A.; Trapido, E., Epidemiology—identifying the causes and preventability of cancer? *Nature Reviews Cancer* **2005,** *6* (1), 75-83.
53. Foye, W. O.; Lemke, T. L.; Williams, D. A., *Foye's principles of medicinal chemistry*. 6th ed.; Lippincott Williams & Wilkins: Philadelphia, 2008.
54. Reece, J. B.; Urry, L. A.; Cain, M. L.; Wasserman, S. A.; Minorsky, P. V.; Jackson, R. B., *Campbell biology*. 9th ed.; Benjamin Cummings / Pearson: Boston, 2011.
55. Ryan, M. B.; Corcoran, R. B., Therapeutic strategies to target RAS-mutant cancers. *Nature Reviews Clinical Oncology* **2018,** *15* (11), 709-720.
56. Mendelsohn, J.; Howley, P. M.; Israel, M. A.; Gray, J. W.; Thompson, C. B., *The Molecular Basis of Cancer* 4th ed.; Elsevier Saunders: Philadelphia, 2014.
57. Lodish, H.; Berk, A.; Kaiser, C. A.; Krieger, M.; Scott, M. P.; Bretscher, A.; Ploegh, H.; Matsudaira, P., *Molecular cell biology*. W. H. Freeman and Company,: New York, 2008.
58. Harrington, K. J., The biology of cancer. *Medicine* **2016,** *44* (1), 1-5.
59. Hanahan, D.; Weinberg, Robert A., Hallmarks of Cancer: The Next Generation. *Cell* **2011,** *144* (5), 646-674.
60. Lesterhuis, W. J.; Haanen, J. B. A. G.; Punt, C. J. A., Cancer immunotherapy – revisited. *Nature Reviews Drug Discovery* **2011,** *10*, 591.
61. De Luca, M.; Aiuti, A.; Cossu, G.; Parmar, M.; Pellegrini, G.; Robey, P. G., Advances in stem cell research and therapeutic development. *Nature Cell Biology* **2019**.
62. American Cancer Society, How is surgey used for cancer?, Treatment & Support, Treatments and Side Effects. http://www.cancer.org/treatment/treatmentsandsideeffects/treatmenttypes/surgery/surgery-how-is-surgery-used-for-cancer (accessed 17/10/2015).
63. Cuzick, J., Preventive therapy for cancer. *The Lancet Oncology* **2017,** *18* (8), e472-e482.
64. Reed, M., Principles of cancer treatment by surgery. *Surgery (Oxford)* **2009,** *27* (4), 178-181.

65. MD Anderson Cancer Centre-The University of Texas, Cancer Surgery, Diagnosis & Treatment, Treatment Options. **2013**.
66. NHS Choices-UK, Overview-Radiotherapy, Health A to Z. http://www.nhs.uk/Conditions/Radiotherapy/Pages/Introduction.aspx (accessed 17/10/2015).
67. St.Luke's Hospital-Radiation Oncology Network, Radiotherapy treatments. **2013**.
68. Falk, S., Principles of cancer treatment by radiotherapy. *Surgery (Oxford)* **2006,** *24* (2), 62-65.
69. Caley, A.; Jones, R., The principles of cancer treatment by chemotherapy. *Surgery (Oxford)* **2012,** *30* (4), 186-190.
70. Dickens, E.; Ahmed, S., Principles of cancer treatment by chemotherapy. *Surgery (Oxford)* **2018,** *36* (3), 134-138.
71. Weinberg, R. A., *The Biology of Cancer: Second International Student Edition*. WW Norton & Company: New York, 2013.
72. Fernando, J.; Kumar, S., Principles of cancer treatment by immunotherapy. *Surgery (Oxford)* **2015,** *33* (3), 117-121.
73. Androulla, N. M.; Lefkothea, C. P., CAR T-cell Therapy: A New Era in Cancer Immunotherapy. *Current Pharmaceutical Biotechnology* **2018,** *19* (1), 5-18.
74. World Cancer Research Fund, Worldwide cancer data: Global cancer statistics for the most common cancers, Cancer Trends. https://www.wcrf.org/dietandcancer/cancer-trends/worldwide-cancer-data (accessed 26/04/19).
75. Nogai, H.; Dörken, B.; Lenz, G., Pathogenesis of non-Hodgkin's lymphoma. *Journal of clinical oncology : official journal of the American Society of Clinical Oncology* **2011,** *29* (14), 1803-1811.
76. Malcolm, T. I. M.; Hodson, D. J.; Macintyre, E. A.; Turner, S. D., Challenging perspectives on the cellular origins of lymphoma. *Open Biol* **2016,** *6* (9), 160232.
77. Molyneux, E. M.; Rochford, R.; Griffin, B.; Newton, R.; Jackson, G.; Menon, G.; Harrison, C. J.; lsraels, T.; Bailey, S., Burkitt's lymphoma. *Lancet* **2012,** *379* (9822), 1234-1244.
78. Casulo, C.; Friedberg, J., Burkitt lymphoma-a rare but challenging lymphoma. *Best Practice & Research Clinical Haematology* **2018**.
79. Parkin, D. M.; Stiller, C. A.; Draper, G. J.; Bieber, C. A., The international incidence of childhood cancer. *International journal of cancer. Journal international du cancer* **1988,** *42* (4), 511-20.
80. Stiller, C. A.; Parkin, D. M., Geographic and ethnic variations in the incidence of childhood cancer. *British Medical Bulletin* **1996,** *52* (4), 682-703.
81. Burkitt, D., A sarcoma involving the jaws in african children. *British Journal of Surgery* **1958,** *46* (197), 218-223.
82. World Health Organizaiton-International Agency for Research on Cancer *Cancer in Africa: Epidemiology and prevention.*; Lyon, 2003.
83. Jaffe, E. S., The 2008 WHO classification of lymphomas: implications for clinical practice and translational research. *Hematology Am Soc Hematol Educ Program* **2009,** *2009* (1), 523-531.
84. Rochford, R.; Cannon, M. J.; Moormann, A. M., Endemic Burkitt's lymphoma: a polymicrobial disease? *Nat Rev Micro* **2005,** *3* (2), 182-187.
85. Haddow, A., An Improved Map for the Study of Burkitt's Lymphoma Syndrome in Africa. *East African medical journal* **1963,** *40* (9), 429-32.

86. Epstein, M. A.; Achong, B.; Barr, Y., Virus particles in cultured lymphoblasts from Burkitt's lymphoma. *The Lancet* **1964,** *283* (7335), 702-703.
87. Biggar, R. J.; Henle, W.; Fleisher, G.; Böcker, J.; Lennette, E. T.; Henle, G., Primary epstein-barr virus infections in african infants. I. Decline of maternal antibodies and time of infection. *International Journal of Cancer* **1978,** *22* (3), 239-243.
88. Geser, A.; Brubaker, G.; Olwit, G. W., The frequency of Epstein-Barr virus infection and Burkitt's lymphoma at high and low altitudes in East Africa. *Revue d'epidemiologie et de sante publique* **1980,** *28* (3), 307-21.
89. Gabrielsen, A. A., Jr.; Jensen, J. B., Mitogenic activity of extracts from continuous cultures of Plasmodium falciparum. *Am J Trop Med Hyg* **1982,** *31* (3 Pt 1), 441-8.
90. Moss, D.; Burrows, S.; Castelino, D.; Kane, R.; Pope, J.; Rickinson, A.; Alpers, M.; Heywood, P., A comparison of epstein-barr virus-specific T-cell immunity in malaria-endemic and-nonendemic regions of Papua New Guinea. *International Journal of Cancer* **1983,** *31* (6), 727-732.
91. Liu, H.; Andreansky, S.; Diaz, G.; Turner, S. J.; Wodarz, D.; Doherty, P. C., Quantitative analysis of long-term virus-specific CD8+-T-cell memory in mice challenged with unrelated pathogens. *Journal of virology* **2003,** *77* (14), 7756-7763.
92. Kamranvar, S. A.; Gruhne, B.; Szeles, A.; Masucci, M. G., Epstein-Barr virus promotes genomic instability in Burkitt's lymphoma. *Oncogene* **2007,** *26* (35), 5115-5123.
93. Biggar, R. J.; Chaturvedi, A. K.; Goedert, J. J.; Engels, E. A., AIDS-Related Cancer and Severity of Immunosuppression in Persons With AIDS. *Journal of the National Cancer Institute* **2007,** *99* (12), 962-972.
94. Zech, L.; Haglund, U.; Nilsson, K.; Klein, G., Characteristic chromosomal abnormalities in biopsies and lymphoid-cell lines from patients with burkitt and non-burkitt lymphomas. *International Journal of Cancer* **1976,** *17* (1), 47-56.
95. Kafuko, G.; Burkitt, D., Burkitt's lymphoma and malaria. *International Journal of Cancer* **1970,** *6* (1), 1-9.
96. Hecht, J. L.; Aster, J. C., Molecular Biology of Burkitt's Lymphoma. *Journal of Clinical Oncology* **2000,** *18* (21), 3707-3721.
97. Giulino-Roth, L.; Cesarman, E., Molecular biology of Burkitt lymphoma. In *Burkitt's Lymphoma*, Springer: 2013; pp 211-226.
98. Wade, M.; Wahl, G., c-Myc, genome instability, and tumorigenesis: the devil is in the details. In *The Myc/Max/Mad Transcription Factor Network*, Springer: New York, 2006; pp 169-203.
99. Lossos, C.; Liu, Y.; Kolb, K. E.; Christie, A. L.; Van Scoyk, A.; Prakadan, S. M.; Shigemori, K.; Stevenson, K. E.; Morrow, S.; Plana, O. D., Mechanisms of lymphoma clearance induced by high-dose alkylating agents. *Cancer discovery* **2019**.
100. Egle, A.; Harris, A. W.; Bouillet, P.; Cory, S., Bim is a suppressor of Myc-induced mouse B cell leukemia. *Proceedings of the National Academy of Sciences of the United States of America* **2004,** *101* (16), 6164-6169.
101. Wilson, W. H.; Dunleavy, K.; Pittaluga, S.; Hegde, U.; Grant, N.; Steinberg, S. M.; Raffeld, M.; Gutierrez, M.; Chabner, B. A.; Staudt, L., Phase II study of dose-adjusted EPOCH and rituximab in untreated diffuse large B-cell lymphoma with analysis of germinal center and post-germinal center biomarkers. *Journal of Clinical Oncology* **2008,** *26* (16), 2717-2724.
102. Smeland, S.; Blystad, A. K.; Kvaløy, S. O.; Ikonomou, I. M.; Delabie, J.; Kvalheim, G.; Hammerstrøm, J.; Lauritzsen, G. F.; Holte, H., Treatment of Burkitt's/Burkitt-like lymphoma in adolescents and adults: a 20-year experience from

the Norwegian Radium Hospital with the use of three successive regimens. *Annals of Oncology* **2004,** *15* (7), 1072-1078.
103. Perkins, A. S.; Friedberg, J. W., Burkitt Lymphoma in Adults. *ASH Education Program Book* **2008,** *2008* (1), 341-348.
104. Kalisz, K.; Alessandrino, F.; Beck, R.; Smith, D.; Kikano, E.; Ramaiya, N. H.; Tirumani, S. H., An update on Burkitt lymphoma: a review of pathogenesis and multimodality imaging assessment of disease presentation, treatment response, and recurrence. *Insights into imaging* **2019,** *10* (1), 56.
105. Magrath, I. T.; Haddy, T. B.; Adde, M. A., Treatment of patients with high grade non-Hodgkin's lymphomas and central nervous system involvement: is radiation an essential component of therapy? *Leuk Lymphoma* **1996,** *21* (1-2), 99-105.
106. Modified Magrath Regimens for Adults with Burkitt and Burkitt-Like Lymphomas: Preserved Efficacy with Decreased Toxicity. *Leukemia & Lymphoma* **2004,** *45* (4), 761-767.
107. Lymphoma Action, Rituximab for lymphoma, About Lymphoma. https://lymphoma-action.org.uk/about-lymphoma-treatment-lymphoma-antibody-therapy-including-rituximab/rituximab-lymphoma (accessed 20/04/19).
108. Hoelzer, D.; Walewski, J.; Döhner, H.; Viardot, A.; Hiddemann, W.; Spiekermann, K.; Serve, H.; Dührsen, U.; Hüttmann, A.; Thiel, E.; Dengler, J.; Kneba, M.; Schaich, M.; Schmidt-Wolf, I. G. H.; Beck, J.; Hertenstein, B.; Reichle, A.; Domanska-Czyz, K.; Fietkau, R.; Horst, H.-A.; Rieder, H.; Schwartz, S.; Burmeister, T.; Gökbuget, N., Improved outcome of adult Burkitt lymphoma/leukemia with rituximab and chemotherapy: report of a large prospective multicenter trial. *Blood* **2014,** *124* (26), 3870.
109. Marcus, R.; Imrie, K.; Belch, A.; Cunningham, D.; Flores, E.; Catalano, J.; Solal-Celigny, P.; Offner, F.; Walewski, J.; Raposo, J., CVP chemotherapy plus rituximab compared with CVP as first-line treatment for advanced follicular lymphoma. *Blood* **2005,** *105* (4), 1417-1423.
110. Thomas, D. A.; Faderl, S.; O'Brien, S.; Bueso-Ramos, C.; Cortes, J.; Garcia-Manero, G.; Giles, F. J.; Verstovsek, S.; Wierda, W. G.; Pierce, S. A., Chemoimmunotherapy with hyper-CVAD plus rituximab for the treatment of adult Burkitt and Burkitt-type lymphoma or acute lymphoblastic leukemia. *Cancer* **2006,** *106* (7), 1569-1580.
111. Thomas, D. A.; Cortes, J.; O'Brien, S.; Pierce, S.; Faderl, S.; Albitar, M.; Hagemeister, F. B.; Cabanillas, F. F.; Murphy, S.; Keating, M. J., Hyper-CVAD program in Burkitt's-type adult acute lymphoblastic leukemia. *Journal of Clinical Oncology* **1999,** *17* (8), 2461-2461.
112. Noy, A.; Lee, J. Y.; Cesarman, E.; Ambinder, R.; Baiocchi, R.; Reid, E.; Ratner, L.; Wagner-Johnston, N.; Kaplan, L., AMC 048: modified CODOX-M/IVAC-rituximab is safe and effective for HIV-associated Burkitt lymphoma. *Blood* **2015,** *126* (2), 160.
113. Galicier, L.; Fieschi, C.; Borie, R.; Meignin, V.; Daniel, M.-T.; Gérard, L.; Oksenhendler, E., Intensive chemotherapy regimen (LMB86) for St Jude stage IV AIDS-related Burkitt lymphoma/leukemia: a prospective study. *Blood* **2007,** *110* (8), 2846-2854.
114. Meegan, M. J.; Cloonan, S. M.; Keating, J. J.; Corrigan, D.; O' Brien, J. E.; Kavanagh, P. V.; Williams, C., Synthesis and in vitro toxicity of 4-MTA, its characteristic clandestine synthesis by-products and related sulphur substituted alpha-alkylthioamphetamines. *Bioorganic & Medicinal Chemistry* **2010,** *18*, 4009-4031.

115. McNamara, Y. M.; Cloonan, S. M.; Knox, A. J. S.; Keating, J. J.; Butler, S. G.; Peters, G. H.; Meegan, M. J.; Williams, D. C., Synthesis and serotonin transporter activity of 1,3-bis(aryl)-2-nitro-1-propenes as a new class of anticancer agents. *Bioorganic & Medicinal Chemistry* **2011,** *19* (3), 1328-1348.
116. Mc Namara, Y. M., Bright , S.A. , Byrne, A.J. , Williams, D.C. , Meegan, M.J., Synthesis and biochemical evaluation of a novel series of maprotiline analogues. *European Journal of Medicinal Chemistry* **2013,** *71*, 333-353.
117. S.M. Cloonan, A. D., D. Fayne, D.C. Williams, The antidepressants maprotiline and fluoxetine have potent selective antiproliferative effects against Burkitt lymphoma independently of the norepinephrine and serotonin transporters. *Leukemia & Lymphoma* **2010,** *51* (3), 523-539.
118. Cloonan, S. M.; Williams, D. C., The antidepressants maprotiline and fluoxetine induce Type II autophagic cell death in drug-resistant Burkitt's lymphoma. *International Journal of Cancer* **2011,** *128* (7), 1712-1723.
119. Kaap, S.; Quentin, I.; Tamiru, D.; Shaheen, M.; Eger, K.; Steinfelder, H. J., Structure activity analysis of the pro-apoptotic, antitumor effect of nitrostyrene adducts and related compounds. *Biochemical Pharmacology* **2003,** *65* (4), 603-610.
120. Pettit, R. K.; Pettit, G. R.; Hamel, E.; Hogan, F.; Moser, B. R.; Wolf, S.; Pon, S.; Chapuis, J.-C.; Schmidt, J. M., E-Combretastatin and E-resveratrol structural modifications: Antimicrobial and cancer cell growth inhibitory β-E-nitrostyrenes. *Bioorganic & Medicinal Chemistry* **2009,** *17* (18), 6606-6612.
121. Chen, J.; Odenike, O.; Rowley, J. D., Leukemogenesis: More than mutant genes. *Nature reviews. Cancer* **2010,** *10* (1), 23.
122. Jones, P. A.; Archer, T. K.; Baylin, S. B.; Beck, S.; Berger, S.; Bernstein, B. E.; Carpten, J. D.; Clark, S. J.; Costello, J. F.; Doerge, R. W., Moving AHEAD with an international human epigenome project. *Nature* **2008,** *454* (7205), 711-715.
123. Niederhuber, J. E.; Armitage, J. O.; Doroshow, J. H.; Kastan, M. B.; Tepper, J. E., *Abeloff's Clinical Oncology E-Book*. Elsevier Health Sciences: 2019.
124. National Cancer Institute (NCI), Childhood Acute Lymphoblastic Leukemia Treatment (PDQ®)–Patient Version. https://www.cancer.gov/types/leukemia/patient/child-all-treatment-pdq (accessed 15/09/17).
125. Leukaemia Care, Leukaemia, Blood cancer information. http://www.leukaemiacare.org.uk/leukaemia (accessed 15/09/17).
126. Blood Cancer Network Ireland (BCNI), Leukaemia, Information for patients-Blood Cancers. http://www.bloodcancers.ie/bloodcancers/informationforpatients/leukaemia/ (accessed 15/09/2017).
127. Leukaemia Foundation Austrailia, Leukaemias, Types of Blood Cancer. . http://www.leukaemia.org.au/blood-cancers/leukaemias (accessed 15/09/2017).
128. Govindan, R., *The Washington manual of oncology*. 2nd ed.; Lippincott Williams & Wilkins: Philadelphia, 2008.
129. American Cancer Society, Key Statistics for Acute Myeloid Leukemia (AML), About Acute Myeloid Leukaemia. https://www.cancer.org/cancer/acute-myeloid-leukemia/about/key-statistics.html (accessed 15/03/19).
130. Mwirigi, A.; Dillon, R.; Raj, K., Acute leukaemia. *Medicine* **2017,** *45* (5), 280-286.
131. Hanlon, K.; Copland, M., Chronic myeloid leukaemia. *Medicine* **2017,** *45* (5), 287-291.

132. Hallek, M.; Cheson, B. D.; Catovsky, D.; Caligaris-Cappio, F.; Dighiero, G.; Döhner, H.; Hillmen, P.; Keating, M. J.; Montserrat, E.; Rai, K. R., Guidelines for the diagnosis and treatment of chronic lymphocytic leukemia: a report from the International Workshop on Chronic Lymphocytic Leukemia updating the National Cancer Institute–Working Group 1996 guidelines. *Blood* **2008,** *111* (12), 5446-5456.
133. Devereux, S.; Cuthill, K., Chronic lymphocytic leukaemia. *Medicine* **2017,** *45* (5), 292-296.
134. Scarfò, L.; Ferreri, A. J. M.; Ghia, P., Chronic lymphocytic leukaemia. *Critical Reviews in Oncology/Hematology* **2016,** *104*, 169-182.
135. Howlader, N.; Noone, A.; Krapcho, M.; Miller, D.; Bishop, K.; Altekruse, S.; Kosary, C.; Yu, M.; Ruhl, J.; Tatalovich, Z. *SEER Cancer Statistics Review, 1975-2013.*; Bethesda, 2016.
136. Redaelli, A.; Laskin, B. L.; Stephens, J. M.; Botteman, M. F.; Pashos, C. L., The clinical and epidemiological burden of chronic lymphocytic leukaemia. *European Journal of Cancer Care* **2004,** *13* (3), 279-287.
137. Miranda-Filho, A.; Pineros, M.; Ferlay, J.; Soerjomataram, I.; Monnereau, A.; Bray, F., Epidemiological patterns of leukaemia in 184 countries: a population-based study. *The Lancet. Haematology* **2018,** *5* (1), e14-e24.
138. García-Escobar, I.; Sepúlveda, J.; Castellano, D.; Cortés-Funes, H., Therapeutic management of chronic lymphocytic leukaemia. *Critical Reviews in Oncology/Hematology* **2011,** *80* (1), 100-113.
139. Puente, X. S.; Pinyol, M.; Quesada, V.; Conde, L.; Ordonez, G. R.; Villamor, N.; Escaramis, G.; Jares, P.; Bea, S.; Gonzalez-Diaz, M.; Bassaganyas, L.; Baumann, T.; Juan, M.; Lopez-Guerra, M.; Colomer, D.; Tubio, J. M. C.; Lopez, C.; Navarro, A.; Tornador, C.; Aymerich, M.; Rozman, M.; Hernandez, J. M.; Puente, D. A.; Freije, J. M. P.; Velasco, G.; Gutierrez-Fernandez, A.; Costa, D.; Carrio, A.; Guijarro, S.; Enjuanes, A.; Hernandez, L.; Yague, J.; Nicolas, P.; Romeo-Casabona, C. M.; Himmelbauer, H.; Castillo, E.; Dohm, J. C.; de Sanjose, S.; Piris, M. A.; de Alava, E.; Miguel, J. S.; Royo, R.; Gelpi, J. L.; Torrents, D.; Orozco, M.; Pisano, D. G.; Valencia, A.; Guigo, R.; Bayes, M.; Heath, S.; Gut, M.; Klatt, P.; Marshall, J.; Raine, K.; Stebbings, L. A.; Futreal, P. A.; Stratton, M. R.; Campbell, P. J.; Gut, I.; Lopez-Guillermo, A.; Estivill, X.; Montserrat, E.; Lopez-Otin, C.; Campo, E., Whole-genome sequencing identifies recurrent mutations in chronic lymphocytic leukaemia. *Nature* **2011,** *475* (7354), 101-105.
140. Hallek, M.; Shanafelt, T. D.; Eichhorst, B., Chronic lymphocytic leukaemia. *The Lancet* **2018,** *391* (10129), 1524-1537.
141. Kikushige, Y.; Ishikawa, F.; Miyamoto, T.; Shima, T.; Urata, S.; Yoshimoto, G.; Mori, Y.; Iino, T.; Yamauchi, T.; Eto, T., Self-renewing hematopoietic stem cell is the primary target in pathogenesis of human chronic lymphocytic leukemia. *Cancer cell* **2011,** *20* (2), 246-259.
142. Nowakowski, G. S.; Hoyer, J. D.; Shanafelt, T. D.; Zent, C. S.; Call, T. G.; Bone, N. D.; LaPlant, B.; Dewald, G. W.; Tschumper, R. C.; Jelinek, D. F., Percentage of smudge cells on routine blood smear predicts survival in chronic lymphocytic leukemia. *Journal of Clinical Oncology* **2009,** *27* (11), 1844.
143. Go, R. S., Smudge cells, serum albumin, and prognosis in B-cell chronic lymphocytic leukemia. *Journal of Clinical Oncology* **2009,** *27* (22), e44-e44.
144. Jevremovic, D.; Dronca, R. S.; Morice, W. G.; McPhail, E. D.; Kurtin, P. J.; Zent, C. S.; Hanson, C. A., CD5+ B-cell lymphoproliferative disorders: beyond chronic lymphocytic leukemia and mantle cell lymphoma. *Leukemia research* **2010,** *34* (9), 1235-1238.

145. Döhner, H.; Stilgenbauer, S.; Benner, A.; Leupolt, E.; Kröber, A.; Bullinger, L.; Döhner, K.; Bentz, M.; Lichter, P., Genomic aberrations and survival in chronic lymphocytic leukemia. *New England Journal of Medicine* **2000,** *343* (26), 1910-1916.
146. Buhmann, R.; Kurzeder, C.; Rehklau, J.; Westhaus, D.; Bursch, S.; Hiddemann, W.; Haferlach, T.; Hallek, M.; Schoch, C., CD40L stimulation enhances the ability of conventional metaphase cytogenetics to detect chromosome aberrations in B-cell chronic lymphocytic leukaemia cells. *British Journal of Haematology* **2002,** *118* (4), 968-975.
147. Hallek, M.; Cheson, B. D.; Catovsky, D.; Caligaris-Cappio, F.; Dighiero, G.; Döhner, H.; Hillmen, P.; Keating, M.; Montserrat, E.; Chiorazzi, N.; Stilgenbauer, S.; Rai, K. R.; Byrd, J. C.; Eichhorst, B.; O'Brien, S.; Robak, T.; Seymour, J. F.; Kipps, T. J., iwCLL guidelines for diagnosis, indications for treatment, response assessment, and supportive management of CLL. *Blood* **2018,** *131* (25), 2745-2760.
148. Morice, W. G.; Kurtin, P. J.; Hodnefield, J. M.; Shanafelt, T. D.; Hoyer, J. D.; Remstein, E. D.; Hanson, C. A. In *Predictive value of blood and bone marrow flow cytometry in B-cell lymphoma classification: comparative analysis of flow cytometry and tissue biopsy in 252 patients*, Mayo Clinic Proceedings, Elsevier: 2008; pp 776-785.
149. Marti, G. E.; Rawstron, A. C.; Ghia, P.; Hillmen, P.; Houlston, R. S.; Kay, N.; Schleinitz, T. A.; Caporaso, N., Diagnostic criteria for monoclonal B-cell lymphocytosis. *British Journal of Haematology* **2005,** *130* (3), 325-332.
150. Dighiero, G.; Hamblin, T., Chronic lymphocytic leukaemia. *The Lancet* **2008,** *371* (9617), 1017-1029.
151. Rai, K. R.; Sawitsky, A.; Cronkite, E. P.; Chanana, A. D.; Levy, R. N.; Pasternack, B., Clinical staging of chronic lymphocytic leukemia. *Blood* **1975,** *46* (2), 219-234.
152. Binet, J.; Leporrier, M.; Dighiero, G.; Charron, D.; Vaugier, G.; Beral, H. M.; Natali, J. C.; Raphael, M.; Nizet, B.; Follezou, J., A clinical staging system for chronic lymphocytic leukemia. Prognostic significance. *Cancer* **1977,** *40* (2), 855-864.
153. Langerbeins, P.; Bahlo, J.; Rhein, C.; Cramer, P.; Pflug, N.; Fischer, K.; Stilgenbauer, S.; Kreuzer, K. A.; Wendtner, C.-M.; Eichhorst, B., The CLL12 trial protocol: a placebo-controlled double-blind Phase III study of ibrutinib in the treatment of early-stage chronic lymphocytic leukemia patients with risk of early disease progression. *Future Oncology* **2015,** *11* (13), 1895-1903.
154. Hallek, M.; Pflug, N., State of the art treatment of chronic lymphocytic leukaemia. *Blood Reviews* **2011,** *25* (1), 1-9.
155. Greaves, M.; Maley, C. C., Clonal evolution in cancer. *Nature* **2012,** *481* (7381), 306-313.
156. Ten Hacken, E.; Burger, J. A., Microenvironment interactions and B-cell receptor signaling in Chronic Lymphocytic Leukemia: Implications for disease pathogenesis and treatment. *Biochimica et biophysica acta* **2016,** *1863* (3), 401-413.
157. Takahashi, K.; Sivina, M.; Hoellenriegel, J.; Oki, Y.; Hagemeister, F. B.; Fayad, L.; Romaguera, J. E.; Fowler, N.; Fanale, M. A.; Kwak, L. W.; Samaniego, F.; Neelapu, S.; Xiao, L.; Huang, X.; Kantarjian, H.; Keating, M. J.; Wierda, W.; Fu, K.; Chan, W. C.; Vose, J. M.; O'Brien, S.; Davis, R. E.; Burger, J. A., CCL3 and CCL4 are biomarkers for B cell receptor pathway activation and prognostic serum markers in diffuse large B cell lymphoma. *British Journal of Haematology* **2015,** *171* (5), 726-35.

158. O'Reilly, A.; Murphy, J.; Rawe, S.; Garvey, M., Chronic lymphocytic leukemia: a review of front-line treatment options, with a focus on elderly CLL patients. *Clinical Lymphoma Myeloma and Leukemia* **2018,** *18* (4), 249-256.
159. Bergmann, M. A.; Eichhorst, B. F.; Busch, R.; Adorf, D.; Stilgenbauer, S.; Eckart, M. J.; Wendtner, C.-M.; Hallek, M., Prospective Evaluation of Prognostic Parameters in Early Stage Chronic Lymphocytic Leukemia (CLL): Results of the CLL1-Protocol of the German CLL Study Group (GCLLSG). *Blood* **2007,** *110* (11), 625-625.
160. Wiestner, A.; Rosenwald, A.; Barry, T. S.; Wright, G.; Davis, R. E.; Henrickson, S. E.; Zhao, H.; Ibbotson, R. E.; Orchard, J. A.; Davis, Z.; Stetler-Stevenson, M.; Raffeld, M.; Arthur, D. C.; Marti, G. E.; Wilson, W. H.; Hamblin, T. J.; Oscier, D. G.; Staudt, L. M., ZAP-70 expression identifies a chronic lymphocytic leukemia subtype with unmutated immunoglobulin genes, inferior clinical outcome, and distinct gene expression profile. *Blood* **2003,** *101* (12), 4944.
161. Rassenti, L. Z.; Huynh, L.; Toy, T. L.; Chen, L.; Keating, M. J.; Gribben, J. G.; Neuberg, D. S.; Flinn, I. W.; Rai, K. R.; Byrd, J. C., ZAP-70 compared with immunoglobulin heavy-chain gene mutation status as a predictor of disease progression in chronic lymphocytic leukemia. *New England Journal of Medicine* **2004,** *351* (9), 893-901.
162. Suresh, S.; Irvine, A. E., The NOTCH signaling pathway in normal and malignant blood cell production. *Journal of Cell Communication and Signaling* **2015,** *9* (1), 5-13.
163. Cretu, C.; Schmitzová, J.; Ponce-Salvatierra, A.; Dybkov, O.; De Laurentiis, Evelina I.; Sharma, K.; Will, Cindy L.; Urlaub, H.; Lührmann, R.; Pena, V., Molecular Architecture of SF3b and Structural Consequences of Its Cancer-Related Mutations. *Molecular Cell* **2016,** *64* (2), 307-319.
164. Wang, L.; Lawrence, M. S.; Wan, Y.; Stojanov, P.; Sougnez, C.; Stevenson, K.; Werner, L.; Sivachenko, A.; DeLuca, D. S.; Zhang, L.; Zhang, W.; Vartanov, A. R.; Fernandes, S. M.; Goldstein, N. R.; Folco, E. G.; Cibulskis, K.; Tesar, B.; Sievers, Q. L.; Shefler, E.; Gabriel, S.; Hacohen, N.; Reed, R.; Meyerson, M.; Golub, T. R.; Lander, E. S.; Neuberg, D.; Brown, J. R.; Getz, G.; Wu, C. J., SF3B1 and Other Novel Cancer Genes in Chronic Lymphocytic Leukemia. *New England Journal of Medicine* **2011,** *365* (26), 2497-2506.
165. Wierda, W. G.; O'Brien, S.; Wang, X.; Faderl, S.; Ferrajoli, A.; Do, K.-A.; Cortes, J.; Thomas, D.; Garcia-Manero, G.; Koller, C., Prognostic nomogram and index for overall survival in previously untreated patients with chronic lymphocytic leukemia. *Blood* **2007,** *109* (11), 4679-4685.
166. Jaksic, B.; Brugiatelli, M.; Krc, I.; Losonczi, H.; Holowiecki, J.; Planinc-Peraica, A.; Kusec, R.; Morabito, F.; Iacopino, P.; Lutz, D., High dose chlorambucil versus Binet's modified cyclophosphamide, doxorubicin, vincristine, and prednisone regimen in the treatment of patients with advanced B-cell chronic lymphocytic leukemia. *Cancer* **1997,** *79* (11), 2107-2114.
167. Robak, T.; Błoński, J. Z.; Kasznicki, M.; Góra-Tybor, J.; Dmoszyńska, A.; Wojtaszko, M.; Skotnicki, A. B.; Nowak, W.; Hellmann, A.; Lewandowski, K., Comparison of cladribine plus prednisone with chlorambucil plus prednisone in patients with chronic lymphocytic leukemia: Final report of the Polish Adult Leukemia Group (PALGCLL1). *Medical Science Monitor* **2005,** *11* (10), 171-179.
168. Dave, S. S.; Fu, K.; Wright, G. W.; Lam, L. T.; Kluin, P.; Boerma, E.-J.; Greiner, T. C.; Weisenburger, D. D.; Rosenwald, A.; Ott, G.; Müller-Hermelink, H.-K.; Gascoyne, R. D.; Delabie, J.; Rimsza, L. M.; Braziel, R. M.; Grogan, T. M.;

Campo, E.; Jaffe, E. S.; Dave, B. J.; Sanger, W.; Bast, M.; Vose, J. M.; Armitage, J. O.; Connors, J. M.; Smeland, E. B.; Kvaloy, S.; Holte, H.; Fisher, R. I.; Miller, T. P.; Montserrat, E.; Wilson, W. H.; Bahl, M.; Zhao, H.; Yang, L.; Powell, J.; Simon, R.; Chan, W. C.; Staudt, L. M., Molecular Diagnosis of Burkitt's Lymphoma. *New England Journal of Medicine* **2006,** *354* (23), 2431-2442.
169. Armitage, J. O.; Gascoyne, R. D.; Lunning, M. A.; Cavalli, F., Non-Hodgkin lymphoma. *The Lancet* **2017,** *390* (10091), 298-310.
170. CLL Trialists' Collaborative Group, Chemotherapeutic options in chronic lymphocytic leukemia: a meta-analysis of the randomized trials. *Journal of the National Cancer Institute* **1999,** *91* (10), 861-868.
171. Raphael, B.; Andersen, J. W.; Silber, R.; Oken, M.; Moore, D.; Bennett, J.; Bonner, H.; Hahn, R.; Knospe, W. H.; Mazza, J., Comparison of chlorambucil and prednisone versus cyclophosphamide, vincristine, and prednisone as initial treatment for chronic lymphocytic leukemia: long-term follow-up of an Eastern Cooperative Oncology Group randomized clinical trial. *Journal of Clinical Oncology* **1991,** *9* (5), 770-776.
172. Kimby, E.; Mellstedt, H., Chlorambucil/prednisone versus CHOP in symptomatic chronic lymphocytic leukemias of B-cell type. A randomized trial. *Leukemia & lymphoma* **1991,** *5* (sup1), 93-96.
173. Rai, K. R.; Peterson, B. L.; Appelbaum, F. R.; Kolitz, J.; Elias, L.; Shepherd, L.; Hines, J.; Threatte, G. A.; Larson, R. A.; Cheson, B. D., Fludarabine compared with chlorambucil as primary therapy for chronic lymphocytic leukemia. *New England Journal of Medicine* **2000,** *343* (24), 1750-1757.
174. Eichhorst, B. F.; Busch, R.; Hopfinger, G.; Pasold, R.; Hensel, M.; Steinbrecher, C.; Siehl, S.; Jäger, U.; Bergmann, M.; Stilgenbauer, S., Fludarabine plus cyclophosphamide versus fludarabine alone in first-line therapy of younger patients with chronic lymphocytic leukemia. *Blood* **2006,** *107* (3), 885-891.
175. Flinn, I. W.; Neuberg, D. S.; Grever, M. R.; Dewald, G. W.; Bennett, J. M.; Paietta, E. M.; Hussein, M. A.; Appelbaum, F. R.; Larson, R. A.; Moore Jr, D. F., Phase III trial of fludarabine plus cyclophosphamide compared with fludarabine for patients with previously untreated chronic lymphocytic leukemia: US Intergroup Trial E2997. *Journal of Clinical Oncology* **2007,** *25* (7), 793-798.
176. Hallek, M.; Fischer, K.; Fingerle-Rowson, G.; Fink, A. M.; Busch, R.; Mayer, J.; Hensel, M.; Hopfinger, G.; Hess, G.; Von Grünhagen, U., Addition of rituximab to fludarabine and cyclophosphamide in patients with chronic lymphocytic leukaemia: a randomised, open-label, phase 3 trial. *The Lancet* **2010,** *376* (9747), 1164-1174.
177. O'Brien, S. M.; Kantarjian, H.; Thomas, D. A.; Giles, F. J.; Freireich, E. J.; Cortes, J.; Lerner, S.; Keating, M. J., Rituximab dose-escalation trial in chronic lymphocytic leukemia. *Journal of Clinical Oncology* **2001,** *19* (8), 2165-2170.
178. Wiestner, A., Choosing frontline chemoimmunotherapy for CLL. *The Lancet Oncology* **2016,** *17* (7), 852-854.
179. Hale, G.; Bright, S.; Chumbley, G.; Hoang, T.; Metcalf, D.; Munro, A.; Waldmann, H., Removal of T cells from bone marrow for transplantation: a monoclonal antilymphocyte antibody that fixes human complement. *Blood* **1983,** *62* (4), 873-882.
180. Hillmen, P.; Skotnicki, A. B.; Robak, T.; Jaksic, B.; Dmoszynska, A.; Wu, J.; Sirard, C.; Mayer, J., Alemtuzumab compared with chlorambucil as first-line therapy for chronic lymphocytic leukemia. *J Clin Oncol* **2007,** *25* (35), 5616-23.
181. Cancer Trials Ireland *DSSG Digest Autumn 2017*; Dublin, 2017.

182. Lee, H.-Z.; Miller, B. W.; Kwitkowski, V. E.; Ricci, S.; DelValle, P.; Saber, H.; Grillo, J.; Bullock, J.; Florian, J.; Mehrotra, N.; Ko, C.-W.; Nie, L.; Shapiro, M.; Tolnay, M.; Kane, R. C.; Kaminskas, E.; Justice, R.; Farrell, A. T.; Pazdur, R., U.S. Food and Drug Administration Approval: Obinutuzumab in Combination with Chlorambucil for the Treatment of Previously Untreated Chronic Lymphocytic Leukemia. *Clinical Cancer Research* **2014,** *20* (15), 3902-3907.
183. Genentech Incorporated, GAZYVA-Full prescribing information, Healthcare professional resources. https://www.gazyva.com/hcp/cll/resources/professional.html.
184. Rey, J.; Fauriat, C.; Moretta, A.; Costello, R.; Olive, D., Natural killer cells in leukaemia A2 - Lotze, Michael T. In *Natural Killer Cells*, Thomson, A. W., Ed. Academic Press: San Diego, 2010; pp 533-541.
185. Cartron, G.; De Guibert, S.; Dilhuydy, M.-S.; Morschhauser, F.; Leblond, V.; Dupuis, J.; Mahe, B.; Bouabdallah, R.; Lei, G.; Wenger, M., Obinutuzumab (GA101) in relapsed/refractory chronic lymphocytic leukemia: final data from the phase 1/2 GAUGUIN study. *Blood* **2014,** *124* (14), 2196-2202.
186. Goede , V.; Fischer , K.; Busch , R.; Engelke , A.; Eichhorst , B.; Wendtner , C. M.; Chagorova , T.; de la Serna , J.; Dilhuydy , M.-S.; Illmer , T.; Opat , S.; Owen , C. J.; Samoylova , O.; Kreuzer , K.-A.; Stilgenbauer , S.; Döhner , H.; Langerak , A. W.; Ritgen , M.; Kneba , M.; Asikanius , E.; Humphrey , K.; Wenger , M.; Hallek , M., Obinutuzumab plus Chlorambucil in Patients with CLL and Coexisting Conditions. *New England Journal of Medicine* **2014,** *370* (12), 1101-1110.
187. Roberts, A. W.; Davids, M. S.; Pagel, J. M.; Kahl, B. S.; Puvvada, S. D.; Gerecitano, J. F.; Kipps, T. J.; Anderson, M. A.; Brown, J. R.; Gressick, L.; Wong, S.; Dunbar, M.; Zhu, M.; Desai, M. B.; Cerri, E.; Heitner Enschede, S.; Humerickhouse, R. A.; Wierda, W. G.; Seymour, J. F., Targeting BCL2 with Venetoclax in Relapsed Chronic Lymphocytic Leukemia. *New England Journal of Medicine* **2016,** *374* (4), 311-322.
188. AbbVie Limited, Summary of Product Characteristics: Venclyxto 10mg, 50mg and 100mg Film-coated Tablets. http://www.medicines.ie/medicine/17008/SPC/Venclyxto+10mg,+50mg+and+100mg+Film-coated+Tablets/ (accessed 20/10/17).
189. Scheffold, A.; Jebaraj, B. M. C.; Stilgenbauer, S., Venetoclax: Targeting BCL2 in Hematological Cancers. In *Small Molecules in Hematology*, Martens, U. M., Ed. Springer International Publishing: Cham, 2018; pp 215-242.
190. Deeks, E. D., Venetoclax: First Global Approval. *Drugs* **2016,** *76* (9), 979-987.
191. Hughes, D. L., Patent Review of Manufacturing Routes to Oncology Drugs: Carfilzomib, Osimertinib, and Venetoclax. *Organic Process Research & Development* **2016,** *20* (12), 2028-2042.
192. Hexamer, L. A.; Ding, H.; Elmore, S. W.; Kunzer, A. R.; Song, X.; Souers, A. J.; Sullivan, G. M.; Tao, Z.-F.; Wendt, M. D. Apoptosis-inducing agents for the treatment of cancer and immune and autoimmune diseases. 2013.
193. Catron, N.; Chen, S.; Gong, Y.; Zhang, G. G. Salts and crystalline forms of 4-(4-{[2-(4-chlorophenyl)-4,4-dimethylcyclohex-1-en-1-yl]methyl}piperazin-1-yl)-N-({3-nitro-4-[(tetrahydro-2H-pyran-4-ylmethyl)amino]phenyl}-sulfonyl)-2-(1H-pyrrolo[2,3-b]pyridin-5-yloxy)benzamide are suitable active pharmaceutical ingredients for pharmaceutical compositions useful in treatment of a disease characterized by overexpression of one or more anti-apoptotic Bcl-2 family proteins, for example cancer. 2014.
194. Chan, V. S.; Christesen, A. C.; Grieme, T. A.; Ku, Y.-Y.; Mulhern, M. M.; Pu, Y.-M. M. Processes for the preparation of an apoptosis-inducing agent. 2015.

195. Liu, N.; Hoogendoorn, S.; van de Kar, B.; Kaptein, A.; Barf, T.; Driessen, C.; Filippov, D. V.; van der Marel, G. A.; van der Stelt, M.; Overkleeft, H. S., Direct and two-step bioorthogonal probes for Bruton's tyrosine kinase based on ibrutinib: a comparative study. *Organic & Biomolecular Chemistry* **2015,** *13* (18), 5147-5157.
196. Pan, Z.; Scheerens, H.; Li, S. J.; Schultz, B. E.; Sprengeler, P. A.; Burrill, L. C.; Mendonca, R. V.; Sweeney, M. D.; Scott, K. C. K.; Grothaus, P. G.; Jeffery, D. A.; Spoerke, J. M.; Honigberg, L. A.; Young, P. R.; Dalrymple, S. A.; Palmer, J. T., Discovery of Selective Irreversible Inhibitors for Bruton's Tyrosine Kinase. *ChemMedChem* **2007,** *2* (1), 58-61.
197. Byrd , J. C.; Furman , R. R.; Coutre , S. E.; Flinn , I. W.; Burger , J. A.; Blum , K. A.; Grant , B.; Sharman , J. P.; Coleman , M.; Wierda , W. G.; Jones , J. A.; Zhao , W.; Heerema , N. A.; Johnson , A. J.; Sukbuntherng , J.; Chang , B. Y.; Clow , F.; Hedrick , E.; Buggy , J. J.; James , D. F.; O'Brien , S., Targeting BTK with Ibrutinib in Relapsed Chronic Lymphocytic Leukemia. *New England Journal of Medicine* **2013,** *369* (1), 32-42.
198. Janssen-Cilag, Summary of Product Characteristics: Imbruvica 140 mg hard capsules. https://www.medicines.org.uk/emc/medicine/29383#PHARMACODYNAMIC_PROPS (accessed 20/10/17).
199. O'Brien, S.; Furman, R. R.; Coutre, S. E.; Sharman, J. P.; Burger, J. A.; Blum, K. A.; Grant, B.; Richards, D. A.; Coleman, M.; Wierda, W. G., Ibrutinib as initial therapy for elderly patients with chronic lymphocytic leukaemia or small lymphocytic lymphoma: an open-label, multicentre, phase 1b/2 trial. *The Lancet Oncology* **2014,** *15* (1), 48-58.
200. O'Brien, S.; Jones, J. A.; Coutre, S. E.; Mato, A. R.; Hillmen, P.; Tam, C.; Österborg, A.; Siddiqi, T.; Thirman, M. J.; Furman, R. R., Ibrutinib for patients with relapsed or refractory chronic lymphocytic leukaemia with 17p deletion (RESONATE-17): a phase 2, open-label, multicentre study. *The Lancet Oncology* **2016,** *17* (10), 1409-1418.
201. Ding, H. X.; Leverett, C. A.; Kyne Jr, R. E.; Liu, K. K.-C.; Fink, S. J.; Flick, A. C.; O'Donnell, C. J., Synthetic approaches to the 2013 new drugs. *Bioorganic & Medicinal Chemistry* **2015,** *23* (9), 1895-1922.
202. Chen, W.; Loury, D. J.; Mody, T. D. Pyrazolo-pyrimidine inhibitors of bruton's tyrosine kinase. 2010.
203. Xu, X. Method for preparing Ibrutinib, US Patent, US20160264584A1. 2017.
204. Brown, J. R., The PI3K pathway: clinical inhibition in chronic lymphocytic leukemia. *Seminars in oncology* **2016,** *43* (2), 260-264.
205. Vanhaesebroeck, B.; Guillermet-Guibert, J.; Graupera, M.; Bilanges, B., The emerging mechanisms of isoform-specific PI3K signalling. *Nature Reviews Molecular Cell Biology* **2010,** *11* (5), 329.
206. Clayton, E.; Bardi, G.; Bell, S. E.; Chantry, D.; Downes, C. P.; Gray, A.; Humphries, L. A.; Rawlings, D.; Reynolds, H.; Vigorito, E., A crucial role for the p110δ subunit of phosphatidylinositol 3-kinase in B cell development and activation. *Journal of Experimental Medicine* **2002,** *196* (6), 753-763.
207. Gopal, A. K.; Kahl, B. S.; de Vos, S.; Wagner-Johnston, N. D.; Schuster, S. J.; Jurczak, W. J.; Flinn, I. W.; Flowers, C. R.; Martin, P.; Viardot, A., PI3Kδ inhibition by idelalisib in patients with relapsed indolent lymphoma. *New England Journal of Medicine* **2014,** *370* (11), 1008-1018.

208. Yang, Q.; Modi, P.; Ramanathan, S.; Quéva, C.; Gandhi, V., Idelalisib for the treatment of B-cell malignancies. *Expert Opinion on Orphan Drugs* **2015,** *3* (1), 109-123.
209. Gilead Sciences Ltd, Summary of product characteristics-Zydelig 100 mg film-coated tablets. https://www.medicines.org.uk/emc/product/3330/smpc#CLINICAL_PARTS (accessed 17/05/19).
210. Kesicki Edward, A.; Zhichkin, P. Method Of Preparing 3-phenyl-2-[9h-purin-6-ylamino)-methyl]-3h-quinazolin-4-one And Substituted And Related Compounds. WO 2005/113554 A2, 2005/05/12, 2005.
211. Mekala, N.; Buddepu, S. R.; Dehury, S. K.; Moturu, K. M. V. R.; Indukuri, S. K. V.; Vasireddi, U. R.; Parimi, A. R., A novel strategy for the manufacture of idelalisib: controlling the formation of an enantiomer. *RSC Advances* **2018,** *8* (28), 15863-15869.
212. Ferla, S.; Aboraia, A. S.; Brancale, A.; Pepper, C. J.; Zhu, J.; Ochalek, J. T.; DeLuca, H. F.; Simons, C., Small-molecule inhibitors of 25-hydroxyvitamin D-24-hydroxylase (CYP24A1): synthesis and biological evaluation. *Journal of Medicinal Chemistry* **2014,** *57* (18), 7702-7715.
213. Rosenwald, A.; Alizadeh, A. A.; Widhopf, G.; Simon, R.; Davis, R. E.; Yu, X.; Yang, L.; Pickeral, O. K.; Rassenti, L. Z.; Powell, J.; Botstein, D.; Byrd, J. C.; Grever, M. R.; Cheson, B. D.; Chiorazzi, N.; Wilson, W. H.; Kipps, T. J.; Brown, P. O.; Staudt, L. M., Relation of gene expression phenotype to immunoglobulin mutation genotype in B cell chronic lymphocytic leukemia. *Journal of Experimental Medicine* **2001,** *194* (11), 1639-47.
214. Pepper, C.; Thomas, A.; Hoy, T.; Milligan, D.; Bentley, P.; Fegan, C., The vitamin D3 analog EB1089 induces apoptosis via a p53-independent mechanism involving p38 MAP kinase activation and suppression of ERK activity in B-cell chronic lymphocytic leukemia cells in vitro. *Blood* **2003,** *101* (7), 2454-60.
215. Rosemary Siafakas, A.; Richardson, D. R., Growth arrest and DNA damage-45 alpha (GADD45α). *The International Journal of Biochemistry & Cell Biology* **2009,** *41* (5), 986-989.
216. Javelaud, D.; Besançon, F. CDKN1A (cyclin-dependent kinase inhibitor 1A), Atlas of Genetics and Cytogenetics in Oncology and Haematology. http://atlasgeneticsoncology.org/Genes/GC_CDKN1A.html (accessed 20/12/19).
217. Zhu, F.; Khatri, I.; Spaner, D.; Gorczynski, R. M., An autologous tumor vaccine for CLL. *Leukaemia Research* **2018,** *68*, 40-47.
218. Schetelig, J.; Thiede, C.; Bornhäuser, M.; Schwerdtfeger, R.; Kiehl, M.; Beyer, J.; Sayer, H. G.; Kröger, N.; Hensel, M.; Scheffold, C.; Held, T. K.; Höffken, K.; Ho, A. D.; Kienast, J.; Neubauer, A.; Zander, A. R.; Fauser, A. A.; Ehninger, G.; Siegert, W., Evidence of a Graft-Versus-Leukemia Effect in Chronic Lymphocytic Leukemia After Reduced-Intensity Conditioning and Allogeneic Stem-Cell Transplantation: The Cooperative German Transplant Study Group. *Journal of Clinical Oncology* **2003,** *21* (14), 2747-2753.
219. Ribera, J. M.; Vinolas, N.; Urbano-Ispizua, A.; Gallart, T.; Montserrat, E.; Rozman, C., 'Spontaneous' complete remissions in chronic lymphocytic leukemia: Report of three cases and review of the literature. *Blood Cells* **1987,** *12* (2), 471-479.
220. Ziegler-Heitbrock, H. W. L.; Schlag, R.; Flieger, D.; Thiel, E., Favorable response of early stage B CLL patients to treatment with IFN-α2. *Blood* **1989,** *73* (6), 1426-1430.

221. Gitelson, E.; Hammond, C.; Mena, J.; Lorenzo, M.; Buckstein, R.; Berinstein, N. L.; Imrie, K.; Spaner, D. E., Chronic lymphocytic leukemia-reactive T cells during disease progression and after autologous tumor cell vaccines. *Clinical Cancer Research* **2003,** *9* (5), 1656-1665.
222. Coles, S.; Hills, R. K.; Wang, E. C. Y.; Burnett, A. K.; Man, S.; Darley, R. L.; Tonks, A., Expression of CD200 on AML blasts directly suppresses memory T-cell function. *Leukemia* **2012,** *26* (9), 2148.
223. Coles, S.; Wang, E. C. Y.; Man, S.; Hills, R. K.; Burnett, A. K.; Tonks, A.; Darley, R. L., CD200 expression suppresses natural killer cell function and directly inhibits patient anti-tumor response in acute myeloid leukemia. *Leukemia* **2011,** *25* (5), 792.
224. D'Arena, G.; Valvano, L.; Vitale, C.; Coscia, M.; Statuto, T.; Bellesi, S.; Lamorte, D.; Musto, P.; Laurenti, L.; D'Auria, F., CD200 and prognosis in chronic lymphocytic leukemia: Conflicting results. *Leukemia Research* **2019,** *83*, 106169.
225. Novartis Pharmaceuticals, Phase Ib Open-label Study of VAY736 and Ibrutinib in Patients With Chronic Lymphocytic Leukemia (CLL) on Ibrutinib Therapy. https://clinicaltrials.gov/ct2/show/NCT03400176?recrs=abdfm&cond=CLL&rank=5 (accessed 04/02/19).
226. Smulski, C. R.; Eibel, H., BAFF and BAFF-Receptor in B Cell Selection and Survival. *Frontiers in Immunology* **2018,** *9* (2285).
227. Dörner, T.; Posch, M. G.; Li, Y.; Petricoul, O.; Cabanski, M.; Milojevic, J. M.; Kamphausen, E.; Valentin, M.-A.; Simonett, C.; Mooney, L.; Hüser, A.; Gram, H.; Wagner, F. D.; Oliver, S. J., Treatment of primary Sjögren's syndrome with ianalumab (VAY736) targeting B cells by BAFF receptor blockade coupled with enhanced, antibody-dependent cellular cytotoxicity. *Annals of the Rheumatic Diseases* **2019,** *78* (5), 641.
228. Wells, B. G.; Gelenberg, A. J., Chemistry, pharmacology, pharmacokinetics, adverse effects, and efficacy of the antidepressant maprotiline hydrochloride. *Pharmacotherapy: The Journal of Human Pharmacology and Drug Therapy* **1981,** *1* (2), 121-138.
229. Tatsumi, M.; Groshan, K.; Blakely, R. D.; Richelson, E., Pharmacological profile of antidepressants and related compounds at human monoamine transporters. *European Journal of Pharmacology* **1997,** *340* (2–3), 249-258.
230. Richelson, E., Antimuscarinic and other receptor-blocking properties of antidepressants. *Mayo Clinic proceedings. Mayo Clinic* **1983,** *58* (1), 40-46.
231. Gareri, P.; Falconi, U.; De Fazio, P.; De Sarro, G., Conventional and new antidepressant drugs in the elderly. *Progress in neurobiology* **2000,** *61* (4), 353-96.
232. Hajhashemi, V.; Sadeghi, H.; Minaiyan, M.; Movahedian, A.; Talebi, A., Central and peripheral anti-inflammatory effects of maprotiline on carrageenan-induced paw edema in rats. *Inflammation Research* **2010,** *59* (12), 1053-1059.
233. Wilhelm, M.; Schmidt, P., Synthese und Eigenschaften von 1-Aminoalkyl-dibenzo[b, e]bicyclo[2.2.2]octadienen. *Helvetica Chimica Acta* **1969,** *52* (6), 1385-1395.
234. Thomas, C. L., Cristol, S.J., Hauser, J., Mechanisms of Elimination Reactions. V. Preparation and Elimination Reactions of cis- and trans-11,12-Dichloro-9,10-dihydro-9,10-ethanoanthracene. *Journal of the American Chemical Society* **1952,** *74* (2196).
235. Szabó, D.; Szabó Jr, G.; Ocsovszki, I.; Aszalos, A.; Molnár, J., Anti-psychotic drugs reverse multidrug resistance of tumor cell lines and human AML cells ex-vivo. *Cancer Letters* **1999,** *139* (1), 115-119.

236. Salama, A.; Facer, C., Desipramine reversal of chloroquine resistance in wild isolates of Plasmodium falciparum. *Lancet* **1990,** *335* (8682), 164-165.
237. van Schalkwyk, D. A.; Egan, T. J., Quinoline-resistance reversing agents for the malaria parasite Plasmodium falciparum. *Drug Resistance Updates* **2006,** *9* (4–5), 211-226.
238. Alibert, S.; Santelli-Rouvier, C.; Castaing, M.; Berthelot, M.; Spengler, G.; Molnar, J.; Barbe, J., Effects of a series of dihydroanthracene derivatives on drug efflux in multidrug resistant cancer cells. *European journal of medicinal chemistry* **2003,** *38* (3), 253-263.
239. McNamara, Y. M.; Bright, S. A.; Byrne, A. J.; Cloonan, S. M.; McCabe, T.; Williams, D. C.; Meegan, M. J., Synthesis and antiproliferative action of a novel series of maprotiline analogues. *European Journal of Medicinal Chemistry* **2014,** *71*, 333-353.
240. Halimehjani, A. Z.; Namboothiri, I. N.; Hooshmand, S. E., Part I: Nitroalkenes in the synthesis of heterocyclic compounds. *RSC Advances* **2014,** *4* (89), 48022-48084.
241. Ballini, R.; Gabrielli, S.; Palmieri, A., β-Nitroacrylates as an Emerging, Versatile Class of Functionalized Nitroalkenes for the Synthesis of a Variety of Chemicals. *Current Organic Chemistry* **2010,** *14* (1), 65-83.
242. Milner, S. E.; Moody, T. S.; Maguire, A. R., Biocatalytic approaches to the Henry (nitroaldol) reaction. *European Journal of Organic Chemistry* **2012,** *2012* (16), 3059-3067.
243. Noble, A.; Anderson, J. C., Nitro-mannich reaction. *Chemical Reviews* **2013,** *113* (5), 2887-2939.
244. Milhazes, N.; Calheiros, R.; Marques, M. P. M.; Garrido, J.; Cordeiro, M. N. D. S.; Rodrigues, C.; Quinteira, S.; Novais, C.; Peixe, L.; Borges, F., β-Nitrostyrene derivatives as potential antibacterial agents: A structure-property-activity relationship study. *Bioorganic and Medicinal Chemistry* **2006,** *14* (12), 4078-4088.
245. Kim, J. H.; Kim, J. H.; Lee, G. E.; Lee, J. E.; Chung, I. K., Potent inhibition of human telomerase by nitrostyrene derivatives. *Molecular Pharmacology* **2003,** *63* (5), 1117-1124.
246. Wijkander, J.; O'Flaherty, J. T.; Nixon, A. B.; Wykle, R. L., 5-Lipoxygenase products modulate the activity of the 85-kDa phospholipase A2 in human neutrophils. *Journal of Biological Chemistry* **1995,** *270* (44), 26543-26549.
247. Funk, C. D., Prostaglandins and leukotrienes: advances in eicosanoid biology. *Science* **2001,** *294* (5548), 1871-1875.
248. Villar, J.; Lima, F.; Veber, C.; Oliveira, A.; Calgarotto, A.; Marangoni, S.; Da Silva, S., Synthesis and evaluation of nitrostyrene derivative compounds, new snake venom phospholipase A2 inhibitors. *Toxicon* **2008,** *51* (8), 1467-1478.
249. Balsinde, J.; Winstead, M. V.; Dennis, E. A., Phospholipase A2 regulation of arachidonic acid mobilization. *FEBS Letters* **2002,** *531* (1), 2-6.
250. Tsai, C.-H.; Hsieh, P.-W.; Lee, Y.-C.; Wang, C.-H.; Chiu, W.-C.; Lu, C.-W.; Wang, Y.-Y.; Hu, S. C.-S.; Cheng, T.-L.; Yuan, S.-S. F., 3′-Hydroxy-4′-methoxy-β-methyl-β-nitrostyrene inhibits tumor growth through ROS generation and GSH depletion in lung cancer cells. *Life sciences* **2017,** *172*, 19-26.
251. Wu, C.; Sun, M.; Liu, L.; Zhou, G. W., The function of the protein tyrosine phosphatase SHP-1 in cancer. *Gene* **2003,** *306*, 1-12.
252. Pettit, R. K.; Hamel, E.; Verdier-Pinard, P.; Roberson, R. W.; Hazen, K. C.; Pettit, G. R.; Crews, L. C., Antifungal and cancer cell growth inhibitory activities of 1-(3′,4′,5′-trimethoxyphenyl)-2-nitro-ethylene. *Mycoses* **2002,** *45* (3-4), 65-74.
253. Reddy, M. A.; Jain, N.; Yada, D.; Kishore, C.; Vangala, J. R.; P. Surendra, R.; Addlagatta, A.; Kalivendi, S. V.; Sreedhar, B., Design and synthesis of resveratrol-

based nitrovinylstilbenes as antimitotic agents. *Journal of Medicinal Chemistry* **2011,** *54* (19), 6751-6760.
254. He, Y.; Varadarajan, S.; Muñoz-Planillo, R.; Burberry, A.; Nakamura, Y.; Núñez, G., 3,4-Methylenedioxy-β-nitrostyrene Inhibits NLRP3 Inflammasome Activation by Blocking Assembly of the Inflammasome. *Journal of Biological Chemistry* **2014,** *289* (2), 1142-1150.
255. Baldwin, A. G.; Brough, D.; Freeman, S., Inhibiting the Inflammasome: A Chemical Perspective. *Journal of Medicinal Chemistry* **2016,** *59* (5), 1691-1710.
256. Brian, P. W.; Grove, J. F.; McGowan, J. C., Fungistatic Activity of Ethylenic and Acetylenic Compounds. *Nature* **1946,** *158* (4024), 876-876.
257. Worthen, L. R.; Bond, H. W., Antimicrobial Activity of Some β-Nitrostyrenes. *Journal of Pharmaceutical Sciences* **1970,** *59* (8), 1185-1186.
258. Nicoletti, G.; Cornell, H. J.; Hugel, H. M.; White, K. S.; Nguyen, T.; Zalizniak, L.; Nugegoda, D., Synthesis and antimicrobial activity of nitroalkenyl arenes. *Anti-Infective Agents* **2013,** *11* (2), 179-191.
259. Ajiboye, T., 2-(2-Nitrovinyl) furan exacerbates oxidative stress response of Escherichia coli to bacteriostatic and bactericidal antibiotics. *Microbial pathogenesis* **2018,** *116*, 130-134.
260. Cornell, H.; Nguyen, T.; Nicoletti, G.; Jackson, N.; Hügel, H., Comparisons of halogenated β-nitrostyrenes as antimicrobial agents. *Applied Sciences* **2014,** *4* (3), 380-389.
261. List , B., Emil Knoevenagel and the Roots of Aminocatalysis. *Angwandte Chemie International Edition* **2010,** *49*, 1730-1734.
262. Jones , G., The Knoevenagel Condensation. In *Organic Reactions*, John Wiley & Sons Inc.: Hoboken (N.J.), 1967; Vol. 15, pp 204-599.
263. Bruckner, R., *Advanced Organic Chemistry - Reaction Mechanisms.* . Academic Press: London, 2002.
264. Smith, M.; March, J., *March's advanced organic chemistry : reactions, mechanisms, and structure*. Seventh edition / ed.; 2013; p xxv, 2047 pages.
265. Clayden, J.; Greeves, N.; Warren, S. G., *Organic chemistry*. 2nd ed.; Oxford University Press: Oxford, 2012; p xxv, 1234 p.
266. Parker, M. A.; Kurrasch, D. M.; Nichols, D. E., The role of lipophilicity in determining binding affinity and functional activity for 5-HT2A receptor ligands. *Bioorganic & Medicinal Chemistry* **2008,** *16* (8), 4661-4669.
267. Wang, Z., Henry Reaction. In *Comprehensive Organic Name Reactions and Reagents*, John Wiley & Sons Inc.: Hoboken (N.J.), 2010; pp 1383-1387.
268. Luzzio, F. A., The Henry reaction: recent examples. *Tetrahedron* **2001,** *57* (6), 915-945.
269. Bloom, J. D.; Dutia, M. D.; Johnson, B. D.; Wissner, A.; Burns, M. G.; Largis, E. E.; Dolan, J. A.; Claus, T. H., Disodium (R,R)-5-[2-[[2-(3-chlorophenyl)-2-hydroxyethyl]amino]propyl]-1,3-benzodioxole-2,2-dicarboxylate (CL 316,243). A potent .beta.-adrenergic agonist virtually specific for .beta.3 receptors. A promising antidiabetic and antiobesity agent. *Journal of Medicinal Chemistry* **1992,** *35* (16), 3081-3084.
270. Sasai, H.; Suzuki, T.; Arai, S.; Arai, T.; Shibasaki, M., Basic character of rare earth metal alkoxides. Utilization in catalytic carbon-carbon bond-forming reactions and catalytic asymmetric nitroaldol reactions. *Journal of the American Chemical Society* **1992,** *114* (11), 4418-4420.

271. Borah, J. C.; Gogoi, S.; Boruwa, J.; Kalita, B.; Barua, N. C., A highly efficient synthesis of the C-13 side-chain of taxol using Shibasaki's asymmetric Henry reaction. *Tetrahedron Letters* **2004,** *45* (18), 3689-3691.
272. Kühbeck, D.; Mayr, J.; Häring, M.; Hofmann, M.; Quignard, F.; Díaz Díaz, D., Evaluation of the nitroaldol reaction in the presence of metal ion-crosslinked alginates. *New Journal of Chemistry* **2015,** *39* (3), 2306-2315.
273. Carey, F. A.; Sundberg, R. J. Advanced organic chemistry. Part B, Reactions and synthesis.
274. van Schijndel, J.; Canalle, L. A.; Molendijk, D.; Meuldijk, J., The green Knoevenagel condensation: solvent-free condensation of benzaldehydes. *Green Chemistry Letters and Reviews* **2017,** *10* (4), 404-411.
275. Sohtome, Y.; Takemura, N.; Iguchi, T.; Hashimoto, Y.; Nagasawa, K., Diastereoselective Henry Reaction Catalyzed by Guanidine-Thiourea Bifunctional Organocatalyst. *Synlett* **2006,** *2006* (01), 0144-0146.
276. Clayden, J.; Greeves, N.; Warren, S. G., *Organic chemistry*. Oxford University Press: New York, 2012.
277. Bova, S.; Saponara, S.; Rampa, A.; Gobbi, S.; Cima, L.; Fusi, F.; Sgaragli, G.; Cavalli, M.; De Los Rios, C.; Striessnig, J., Anthracene based compounds as new L-type Ca2+ channel blockers: design, synthesis, and full biological profile. *Journal of Medicinal Chemistry* **2009,** *52* (5), 1259-1262.
278. Bonvicini, F.; Manet, I.; Belluti, F.; Gobbi, S.; Rampa, A.; Gentilomi, G. A.; Bisi, A., Targeting the bacterial membrane with a new polycyclic privileged structure: a powerful tool to face Staphylococcus aureus infections. *ACS Infectious Diseases* **2019,** *5* (9), 1524-1534.
279. Bisi, A.; Mokhtar Mahmoud, A.; Allará, M.; Naldi, M.; Belluti, F.; Gobbi, S.; Ligresti, A.; Rampa, A., Polycyclic maleimide-based scaffold as new privileged structure for navigating the cannabinoid system opportunities. *ACS Medicinal Chemistry Letters* **2019,** *10* (4), 596-600.
280. Arya, S.; Kumar, S.; Rani, R.; Kumar, N.; Roy, P.; Sondhi, S. M., Synthesis, anti-inflammatory, and cytotoxicity evaluation of 9, 10-dihydroanthracene-9, 10-α, β-succinimide and bis-succinimide derivatives. *Medicinal Chemistry Research* **2013,** *22* (9), 4278-4285.
281. Rossiter, S.; Kirton, S. B.; Camara, R. Anthracene based compounds and their uses. 2018.
282. Ji, Y.-F.; Huang, H.; Jiang, F.; Ni, R.-Z.; Xiao, M.-B., S100 family signaling network and related proteins in pancreatic cancer. *International Journal of Molecular Medicine* **2014,** *33* (4), 769-776.
283. Diels, O.; Alder, K., Synthesen in der hydroaromatischen Reihe. *Justus Liebigs Annalen der Chemie* **1928,** *460* (1), 98-122.
284. Tasdelen, M. A., Diels–Alder "click" reactions: recent applications in polymer and material science. *Polymer Chemistry* **2011,** *2* (10), 2133-2145.
285. Eliel, E. L.; Mander, L. N.; Wilen, S. H., *Stereochemistry of organic compounds*. Wiley: New York 1994.
286. Sauer, J.; Lang, D.; Mielert, A., The Order of Reactivity of Dienes towards Maleic Anhydride in the Diels-Alder Reaction. *Angewandte Chemie International Edition in English* **1962,** *1* (5), 268-269.
287. Khan, R.; Ningombam, A.; Singh, K. B.; Singh, M. D., Stereoelectronic effects in the Stereoselectivity of the Diels-Alder Reactions: Reactions of Aminoanthracenes with N-phenylmaleimide *Journal of Chemical and Pharmaceutical Research* **2012,** *4* (3), 1532-1538.

288. Nicolaou, K.; Snyder, S. A.; Montagnon, T.; Vassilikogiannakis, G., The Diels–Alder reaction in total synthesis. *Angewandte Chemie International Edition* **2002,** *41* (10), 1668-1698.
289. Alder, K.; Stein, G.; von Budedenbrock, F.; Eckardt, W.; Frercks, W.; Schneider, S., Steric course of addition and substitution reactions, I: Stereochemistry of the diene synthesis. *Justus Liebigs Ann. Chem* **1934,** *514*, 1-33.
290. Pellissier, H., *Chiral Sulfur Ligands: Asymmetric Catalysis*. RSC Publishing: Cambridge, 2009.
291. Laue, T.; Plagens, A., *Named Organic Reactions 2nd Edition*. 2nd ed.; Wiley Chichester, 2005.
292. Seguchi, K.; Sera, A.; Maruyama, K., The Effect of Pressure on the Diels-Alder Reaction. *Bulletin of the Chemical Society of Japan* **1974,** *47* (9), 2242-2246.
293. Matsumoto, K.; Sera, A., Organic Synthesis under High Pressure; II. *Synthesis* **1985,** *1985* (11), 999-1027.
294. Ichihara, A., Discoveries of the Diels-Alderases. In *Studies in Natural Products Chemistry*, Atta ur, R., Ed. Elsevier: 2008; Vol. 34, pp 129-171.
295. Kim, H. J.; Ruszczycky, M. W.; Liu, H.-w., Current developments and challenges in the search for a naturally selected Diels-Alderase. *Current Opinion in Chemical Biology* **2012,** *16* (1), 124-131.
296. Zheng, Q.; Tian, Z.; Liu, W., Recent advances in understanding the enzymatic reactions of [4+2] cycloaddition and spiroketalization. *Current Opinion in Chemical Biology* **2016,** *31*, 95-102.
297. Edward, S. N. Synthesis of nu-aryl-maleimides. 1948.
298. Deshpande, S. R.; Maybhate, S. P.; Likhite, A. P.; Chaudhary, P. M., A facile synthesis of N-substituted maleimides. *Indian Journal of chemistry* **2010,** *49B* (April 2014), 487-488.
299. Garad, D. N.; Tanpure, S. D.; Mhaske, S. B., Radical-mediated dehydrative preparation of cyclic imides using (NH(4))(2)S(2)O(8)–DMSO: application to the synthesis of vernakalant. *Beilstein Journal of Organic Chemistry* **2015,** *11*, 1008-1016.
300. Smith, N. M.; Iyer, K. S.; Corry, B., The confined space inside carbon nanotubes can dictate the stereo-and regioselectivity of Diels–Alder reactions. *Physical Chemistry Chemical Physics* **2014,** *16* (15), 6986-6989.
301. Zhuang, C.; Zhang, W.; Sheng, C.; Zhang, W.; Xing, C.; Miao, Z., Chalcone: A Privileged Structure in Medicinal Chemistry. *Chemical Reviews* **2017**.
302. Orlikova, B.; Tasdemir, D.; Golais, F.; Dicato, M.; Diederich, M., Dietary chalcones with chemopreventive and chemotherapeutic potential. *Genes & nutrition* **2011,** *6* (2), 125-47.
303. Żyszka, B.; Anioł, M.; Lipok, J., Highly effective, regiospecific reduction of chalcone by cyanobacteria leads to the formation of dihydrochalcone: two steps towards natural sweetness. *Microbial Cell Factories* **2017,** *16* (1), 136.
304. K Sahu, N.; S Balbhadra, S.; Choudhary, J.; V Kohli, D., Exploring pharmacological significance of chalcone scaffold: a review. *Current Medicinal Chemistry* **2012,** *19* (2), 209-225.
305. Lin, D.; Xiao, M.; Zhao, J.; Li, Z.; Xing, B.; Li, X.; Kong, M.; Li, L.; Zhang, Q.; Liu, Y., An overview of plant phenolic compounds and their importance in human nutrition and management of type 2 diabetes. *Molecules* **2016,** *21* (10), 1374.
306. Aksöz, B. E.; Ertan, R., Chemical and structural properties of chalcones *FABAD Journal of Pharmaceutical Sciences* **2011,** *36*, 223-242.

307. Singh, P.; Anand, A.; Kumar, V., Recent developments in biological activities of chalcones: A mini review. *European Journal of Medicinal Chemistry* **2014,** *85*, 758-777.
308. Batovska, D. I.; Todorova, I. T., Trends in utilization of the pharmacological potential of chalcones. *Current Clinical Pharmacology* **2010,** *5* (1), 1-29.
309. Salum, L. B.; Altei, W. F.; Chiaradia, L. D.; Cordeiro, M. N.; Canevarolo, R. R.; Melo, C. P.; Winter, E.; Mattei, B.; Daghestani, H. N.; Santos-Silva, M. C., Cytotoxic 3, 4, 5-trimethoxychalcones as mitotic arresters and cell migration inhibitors. *European Journal of Medicinal Chemistry* **2013,** *63*, 501-510.
310. Ducki, S.; Rennison, D.; Woo, M.; Kendall, A.; Chabert, J. F. D.; McGown, A. T.; Lawrence, N. J., Combretastatin-like chalcones as inhibitors of microtubule polymerization. Part 1: Synthesis and biological evaluation of antivascular activity. *Bioorganic & Medicinal Chemistry* **2009,** *17* (22), 7698-7710.
311. Ducki, S.; Mackenzie, G.; Lawrence, N. J.; Snyder, J. P., Quantitative structure− activity relationship (5D-QSAR) study of combretastatin-like analogues as inhibitors of tubulin assembly. *Journal of Medicinal Chemistry* **2005,** *48* (2), 457-465.
312. Dong, J.; Huang, G.; Zhang, Q.; Wang, Z.; Cui, J.; Wu, Y.; Meng, Q.; Li, S., Development of benzochalcone derivatives as selective CYP1B1 inhibitors and anticancer agents. *MedChemComm* **2019**.
313. Lawrence, N. J.; Rennison, D.; McGown, A. T.; Hadfield, J. A., The total synthesis of an aurone isolated from Uvaria hamiltonii: aurones and flavones as anticancer agents. *Bioorganic & Medicinal Chemistry Letters* **2003,** *13* (21), 3759-3763.
314. Park, S.; Kim, E. H.; Kim, J.; Kim, S. H.; Kim, I., Biological evaluation of indolizine-chalcone hybrids as new anticancer agents. *European Journal of Medicinal Chemistry* **2018,** *144*, 435-443.
315. Gomes, M.; Muratov, E.; Pereira, M.; Peixoto, J.; Rosseto, L.; Cravo, P.; Andrade, C.; Neves, B. J. M., Chalcone derivatives: promising starting points for drug design. *Molecules* **2017,** *22* (8), 1210.
316. Pandey, M. K.; Sandur, S. K.; Sung, B.; Sethi, G.; Kunnumakkara, A. B.; Aggarwal, B. B., Butein, a Tetrahydroxychalcone, Inhibits Nuclear Factor (NF)-κB and NF-κB-regulated Gene Expression through Direct Inhibition of IκBα Kinase β on Cysteine 179 Residue. *Journal of Biological Chemistry* **2007,** *282* (24), 17340-17350.
317. Liu, F.; Xia, Y.; Parker, A. S.; Verma, I. M., IKK biology. *Immunol Rev* **2012,** *246* (1), 239-253.
318. Cai, L.; Sutter, B. M.; Li, B.; Tu, B. P., Acetyl-CoA induces cell growth and proliferation by promoting the acetylation of histones at growth genes. *Molecular Cell* **2011,** *42* (4), 426-437.
319. Zhuang, C.; Wu, Z.; Xing, C.; Miao, Z., Small molecules inhibiting Keap1–Nrf2 protein–protein interactions: a novel approach to activate Nrf2 function. *MedChemComm* **2017,** *8* (2), 286-294.
320. Zhuang, C.; Miao, Z.; Sheng, C.; Zhang, W., Updated research and applications of small molecule inhibitors of Keap1-Nrf2 protein-protein interaction: a review. *Current Medicinak Chemistry* **2014,** *21* (16), 1861-1870.
321. Kumar, V.; Kumar, S.; Hassan, M.; Wu, H.; Thimmulappa, R. K.; Kumar, A.; Sharma, S. K.; Parmar, V. S.; Biswal, S.; Malhotra, S. V., Novel chalcone derivatives as potent Nrf2 activators in mice and human lung epithelial cells. *Journal of Medicinal Chemistry* **2011,** *54* (12), 4147-4159.

322. Yang, E. B.; Zhang, K.; Cheng, L. Y.; Mack, P., Butein, a specific protein tyrosine kinase inhibitor. *Biochemical and biophysical research communications* **1998,** *245* (2), 435-8.
323. Claisen, L.; Claparède, A., Condensationen von Ketonen mit Aldehyden. *Berichte der deutschen chemischen Gesellschaft* **1881,** *14* (2), 2460-2468.
324. Mahrwald, R.; Gündogan, B., Highly Regioselective Lewis Acid-Mediated Aldol Additions at the More Encumbered α-Side of Unsymmetrical Ketones. *Journal of the American Chemical Society* **1998,** *120* (2), 413-414.
325. P. James, J.; Ishwar Bhat, K.; More, U. A.; Joshi, S. D., Design, synthesis, molecular modeling, and ADMET studies of some pyrazoline derivatives as shikimate kinase inhibitors. *Medicinal Chemistry Research* **2018,** *27* (2), 546-559.
326. Carey, F. A.; Giuliano, R. M., *Organic chemistry*. 10th ed.; Mc Graw Hill Education: New York, 2017.
327. Smith, M. B., *March's Advanced Organic Chemistry: Reactions, Mechanisms, and Structure*. 5th ed.; J. Wiley and Sons: Hoboken (N.J.), 2014.
328. Wyatt, P.; Warren, S., *Organic Synthesis Strategy and Control*. John Wiley & Sons Inc.: Hoboken (N.J.), 2007.
329. Carey, F. A.; Sundberg, R. J., *Advanced organic chemistry : Part B : reactions and synthesis*. Springer: New York, 2007.
330. Eddarir, S.; Cotelle, N.; Bakkour, Y.; Rolando, C., An efficient synthesis of chalcones based on the Suzuki reaction. *Tetrahedron Letters* **2003,** *44* (28), 5359-5363.
331. Xu, C.; Chen, G.; Huang, X., Chalcones by the Wittig reaction of a stable ylide with aldehydes under microwave irradiation. *Organic Preparations and Procedures International* **1995,** *27* (5), 559-561.
332. Kumar, A.; Sharma, S.; Tripathi, V. D.; Srivastava, S., Synthesis of chalcones and flavanones using Julia–Kocienski olefination. *Tetrahedron* **2010,** *66* (48), 9445-9449.
333. Shotter, R.; Johnston, K.; Jones, J., Reactions of unsaturated acid halides—IV.: Competitive friedel-crafts acylations and alkylations of monohalogenobenzenes by the bifunctional cinnamoyl chloride. *Tetrahedron* **1978,** *34* (6), 741-746.
334. Miyaura, N.; Yamada, K.; Suzuki, A., A new stereospecific cross-coupling by the palladium-catalyzed reaction of 1-alkenylboranes with 1-alkenyl or 1-alkynyl halides. *Tetrahedron Letters* **1979,** *20* (36), 3437-3440.
335. Haddach, M.; McCarthy, J. R., A new method for the synthesis of ketones: The palladium-catalyzed cross-coupling of acid chlorides with arylboronic acids. *Tetrahedron Letters* **1999,** *40* (16), 3109-3112.
336. Wittig, G.; Haag, W., Über Triphenyl-phosphinmethylene als olefinbildende Reagenzien (II. Mitteil. 1). *Chemische Berichte* **1955,** *88* (11), 1654-1666.
337. Wang, Z., Wittig Reaction. In *Comprehensive Organic Name Reactions and Reagents*, John Wiley & Sons Inc.: Hoboken (N.J.), 2010; pp 3031-3042.
338. Bandowe, B. A. M.; Meusel, H., Nitrated polycyclic aromatic hydrocarbons (nitro-PAHs) in the environment – A review. *Science of The Total Environment* **2017,** *581*, 237-257.
339. Wu, R. P.; Hayashi, T.; Cottam, H. B.; Jin, G.; Yao, S.; Wu, C. C.; Rosenbach, M. D.; Corr, M.; Schwab, R. B.; Carson, D. A., Nrf2 responses and the therapeutic selectivity of electrophilic compounds in chronic lymphocytic leukemia. *Proceedings of the National Academy of Sciences* **2010,** *107* (16), 7479-7484.
340. Hassan, S. Y., Synthesis and biological activity of some new pyrazoline and pyrimidine derivatives. *Journal of the Brazilian Chemical Society* **2011,** *22*, 1286-1298.

341. Arshad, M. N.; Asiri, A. M.; Alamry, K. A.; Mahmood, T.; Gilani, M. A.; Ayub, K.; Birinji, A. S., Synthesis, crystal structure, spectroscopic and density functional theory (DFT) study of N-[3-anthracen-9-yl-1-(4-bromo-phenyl)-allylidene]-N-benzenesulfonohydrazine. *Spectrochimica Acta Part A: Molecular and Biomolecular Spectroscopy* **2015,** *142*, 364-374.
342. Larionov, V. A.; Markelova, E. P.; Smol'yakov, A. F.; Savel'yeva, T. y. F.; Maleev, V. I.; Belokon, Y. N., Chiral octahedral complexes of Co(iii) as catalysts for asymmetric epoxidation of chalcones under phase transfer conditions. *RSC Advances* **2015,** *5* (89), 72764-72771.
343. Vázquez-Vuelvas, O. F.; Enriquez-Figueroa, R. A.; Garcia-Ortega, H.; Flores-Alamo, M.; Pineda-Contreras, A., Crystal structure of the chalcone (E)-3-(furan-2-yl)-1-phenylprop-2-en-1-one. *Acta Crystallographica Section E: Crystallographic Communications* **2015,** *71* (2), 161-164.
344. Sun, H.; Khan, A.; Usman, R.; Wang, M., Understanding relationship between stacking modes and optical properties of organic charge transfer cocrystals involving anthracyl chalcones and TCNB. *Journal of Photochemistry and Photobiology A: Chemistry* **2019,** *371*, 315-326.
345. Feng, Q.; Wang, J.; Huan, W.; Shen, C.; Guo, F.; Lu, J.; Diao, G., Polymorphism and configurational isomerism in 3-(9-anthryl)-1-(3-hydroxyphenyl)prop-2-en-1-one. *Journal of Molecular Structure* **2019,** *1195*, 355-363.
346. Yoshizawa, K.; Shioiri, T., Convenient stereoselective synthesis of (Z)-chalcone derivatives from 1, 3-diaryl-2-propynyl silyl ethers. *Tetrahedron letters* **2006,** *47* (28), 4943-4945.
347. Johnson, M. R.; Rickborn, B., Sodium borohydride reduction of conjugated aldehydes and ketones. *The Journal of Organic Chemistry* **1970,** *35* (4), 1041-1045.
348. Mason, T., In memory of Jean-Louis Luche. *Ultrasonics sonochemistry* **2015,** *25*, 4-7.
349. Chan, C.-K.; Tsai, Y.-L.; Chang, M.-Y., Bi(OTf)3 catalyzed disproportionation reaction of cinnamyl alcohols. *Tetrahedron* **2017,** *73* (24), 3368-3376.
350. Luche, J. L., Lanthanides in organic chemistry. 1. Selective 1,2 reductions of conjugated ketones. *Journal of the American Chemical Society* **1978,** *100* (7), 2226-2227.
351. Gemal, A. L.; Luche, J. L., Lanthanoids in organic synthesis. 6. Reduction of .alpha.-enones by sodium borohydride in the presence of lanthanoid chlorides: synthetic and mechanistic aspects. *Journal of the American Chemical Society* **1981,** *103* (18), 5454-5459.
352. Jones-Mensah, E.; Nickerson, L. A.; Deobald, J. L.; Knox, H. J.; Ertel, A. B.; Magolan, J., Cerium-free Luche reduction directed by rehydrated alumina. *Tetrahedron* **2016,** *72* (26), 3748-3753.
353. Forkel, N. V.; Henderson, D. A.; Fuchter, M. J., Calcium-mediated stereoselective reduction of α,β-epoxy ketones. *Tetrahedron Letters* **2014,** *55* (40), 5511-5514.
354. Nakata, T.; Tanaka, T.; Oishi, T., Highly stereoselective synthesis of erythro-α, β-epoxy alcohols by the reduction of α, β-epoxy ketones with zinc borohydride. *Tetrahedron Letters* **1981,** *22* (47), 4723-4726.
355. Lauret, C., Epoxy ketones as versatile building blocks in organic synthesis. *Tetrahedron: Asymmetry* **2001,** *12* (17), 2359-2383.
356. Knorr, L., Einwirkung von Acetessigester auf Phenylhydrazin. *European Journal of Inorganic Chemistry* **1883,** *16* (2), 2597-2599.

357. Varghese, B.; Al-Busafi, S. N.; Suliman, F. O.; Al-Kindy, S. M. J. R. A., Unveiling a versatile heterocycle: pyrazoline–a review. *RSC Advances* **2017,** *7* (74), 46999-47016.
358. Mishra, N.; Sasmal, D., Development of selective and reversible pyrazoline based MAO-B inhibitors: Virtual screening, synthesis and biological evaluation. *Bioorganic & Medicinal Chemistry Letters* **2011,** *21* (7), 1969-1973.
359. George, R. F.; Fouad, M. A.; Gomaa, I. E., Synthesis and cytotoxic activities of some pyrazoline derivatives bearing phenyl pyridazine core as new apoptosis inducers. *European Journal of Medicinal Chemistry* **2016,** *112*, 48-59.
360. Stefanes, N. M.; Toigo, J.; Maioral, M. F.; Jacques, A. V.; Chiaradia-Delatorre, L. D.; Perondi, D. M.; Ribeiro, A. A. B.; Bigolin, Á.; Pirath, I. M. S.; Duarte, B. F., Synthesis of novel pyrazoline derivatives and the evaluation of death mechanisms involved in their antileukemic activity. *Bioorganic & Medicinal Chemistry* **2019,** *27* (2), 375-382.
361. Fioravanti, R.; Bolasco, A.; Manna, F.; Rossi, F.; Orallo, F.; Ortuso, F.; Alcaro, S.; Cirilli, R., Synthesis and biological evaluation of N-substituted-3, 5-diphenyl-2-pyrazoline derivatives as cyclooxygenase (COX-2) inhibitors. *European Journal of Medicinal Chemistry* **2010,** *45* (12), 6135-6138.
362. Jadhav, S. Y.; Shirame, S. P.; Kulkarni, S. D.; Patil, S. B.; Pasale, S. K.; Bhosale, R. B., PEG mediated synthesis and pharmacological evaluation of some fluoro substituted pyrazoline derivatives as antiinflammatory and analgesic agents. *Bioorganic & Medicinal Chemistry Letters* **2013,** *23* (9), 2575-2578.
363. Kumar, G.; Tanwar, O.; Kumar, J.; Akhter, M.; Sharma, S.; Pillai, C.; Alam, M. M.; Zama, M., Pyrazole-pyrazoline as promising novel antimalarial agents: A mechanistic study. *European Journal of Medicinal Chemistry* **2018,** *149*, 139-147.
364. Unsal-Tan, O.; Küçükkılınç, T. T.; Ayazgök, B.; Balkan, A.; Ozadali-Sari, K., Synthesis, molecular docking, and biological evaluation of novel 2-pyrazoline derivatives as multifunctional agents for the treatment of Alzheimer's disease. *MedChemComm* **2019**.
365. Kitawat, B. S.; Singh, M., Synthesis, characterization, antibacterial, antioxidant, DNA binding and SAR study of a novel pyrazine moiety bearing 2-pyrazoline derivatives. *New Journal of Chemistry* **2014,** *38* (9), 4290-4299.
366. Kemnitz, C. R.; Loewen, M. J., "Amide Resonance" Correlates with a Breadth of C− N Rotation Barriers. *Journal of the American Chemical Society* **2007,** *129* (9), 2521-2528.
367. Dastoorani, P.; Maghsoodlou, M. T.; Khalilzadeh, M. A.; Sarina, E., Synthesis of new dibenzofuran derivatives via Diels–Alder reaction of euparin with activated acetylenic esters. *Tetrahedron Letters* **2016,** *57* (3), 314-316.
368. Loftsson, T., *Drug stability for pharmaceutical scientists*. 1st ed.; Academic Press: Oxford, 2014.
369. Wong, A. W.; Datla, A., Chapter 13 - Assay and Stability Testing. In *Separation Science and Technology*, Ahuja, S.; Dong, M. W., Eds. Academic Press: 2005; Vol. 6, pp 335-358.
370. European Medicines Agency (EMA) *ICH Q1A (R2) Harmonised Tripartite Guideline , Stability testing of new drug substances and products*; London, 2003.
371. Snyder, L. R.; Kirkland, J. J.; Glajch, J. L., *Practical HPLC method development*. 2nd ed.; John Wiley & Sons: Hoboken, (N.J.), 2012.
372. Singh, R., HPLC method development and validation-an overview. *Journal of Pharmaceutical Education & Research* **2013,** *4* (1).

373. Chan, C. C.; Lee, Y.; Lam, H.; Zhang, X.-M., *Analytical method validation and instrument performance verification*. John Wiley & Sons: 2004.
374. Sato, Y.; Kojima, T.; Goto, T.; Oomikawa, R.; Watanabe, H.; Wakabayashi, K., Hydrolysis and phytotoxic activity of cyclic imides. *Agricultural and Biological Chemistry* **1991,** *55* (11), 2677-2681.
375. US National Library of Medicine-National Centre for Biotechnology Information, PubChem: Compound Summary-beta Nitrostyrene https://pubchem.ncbi.nlm.nih.gov/compound/beta-Nitrostyrene (accessed 05/07/19).
376. Royal Society of Chemistry, ChemSpider: trans-β-Nitrostyrene. http://www.chemspider.com/Chemical-Structure.4447524.html?rid=07ebe006-9b68-461a-9b99-cd680057f26a&page_num=0 (accessed 02/06/19).
377. Shriner, R.; Kurosawa, T., Chalcones. ii. decomposition by alkali. *Journal of the American Chemical Society* **1930,** *52* (6), 2538-2540.
378. Leibniz InstituteDSMZ-German Collection of Microorganisms and Cell Cultures, HG-3 (ACC 765). https://www.dsmz.de/collection/catalogue/details/culture/ACC-765 (accessed 14/10/19).
379. Rosén, A.; Bergh, A.-C.; Gogok, P.; Evaldsson, C.; Myhrinder, A. L.; Hellqvist, E.; Rasul, A.; Björkholm, M.; Jansson, M.; Mansouri, L. J. O., Lymphoblastoid cell line with B1 cell characteristics established from a chronic lymphocytic leukemia clone by in vitro EBV infection. *Oncoimmunology* **2012,** *1* (1), 18-27.
380. Leibniz Institute, DSMZ-German Collection of Microorganisms and Cell Cultures, PGA-1 (ACC 766). https://www.dsmz.de/collection/catalogue/details/culture/ACC-766 (accessed 14/10/19).
381. Lanemo Myhrinder, A.; Hellqvist, E.; Bergh, A.-C.; Jansson, M.; Nilsson, K.; Hultman, P.; Jonasson, J.; Buhl, A. M.; Bredo Pedersen, L.; Jurlander, J., Molecular characterization of neoplastic and normal "sister" lymphoblastoid B-cell lines from chronic lymphocytic leukemia. *Leukemia & Lymphoma* **2013,** *54* (8), 1769-1779.
382. Byrne, A. J. Design, synthesis and biochemical evaluation of novel anthracenes, ethanoanthracenes and related compounds to target Burkitt's lymphoma (PhD Thesis). Trinity College Dublin, 2015.
383. Elkamhawy, A.; Park, J.-e.; Cho, N.-C.; Sim, T.; Pae, A. N.; Roh, E. J., Discovery of a broad spectrum antiproliferative agent with selectivity for DDR1 kinase: cell line-based assay, kinase panel, molecular docking, and toxicity studies. *Journal of Enzyme Inhibition and Medicinal Chemistry* **2016,** *31* (1), 158-166.
384. National Cancer Institute (NCI), NCI-60 Screening Methodology. https://dtp.cancer.gov/discovery_development/nci-60/methodology.htm (accessed 01/11/19).
385. Cleaveland, E. S.; Monks, A.; Vaigro-Wolff, A.; Zaharevitz, D. W.; Paull, K.; Ardalan, K.; Cooney, D. A.; Ford Jr, H., Site of action of two novel pyrimidine biosynthesis inhibitors accurately predicted by the COMPARE program. *Biochemical Pharmacology* **1995,** *49* (7), 947-954.
386. National Center for Biotechnology Information (NCBI), PubChem Database-Diacetoxyscirpenol, CID=91518. https://pubchem.ncbi.nlm.nih.gov/compound/Diacetoxyscirpenol (accessed 21/10/19).
387. Knutsen, H. K.; Alexander, J.; Barregård, L.; Bignami, M.; Brüschweiler, B.; Ceccatelli, S.; Cottrill, B.; Dinovi, M.; Grasl-Kraupp, B., Risk to human and animal

health related to the presence of 4, 15-diacetoxyscirpenol in food and feed. *EFSA Journal* **2018,** *16* (8), e05367.
388. Dorr, R. T., Bleomycin pharmacology: mechanism of action and resistance, and clinical pharmacokinetics. *Seminars in oncology* **1992,** *19* (2 Suppl 5), 3-8.
389. National Center for Biotechnology Information (NCBI), PubChem Database-Bleomycin, CID=5460769,. https://pubchem.ncbi.nlm.nih.gov/compound/Bleomycin (accessed 21/10/19).
390. Moore, E. C.; Booth, B. A.; Sartorelli, A. C., Inhibition of Deoxyribonucleotide Synthesis by Pyridine Carboxaldehyde Thiosemicarbazones. *Cancer Research* **1971,** *31* (3), 235.
391. Head, R. J.; Fay, M. F.; Cosgrove, L.; Y C Fung, K.; Rundle-Thiele, D.; Martin, J. H., Persistence of DNA adducts, hypermutation and acquisition of cellular resistance to alkylating agents in glioblastoma. *Cancer Biology & Therapy* **2017,** *18* (12), 917-926.
392. National Center for Biotechnology Information (NCBI), PubChem Database-2-Amino-6-methoxypurine, CID=65275. https://pubchem.ncbi.nlm.nih.gov/compound/2-Amino-6-methoxypurine (accessed 22/10/19).
393. Wiek, C.; Schmidt, E. M.; Roellecke, K.; Freund, M.; Nakano, M.; Kelly, E. J.; Kaisers, W.; Yarov-Yarovoy, V.; Kramm, C. M.; Rettie, A. E.; Hanenberg, H., Identification of amino acid determinants in CYP4B1 for optimal catalytic processing of 4-ipomeanol. *Biochem J* **2015,** *465* (1), 103-114.
394. Skeel, R. T.; Sawicki, W. L.; Cashmore, A. R.; Bertino, J. R., Inhibition of DNA Synthesis in Normal and Malignant Human Cells by Triazinate (Baker's Antifol) and Methotrexate. *Cancer Research* **1976,** *36* (10), 3659.
395. (NCBI), N. C. f. B. I. PubChem Database-Tamoxifen, CID=2733526. https://pubchem.ncbi.nlm.nih.gov/compound/Tamoxifen (accessed 22/10/19).
396. Plagemann, P. G.; Graff, J. C.; Behrens, M., Mechanism of action of inosine dialdehyde (NSC 118994) in the inhibition of proliferation of tumor cells in culture. *Cancer Research* **1977,** *37* (7 Pt 1), 2188-95.
397. Cory, J. G.; Parker, S. H.; Fox, C. S., Inhibition of RNA Synthesis in Ehrlich Tumor Cells by the Dialdehyde Derivative of Inosine (NSC 118994). *Cancer Research* **1978,** *38* (3), 815.
398. National Center for Biotechnology Information (NCBI), PubChem Database. Pentostatin, CID=439693. https://pubchem.ncbi.nlm.nih.gov/compound/Pentostatin (accessed 23/10/19).
399. Wishart, D. S.; Feunang, Y. D.; Guo, A. C.; Lo, E. J.; Marcu, A.; Grant, J. R.; Sajed, T.; Johnson, D.; Li, C.; Sayeeda, Z., DrugBank 5.0: a major update to the DrugBank database for 2018. *Nucleic Acids Research* **2017,** *46* (D1), 1074-1082.
400. National Center for Biotechnology Information., C. PubChem Database-Caracemide. https://pubchem.ncbi.nlm.nih.gov/compound/Caracemide (accessed 23/10/19).
401. National Cancer Institute (NCI), C29042: Fluorodopan, NCIt Antineoplastic Agent Terminology. https://ncithesaurus.nci.nih.gov/ncitbrowser/ConceptReport.jsp?dictionary=NCI_Thesaurus&version=20.10d&code=C29042&ns=ncit (accessed 02/4/19).
402. National Cancer Institute (NCI), NCI Drug dictionary, Hydroxyurea. https://www.cancer.gov/publications/dictionaries/cancer-drug/def/hydroxyurea (accessed 16/5/19).
403. Krajewska, M.; Zapata, J. M.; Meinhold-Heerlein, I.; Hedayat, H.; Monks, A.; Bettendorf, H.; Shabaik, A.; Bubendorf, L.; Kallioniemi, O.-P.; Kim, H.;

Reifenberger, G.; Reed, J. C.; Krajewski, S., Expression of Bcl-2 Family Member Bid in Normal and Malignant Tissues. *Neoplasia* **2002,** *4* (2), 129-140.
404. Drugbank ,Glyoxylic acid. https://www.drugbank.ca/drugs/DB04343 (accessed 04/11/19).
405. Kelsen, D.; Scher, H.; Alcock, N.; Leyland-Jones, B.; Donner, A.; Williams, L.; Greene, G.; Burchenal, J.; Tan, C.; Philips, F., Phase I clinical trial and pharmacokinetics of 4′-carboxyphthalato-(1, 2-diaminocyclohexane) platinum (II). *Cancer Research* **1982,** *42* (11), 4831-4835.
406. Johnstone, T. C.; Park, G. Y.; Lippard, S. J., Understanding and improving platinum anticancer drugs--phenanthriplatin. *Anticancer Res* **2014,** *34* (1), 471-476.
407. Decker, T.; Lohmann-Matthes, M.-L., A quick and simple method for the quantitation of lactate dehydrogenase release in measurements of cellular cytotoxicity and tumor necrosis factor (TNF) activity. *Journal of Immunological Methods* **1988,** *115* (1), 61-69.
408. Nachlas, M. M.; Margulies, S. I.; Goldberg, J. D.; Seligman, A. M., The determination of lactic dehydrogenase with a tetrazolium salt. *Analytical Biochemistry* **1960,** *1* (4-5), 317-326.
409. Thermo Scientific, Pierce LDH Cytotoxicity Assay Kit (product insert). 2015.
410. Gupta, A.; Moore, J. A., Tumor Lysis Syndrome. *JAMA Oncology* **2018,** *4* (6), 895-895.
411. Schlegel, R.; Williamson, P., Phosphatidylserine, a death knell. *Cell Death and Differentiation* **2001,** *8* (6), 551.
412. Segawa, K.; Nagata, S., An Apoptotic 'Eat Me' Signal: Phosphatidylserine Exposure. *Trends in Cell Biology* **2015,** *25* (11), 639-650.
413. Mariño, G.; Kroemer, G., Mechanisms of apoptotic phosphatidylserine exposure. *Cell Research* **2013,** *23* (11), 1247-1248.
414. National Centre for Biotechnology Information, ANXA5 annexin A5 [Homo sapiens (human)] (NCBI). https://www.ncbi.nlm.nih.gov/gene/308 (accessed 15/08/2017).
415. Rieger, A. M.; Nelson, K. L.; Konowalchuk, J. D.; Barreda, D. R., Modified Annexin V/Propidium Iodide Apoptosis Assay For Accurate Assessment of Cell Death. *Journal of Visualized Experiments : JoVE* **2011,** (50), 2597.
416. Wilkins, R.; Kutzner, B.; Truong, M.; Sanchez-Dardon, J.; McLean, J., Analysis of radiation-induced apoptosis in human lymphocytes: flow cytometry using Annexin V and propidium iodide versus the neutral comet assay. *Cytometry Part A* **2002,** *48* (1), 14-19.
417. Nathan, C.; Ding, A., SnapShot: Reactive Oxygen Intermediates (ROI). *Cell* **2010,** *140* (6), 951-951.e2.
418. Finkel, T.; Holbrook, N. J., Oxidants, oxidative stress and the biology of ageing. *Nature* **2000,** *408* (6809), 239-47.
419. Redza-Dutordoir, M.; Averill-Bates, D. A., Activation of apoptosis signalling pathways by reactive oxygen species. *Biochimica et Biophysica Acta (BBA) - Molecular Cell Research* **2016,** *1863* (12), 2977-2992.
420. Djordjević, V. B., Free Radicals in Cell Biology. In *International Review of Cytology*, Academic Press: 2004; Vol. 237, pp 57-89.
421. Thimraj, T. A.; George, L.; Asrafuzzaman, S.; Upadhyay, S.; Ganguly, K., Chapter 7 - Oxidative Signaling in Chronic Obstructive Airway Diseases. In *Immunity and Inflammation in Health and Disease*, Chatterjee, S.; Jungraithmayr, W.; Bagchi, D., Eds. Academic Press: 2018; pp 79-98.

422. Messner, D. J.; Murray, K. F.; Kowdley, K. V., Chapter 55 - Mechanisms of Hepatocyte Detoxification. In *Physiology of the Gastrointestinal Tract (Fifth Edition)*, Johnson, L. R.; Ghishan, F. K.; Kaunitz, J. D.; Merchant, J. L.; Said, H. M.; Wood, J. D., Eds. Academic Press: Boston, 2012; pp 1507-1527.
423. Lumb, A. B., Chapter 24 - Oxygen Toxicity and Hyperoxia. In *Nunn's Applied Respiratory Physiology (Eighth Edition)*, Lumb, A. B., Ed. Elsevier: 2017; pp 341-356.e2.
424. Aldred, E. M.; Buck, C.; Vall, K., Chapter 7 - Free radicals. In *Pharmacology*, Aldred, E. M.; Buck, C.; Vall, K., Eds. Churchill Livingstone: Edinburgh, 2009; pp 41-52.
425. Corso, C. R.; Acco, A., Glutathione system in animal model of solid tumors: From regulation to therapeutic target. *Critical reviews in oncology/hematology* **2018,** *128*, 43-57.
426. Zhang, H.; Limphong, P.; Pieper, J.; Liu, Q.; Rodesch, C. K.; Christians, E.; Benjamin, I. J., Glutathione-dependent reductive stress triggers mitochondrial oxidation and cytotoxicity. *The FASEB Journal* **2012,** *26* (4), 1442-1451.
427. Lu, J.; Holmgren, A., The thioredoxin antioxidant system. *Free Radical Biology and Medicine* **2014,** *66*, 75-87.
428. Chae, H. Z.; Chung, S. J.; Rhee, S. G., Thioredoxin-dependent peroxide reductase from yeast. *Journal of Biological Chemistry* **1994,** *269* (44), 27670-27678.
429. Rhee, S. G.; Woo, H. A.; Kil, I. S.; Bae, S. H., Peroxiredoxin Functions as a Peroxidase and a Regulator and Sensor of Local Peroxides. *Journal of Biological Chemistry* **2012,** *287* (7), 4403-4410.
430. Rhee, S. G.; Chae, H. Z.; Kim, K., Peroxiredoxins: A historical overview and speculative preview of novel mechanisms and emerging concepts in cell signaling. *Free Radical Biology and Medicine* **2005,** *38* (12), 1543-1552.
431. Perkins, A.; Nelson, K. J.; Parsonage, D.; Poole, L. B.; Karplus, P. A., Peroxiredoxins: guardians against oxidative stress and modulators of peroxide signaling. *Trends in Biochemical Sciences* **2015,** *40* (8), 435-45.
432. Smirnoff, N., Ascorbic acid metabolism and functions: A comparison of plants and mammals. *Free Radical Biology and Medicine* **2018,** *122*, 116-129.
433. Peh, H. Y.; Tan, W. S. D.; Liao, W.; Wong, W. S. F., Vitamin E therapy beyond cancer: Tocopherol versus tocotrienol. *Pharmacology & Therapeutics* **2016,** *162*, 152-169.
434. O'Donnell-Tormey, J.; Nathan, C. F.; Lanks, K.; DeBoer, C. J.; de la Harpe, J., Secretion of pyruvate. An antioxidant defense of mammalian cells. *Journal of Experimental Medicine* **1987,** *165* (2), 500-14.
435. Nathan, C.; Cunningham-Bussel, A., Beyond oxidative stress: an immunologist's guide to reactive oxygen species. *Nature Reviews Immunology* **2013,** *13*, 349.
436. Panieri, E.; Santoro, M., ROS homeostasis and metabolism: a dangerous liason in cancer cells. *Cell Death & Disease* **2016,** *7* (6), e2253.
437. Vander Heiden, M. G., Targeting cancer metabolism: a therapeutic window opens. *Nature Reviews Drug Discovery* **2011,** *10*, 671.
438. Sanderson, S. M.; Locasale, J. W., Revisiting the Warburg Effect: Some Tumors Hold Their Breath. *Cell Metabolism* **2018,** *28* (5), 669-670.
439. Liberti, M. V.; Locasale, J. W., The Warburg Effect: How Does it Benefit Cancer Cells? *Trends in Biochemical Sciences* **2016,** *41* (3), 211-218.

440. Slavov, N.; Budnik, B. A.; Schwab, D.; Airoldi, E. M.; van Oudenaarden, A., Constant growth rate can be supported by decreasing energy flux and increasing aerobic glycolysis. *Cell Reports* **2014,** *7* (3), 705-714.
441. Shestov, A. A.; Liu, X.; Ser, Z.; Cluntun, A. A.; Hung, Y. P.; Huang, L.; Kim, D.; Le, A.; Yellen, G.; Albeck, J. G.; Locasale, J. W., Quantitative determinants of aerobic glycolysis identify flux through the enzyme GAPDH as a limiting step. *eLife* **2014,** *3*, e03342.
442. Epstein, T.; Gatenby, R. A.; Brown, J. S., The Warburg effect as an adaptation of cancer cells to rapid fluctuations in energy demand. *PLoS ONE* **2017,** *12* (9), e0185085.
443. Vander Heiden, M. G.; Cantley, L. C.; Thompson, C. B., Understanding the Warburg effect: the metabolic requirements of cell proliferation. *Science* **2009,** *324* (5930), 1029-1033.
444. Boroughs, L. K.; DeBerardinis, R. J., Metabolic pathways promoting cancer cell survival and growth. *Nature Cell Biology* **2015,** *17* (4), 351.
445. Arteaga, C. L.; Sliwkowski, M. X.; Osborne, C. K.; Perez, E. A.; Puglisi, F.; Gianni, L., Treatment of HER2-positive breast cancer: current status and future perspectives. *Nature Reviews Clinical Oncology* **2012,** *9* (1), 16.
446. Corbet, C.; Feron, O., Tumour acidosis: from the passenger to the driver's seat. *Nature Reviews Cancer* **2017,** *17*, 577.
447. Estrella, V.; Chen, T.; Lloyd, M.; Wojtkowiak, J.; Cornnell, H. H.; Ibrahim-Hashim, A.; Bailey, K.; Balagurunathan, Y.; Rothberg, J. M.; Sloane, B. F.; Johnson, J.; Gatenby, R. A.; Gillies, R. J., Acidity Generated by the Tumor Microenvironment Drives Local Invasion. *Cancer Research* **2013,** *73* (5), 1524.
448. Vaupel, P.; Schmidberger, H.; Mayer, A., The Warburg effect: essential part of metabolic reprogramming and central contributor to cancer progression. *International Journal of Radiation Biology* **2019**, 1-8.
449. Chang, C.-H.; Curtis, Jonathan D.; Maggi, Leonard B.; Faubert, B.; Villarino, Alejandro V.; O'Sullivan, D.; Huang, Stanley C.-C.; van der Windt, Gerritje J. W.; Blagih, J.; Qiu, J.; Weber, Jason D.; Pearce, Edward J.; Jones, Russell G.; Pearce, Erika L., Posttranscriptional Control of T Cell Effector Function by Aerobic Glycolysis. *Cell* **2013,** *153* (6), 1239-1251.
450. Hamanaka, R. B.; Chandel, N. S., Warburg Effect and Redox Balance. *Science* **2011,** *334* (6060), 1219.
451. Gorrini, C.; Harris, I. S.; Mak, T. W., Modulation of oxidative stress as an anticancer strategy. *Nature Reviews Drug Discovery* **2013,** *12*, 931.
452. Schieber, M.; Chandel, Navdeep S., ROS Function in Redox Signaling and Oxidative Stress. *Current Biology* **2014,** *24* (10), 453-462.
453. Kong, H.; Chandel, N. S., Regulation of redox balance in cancer and T cells. *Journal of Biological Chemistry* **2018,** *293* (20), 7499-7507.
454. Zhu, J.; Thompson, C. B., Metabolic regulation of cell growth and proliferation. *Nature Reviews Molecular Cell Biology* **2019**, 1.
455. Lewis, C. A.; Parker, S. J.; Fiske, B. P.; McCloskey, D.; Gui, D. Y.; Green, C. R.; Vokes, N. I.; Feist, A. M.; Vander Heiden, M. G.; Metallo, C. M., Tracing compartmentalized NADPH metabolism in the cytosol and mitochondria of mammalian cells. *Molecular Cell* **2014,** *55* (2), 253-263.
456. Liu, X.-l.; Ding, J.; Meng, L.-h., Oncogene-induced senescence: a double edged sword in cancer. *Acta Pharmacologica Sinica* **2018,** *39* (10), 1553-1558.

457. Ye, J.; Fan, J.; Venneti, S.; Wan, Y.-W.; Pawel, B. R.; Zhang, J.; Finley, L. W.; Lu, C.; Lindsten, T.; Cross, J. R., Serine catabolism regulates mitochondrial redox control during hypoxia. *Cancer Discovery* **2014,** *4* (12), 1406-1417.
458. Fan, J.; Ye, J.; Kamphorst, J. J.; Shlomi, T.; Thompson, C. B.; Rabinowitz, J. D., Quantitative flux analysis reveals folate-dependent NADPH production. *Nature* **2014,** *510* (7504), 298.
459. Liu, X.-S.; Little, J. B.; Yuan, Z.-M., Glycolytic metabolism influences global chromatin structure. *Oncotarget* **2015,** *6* (6), 4214-4225.
460. Cluntun, A. A.; Huang, H.; Dai, L.; Liu, X.; Zhao, Y.; Locasale, J. W., The rate of glycolysis quantitatively mediates specific histone acetylation sites. *Cancer & Metabolism* **2015,** *3* (1), 10.
461. Sebastián, C.; Mostoslavsky, R., The Various Metabolic Sources of Histone Acetylation. *Trends in Endocrinology & Metabolism* **2017,** *28* (2), 85-87.
462. Yu, X.; Ma, R.; Wu, Y.; Zhai, Y.; Li, S., Reciprocal Regulation of Metabolic Reprogramming and Epigenetic Modifications in Cancer. *Front Genet* **2018,** *9*, 394-394.
463. Wellen, K. E.; Hatzivassiliou, G.; Sachdeva, U. M.; Bui, T. V.; Cross, J. R.; Thompson, C. B., ATP-citrate lyase links cellular metabolism to histone acetylation. *Science* **2009,** *324* (5930), 1076-1080.
464. Nieborak, A.; Schneider, R., Metabolic intermediates – Cellular messengers talking to chromatin modifiers. *Molecular Metabolism* **2018,** *14*, 39-52.
465. Wellen, K. E.; Thompson, C. B., A two-way street: reciprocal regulation of metabolism and signalling. *Nature Reviews Molecular Cell Biology* **2012,** *13*, 270.
466. Bezerra, D. P.; Pessoa, C.; de Moraes, M. O.; Saker-Neto, N.; Silveira, E. R.; Costa-Lotufo, L. V., Overview of the therapeutic potential of piplartine (piperlongumine). *European Journal of Pharmaceutical Sciences* **2013,** *48* (3), 453-463.
467. Lee, S. W.; Mandinova, A. Methods for the treatment of cancer using piperlongumine and piperlongumine analogs. U.S Patent 2009312373, Dec 17. 2009.
468. Adams, D. J.; Dai, M.; Pellegrino, G.; Wagner, B. K.; Stern, A. M.; Shamji, A. F.; Schreiber, S. L., Synthesis, cellular evaluation, and mechanism of action of piperlongumine analogs. *Proceedings of the National Academy of Sciences* **2012,** *109* (38), 15115.
469. Duan, C.; Zhang, B.; Deng, C.; Cao, Y.; Zhou, F.; Wu, L.; Chen, M.; Shen, S.; Xu, G.; Zhang, S.; Duan, G.; Yan, H.; Zou, X., Piperlongumine induces gastric cancer cell apoptosis and G2/M cell cycle arrest both in vitro and in vivo. *Tumour Biology* **2016,** *37* (8), 10793-10804.
470. Piska, K.; Gunia-Krzyżak, A.; Koczurkiewicz, P.; Wójcik-Pszczoła, K.; Pękala, E., Piperlongumine (piplartine) as a lead compound for anticancer agents–Synthesis and properties of analogues. *European Journal of Medicinal Chemistry* **2018**.
471. Avendaño, C.; Menendez, J. C., *Medicinal chemistry of anticancer drugs*. 2nd ed.; Elsevier: Amsterdam, 2015.
472. Sigman, D. S.; Graham, D. R.; D'Aurora, V.; Stern, A. M., Oxygen-dependent cleavage of DNA by the 1,10-phenanthroline . cuprous complex. Inhibition of Escherichia coli DNA polymerase I. *Journal of Biological Chemistry* **1979,** *254* (24), 12269-72.
473. Sigman, D. S.; Mazumder, A.; Perrin, D. M., Chemical nucleases. *Chemical Reviews* **1993,** *93* (6), 2295-2316.

474. Englinger, B.; Pirker, C.; Heffeter, P.; Terenzi, A.; Kowol, C. R.; Keppler, B. K.; Berger, W., Metal Drugs and the Anticancer Immune Response. *Chemical Reviews* **2019,** *119* (2), 1519-1624.
475. Kellett, A.; Molphy, Z.; McKee, V.; Slator, C., Recent Advances in Anticancer Copper Compounds. In *Metal-based Anticancer Agents*, RSC Publishing: Cambridge, 2019; pp 91-119.
476. Wehbe, M.; Leung, A. W.; Abrams, M. J.; Orvig, C.; Bally, M. B., A Perspective–can copper complexes be developed as a novel class of therapeutics? *Dalton Transactions* **2017,** *46* (33), 10758-10773.
477. Hartmann, J. T.; Lipp, H.-P., Toxicity of platinum compounds. *Expert Opinion on Pharmacotherapy* **2003,** *4* (6), 889-901.
478. Nathan, C.; Cunningham-Bussel, A., Beyond oxidative stress: an immunologist's guide to reactive oxygen species. *Nature Reviews Immunology* **2013,** *13* (5), 349.
479. Gorrini, C.; Harris, I. S.; Mak, T. W., Modulation of oxidative stress as an anticancer strategy. *Nature Reviews Drug discovery* **2013,** *12* (12), 931.
480. Mace, P. D.; Riedl, S. J.; Salvesen, G. S., Chapter Seven - Caspase Enzymology and Activation Mechanisms. In *Methods in Enzymology*, Ashkenazi, A.; Yuan, J.; Wells, J. A., Eds. Academic Press: San Diego, 2014; Vol. 544, pp 161-178.
481. Morgan, C. W.; Julien, O.; Unger, E. K.; Shah, N. M.; Wells, J. A., Chapter Eight - Turning on Caspases with Genetics and Small Molecules. In *Methods in Enzymology*, Ashkenazi, A.; Yuan, J.; Wells, J. A., Eds. Academic Press: San Diego, 2014; Vol. 544, pp 179-213.
482. Shalini, S.; Dorstyn, L.; Dawar, S.; Kumar, S., Old, new and emerging functions of caspases. *Cell Death & Differentiation* **2015,** *22* (4), 526-539.
483. Olsson, M.; Zhivotovsky, B., Caspases and cancer. *Cell Death & Differentiation* **2011,** *18* (9), 1441-1449.
484. McIlwain, D. R.; Berger, T.; Mak, T. W., Caspase functions in cell death and disease. *Cold Spring Harb Perspect Biol* **2013,** *5* (4), a008656.
485. Bright, S.; Byrne, A.; Vandenberghe, E.; Browne, P.; Mcelligott, A.; Meegan, M.; Williams, D., Selected nitrostyrene compounds demonstrate potent activity in chronic lymphocytic leukaemia cells, including those with poor prognostic markers. *Oncol Rep.* **2019,** *41* (5), 3127-3136.
486. National Center for Biotechnology Information (NCBI)-PubChem Database, Z-VAD-FMK (CID=5497174). https://pubchem.ncbi.nlm.nih.gov/compound/Z-VAD_OMe_-FMK (accessed 25/1/20).
487. Greene, L. M.; O'Boyle, N. M.; Nolan, D. P.; Meegan, M. J.; Zisterer, D. M., The vascular targeting agent Combretastatin-A4 directly induces autophagy in adenocarcinoma-derived colon cancer cells. *Biochemical Pharmacology* **2012,** *84* (5), 612-624.
488. Saha, M. N.; Qiu, L.; Chang, H., Targeting p53 by small molecules in hematological malignancies. *Journal of Hematology & Oncology* **2013,** *6* (1), 23.
489. Parrales, A.; Iwakuma, T., Targeting Oncogenic Mutant p53 for Cancer Therapy. *Frontiers in Oncology* **2015,** *5* (288).
490. Synnott, N. C.; Madden, S. F.; Bykov, V. J.; Crown, J.; Wiman, K. G.; Duffy, M. J., The mutant p53-targeting compound APR-246 induces ROS-modulating genes in breast cancer cells. *Transl Oncol.* **2018,** *11* (6), 1343-1349.
491. Synnott, N. C.; Bauer, M. R.; Madden, S.; Murray, A.; Klinger, R.; O'Donovan, N.; O'Connor, D.; Gallagher, W. M.; Crown, J.; Fersht, A. R.; Duffy, M. J., Mutant p53 as a therapeutic target for the treatment of triple-negative breast cancer:

Preclinical investigation with the anti-p53 drug, PK11007. *Cancer Letters* **2018,** *414*, 99-106.
492. Avonto, C.; Taglialatela-Scafati, O.; Pollastro, F.; Minassi, A.; Di Marzo, V.; De Petrocellis, L.; Appendino, G., An NMR spectroscopic method to identify and classify thiol-trapping agents: revival of Michael acceptors for drug discovery? *Angewandte Chemie International Edition* **2011,** *50* (2), 467-471.
493. ATCC (American Type Culture Collection), Triple-Negative Breast Cancer Panel 3 (ATCC® TCP-1003™). https://www.lgcstandards-atcc.org/products/all/TCP-1003.aspx?geo_country=ie (accessed 11/10/19).
494. ATCC (American Type Culture Collection), SK-BR-3 [SKBR3] (ATCC® HTB-30™). https://www.lgcstandards-atcc.org/products/all/HTB-30.aspx (accessed 11/10/19).
495. Memorial Sloan Kettering Cancer Center, CAMA-1: Human Breast Cancer Cell Line (ATCC HT-21). https://www.mskcc.org/research-advantage/support/technology/tangible-material/human-breast-cell-line-cama-1 (accessed 12/10/19).
496. ATCC (American Type Culture Collection), MCF7 (ATCC® HTB-22™). https://www.lgcstandards-atcc.org/products/all/HTB-22.aspx#documentation (accessed 11/10/19).
497. ATCC (American Type Culture Collection), MTT Cell Proliferation Assay. 2019.
498. Plumb, J. A., Cell Sensitivity Assays: The MTT Assay. In *Cancer Cell Culture: Methods and Protocols*, Langdon, S. P., Ed. Humana Press: Totowa, NJ, 2004; pp 165-169.
499. Bykov, V. J.; Zhang, Q.; Zhang, M.; Ceder, S.; Abrahmsen, L.; Wiman, K. G., Targeting of mutant p53 and the cellular redox balance by APR-246 as a strategy for efficient cancer therapy. *Frontiers in Oncology* **2016,** *6*, 21.
500. Iwakuma, T.; Lozano, G., MDM2, An Introduction. *Molecular Cancer Research* **2003,** *1* (14), 993.
501. National Centre for Biotechnology Information (NCBI), BAX BCL2 associated X, apoptosis regulator [Homo sapiens (human)]. https://www.ncbi.nlm.nih.gov/gene/581 (accessed 16/10/19).
502. National Centre for Biotechnology Information (NCBI), PERP p53 apoptosis effector related to PMP22 [Homo sapiens (human)]. https://www.ncbi.nlm.nih.gov/gene/64065 (accessed 16/10/19).
503. Ploner, C.; Kofler, R.; Villunger, A., Noxa: at the tip of the balance between life and death. *Oncogene* **2008,** *27* (1), S84-S92.
504. Yao, J.-Y.; Chen, J.-K. J. B.; communications, b. r., TAp63 plays compensatory roles in p53-deficient cancer cells under genotoxic stress. *Biochem Biophys Res Commun.* **2010,** *403* (3-4), 310-315.
505. Dötsch, V.; Bernassola, F.; Coutandin, D.; Candi, E.; Melino, G., p63 and p73, the ancestors of p53. *Cold Spring Harb Perspect Biol.* **2010,** *2* (9), a004887.
506. Moll, U. M.; Slade, N., p63 and p73: Roles in Development and Tumor Formation11National Cancer Institute. *J Molecular cancer research* **2004,** *2* (7), 371-386.
507. Nakano, K.; Vousden, K. H., PUMA, a Novel Proapoptotic Gene, Is Induced by p53. *Molecular Cell* **2001,** *7* (3), 683-694.
508. Daina, A.; Michielin, O.; Zoete, V., SwissADME: a free web tool to evaluate pharmacokinetics, drug-likeness and medicinal chemistry friendliness of small molecules. *Sci Rep* **2017,** *7*, 42717-42717.

509. Padron, J.; Carrasco, R.; Pellon, R., Molecular descriptor based on a molar refractivity partition using Randic-type graph-theoretical invariant. *J. Pharm. Pharmaceut. Sci* **2002,** *5* (3), 258-266.
510. Hansch, C.; Leo, A.; Hoekman, D., *Exploring QSAR: fundamentals and applications in chemistry and biology*. American Chemical Society Washington, D.C., 1995; Vol. 1.
511. Todeschini, R.; Consonni, V., *Handbook of molecular descriptors*. John Wiley & Sons: 2008; Vol. 11.
512. Winiwarter, S.; Bonham, N. M.; Ax, F.; Hallberg, A.; Lennernäs, H.; Karlén, A., Correlation of human jejunal permeability (in vivo) of drugs with experimentally and theoretically derived parameters. A multivariate data analysis approach. *Journal of Medicinal Chemistry* **1998,** *41* (25), 4939-4949.
513. Palm, K.; Luthman, K.; Ungell, A.-L.; Strandlund, G.; Artursson, P., Correlation of drug absorption with molecular surface properties. *Journal of Pharmaceutical Sciences* **1996,** *85* (1), 32-39.
514. Palm, K.; Stenberg, P.; Luthman, K.; Artursson, P., Polar Molecular Surface Properties Predict the Intestinal Absorption of Drugs in Humans. *Pharm Res* **1997,** *14* (5), 568-571.
515. Barret, R., Chapter 5- Importance and Evaluation of the Polar Surface Area (PSA and TPSA). In *Therapeutical Chemistry*, Barret, R., Ed. Elsevier: 2018; pp 89-95.
516. Barret, R., Chapter 3 - Importance and Evaluation of Lipophilicity. In *Therapeutical Chemistry*, Barret, R., Ed. Elsevier: 2018; pp 53-78.
517. Arnott, J. A.; Planey, S. L., The influence of lipophilicity in drug discovery and design. *Expert Opinion on Drug Discovery* **2012,** *7* (10), 863-875.
518. Montanari, F.; Ecker, G. F., Prediction of drug–ABC-transporter interaction—Recent advances and future challenges. *Advanced Drug Delivery Reviews* **2015,** *86*, 17-26.
519. Szakács, G.; Váradi, A.; Özvegy-Laczka, C.; Sarkadi, B., The role of ABC transporters in drug absorption, distribution, metabolism, excretion and toxicity (ADME–Tox). *Drug Discovery Today* **2008,** *13* (9-10), 379-393.
520. Testa, B.; Krämer, S. D., The biochemistry of drug metabolism–an introduction: part 1. principles and overview. *Chemistry biodiversity* **2006,** *3* (10), 1053-1101.
521. Daina, A.; Michielin, O.; Zoete, V., SwissADME: a free web tool to evaluate pharmacokinetics, drug-likeness and medicinal chemistry friendliness of small molecules. *Sci Rep* **2017,** *7*, 42717.
522. Sychev, D. A.; Ashraf, G. M.; Svistunov, A. A.; Maksimov, M. L.; Tarasov, V. V.; Chubarev, V. N.; Otdelenov, V. A.; Denisenko, N. j. P.; Barreto, G. E.; Aliev, G., The cytochrome P450 isoenzyme and some new opportunities for the prediction of negative drug interaction in vivo. *Drug Des Devel Ther.* **2018,** *12*, 1147.
523. Hodgson, E., *Introduction to toxicology-A textbook of modern toxicology*. 3rd ed.; John Wiley & Sons Inc.: Hoboken, New Jersey, 2004.
524. Lipinski, C. A.; Lombardo, F.; Dominy, B. W.; Feeney, P. J., Experimental and computational approaches to estimate solubility and permeability in drug discovery and development settings. *Advanced Drug Delivery Reviews* **1997,** *23* (1–3), 3-25.
525. Lipinski, C. A., Lead- and drug-like compounds: the rule-of-five revolution. *Drug Discovery Today: Technologies* **2004,** *1* (4), 337-341.
526. Muegge, I.; Bergner, A.; Kriegl, J. M., Computer-aided drug design at Boehringer Ingelheim. *J Comput Aided Mol Des.* **2017,** *31* (3), 275-285.
527. Muegge, I.; Heald, S. L.; Brittelli, D., Simple selection criteria for drug-like chemical matter. *Journal of Medicinal chCemistry* **2001,** *44* (12), 1841-1846.

528. Ghose, A. K.; Viswanadhan, V. N.; Wendoloski, J. J., A knowledge-based approach in designing combinatorial or medicinal chemistry libraries for drug discovery. 1. A qualitative and quantitative characterization of known drug databases. *J Comb Chem.* **1999,** *1* (1), 55-68.
529. Veber, D. F.; Johnson, S. R.; Cheng, H. Y.; Smith, B. R.; Ward, K. W.; Kopple, K. D., Molecular properties that influence the oral bioavailability of drug candidates. *Journal of Medicinal Chemistry* **2002,** *45* (12), 2615-2623.
530. Egan, W. J.; Merz, K. M.; Baldwin, J. J., Prediction of Drug Absorption Using Multivariate Statistics. *Journal of Medicinal Chemistry* **2000,** *43* (21), 3867-3877.
531. Oprea, T. I.; Davis, A. M.; Teague, S. J.; Leeson, P. D., Is There a Difference between Leads and Drugs? A Historical Perspective. *Journal of Chemical Information and Computer Sciences* **2001,** *41* (5), 1308-1315.
532. Wigglesworth, M. J.; Murray, D. C.; Blackett, C. J.; Kossenjans, M.; Nissink, J. W. M., Increasing the delivery of next generation therapeutics from high throughput screening libraries. *Current opinion in chemical biology* **2015,** *26*, 104-110.
533. Leeson, P., Drug discovery: Chemical beauty contest. *Nature* **2012,** *481* (7382), 455-456.
534. Benet, L. Z.; Hosey, C. M.; Ursu, O.; Oprea, T. I., BDDCS, the Rule of 5 and drugability. *Advanced Drug Delivery Reviews* **2016,** *101*, 89-98.
535. Bickerton, G. R.; Paolini, G. V.; Besnard, J.; Muresan, S.; Hopkins, A. L., Quantifying the chemical beauty of drugs. *Nat Chem* **2012,** *4* (2), 90-98.
536. Baell, J. B.; Holloway, G. A., New Substructure Filters for Removal of Pan Assay Interference Compounds (PAINS) from Screening Libraries and for Their Exclusion in Bioassays. *Journal of Medicinal Chemistry* **2010,** *53* (7), 2719-2740.
537. Brenk, R.; Schipani, A.; James, D.; Krasowski, A.; Gilbert, I. H.; Frearson, J.; Wyatt, P. G., Lessons Learnt from Assembling Screening Libraries for Drug Discovery for Neglected Diseases. **2008,** *3* (3), 435-444.
538. Jain, N.; O'Brien, S., Targeted therapies for CLL: Practical issues with the changing treatment paradigm. *Blood Reviews* **2016,** *30* (3), 233-244.
539. British Pharmacopoeia, Appendix I D. Buffer Solutions. https://www.pharmacopoeia.com/bp-2019/appendices/appendix-01/appendix-01-d/ (accessed 15/04/19).
540. Prabhakar, M.; Merry, T.; Tsurho, S.; Zatsu, R.; Jain, N.; Sataniya, A.; Enaganti, S., Synthesis, characterization and biological evaluation of 9-anthracenyl chalcones as anti-cancer agents. *J Chem Pharm Res* **2017,** *9*, 185-92.
541. Koslov, N. S.; Shmanai, G. S.; Gladchenko, L. F., Anthracene derivatives of benzo[f]quinoline. Synthesis, spectra, and luminescence. *Chemistry of Heterocyclic Compounds* **1985,** *21* (11), 1268-1272.
542. Zhao, Y.; Li, H.; Shao, Z.; Xu, W.; Meng, X.; Song, Y.; Hou, H., Investigation of Regulating Third-Order Nonlinear Optical Property by Coordination Interaction. *Inorganic Chemistry* **2019,** *58* (8), 4792-4801.

Appendicies

(Compact Disc)

A: National Cancer Institute (NCI) 60 cell panel reports

B: X-ray crystallography reports